

Electronic Thesis and Dissertation Repository

2-17-2022 10:00 AM

Illuminating Transfer RNA Variants as Genetic Modifiers in Models of Human Disease

Jeremy T. Lant, *The University of Western Ontario*

Supervisor: O'Donoghue, Patrick, *The University of Western Ontario*

A thesis submitted in partial fulfillment of the requirements for the Doctor of Philosophy degree in Biochemistry

© Jeremy T. Lant 2022

Follow this and additional works at: <https://ir.lib.uwo.ca/etd>



Part of the [Biochemistry Commons](#), [Cell Biology Commons](#), [Genetics Commons](#), [Molecular and Cellular Neuroscience Commons](#), and the [Molecular Biology Commons](#)

Recommended Citation

Lant, Jeremy T., "Illuminating Transfer RNA Variants as Genetic Modifiers in Models of Human Disease" (2022). *Electronic Thesis and Dissertation Repository*. 8416.
<https://ir.lib.uwo.ca/etd/8416>

This Dissertation/Thesis is brought to you for free and open access by Scholarship@Western. It has been accepted for inclusion in Electronic Thesis and Dissertation Repository by an authorized administrator of Scholarship@Western. For more information, please contact wlsadmin@uwo.ca.

Abstract

Transfer RNAs (tRNAs) physically link the genetic code to an amino acid sequence, by recruiting amino acids to three-nucleotide codons in messenger RNAs. To ensure that the genetic code is translated as intended, tRNAs must be accurately aminoacylated and faithfully recognize codons in the ribosome during protein synthesis. Given the critical function of tRNAs, it has often been assumed that mutations in human tRNA genes would be either lethal to cells or not significantly impair tRNA function. My goal was to rigorously test this assumption in mammalian cell models, prompted by the recent discovery of unprecedented variation in human tRNA gene sequences.

First, I review existing knowledge on links between human cytosolic tRNA biology and disease. Next, I demonstrate that synthetic tRNA mutants can elicit significant levels of amino acid misincorporation in human cells, which is surprisingly well tolerated. I then test the effects of mistranslation by synthetic and natural tRNA variants on cellular models of neurodegenerative disease, based on our hypothesis that mistranslation would exacerbate protein-folding stress-associated diseases. I find that a natural tRNA variant occurring in ~2% of the sequenced human population has significant potential to modify the progression and severity of Huntington's disease, amyotrophic lateral sclerosis, and potentially other diseases. Lastly, I investigate methodological approaches which could aid in the characterization of other natural human tRNA variants, while demonstrating that even identical tRNA variants may differ in phenotypic severity and effected tissues depending on local sequence context of the tRNA gene.

Keywords

Transfer RNA, tRNA, mistranslation, amino acid misincorporation, human disease, neurodegenerative disease, Huntington's disease, HTT, amyotrophic lateral sclerosis, FUS, protein aggregation, fluorescence, microscopy.

Summary for Lay Audience

Transfer RNAs, commonly known as tRNAs, are like assembly-line workers for the cell. Their job is to carry amino acids—the building blocks of proteins—to the ribosome, which assembles amino acids into a protein sequence. Proteins carry out most cellular functions. From providing structural support to the cell, to pumping ions across the cell membrane, their functions are astoundingly diverse. Hence, the job of tRNAs is critical to ensure that every protein is produced precisely as encoded by the human genome.

Given the critical function of tRNAs, it has often been assumed that mutations in tRNA genes would be either lethal to cells or not significantly impair tRNA function. However, since tRNAs are genetically encoded molecules themselves, they too are subject to mutation, and some mutations cause tRNAs to carry the wrong amino acids to the ribosome, or misread the genetic code, resulting in the erroneous incorporation of amino acids in proteins. Further, it was recently discovered that tRNA gene sequence variants are common in the human population, with the average individual harboring ~60-70 variants in tRNA genes compared to the human reference genome.

My thesis explores tRNA genes as an underappreciated source of variability in human diseases. First, I found that synthetic tRNA mutants can cause significant levels of amino acid misincorporation (~2-3%) without severely impacting cell viability. Next, I found that a naturally occurring tRNA variant found in ~2% of the sequenced human population had potent modifying effects on cellular models of Huntington's disease and amyotrophic lateral sclerosis, demonstrating that tRNA variants have potential to modify the outcomes of neurodegenerative diseases. Lastly, I investigated several methodological approaches to characterize the many human tRNA sequence variants in the human population, while finding that even identical tRNA gene mutations can have differing severity of effects and in different cell types depending on which identical copy of a tRNA gene is mutated in the genome. Altogether, my work shines a new light on tRNA variants as potentially underappreciated modifiers of human disease and outlines new methods to study them.

Co-Authorship Statement

Chapter 1:

Lant, J.T., Berg, M.D., Heinemann, I.U., Brandl, C.J., O'Donoghue, P. (2019). Pathways to disease from natural variations in human cytoplasmic tRNAs. *Journal of Biological Chemistry*.

J.T. Lant and P. O'Donoghue co-wrote the majority of the review. M.D. Berg analyzed 1000 genomes data shown in figure 1.3 and produced the figure. I.U. Heinemann and J.T. Lant co-wrote the section on "tRNA regulation in human cells" and I.U. Heinemann and C.J. Brandl assisted in editing and consulting on the manuscript throughout.

Chapter 2:

Lant, J.T., Berg, M.D., Sze, D.H.W., Hoffman, K.S., Akinpelu, I.C., Turk, M., Heinemann, I.U., Duennwald, M.L., Brandl, C.J., and O'Donoghue, P. (2017) Visualizing tRNA-dependent mistranslation in human cells. *RNA Biology*.

J.T. Lant, M.D. Berg, and P. O'Donoghue co-wrote the majority of the manuscript. J.T. Lant completed experiments and produced figures 2.3-2.5 and S2.1-2.4. P. O'Donoghue created figure 2.1. D.H.W. Sze and K. Hoffman completed experiment in figure 2.2 and J.T. Lant and M.D. Berg produced the figure. I.C. Akinpelu and M. Turk assisted with mammalian cell culture maintenance and harvesting for western blots. I.U. Heinemann, M.L. Duennwald, and C.J. Brandl assisted in experimental planning and editing the manuscript.

Chapter 3:

Lant, J.T., Kiri, R., Duennwald, M.L., O'Donoghue, P. (2021). Formation and persistence of polyglutamine aggregates in mistranslating cells. *Nucleic Acids Research*

J.T. Lant and P. O'Donoghue co-wrote the majority of the manuscript. P. O'Donoghue created figure 3.1. R. Kiri assisted in cloning DNA plasmids and experimental planning. All other experiments and figures were completed and produced by J.T. Lant. M.L. Duennwald assisted in experimental planning and editing of the manuscript.

Chapter 4:

Lant, J.T., Hasan, F., Briggs, J., and O'Donoghue, P. (2021). Kinetics of amyotrophic lateral sclerosis-associated protein aggregation in mistranslating cells. (unpublished).

J.T. Lant and P. O'Donoghue co-wrote the majority of the chapter. F. Hasan completed the experiment in Fig. 4.4 and produced the figure. J. Briggs completed the experiment in Fig. S4.4 and produced the figure. F. Hasan and J. Briggs also completed DNA cloning work with experimental planning contributions from J.T. Lant. All other experiments and figures were completed and produced by J.T. Lant

Chapter 5:

Lant, J.T., Hasan, F., Seto, A., Briggs, J., and O'Donoghue, P. (2021). Local DNA sequence context alters the phenotypic potency of identical human tRNA variants. (unpublished).

J.T. Lant wrote the majority of the chapter with editing and experimental planning contributions from P. O'Donoghue. F. Hasan completed the experiments in figures 5.3C, 5.3F, and 5.5C, for which J.T. Lant completed data analysis and produced the figures. F. Hasan and J. Briggs assisted with DNA cloning. A. Seto designed the majority of primers used in the genomic PCRs and assisted with initial planning and literature searching. All other experiments and figures were completed and produced by J.T. Lant.

Acknowledgments

Firstly, I wish to thank my supervisor, Dr. Patrick O'Donoghue for your outstanding mentorship throughout my graduate studies. From the moment I first set foot in your office your energy and enthusiasm for science has motivated me to push myself further and grow stronger as a scientist. I will always remember my years in your lab fondly and look forward to our lasting friendship.

Secondly, I wish to thank my fiancée Caitlin Droney, my parents Victoria and David Lant, and all of my other close friends and family who have supported me throughout my graduate studies. Any scientist has good days and bad days and having a strong support network has made things so much easier along the way (and more fun).

I also wish to thank all of the outstanding individuals in the department of Biochemistry at Western who have helped me out, made me laugh, and been an involuntary sounding board for my ideas over the years. In particular, I wish to acknowledge Ilka Heinemann, Martin Duennwald, Murray Junop, and Christopher Brandl as faculty who have provided me with extensive mentorship over the years. I also wish to thank my colleagues David Wright, Nileeka Balasuriya, Farah Hasan, Matthew Berg, Peter Rozik, McShane McKenna, Christina Chung, Mallory Frederick, and many more for their friendship and great ideas. Lastly, I wish to thank the outstanding staff and research associates in our department who have helped me out in countless ways. Kyle Pollard, Laszlo Gyenis, Yumin Bi, Lee-Ann Briere, Victoria Clarke, Lindsay Ralph, Boun Thai, Barbara Green, and Lynn Weir have all significantly contributed to my success as a graduate student, in addition to many others.

Table of Contents

Abstract.....	ii
Keywords.....	ii
Summary for Lay Audience.....	iii
Co-Authorship Statement.....	iv
Acknowledgements.....	vi
Table of Contents.....	vii
List of Tables.....	xiv
List of Figures.....	xiv
List of Supplemental Tables.....	xvi
List Supplemental Figures.....	xvi
List of Appendices.....	xvii
Chapter 1.....	1
1 Pathways to disease from natural variations in human cytoplasmic tRNAs.....	1
1.1 Introduction.....	1
1.2 tRNA function and regulation.....	3
1.2.1 The role of tRNA in decoding the genetic code.....	3
1.2.2 tRNA regulation in human cells.....	6
1.3 Phenotypes of mistranslating cells.....	8
1.4 tRNA variation in humans.....	10
1.5 tRNA variation and disease.....	15
1.5.1 tRNA mutants linked to disease.....	15
1.5.2 Imbalanced tRNA expression and disease.....	16
1.5.3 tRNA modification defects in disease.....	18
1.5.4 tRNA variants in neurodegeneration.....	20

1.6 Conclusion.....	21
1.7 References.....	23
1.8 Supplemental information.....	33
1.8.1 Supplemental tables.....	33
1.8.2 Supplemental references.....	34
Chapter 2.....	36
2. Visualizing tRNA-dependent mistranslation in human cells.....	36
2.1 Introduction.....	36
2.2 Materials and methods.....	39
2.2.1 Plasmids and strains.....	39
2.2.2 <i>In vitro</i> tRNA transcription and radiolabeling.....	39
2.2.3 <i>In vitro</i> tRNA aminoacylation.....	39
2.2.4 HEK293T cell transfection.....	40
2.2.5 Fluorescence quantitation of enhanced GFP (EGFP) reporter.....	40
2.2.6 Western blotting.....	41
2.2.7 Cell viability assay.....	41
2.3 Results.....	42
2.3.1 Biochemical characterization of a mistranslating human tRNA ^{Pro} (G3:U70).....	42
2.3.2 GFP reporter illuminates mistranslation in living cells.....	43
2.3.3 Mistranslation following antibiotic selection.....	46
2.3.4 Mistranslation by tRNA ^{Pro} (G3:U70) does not induce a heat-shock response.....	47
2.3.5 Viability in mistranslating cells.....	48
2.4 Discussion.....	48
2.4.1 Transfer RNA genes occur in excess.....	48
2.4.2 A single tRNA mutant induces mistranslation in human cells.....	49

2.4.3 tRNA-dependent mistranslation linked to disease.....	50
2.4.4 Detecting tRNA-dependent mistranslation in live cells.....	50
2.4.5 Cellular adaptation to mistranslation.....	51
2.5 Conclusion.....	52
2.6 References.....	52
2.7 Supplemental information.....	56
2.7.1 Methods.....	56
2.7.2 Tables.....	57
2.7.3 Figures.....	58
2.7.4 References.....	61
Chapter 3.....	62
3. Formation and persistence of polyglutamine aggregates in mistranslating cells.....	62
3.1 Introduction.....	62
3.2 Materials and methods.....	65
3.2.1 Plasmids and strains.....	65
3.2.2 Cell culture and transfection.....	65
3.2.3 Small molecules and peptides.....	65
3.2.4 Cellular viability and toxicity assays.....	66
3.2.5 Western blotting.....	66
3.2.6 Mass spectrometry.....	66
3.2.7 Fluorescence microscopy.....	66
3.2.8 Cycloheximide chase protein degradation assays.....	67
3.2.9 Semi-denaturing detergent agarose gel electrophoresis (SDD-AGE)..	67
3.2.10 Protein aggregation clearance assay.....	68
3.3 Results.....	68
3.3.1 Transfer RNA variants used in this study.....	68

3.3.2 tRNA ^{Ser} _{AAA} -dependent amino acid misincorporation.....	71
3.3.3 Reduced protein levels in mistranslating cells.....	73
3.3.4 tRNA-dependent toxicity in human and mouse cellular models of HD.....	75
3.3.5 Interaction of polyQ HTT alleles with tRNA ^{Ser} mutants.....	77
3.3.6 Kinetics of polyQ aggregate formation in mistranslating cells.....	78
3.3.7 Mistranslating cells accumulate smaller and fewer polyQ aggregates.....	79
3.3.8 Heat shock protein levels in mistranslating cells.....	82
3.3.9 Regulation of translation initiation and elongation in mistranslating cells.....	82
3.3.10 Mistranslating cells are resistant to the integrated stress response inhibitor.....	83
3.3.11 Defective protein turnover and aggregate clearance in mistranslating cells.....	85
3.4 Discussion.....	87
3.4.1 Huntingtin protein aggregation in mistranslating cells.....	87
3.4.2 Huntingtin protein aggregation and defects in protein quality control.....	88
3.4.3 Compromised proteostasis in cells expressing mistranslating tRNAs.....	89
3.5 Conclusion.....	91
3.6 Data availability.....	92
3.7 References.....	92
3.8 Supplemental information.....	98
3.8.1 Methods.....	98
3.8.2 Tables.....	102

3.8.3 Figures.....	104
3.8.4 Data files.....	113
3.8.5 Appendix: ImageJ macros.....	113
3.8.6 Supplemental References.....	119
Chapter 4.....	120
4. Kinetics of amyotrophic lateral sclerosis-associated protein aggregation in mistranslating cells.....	120
4.1 Introduction.....	120
4.2 Materials and Methods.....	122
4.2.1 Plasmids and strains.....	122
4.2.2 Cell culture and transfections.....	123
4.2.3 Cytotoxicity assay.....	123
4.2.4 Fluorescence microscopy.....	124
4.2.5 Cell harvesting and western blotting.....	124
4.2.6 Semi-denaturing detergent agarose gel electrophoresis (SDD-AGE).....	125
4.2.7 Statistical analysis.....	126
4.3 Results.....	126
4.3.1 FUS protein synthesis in mistranslating cells.....	126
4.3.2 Toxicity of FUS alleles in mistranslating cells.....	129
4.3.3 Aggregation kinetics of FUS in normal and mistranslating cells.....	130
4.3.4 Measuring insoluble FUS aggregates in mistranslating cells.....	133
4.4 Discussion.....	135
4.4.1 Protein synthesis de-regulation in ALS models and mistranslating cells.....	135
4.4.2 Influence of tRNAs on FUS aggregation.....	136
4.5 References.....	138

4.6 Supplemental information.....	143
4.6.1 Tables.....	143
4.6.2 Figures.....	143
4.6.3 Appendix: Fiji/ImageJ macros.....	149
Chapter 5.....	155
5. Local DNA sequence context alters the phenotypic potency of identical human tRNA variants.....	155
5.1 Introduction.....	155
5.2 Materials and methods.....	157
5.2.1 tRNA gene alignments.....	157
5.2.2 Plasmids and strains.....	157
5.2.3 Cell culture and transfection.....	158
5.2.4 Small molecules and peptides.....	159
5.2.5 Fluorescence microscopy.....	159
5.2.6 tRNA sequencing.....	159
5.2.7 Cell harvesting and western blotting.....	160
5.2.8 RFP-trap immunoprecipitation.....	161
5.2.9 Cytotoxicity assays.....	162
5.2.10 Cell migration assay.....	162
5.3 Results.....	163
5.3.1 tRNA gene alignments and variant frequencies.....	163
5.3.2 Single nucleotide variants allow detection of tRNA expression by tRNAseq.....	164
5.3.3 tRNA gene expression predictions.....	169
5.3.4 Mistranslating tRNAs reduce protein synthesis to varying degrees depending on local sequence context.....	174
5.3.5 Precise detection of tRNA-dependent codon misreading with MS-READ.....	176

5.3.6 Cytotoxicity of a mistranslating tRNA variant expressed from different sequence contexts.....	180
5.3.7 Migration kinetics of cells expressing a mistranslating tRNA variant from different sequence contexts.....	182
5.4 Discussion.....	184
5.4.1 tRNA gene copy number does not imply redundancy.....	184
5.4.2 Using variants as tools to detect tRNA expression.....	185
5.4.3 Detecting amino acid misincorporation by mass spectrometry.....	186
5.4.4 Phenotypic assays enable high sensitivity and throughput in tRNA variant testing.....	187
5.6 References.....	189
5.7 Supplemental information.....	193
5.7.1 Methods.....	193
5.7.2 Tables.....	195
5.7.3 Figures.....	199
5.7.4 Appendix: Fiji/ImageJ macros and TrackMate analysis.....	204
Chapter 6.....	207
6. Conclusions and future perspectives.....	207
6.1 Summary and conclusions.....	207
6.2 Future directions.....	216
6.2.1 Mechanisms of protein synthesis inhibition in mistranslating cells....	216
6.2.2 Fluorescent reporters of amino acid misincorporation.....	217
6.2.3 Sequencing tRNA genes in disease cohorts.....	218
6.3 Conclusion.....	218
6.4 References.....	219
Copyright permissions.....	223
Curriculum vitae.....	225

List of Tables

Table 1.1 Human tRNA anticodon variants.....	14
Table 1.2 Human tRNA variants that introduce a G3:U70 base pair.....	15
Table 1.3 Human tRNA ^{Arg} C50T variants.....	21
Table 3.1 tRNA genes and variants.....	69
Table 3.2 Selected observed peptides showing Ser mis-incorporation at Phe codons in mCherry.....	72
Table 3.3 Observed spectral counts for Ser or Phe incorporation at Phe codons in mCherry.....	72
Table 5.1 tRNA-Ser-AGA-2- <i>n</i> gene loci and variant frequencies.....	164
Table 5.2 tRNAseq unique read counts for all tRNA-Ser isodecoders.....	167
Table 5.3 tRNAseq multi-map-corrected read counts for all tRNA-Ser isodecoders.....	168
Table 5.4 Extended tRNA gene activity prediction scores.....	172
Table 5.5 LC-MS/MS area under the curve and spectral counts for MS-READ peptides...	179
Table 5.6 Mechanism of action of common selectable markers used in mammalian cell line selection.....	188

List of Figures

Figure 1.1 tRNA structure.....	3
Figure 1.2 Phylogenetic relationships of human and yeast tRNA ^{Ala}	5
Figure 1.3 Transfer RNA variants observed in the 1000 Genomes Project.....	11
Figure 1.4 Phenotypic consequences of tRNA variation.....	22
Figure 2.1 Structure of AlaRS and tRNA ^{Ala} complex.....	38
Figure 2.2 <i>In vitro</i> amino-acylation of tRNA ^{Pro} (G3:U70).....	43
Figure 2.3 tRNA-dependent mistranslation increases under glucose and serum starvation.....	44
Figure 2.4 Mistranslation caused no detectable induction of heat shock response.....	46

Figure 2.5 Viability of mistranslating cells.....	47
Figure 3.1 Mechanisms of tRNA-dependent mistranslation.....	70
Figure 3.2 Fluorescence and expression of mCherry protein in mistranslating cells.....	74
Figure 3.3 Toxic interaction of tRNA variants with a deleterious polyQ allele or proteasome inhibition.....	76
Figure 3.4 Formation of polyQ aggregates in mistranslating cells.....	78
Figure 3.5 Insoluble polyQ aggregate size and levels in mistranslating cells.....	80
Figure 3.6 Fluorescence and cytotoxicity of mistranslating cells treated with p-eIf2 α Antagonist ISRIB.....	84
Figure 3.7 Protein turnover and clearance of polyQ aggregates in mistranslating cells.....	86
Figure 4.1 Kinetics of FUS protein synthesis in wild-type and mistranslating cells.....	127
Figure 4.2 Synthetic toxicity of mistranslation and FUS R521C aggregation.....	129
Figure 4.3 Kinetics of FUS protein aggregation in wild-type and mistranslating cells.....	131
Figure 4.4 FUS protein and aggregate production in wild-type and mistranslating cells....	134
Figure 5.1 tRNA and tRNA variant expression in N2a cells revealed by tRNAseq.....	166
Figure 5.2 tRNA gene expression activity predictions from publicly available datasets.....	170
Figure 5.3 Fluorescence of cells expressing tRNA-Ser-AAA-2- <i>n</i> variants.....	175
Figure 5.4 tRNA-dependent Phe to Ser misincorporation detected by MS-READ.....	178
Figure 5.5 Cytotoxicity of tRNA ^{Ser} _{AAA} variants in different cell lines and sequence contexts.....	181
Figure 5.6 Migration kinetics of cells expressing tRNA-Ser-AAA-2- <i>n</i> variants.....	183

List of Supplemental Tables

Table S1.1 Human tRNA variants that introduce a G4:U69 base pair.....	33
Table S1.2 List of tRNA counts in selected genomes.....	34
Table S2.1 Sequences of tRNA construct oligos.....	57
Table S2.2 Sequences of primers for template PCR.....	58
Table S3.1 Oligonucleotide sequences.....	102
Table S3.2 tRNA gene sequences and identifiers.....	103
Table S4.1 Oligonucleotide sequences.....	143
Table S5.1 Oligonucleotide sequences.....	195
Table S5.2 tRNAseq RNA yields and purity.....	197
Table S5.3 tRNAseq read mapping summary.....	197
Table S5.4 UCSC genome browser data representing basal tRNA transcription initiation complex proteins.....	198

List of Supplemental Figures

Figure S2.1 Overexpression of tRNA ^{Pro} G3:U70 had no obvious effect on cell morphology compared to wildtype tRNA ^{Pro}	58
Figure S2.2 Visualizing mistranslation after selection in Geneticin.....	59
Figure S2.3 Additional images from low serum low glucose growth, experiment day 5....	60
Figure S2.4 Mistranslation under glucose and serum starvation.....	61
Figure S3.1 Detailed y and b ion spectra of observed Ser mistranslation at Phe codons.....	104
Figure S3.2 HEK293 cells expressing tRNA ^{Pro} G3:U70 and cis/trans-plasmid expression tests od N2a cells expressing tRNA ^{Ser} _{AAA}	105
Figure S3.3 Viability of cells mistranslating Phe or Pro codons with Ser and expressing HTTexon1 variants.....	106
Figure S3.4 Quantitation of aggregate fluorescence and area in ImageJ.....	107
Figure S3.5 Live cell imaging raw fluorescence and number of aggregates (N _{aggregates}).....	108

Figure S3.6 Semi-denaturing detergent agarose gel electrophoresis (SDD-AGE).....	108
Figure S3.7 Heat shock protein levels in mistranslating cells.....	109
Figure S3.8 Regulation of translation initiation and elongation in mistranslating cells.....	110
Figure S3.9 Cycloheximide concentration testing.....	111
Figure S3.10 Aggregate counting in PC12 cells transfected with mCherry-tRNA plasmids.....	112
Figure S4.1 FUS-mCherry construct and fluorescence in HEK293T cells.....	143
Figure S4.2 FUS-mCherry fluorescence timecourse statistical analysis and mCherry control transfections.....	144
Figure S4.3 Cell death assay for N2a cells co-expressing tRNA ^{Ser} variants with mCherry or FUS-mCherry variants.....	145
Figure S4.4 FUS aggregate formation in cells expressing wild-type and G3:U70 tRNA ^{Pro}	146
Figure S4.5 FUS-mCherry aggregation timecourse statistical analysis.....	147
Figure S4.6 Insoluble FUS aggregate levels in wild-type and mistranslating cells.....	148
Figure S5.1 tRNA-Ser-AGA-2- <i>n</i> gene alignment.....	199
Figure S5.2 tRNAseq transfection images.....	200
Figure S5.3 CHIP-seq and DNase-seq data for all tRNA-Ser-AGA genes.....	201
Figure S5.4 Representative y and b ion spectra for Leu-containing MS-READ peptides...	202
Figure S5.5 Representative y and b ion spectra for Ser-containing MS-READ peptides....	202
Figure S5.6 Supplemental HEK 293T cell cytotoxicity data.....	203

List of Appendices

3.8.5 Supplemental appendix: ImageJ macros.....	113
4.6.2 Supplemental appendix: Fiji/ImageJ macros.....	149
5.7.4 Fiji/ImageJ macros and TrackMate analysis.....	204

Chapter 1

1. Pathways to disease from natural variations in human cytoplasmic tRNAs¹

1.1 Introduction

Protein synthesis is an evolutionarily conserved process that is required by all life. In the interpretation of the genetic code, transfer RNAs (tRNAs) play a central role as they physically link amino acids to codons. Crick's adaptor hypothesis predicted the existence of tRNAs in 1955: "*each amino acid would combine chemically, at a special enzyme, with a small molecule which, having a specific hydrogen-bonding surface, would combine specifically with the nucleic acid template.*" (1). Just three years later, the first tRNAs were discovered as soluble RNAs involved in protein synthesis (2). Working in yeast, Holley isolated tRNAs and determined the first tRNA sequence (3). The first codons were mapped to amino acids using repeating poly-ribonucleotides as templates for protein synthesis (4,5). The labs of Nirenberg (6) and Khorana (7) then raced to solve the complete codon catalogue using a technique that monitored the binding of radiolabeled aminoacyl-tRNAs to ribosomes separately prepared with each of the possible 64 trinucleotide codons. These efforts established the standard genetic code table for which Holley, Khorana, and Nirenberg were awarded the Nobel prize in Physiology or Medicine in 1968.

Fascinatingly, by the time the prize was awarded, exceptions to the genetic code had already been identified. In 1966, Yanofsky and colleagues demonstrated tRNA mutants enabled missense suppression or amino acid mis-incorporation using a defective tryptophan synthase A gene in *Escherichia coli* (8). Early in 1968, Atkins identified the first exception to triplet decoding with the discovery of frame-shifting in *Salmonella typhimurium* (9). Indeed, while the genetic code is *nearly* universal in the living world, several exceptions to the standard code occur in diverse organisms (10). Genome sequences, genetic and biochemical data reveal that in organisms from microbes to humans, codons can be ambiguously decoded (8,11-13), reassigned (14,15), or site-specifically recoded (16-18) to incorporate unexpected amino acids or amino acids beyond the standard set of 20.

¹Work in this chapter was published in: Lant, J.T., Berg, M.D., Heinemann, I.U., Brandl, C.J., O'Donoghue, P. (2019). Pathways to disease from natural variations in human cytoplasmic tRNAs. *Journal of Biological Chemistry*.

Given the importance of cytosolic tRNAs to facilitate accurate synthesis of the proteome, surprisingly few examples have linked a cytosolic tRNA mutation to human disease thus far. Yet, recent examples directly connecting cytosolic tRNA mutations to disease in humans (19) and separately to neurodegeneration (20,21) and cancer (22) in mice suggest that cytosolic tRNA variants play a greater role in disease than previously imagined. It is possible that significant changes to tRNA function are not usually tolerated in the genome or that defective tRNA alleles may be genetically buffered by multiple copies of each iso-decoder. Nevertheless, two empirical observations suggest tRNAs have a larger role in disease than previously recognized: *i*) the unexpectedly large number of tRNA variants in the human population (Tables 1.1, 1.2, 1.3, S1.1) and *ii*) the fact that even a single nucleotide change in a single tRNA gene can cause mistranslation or stall translation leading to molecular and cellular defects (e.g., (13,21,23)). The majority of research connecting human tRNA function to disease is focused on mutations in aminoacyl-tRNA synthetases (AARSs) (reviewed in (24)), on proteins that modify nucleotides in cytosolic tRNAs (25,26), or on the smaller pool of mitochondrial tRNAs (27-29). Two major reasons for this are a relative lack in available sequence data for cytosolic tRNAs, and a long-held assumption that excessive tRNA copy number should ‘buffer’ potential phenotypes resulting from a single mutant.

In this review, we outline the complexity of cytosolic tRNA function and regulation in eukaryotic cells. We then summarize recent studies demonstrating examples of single nucleotide tRNA variants that elicit significant levels of amino acid mis-incorporation, which can be surprisingly well-tolerated in eukaryotic cells. Using data from the 1000 Genomes Project, we analyzed the location and frequency of naturally occurring human tRNA variants. These data reveal an abundance of mistranslating tRNAs in the human population. Finally, we summarize recent evidence linking tRNA mutations and de-regulated tRNA expression and nucleotide modification to disease in humans and model systems. Some of the studies point to the idea that tRNA mutations, which are otherwise tolerated or benign, contribute to disease in the context of other coincidental cellular defects.

1.2 tRNA function and regulation

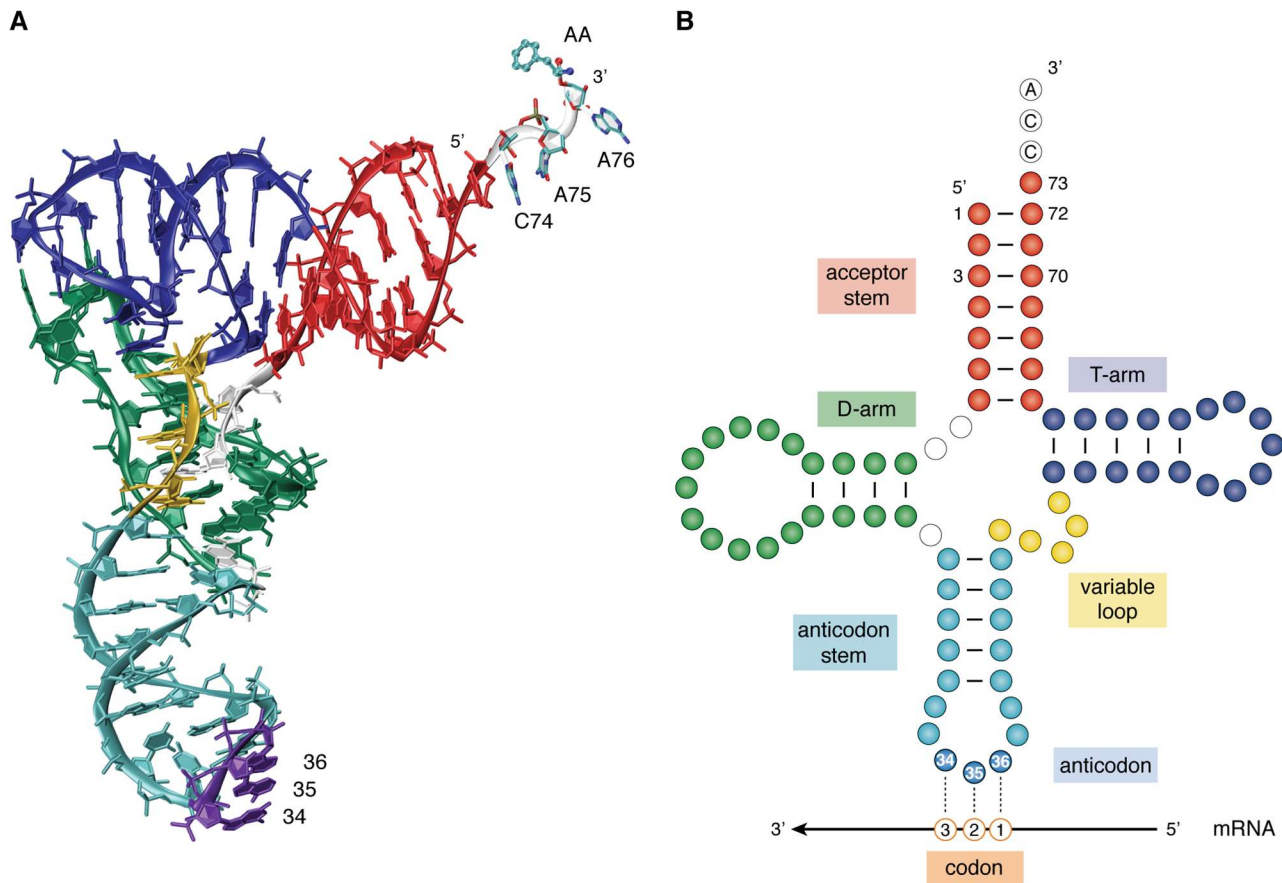


Figure 1.1. tRNA structure. (A) Transfer RNAs fold into an L-shaped 3-dimensional structure with extensive intramolecular base-pairing. This tRNA^{Phe} structure (PDB: 1OB5) (134) is aminoacylated with phenylalanine (AA). (B) In a two-dimensional representation, tRNA resembles a cloverleaf. In both diagrams, the tRNA is colored by structural elements: acceptor stem (red), dihydrouridine (D)-arm (green), anticodon stem (cyan), anticodon (bases 34, 35, 36 in purple), variable loop (yellow), T Ψ C (T) arm (navy), and the conserved CCA-3' end (white). A schematic mRNA is shown below the tRNA diagram to indicate the tRNA nucleotides that base pair with each codon position.

1.2.1 The role of tRNA in decoding the genetic code.

Transfer RNAs are best known for their role in translation of RNA messages into proteins. tRNAs are relatively small RNA molecules, typically consisting of 76 - 90 nucleotides, and fold into a conserved three-dimensional structure in the shape of an upside-down L (Fig. 1.1A). The anticodon resides at the

long end of the L-shape and binds to cognate codons in the messenger RNA (mRNA) on the ribosome. On the opposite end of the tRNA, the amino acid is ligated to the 3' terminal adenosine residue in the acceptor stem. Accurate tRNA aminoacylation and high-fidelity decoding of codons on the ribosome are key determinants to accurate protein production.

Codon recognition is determined by the tRNA anticodon, which base-pairs with tri-nucleotide codons in mRNAs during protein synthesis (Fig. 1.1B). The essential interaction between codon and anticodon is established not only by Watson-Crick base pairing, but also by nucleotide modifications in tRNAs (30,31), competition between cognate and near-cognate decoding (32,33), and wobble decoding. Generally, the first two positions of a codon form Watson-Crick pairs with the tRNA, while the third position is more flexible (30). In back-to-back publications, Crick hypothesized (34) what Söll *et al.* determined experimentally (35), that the third position of a codon can involve G:U or U:G wobble pairing with the 1st position of the anticodon at tRNA nucleotide 34. Indeed, the initial discoveries also included examples of extended wobble decoding in yeast arginine and alanine tRNAs that read codons ending in U, C, or A (35). Extended wobble decoding is facilitated by post-transcriptional tRNA modification, where adenosine residues at position 34 are modified to inosine, which pairs with U, C, or A in the third codon position (30). Additional nucleotide modifications in the anticodon loop (particularly at positions 34 and 37) also impact translation fidelity and reading-frame maintenance (36,37). For example, in yeast, a 5-methoxycarbonylmethyl-2-thiouridine modification at anti-codon base U34 represses +1 frame-shifting. Lack of the modification or hypo-modification at this site in a variety of tRNAs leads to 1.5 to 3.0-fold increases in ribosomal frame-shifting (38). Similarly, absence of the modified base N⁶-threonylcarbamoyladenosine (t⁶A) at the anticodon adjacent position 37 also increases frame-shifting in yeast by 2-fold (39).

The standard genetic code is comprised of 61 sense codons which encode 20 amino acids and 3 codons (UGA, UAG and UAA) that usually signal termination of protein synthesis. Since certain tRNAs decode up to three or four different codons, the theoretical minimum number of tRNAs for an organism to encode 20 amino acids is 32 (34). Söll *et al.* observed (35) that the “*minimum number of sRNA [tRNA] molecules required for recognition of all of the meaningful codons is relatively small, and this conclusion in turn raises the question of redundancy in the sRNA pool of a cell.*” This question, raised the year after the code was solved, is still unanswered today. As a result of the genome sequencing revolution, we know now that nature contains examples of organisms with tRNA gene complements that are well below and vastly greater than this apparent minimal requirement. There are examples of organelles (e.g., human mitochondria with 22 tRNA genes) and even parasitic microbes (e.g., *Mycoplasma mobile* with 28 tRNA

genes (40)) with fewer than 32 tRNA genes. Their survival depends on importing the missing tRNAs from a different cellular compartment (41) or presumably a host cell.

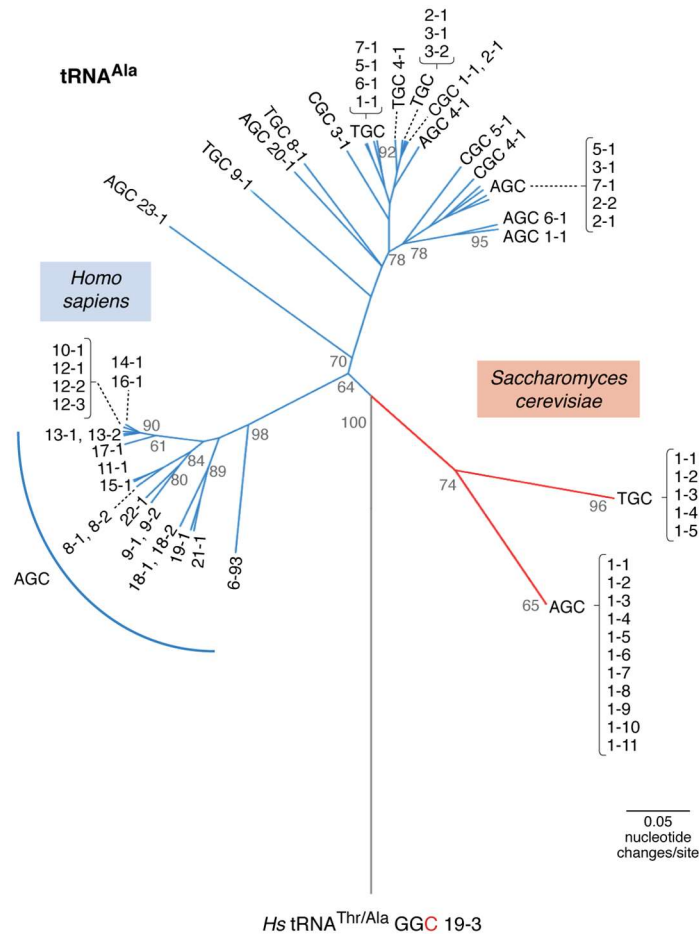


Figure 1.2 Phylogenetic relationships of human and yeast tRNA^{Ala}. The tree is based on an alignment of all known human and yeast tRNA^{Ala} iso-acceptors. The vastly expanded number and greater diversity of human tRNA^{Ala} genes compared to their yeast counterparts is evident. The tRNAs are labeled according to gene names in the genomic tRNA database (43), which include anticodon sequence followed by a numbering system where the first number indicates similar sequences, and the second a gene copy identifier. The human reference genome contains a misannotated tRNA^{Ala}, which was used to root the tree. This gene, tRNA^{Ala}-GGC-19-3, is a tRNA^{Thr} with a mutation (T36C) endowing the tRNA with an alanine anticodon. This is the only example of the alanine GGC anticodon in humans. Scale bar indicates the number of nucleotide changes per site in the tRNA sequences. The tree was calculated similarly as before (135). Briefly, a starting tree computed in MultiSeq 2.0 (136) was optimized to identify the maximum likelihood tree using PhyML 3.1 (137). Statistical branch support (out of 100) was calculated based on an approximate likelihood ratio test method (138) as implemented in PhyML.

Escherichia coli encodes 88 tRNA genes, while yeast has a small tRNAome for a eukaryote at 275 tRNA genes. Eukaryotes typically have hundreds of tRNA genes that display a general trend to increase in number and sequence diversity with the complexity of the organism (42). Unicellular protozoans encode near the theoretical minimum of tRNA genes, such as the malaria parasite *Plasmodium falciparum*, which has only 35 tRNA genes (43). *P. falciparum* was recently found to import additional tRNAs from its host (44). Some species of fish have astoundingly high tRNA gene numbers (Table S1.2), such as the elephant shark (*Callorhynchus milii*), which encodes 13,724 tRNAs (43). As exemplified in a phylogenetic comparison of yeast and human alanine tRNAs (Fig. 1.2), the sequence variations among tRNA iso-acceptors appears to increase with complexity as well. Yeast has 16 tRNA^{Ala} iso-acceptors including 11 identical genes with the AGC anticodon and 5 identical genes with the TGC anticodon. In contrast, humans encode 45 tRNA^{Ala} iso-acceptors with markedly greater sequence diversity than their yeast counterparts including examples with CGC anticodons not seen in yeast (Fig 1.2).

1.2.2 tRNA regulation in human cells.

The number of expressed tRNA genes in human cells is not well defined. Of the 610 tRNA genes in humans, the genomic tRNA database predicts 417 genes in their high confidence set, indicating the tRNA is likely to function in protein synthesis (43). Comprehensive profiling of RNAs in human serum suggests 411 expressed tRNA genes (45). According to CHIP-seq analysis of RNA Polymerase III and transcription factor occupancy, ~350 tRNA genes are actively transcribed in a single human cell line (IMR90hTert) (46). Gogakos *et al.* (98) reported the expression of 288-349 tRNAs in HEK 293 cells based on two different RNA sequencing methods (47). Together the data suggest 300-400 tRNA genes are expressed in any individual human cell.

The degree to which each human tRNA contributes to protein synthesis has not been determined, but evidence that cells regulate tRNA expression to control protein production is emerging. First, expression of individual tRNA genes varies between tissues (48,49). Further, the steady-state level of different tRNAs correlates with the expression of matched-codon biased mRNA transcripts (48). The observation suggests that cells can fine-tune tRNA expression profiles to match codon usage in expressed mRNAs. Indeed, the fact that efficient protein expression requires tRNA levels and decoding capacity match the distribution of codons in mRNA is well known. Multiple *E. coli* strains and bioinformatic tools for codon adaptation were developed based on this principle to enhance the production of eukaryotic and other recombinant proteins in bacteria (50).

Once transcribed, tRNAs are processed via the removal and addition of nucleotides to produce a mature tRNA. Introns, 5'-leader and 3'-trailer sequences in the original transcript are removed (51). Next, the CCA-adding enzyme elongates the pre-tRNA with the conserved CCA 3'-end. CCA-adding enzymes can append a second CCA to certain tRNAs with mismatches or excessive G:U pairs in their acceptor stems (52). The double CCA addition primes tRNAs for exonucleolytic digestion via the rapid tRNA decay pathway (53). The human CCA adding enzyme (TRNT1) is implicated in disease. Complete loss-of-function in TRNT1 is embryonic lethal, and partial loss-of-function mutations cause congenital sideroblastic anemia with immunodeficiency, fevers, and developmental delay (SIFD) (54).

tRNAs are further processed with a variety of post-transcriptional nucleotide modifications, including 2' O-methylation of the ribose, N-acetylation and N-methylation of the nucleotide bases as well as more complex modifications that form bases such as Wybutosine (reviewed in (55)).

In eukaryotes, tRNA^{His} is post-transcriptionally edited to add an extra guanine (G⁻¹) to the 5'-end of the tRNA, a unique feature recognized and required by the cognate histidyl-tRNA synthetase (56). Depleting the tRNA^{His} guanylyltransferase that catalyzes G⁻¹ addition leads to accumulation of un-aminoacylated and un-guanylated, yet hyper-methylated tRNA^{His} in the nucleus (57). Subsequent studies point to tRNA^{His} m⁵C hypermethylation as a response to growth arrest in *S. cerevisiae*, although the significance of the increase in m⁵C methylation is yet unclear (58). Monomethylation of the 5'-monophosphate of tRNA^{His} by Bicoid interacting 3 domain containing RNA methyltransferase (BCDIN3D) is thought to protect tRNA^{His} from degradation. BCDIN3D is overexpressed in breast cancer cells, and monomethylated tRNA^{His} is more abundant in breast cancer cells, yet the overall level of tRNA^{His} is not impacted (59). It is thought that monomethylation contributes to the formation of tRNA^{His}-derived fragments in breast cancer cells, which in turn regulates tumorigenic genes involved in breast cancers (60).

In fact, tRNAs are the most frequently modified non-coding RNA known, containing an average of 13 modifications per molecule (61). The combined number of expressed tRNA genes and their multiple modification states imply the existence of a large combinatorial number of tRNA microspecies in the human cell (62). Since tRNA modifications are important for translation fidelity and reading frame maintenance (34,36,37,63), these microspecies have the potential to impact cellular function and disease. Modifications are also essential for regulating tRNA turnover (64) and for proper structure, folding, and stability of the tRNA (55). Indeed, many tRNA modifying enzymes are already linked to disease (26). As described below, tRNA modification can also dynamically up- or down-regulate sets of tRNAs (65-67).

The mature and active tRNA is a substrate for amino acid ligation catalyzed by the AARS enzymes in an ATP-dependent reaction (68). Each AARS enzyme has specificity both for an amino acid and a distinct set of cognate tRNA iso-acceptors. Amino acids are ligated to the 3'-end of tRNAs, requiring the presence of a CCA 3'-tail. To ensure tRNA recognition fidelity, AARSs make essential contacts with nucleotides in their cognate tRNAs, called identity elements (69). Aminoacyl-tRNAs are then substrates for protein synthesis. The likelihood that a given aminoacyl-tRNA acts in translation depends upon many factors including the stability of the tRNA, the number of aminoacylated-tRNAs competing for the same codon, and the expression of mRNAs containing codons read by the tRNA. tRNAs unfit for translation are degraded by rapid tRNA decay pathway (70). Cytoplasmic tRNA levels are also regulated by export processes to other cellular compartments, including into mitochondria (71), or retrograde transport into the nucleus (72). As reviewed elsewhere (62), tRNAs perform additional functions outside of translation, either as whole tRNAs (73) or tRNA-derived fragments (74).

1.3 Phenotypes of mistranslating cells

Mistranslation occurs in all cells (75) as a result of multiple different mechanisms. Considering the small size, multitude of protein partners and essential cellular role of tRNAs, single nucleotide changes can have a profound impact on their function and on the efficiency and fidelity of protein synthesis (12,13,23,69). Proteins encoded by mRNAs containing rare codons or strongly biased codon compositions are most susceptible to the effects of tRNA variants. Loss-of-function mutations in tRNAs can cause ribosome stalling to de-regulate protein synthesis, while gain-of-function mutations in tRNAs can lead to mis-aminoacylation and mistranslation (12,21).

Mistranslating tRNAs can arise from surprisingly minor changes to the nucleotide sequence. Although many tRNAs harbor major identity determinants in their anticodon, coupling aminoacylation fidelity to codon assignment; alanyl-, leucyl-, and seryl-tRNA synthetases do not recognize the anticodon nucleotides on their cognate tRNAs. Anticodon mutations in these tRNAs often elicit amino acid mis-incorporation (69). The accumulation of highly active tRNA^{Ser} anticodon mutants is toxic to yeast cells, causing proteome wide mistranslation (23). In yeast, the degree of anticodon mutant toxicity varies, depending on competition with wild type tRNAs, chemical properties of the amino acids and tRNA modifications (76).

Santos *et al.* analyzed tRNA^{Ser} variants containing Ala or Leu anticodons in murine NIH 3T3 cells grown in culture and subsequently xenografted to live mice (22). As determined by mass spectrometry in tumor samples recovered from the mice, the rate of mistranslation increased by ~2-fold

in the cells expressing tRNA^{Ser} containing an alanine anticodon, but only marginally in cells expressing tRNA^{Ser} with a leucine anticodon. Mistranslation was not toxic to the NIH 3T3 cells when grown in culture as determined by cellular viability, necrosis, and proliferation assays, indicating that increased cytosolic tRNA-dependent mistranslation was initially well-tolerated. Interestingly, expressing the mistranslating tRNAs promoted the formation of foci *in vitro*, suggesting a link to tumorigenesis (22). Briefly, foci formation occurs when cancer-like cells form dense clusters resembling early-stage tumors on a petri dish (77). Mistranslating tRNAs promoted the activation of the oncogenic factors protein kinase B (Akt) and p38 when cells were treated with tumor necrosis factor alpha (TNF- α), to a greater extent than cells expressing the wildtype tRNAs. Furthermore, cells mistranslating alanine codons with serine promoted angiogenesis in a chick chorioallantoic membrane assay (CAM) and were highly tumorigenic when introduced in mice. In comparison to the parent cells in culture, expression of the mistranslating tRNAs increased ~8-fold in cells recovered from mouse tumors. Although mistranslating tRNAs variants had undetectable cytotoxicity in cells in culture, the mutant tRNAs exacerbated or accelerated cellular pathways to cancer in a mammalian model of disease (22).

Identity element mutations are another route to mistranslating tRNAs. The phenotypic consequences of a single tRNA variant of this type are the subject of a number of recent studies. AlaRS recognizes two critical identity determinants at the 3rd base pair in the acceptor stem (G3:U70) (78), and also aminoacylates tRNAs bearing GU pair at the 4th acceptor stem base pair (76). tRNA variants that convert non-alanine tRNAs to alanine accepting tRNAs by creating these identity elements are common in mammalian genomes (79). Some human tRNA^{Cys} and tRNA^{Thr} species with G4:U69 base pairs are natural alanine acceptors, and cysteine to alanine mistranslation was detected in HEK 293 cells (79). An Animalia specific tRNA deacylase was recently discovered that co-occurs with tRNA^{Thr} G4:U69 variants in animal genomes and de-acylates mis-charged Ala-tRNA^{Thr} (80). This enzyme may protect human cells from alanine mistranslation at threonine codons.

In our work on tRNA-dependent mistranslation, we expressed a mutant of human tRNA^{Pro} containing a G3:U70 base pair in human cells. The human tRNA^{Pro} mutant was an efficient alanine acceptor *in vitro* that no longer accepted proline. Our previous work in yeast demonstrated that a homologous tRNA^{Pro} mutant mistranslated multiple proline codons with alanine (13). We developed a green fluorescent protein reporter (D129P) that fluoresces in response to mistranslation at the Pro129 codon. In HEK 293 cells (12), we did not observe significant mistranslation in rich media compared to cells expressing wildtype tRNA^{Pro}. When the cells were starved of serum and glucose over a period of days, mistranslation accumulated to 2-5% according to the GFP reporter. Strikingly, and similar to the

report of Santos *et al.* (22), we did not observe a loss in cellular viability or induction of the heat shock response compared to cells expressing the wildtype tRNA, indicating that this level of mistranslation was well tolerated. In yeast, a mistranslating tRNA did show synthetic slow growth when coupled with deletion mutants lacking the proteome regulatory transcription factor Rpn4 (13). The above examples illustrate how phenotypes driven by a mistranslating tRNA variant can remain hidden; yet, in conditions of stress or in models of disease, an otherwise neutral tRNA variant can interact synthetically with a stressor or a second mutation to cause phenotypic defects.

Errors in protein synthesis are normally thought to be deleterious, yet mistranslation is an adaptive response in diverse organisms from bacteria (81) to yeast (13) to human cells (82). In some of these cases mistranslation provides a selective advantage. As reviewed elsewhere (83), a recurrent finding is that stress conditions reduce aminoacylation fidelity (84). For example, upon oxidative stress, methionyl-tRNA synthetase increases its mis-aminoacylation of non-cognate tRNAs up to 10-fold in bacteria and mammalian cells (82,85,86); the additional methionine in proteins is thought to protect the proteome from oxidative damage.

1.4 tRNA variation in humans

Human tRNA variants that likely mistranslate can be readily identified in publicly available sequence data (43) (Tables 1.1, 1.2, S1.1). Some of these natural variants (79) or similar variants designed in the laboratory (12,22) do in fact cause mistranslation in human cells. In addition, tRNA variants which simply impair tRNA folding or function also impact the proteome. The absence of even a single tRNA gene product can alter the tRNA pool and limit the rate of protein synthesis by causing ribosome stalling (21). In both capacities, mutations in tRNA encoding genes represent an important class of potential disease modifiers that could increase the severity of other disease-causing alleles.

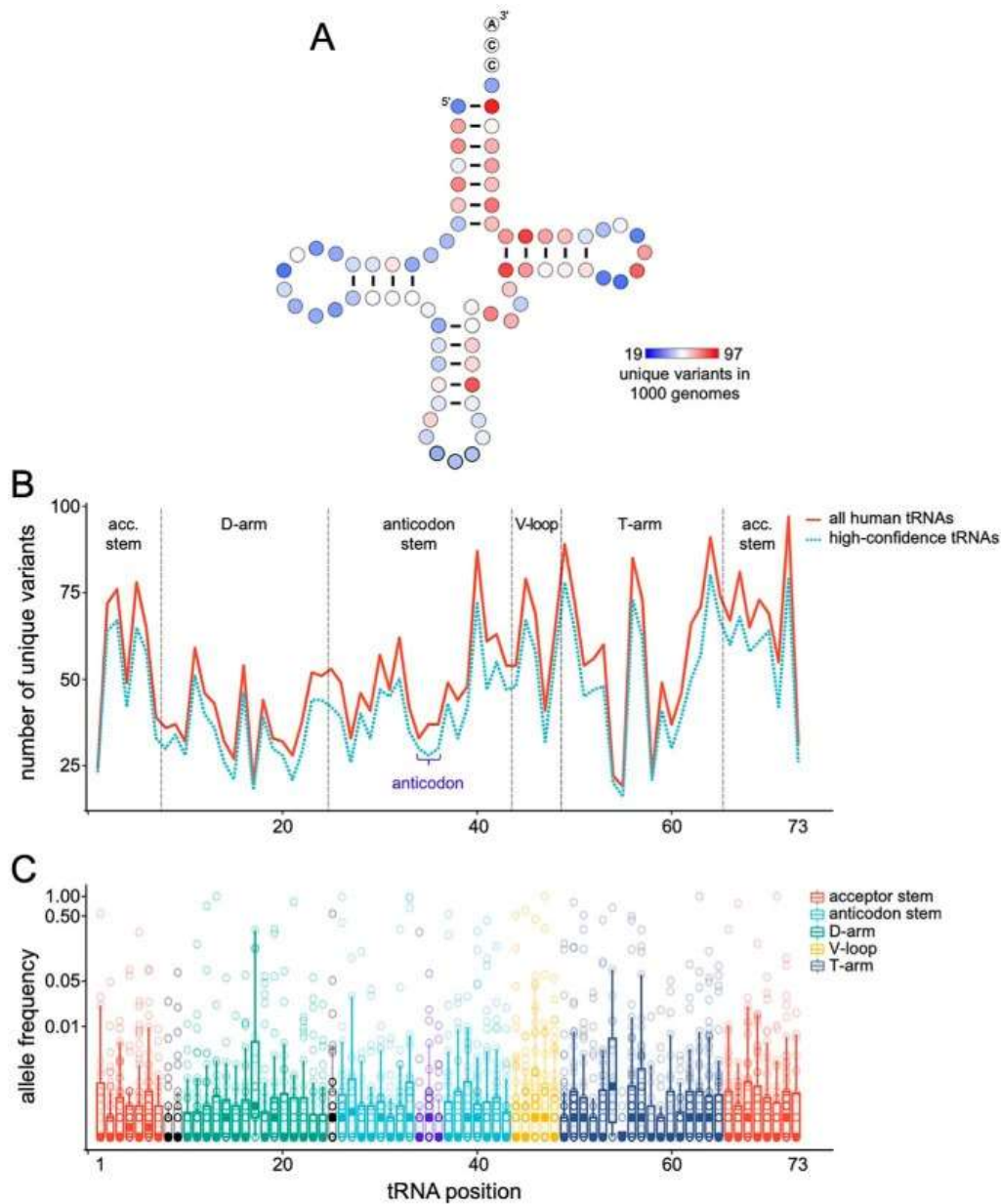


Figure 1.3 Transfer RNA variants observed in the 1000 Genomes Project. (A) Variants that occur within tRNA genes (defined by GtRNAdb(128)) were downloaded from the 1000 Genomes Project phase 3 dataset (<ftp://ftp.1000genomes.ebi.ac.uk/vol1/ftp/release/20130502/>). Insertions and deletions were removed, as were variants with no allele frequency available. Each variant was mapped to its corresponding tRNA position, according to standardized numbering (139), using an in-house Perl script. High confidence tRNAs were defined as tRNAs with a tRNAscan-SE score > 50 (128). For the high confidence tRNA set, unique mutations are mapped to each position in the tRNA. (B) The same data in (A) is plotted for the high-confidence set (cyan dashed line) and for all human tRNA sequences (red line). (C) The allele frequencies (\log_2 scale) of all variants that occur at each tRNA position are

represented in box and whisker plots. Boxes outline quartiles of the allele frequency distribution, filled circles depict the median allele frequency, whiskers show $1.5 \times$ quartile range, and hollow circles depict raw data, i.e., the allele frequencies for each unique tRNA variant at the indicated position.

To visualize the nature and extent of human tRNA variation, we analyzed data from the 1000 Genomes Project and plotted the number of unique variants at each position in an alignment of all human tRNA genes (Fig. 1.3A,B). The number of unique variants were mapped on the tRNA secondary structure (Fig. 1.3A). We also plotted the frequency of occurrence of each of these tRNA mutations in the human population (Fig. 1.3C). Some tRNAs, such as those for leucine, serine, and selenocysteine have significantly larger variable loops; variation from these regions was not included. No position in human tRNA genes is immune to variation, yet some positions are far more variable than others (Fig. 1.3A, B). The allele frequency of these variants indicates that common ($> 5\%$ allele frequency) and rare variants ($< 5\%$ allele frequency) are distributed across nearly all sites in the tRNA (Fig. 1.3C). Some sites, however, lack common variants. Although restricted to rare variants, variation is observed at position 73; this ‘discriminator’ base is a key identity element for many AARSs. The anticodon shows variation at all 3 bases, albeit reduced compared to other regions of the tRNA. The data from 1000 Genomes Project suggests that across all ~ 600 tRNA loci, there are 25-30 unique nucleotide variants at each anticodon base and these include both common and rare variants in the population (Fig. 1.3C).

Positions within the acceptor stem contain large numbers of unique variants. Many AARSs recognize acceptor stem nucleotides to ensure aminoacylation fidelity (69), thus, acceptor stem variants have the potential to elicit mistranslation or lead to a defective tRNA. Another compelling observation is that several important sites of tRNA modification display significant variation (e.g., position 37 in the anticodon loop) (Fig. 1.3). Consistent with this observation, mutations in tRNA-modifying enzymes that act at these positions are implicated in disease (26).

As mentioned above, most human AARSs recognize identity determinants in the tRNA anticodon except for AlaRS, LeuRS, and SerRS (69), thus, non-synonymous anticodon variants in Ala, Leu, and Ser tRNAs are likely to mistranslate. Correspondingly, the tRNA variants that have already been shown to elicit mistranslation in human cells have mutations in the tRNA anticodon or create the identity determinants for AlaRS (12,78,79). Anticodon mutations in other tRNAs typically reduce or ablate amino-acylation (69). However, the degree of amino-acylation loss is not known for all anticodon positions in all tRNAs, and in some cases efficient amino-acylation can be retained even when some identity determinants are mutated (87).

Certainly, mistranslating tRNAs can arise from a variety of mechanisms. In terms of mutations in the tRNA, substitutions at aminoacylation identity elements or anti-determinants that normally exclude non-cognate aminoacylation in nearly any tRNA have the potential to lead to mis-aminoacylated tRNAs and mistranslation. Although such mutants likely occur in the human population, there is a paucity of biochemical data regarding human tRNA identity elements and anti-determinants, thus challenging confident identification of such variants as mistranslating tRNAs from sequence alone. Anti-codon mutations in Ser, Ala, and Leu, however, will undoubtedly lead to amino acid mis-incorporation. For this reason, our discussion of specific mistranslating tRNA examples from human genomes focused on these ‘obvious’ mistranslating tRNAs.

To assess the prevalence of likely tRNA mistranslators in the human population, we searched the Genomic tRNA database (GtRNAdb) for high-confidence Ala, Leu, and Ser tRNAs with anticodon mutations (Table 1.1) or mutations in the 3rd or 4th acceptor stem base pair that create the G3:U70 (Table 1.2) or G4:U69 (Table S1.1) AlaRS identity element. In total, among the human Ala, Leu, and Ser iso-acceptor groups reported in GtRNAdb there are 27 unique anti-codon variants. Of these, there are 14 unique non-synonymous (Table 1.1) and 13 synonymous anticodon variants. Most non-synonymous anticodon variants are rare, but three variants occur in >1% of the population. One alanine tRNA variant containing a glycine anticodon occurs in over 6% of sequenced individuals. The common occurrence of these mutations in cytosolic tRNAs is striking; analogous variants in mitochondrial tRNAs are embryonic lethal (27). Although we found a similar number of unique synonymous anti-codon variants, none were found in > 1% of sequenced individuals. While still encoding the ‘correct’ amino acid, such mutants may more or less efficiently read synonymous codons for a particular amino acid, altering translation rates.

Further complicating this scenario, certain apparently synonymous anticodon variants may become mis-translators through nucleotide modification. For example, tRNAs normally containing an A34 are modified to inosine (I34) by the action of adenine deaminases acting on tRNAs (ADATs) (88). As noted above, I34 enables expanded wobble decoding to codons ending in U, C or A, thus, A34 containing tRNAs are normally restricted to those amino acids with synonymous codons ending in U, C, and A. However, human genomes include examples of tRNAs bearing A34 that, if modified to I34, would lead to mis-translation (e.g., tRNA-Ser-GCT-5-1 single nucleotide polymorphism (SNP) rs550301646; tRNA-Asn-ATT-1-1 and tRNA-Tyr-ATA-1-1 are in the human reference genome). In the case of tRNA^{Asn}, A34I would incorporate Asn at Lys AAA codons. This type of phenomenon was recently examined with anticodon variants of *Methanocaldococcus jannaschii* tRNA^{Tyr} expressed in *E. coli* (89,90). In this case, a tRNA^{Tyr} mutant with an AUG anticodon decoded both histidine CAU and

CAC codons with tyrosine at approximately equal efficiency (2-3%); the mutant tRNA^{Tyr} AUG anticodon was indeed partially modified to IUG (89). Perhaps as a natural defense against mistranslation and resulting of abundant Gln-tRNA^{Gln}_{UUG}, mis-incorporation of tyrosine at glutamine CAA codons was not detected in *E. coli* (89).

Adding to the complexity of human tRNA variation, tRNA genes are particularly susceptible to transcription-associated mutagenesis (TAM) (91), and thus, their sequence can change more rapidly than other genes. Thornlow *et al.* demonstrated that tRNA genes experience 7- to 10- fold higher rates of TAM compared to the genome-wide average (91). TAM occurs when DNA strands are separated during transcription and the non-template strand becomes temporarily isolated, and more accessible to mutagens (92). While tRNA variation is generally selected against on a population scale, this implies that the sequence of tRNA genes within individual cells could change throughout life and that perturbations that increase a tRNAs expression could further increase mutation rates.

Table 1.1 Human tRNA anticodon variants

tRNA gene	variant	MAF (%) ^a	variant count ^a	MAF (%) ^b	variant count ^b	tRNA score ^c	codon identity	tRNA identity	expression ARM ^d	CHIP ^e
Ala-AGC-2-2	G35A	0.02	1	-	-	84.7	Val	Ala	+	+
Ala-AGC-6-1	G35C	6.55	328	6.47	8130	74.1	Gly	Ala	+	+
Ala-AGC-15-1	C36T	0.04	2	0.03	42	56.7	Thr	Ala	+	-
Ala-AGC-16-1	G35A	2.2	11	2.1	269	53.1	Val	Ala	+	-
Ala-CGC-1-1	G35T	-	-	0.0008	1	79.7	Glu	Ala	+	+
Ala-TGC-1-1	G35A	-	-	-	-	80.5	Val	Ala	+	+
Leu-CAA-3-1	A35C	-	-	0.0008	1	77.3	Trp	Leu	+	+
Ser-AGA-2-2	G35A	0.02	1	0.003	4	89.6	Phe	Ser	+	+
Ser-AGA-2-3	G35A	1.82	91	1.87	2347	89.6	Phe	Ser	+	+
Ser-AGA-2-4	G35C	-	-	0.003	4	89.6	Cys	Ser	+	+
Ser-AGA-2-5	_35T	-	-	0.0008	1	89.6	-	-	+	+
Ser-CGA-2-1	_36T	-	-	0.03	34	94	-	-	+	-
Ser-TGA-2-1	G35A	0.04	2	0.02	22	90.4	Leu	Ser	+	+
Ser-TGA-3-1	_36T	-	-	0.0008	1	89.7	-	-	+	+

MAF; minor allele frequency. _##N; inserted nucleotide. ^aData from 1000 Genomes Project (127,128);

^bData from TOPMED sequencing project (128,129); ^ctRNA score was calculated using tRNA-Scan SE

(128); ^dARM = ARM-seq data suggesting expression (128,130); ^eCHIP = CHIP-seq hits for at least 3 of 4 core transcription proteins (RPC155, POLR3G, BRF1, BDP1) (46,129,131-133).

Table 1.2. Human tRNA variants that introduce a G3:U70 base pair

tRNA gene	variant	MAF	variant	MAF	variant	tRNA score ^c	expression	
		(%) ^a	count ^a	(%) ^b	count ^b		ARM ^d	CHIP ^e
Arg-ACG-1-3	C70U	-	-	0.002	2	68	+	+
Cys-GCA-2-3	C70U	-	-	0.02	29	82	+	+
Cys-GCA-1-1	C70U	0.02	1	0.07	86	84	+	-
Cys-GCA-17-1	C70U	-	-	0.002	2	71	+	+
Cys-GCA-12-1	C70U	0.02	1	0.01	16	72	+	+
Gly-CCC-2-1	G70U	-	-	0.05	64	75	+	+
Gly-GCC-2-4	A3G	0.08	4	0.05	63	81	+	-
Gly-GCC-2-5	A3G	0.02	1	0.005	6	81	+	-
Gly-GCC-2-1	A3G	0.02	1	0.02	20	81	+	+
Gly-GCC-2-3	A3G	-	-	-	-	81	+	+
Gly-GCC-1-5	A3G	1.2	61	1.3	1633	81	+	+
Gly-GCC-5-1	A3G	0.02	1	0.1	129	55	-	-
Gly-TCC-2-6	C70U	0.03	14	0.09	111	74	+	+
Ser-AGA-2-6	A3G	-	-	0.01	12	90	+	+

MAF; minor allele frequency. ^aData from 1000 Genomes Project (127,128); ^bData from TOPMED sequencing project (128,129); ^ctRNA score was calculated using tRNA-Scan SE (128); ^dARM = ARM-seq data suggesting expression (128,130); ^eCHIP = CHIP-seq hits for at least 3 of 4 core transcription proteins (RPC155, POLR3G, BRF1, BDP1) (46,129,131-133).

1.5 tRNA variation and disease

Like the involvement of mitochondrial tRNA variants in disease (28), recent studies have identified specific cytosolic tRNA mutants as drivers or modifiers of disease in humans and mice. In addition, tRNA mis-modification and imbalanced tRNA expression also contribute to disease. Here we highlight examples of defective tRNA function in genetic disorders, cancers, and neurodegeneration.

1.5.1 tRNA mutants linked to disease

Kobayashi *et al.* identified the first human tRNA associated with disease in 1990 (90). The mutation, a variant of a mitochondrial tRNA^{Leu} gene, leads to the degradation of the tRNA and causes a rare disorder characterized by stroke and dementia: mitochondrial myopathy, encephalopathy, lactic acidosis and stroke-like episodes (MELAS). Shortly after, a mutation in mitochondrial tRNA^{Lys} was found to cause

another rare neurological disorder: myoclonic epilepsy and ragged-red fiber disease (MERRF) (93). Several other mitochondrial tRNA variants are implicated in major human diseases, including heart disease (94), hypertension (95), metabolic disease (96), and deafness (97).

Two clear examples have emerged where a cytosolic tRNA variant either contributes to or directly causes disease. One case (described in the section *tRNA variants in neurodegeneration*) involves a mutation in a single tRNA^{Arg} gene which causes widespread neurodegeneration in mice when associated with a second mutation in a protein coding gene that sensitizes cells to ribosome stalling (21). The other case (detailed in the section *tRNA modification defects in disease*) is a single nucleotide mutation in the only functional human tRNA^{Sec} gene (98,99) that causes abdominal pain, fatigue, muscle weakness and low plasma selenium levels in a homozygous patient (19). In this case, the tRNA^{Sec} variant appears to be the primary driver of disease (19).

1.5.2 Imbalanced tRNA expression and disease

tRNA copy number variation. The copy number of tRNA genes varies between individuals. Iben and Marais assessed copy number variation among nuclear encoded tRNAs from whole genome sequencing data obtained in the 1000 Genomes Project (100). Their study focused on two sets of two parents and a child, from which > 15-fold read coverage was obtained. While the high similarity of tRNA iso-acceptors complicates this type of analysis, significant copy number variation in at least 11 tRNA gene loci among the six individuals was reported. Further, they validated a homozygous deletion encoding tRNA^{Lys}_{CUU} on chromosome 7 in one individual. Interestingly, modification defects in this tRNA associate with type 2 diabetes in mice. The deletion is common in the human population, and has no known indication of an associated phenotypic defect (101).

Tissue specific tRNA expression. Dittmar *et al.* demonstrated the tissue-dependency of tRNA expression using a tRNA microarray which probed 42 nuclear encoded and 21 mitochondrial encoded tRNAs from 8 different tissues (48). They revealed that human tissues express different sets of cytosolic tRNAs. Comprehensive analysis based on RNA polymerase III occupancy of tRNA genes in mice support this finding (102).

The relevance of tissue-specific tRNA expression to disease was demonstrated by the link between tRNA abundance and cystic fibrosis (103). In this work, Kirchner *et al.* characterized a synonymous single nucleotide polymorphism in the cystic fibrosis transmembrane conductance regulator (CFTR), which substitutes an ACT Thr codon with ACG. This synonymous mutation results in a cell

type-dependent alteration of CFTR protein levels that are not explained by a change in mRNA stability or splicing. The authors discovered that tRNA^{Thr}_{CGU} is a low abundance tRNA in the cystic fibrosis model and human bronchial epithelial cell lines. The polymorphism not only reduces CFTR expression in human bronchial epithelial cells, but also impairs the folding, localization, and membrane conductance of CFTR. The findings point to a translation rate-dependent mechanism, where ribosome stalling on the ACG codon, which is read by a low abundance tRNA, causes the protein product to mis-fold and malfunction.

Phenotypic defects from synonymous codon mutations are observed in numerous other disease-relevant protein coding genes (reviewed in (104)). Examples include multidrug resistance 1 (MDR1) (105), Estrogen receptor α (ER α) (106,107), and surfactant protein-D (SFTPD) (108). Thus, expression of specific tRNA iso-decoders is an important consideration when synonymous mutations result in a phenotype, particularly if the protein synthesis burden is shifted to a low abundance or possibly defective tRNA. Conceivably tRNA synonymous anticodon variants (noted above) could have a similar effect on translation rates and cellular phenotypes.

De-regulated tRNA expression. tRNA expression can change dynamically in disease. Pavon-Eternod *et al.* (107) demonstrated that tRNA expression increases from 3- to 10-fold in breast cancer tumors (109). Oncogenic transcription factors such as Ras and c-Myc promote RNA polymerase (Pol) III transcription, whereas tumor suppressors such as Rb and p53 inhibit Pol III transcription, providing a link between common cancer mechanisms and Pol III-dependent tRNA expression (reviewed in (110)). Although cause or effect has not been established in these cases, tRNA expression changes in cancer may occur through global tRNA upregulation to facilitate increased protein synthesis requirements in tumor cells (111).

Dysregulation of specific tRNA iso-acceptors is also implicated in cancer. Overexpression of the initiator tRNA^{Met} promotes translation reprogramming and cell proliferation in the human breast epithelial cell lines 184A1 and MCF10A (109). This was corroborated in a comprehensive study that quantified tRNA expression profiles using tRNA microarrays and histone modification mapping across 470 patient-derived tissue samples representing various states of proliferation (112). Gingold *et al.* demonstrated that tRNA_i^{Met} expression is highest in the most proliferating samples and lowest in the differentiating cells.

In contrast, reduced tRNA^{Sec} expression was observed in many proliferating and especially cancerous cell samples (112). tRNA^{Sec} is required for the production of selenocysteine-containing

proteins. Depending on the context, selenoprotein synthesis can either prevent or promote cancer (113), thus, up or down-regulation of tRNA^{Sec} may have relevance to disease. tRNA expression changes can also promote cancer through roles for tRNAs beyond protein synthesis. A recent review highlighted examples of tRNAs or tRNA-derived fragments from at least 16 iso-acceptor groups that are specifically de-regulated in cancer (110).

The tRNA expression profile in a particular cell will lead to more or less efficient translation of certain mRNAs depending on codon usage (114,115). Differential expression of tRNAs also promotes cancer through favoring particular “translation programs.” The study of Gingold *et al.* (112) profiled codon usage in transcripts associated with cell cycle versus differentiation. The authors observed a dichotomy where codons with A or U in the 3rd codon position are generally more common in proliferation-associated mRNAs, and G- or C-ending codons more common in differentiation-associated mRNA transcripts (112). The emerging view is that cells dynamically switch between ‘programs’ of protein synthesis, in part by coordinating the transcription of tRNAs with anticodons matching the codon bias in expressed mRNAs.

Differential expression of specific tRNA iso-decoders. The expression of specific tRNA iso-decoders promotes metastasis in breast cancer model cell lines (112). The authors measured the relative abundance of different tRNA iso-decoders in cell lines selected for high rates of metastasis (MDA-LM2, CN-LM1) and parental cell lines (MDA-231, CN34). Two tRNAs (tRNA^{Arg}_{CCG} and tRNA^{Glu}_{UUC}) were highly upregulated in both metastatic lines. These tRNAs were overexpressed in MDA-231 cells to assess changes in the proteome resulting from their increased expression. The abundance of proteins encoded by transcripts enriched in the matching codons (GGC and GAR) increased. As measured by ribosome profiling, two such mRNAs (encoding EXOSC2 and GRIPAP1) showed higher rates of active translation in the cells over-expressing tRNA^{Glu}_{UUC}. RNAi mediated knockdown of these mRNAs reduced *in vitro* invasion capacity of the cells, suggesting that EXOSC2 and GRIPAP1 are required for tRNA^{Glu}_{UUC}-promoted metastasis. Hence, the coordinated expression of tRNA iso-decoders facilitates translational reprogramming in cancer cells and is implicated in the promotion of proliferation as well as metastasis.

1.5.3 tRNA modification defects in disease

As mentioned previously, post-transcriptional modifications are important for tRNA function and stability. Hypo-modification can lead to rapid tRNA decay (116), and many tRNAs require anticodon modifications to ensure faithful codon recognition (34,63). Over 50 different nucleotide modifications

occur in eukaryotic tRNAs (117), and in humans, tRNAs contain an average of 13 modifications per molecule (61). Accordingly, tRNA modification defects are implicated in numerous diseases, including neurological, cardiac, respiratory, and metabolic diseases, as well as cancer and mitochondrial-linked disorders (26). Most diseases that result from defects in tRNA modification are due to mutations in protein coding genes or in mitochondrial tRNA genes, rather than cytosolic tRNA genes.

A recent example, however, provides compelling evidence of a cytosolic tRNA mutant and deregulated nucleotide modification in human disease. A C65G mutation in tRNA^{Sec}_{UCA} was identified in a patient exhibiting abdominal pain, fatigue, muscle weakness and low plasma selenium levels (28). Although humans encode 2 tRNA^{Sec} genes, apparently only one is functional. A mutation in this gene has the potential to impact all 25 human selenoproteins, that are essential for normal development (118). Selenoproteins may be categorized into two groups: housekeeping and stress-related. Synthesis of housekeeping selenoproteins depends on a 5-methoxycarbonylmethyluridine (mcm⁵U) modification at position 34 of tRNA^{Sec}, whereas further modification to 5-methoxycarbonylmethyl-2'-O-methyluridine (mcm⁵Um) promotes synthesis of stress-related selenoproteins (119). The tRNA^{Sec} C65G variant only impaired expression of stress-related selenoproteins. This is attributed to the fact that the variant has markedly reduced levels of both the mcm⁵Um modification at position 34 and the N⁶-isopentenyl adenosine (i⁶A) modification at position 37 (19). The finding underscores the complexity of nucleotide modification in tRNA function by showing that a mutation at one site in tRNA can impact modification at other locations in the tRNA body. In this case, a single nucleotide variant in the T-arm altered modifications in the anticodon stem loop (Fig. 1.1). Although the mechanism is not yet defined, presumably the C65G mutant inhibits or reduces the methyl-transferase activity of the multi-function ALKBH8 gene product that catalyzes conversion of mcm⁵U to mcm⁵Um at position 34 (120).

Modifications can also drive or favor specific translation programs (65,66). For example, melanomas harboring the V600E mutation in the proto-oncogene B-Raf depend on translational reprogramming controlled by upregulation of U₃₄ tRNA-modifying enzymes (67). Similar to the modulation of tRNA expression in metastatic breast cancer (121), the mechanism relies on coordinated regulation of both tRNAs and associated codon-biased transcripts. These modification tunable transcripts (MoTTs) are sensitive to particular tRNA modification states (65). U₃₄ tRNA modification promotes decoding of the '-AA' ending codons AAA, GAA, and CAA (122). Remarkably, upregulation of U₃₄ modifying enzymes promote survival of melanomas dependent on hypoxia-inducible factor (HIF) 1 α metabolism. Elevated levels of HIF-1 correlate with tumor metastasis and poor patient prognosis as well as tumor resistance to therapy (123). Indeed, the HIF1A mRNA is enriched in AAA, GAA, and CAA

codons (67). When U₃₄ modifying enzymes ELP3, CTU1, or CTU2 were knocked down, HIF1 α protein levels decreased even though HIF1A mRNA levels were unchanged. Cancer cells, thus, are able to regulate tRNA modification enzymes to ultimately tune protein synthesis rates and protein levels in favor of oncogenesis.

1.5.4 tRNA variants in neurodegeneration

A common attribute of disorders linked to defective protein homeostasis is the accumulation of mistranslated or misfolded proteins in cells (20,124). In many cell types, this problem can be counteracted through apoptosis or cell division (124). However, post-mitotic cells such as those found in the heart and brain are incapable of diluting misfolded proteins through division, and lack the regenerative capacity to replace apoptotic cells readily (124). Further, protein quality control decreases in post-mitotic tissues with age (125). Post-mitotic tissues may be particularly vulnerable to the consequences of tRNA variants and increasingly so with age.

Girstmair *et al.* (122) proposed a role for cytosolic tRNAs in Huntington disease (HD). HD is caused by an expanded Gln repeat in the huntingtin protein (htt), encoded by a stretch of 40 to 100 repeated CAG codons (126). In some cases, shorter CAG repeats appear to also cause HD, suggesting there are additional disease modifiers. Continuous translation of the repeat depletes charged tRNA^{Gln}_{CUG}, which results in more frequent frameshifting in the translation of the HTT gene, possibly exacerbating the disease phenotype (122). Although tRNA^{Gln}_{CUG} variants are not yet known to exacerbate HD, these findings illustrate the importance of tRNA function and abundance in pathologies of the brain.

Indeed, naturally occurring tRNA variants have the potential to deplete the abundance of a brain-specific tRNA that is essential for health. Ishimura *et al.* (21) uncovered a synthetic toxic effect involving a single cytosolic tRNA variant that causes wide-spread neurodegeneration in mice (21). A pair of mutations in *GTPBP2* (encoding a protein that rescues stalled ribosomes) and *Tr20* (encoding tRNA^{Arg}_{UCU}) were found to co-occur in mice identified in a phenotypic screen for neurodegeneration. Mice carrying both mutations exhibit rapid neurodegeneration and die at 8-9 weeks. At 3 weeks, the mutant mice are indistinguishable from wildtype. The C50T mutation (*n-Tr20*) prevents tRNA^{Arg}_{UCU} maturation and, in combination with the loss of GTPBP2, leads to ribosome stalling. Despite many ‘redundant’ tRNA^{Arg} iso-decoders in the cell, the lack of function of this single tRNA causes ribosome stalling. The authors measured a 3-fold increase in AGA pauses in the *n-Tr20* mutant compared to a mouse containing the wild-type tRNA. Fascinatingly, tRNA^{Arg} C50T variants also occur in the human population, including in a TCT iso-acceptor (Table 1.3).

Table 1.3. Human tRNA^{Arg} C50T variants

tRNA gene	SNP id	MAF	variant	MAF	variant	tRNA score ^c	expression	
		(%) ^a	count ^a	(%) ^b	count ^b		ARM ^d	CHIP ^e
Arg-ACG-1-1	rs6939540	2.42	121	2.2	2765	67.6	+	+
Arg-ACG-1-2	rs186104107	0.02	1	0.01	14	67.6	+	+
Arg-TCG-6-1	rs113170043	16.6	831	20.2	24374	53.7	+	-
Arg-TCT-5-1	rs143334272	0.8	41	0.6	711	61.4	+	-

^aData from 1000 genomes project; ^bData from TOPMED sequencing project (128,129); ^ctRNA score was calculated using tRNA-Scan SE (128); ^dARM = ARM-seq data suggesting expression (128,130); ^eCHIP = CHIP-seq hits for at least 3 of 4 core transcription proteins (RPC155, POLR3G, BRF1, BDP1) (46,129,131-133).

This work exemplifies the ways in which tRNA variants can exacerbate pathways to disease. Two observations from this work may have broader applicability to understanding the roles for tRNA variants in disease. Firstly, the phenotype was tissue specific, since expression of the *n-Tr20* encoded tRNA is only observed in the central nervous system. Further, a co-incident mutation in another gene sensitized cells to the loss-of-function mutation in a single tRNA gene. Together these mutations caused disease in the animal model.

1.6 Conclusion

Humans display a remarkable array of both common and rare tRNA mutants, some with the obvious potential to mistranslate the genetic code (Tables 1.1, 1.2, S1.1) or create defective tRNAs (e.g., Table 1.3). Indeed, such tRNA variants can elicit significant levels of mistranslation in the human cell, and influence protein synthesis and protein homeostasis (Fig. 1.4). Above, we highlighted recent examples showing how tRNA variants and defective tRNA genes contribute to disease. In addition to causing disease, tRNAs variants also act synergistically with other disease-causing alleles by placing additional stress on protein quality control mechanisms or biasing translation programs that drive disease. Further, tissue-specific tRNA expression and de-regulated tRNA expression or modification contributes to disease and phenotypic defects at the cellular level. Together these observations suggest that cytosolic tRNA mutations may have greater importance in disease than previously recognized. We hope that the evidence provided in this review will stimulate new interest in considering cytoplasmic tRNA variants as an important factor in human genetic variation and disease.

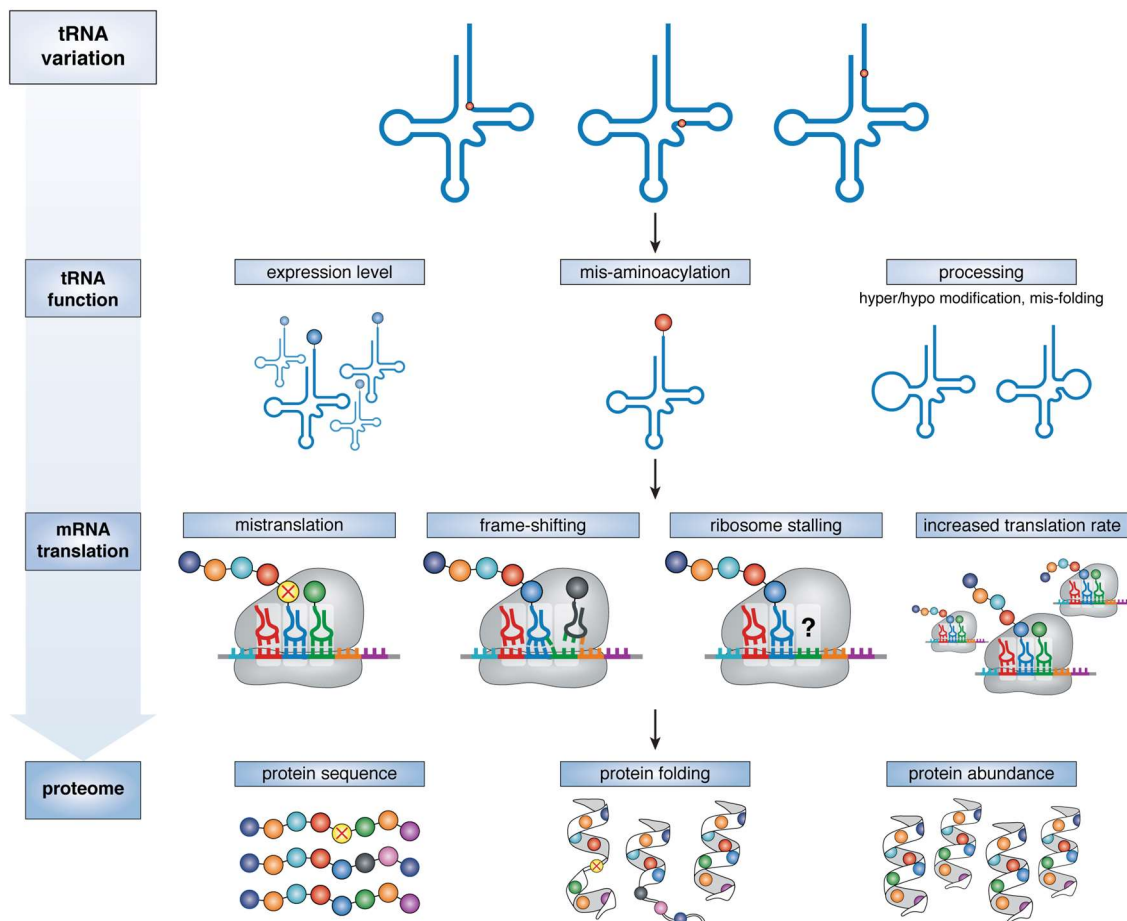


Figure 1.4 Phenotypic consequences of tRNA variation. Transfer RNA variation can impact expression, aminoacylation, or processing and maturation of tRNAs, including nucleotide modification and tRNA folding. Alterations in the functional tRNA pool can impact mRNA translation by causing mistranslation, frame-shifting, ribosome stalling, or increased expression of codon-biased transcripts. These alterations can in turn alter the amino acid sequence, folding, and abundance of proteins across the entire proteome.

1.7 References

1. Crick, F. H. C. (1955) On degenerate templates and the adaptor hypothesis. *A note for the RNA Tie Club*, 1-17
2. Hoagland, M. B., Stephenson, M. L., Scott, J. F., Hecht, L. I., and Zamecnik, P. C. (1958) A soluble ribonucleic acid intermediate in protein synthesis. *J Biol Chem* **231**, 241-257
3. Holley, R. W., Everett, G. A., Madison, J. T., and Zamir, A. (1965) Nucleotide Sequences in the Yeast Alanine Transfer Ribonucleic Acid. *J Biol Chem* **240**, 2122-2128
4. Gardner, R. S., Wahba, A. J., Basilio, C., Miller, R. S., Lengyel, P., and Speyer, J. F. (1962) Synthetic polynucleotides and the amino acid code. VII. *Proc Natl Acad Sci USA* **48**, 2087-2094
5. Nishimura, S., Jones, D. S., and Khorana, H. G. (1965) Studies on polynucleotides. 48. The in vitro synthesis of a co-polypeptide containing two amino acids in alternating sequence dependent upon a DNA-like polymer containing two nucleotides in alternating sequence. *J Mol Biol* **13**, 302-324
6. Nirenberg, M., Leder, P., Bernfield, M., Brimacombe, R., Trupin, J., Rottman, F., and O'Neal, C. (1965) RNA codewords and protein synthesis, VII. On the general nature of the RNA code. *Proc Natl Acad Sci USA* **53**, 1161-1168
7. Söll, D., Ohtsuka, E., Jones, D. S., Lohrmann, R., Hayatsu, H., Nishimura, S., and Khorana, H. G. (1965) Studies on polynucleotides, XLIX. Stimulation of the binding of aminoacyl-sRNA's to ribosomes by ribotrinucleotides and a survey of codon assignments for 20 amino acids. *Proc Natl Acad Sci USA* **54**, 1378-1385
8. Carbon, J., Berg, P., and Yanofsky, C. (1966) Missense suppression due to a genetically altered tRNA. *Cold Spring Harb Symp Quant Biol* **31**, 487-497
9. Riyasaty, S., and Atkins, J. F. (1968) External suppression of a frameshift mutant in salmonella. *J Mol Biol* **34**, 541-557
10. Ling, J., O'Donoghue, P., and Söll, D. (2015) Genetic code flexibility in microorganisms: novel mechanisms and impact on physiology. *Nat Rev Microbiol* **13**, 707-721
11. Bezerra, A. R., Simoes, J., Lee, W., Rung, J., Weil, T., Gut, I. G., Gut, M., Bayes, M., Rizzetto, L., Cavalieri, D., Giovannini, G., Bozza, S., Romani, L., Kapushesky, M., Moura, G. R., and Santos, M. A. (2013) Reversion of a fungal genetic code alteration links proteome instability with genomic and phenotypic diversification. *Proc Natl Acad Sci USA* **110**, 11079-11084
12. Lant, J. T., Berg, M. D., Sze, D. H. W., Hoffman, K. S., Akinpelu, I. C., Turk, M., Heinemann, I. U., Duennwald, M. L., Brandl, C. J., and O'Donoghue, P. (2018) Visualizing tRNA-dependent mistranslation in human cells. *RNA Biology* **15**, 567-575
13. Hoffman, K. S., Berg, M. D., Shilton, B. H., Brandl, C. J., and O'Donoghue, P. (2017) Genetic selection for mistranslation rescues a defective co-chaperone in yeast. *Nucleic Acids Res* **45**, 3407-3421
14. Barrell, B. G., Bankier, A. T., and Drouin, J. (1979) A different genetic code in human mitochondria. *Nature* **282**, 189-194
15. Campbell, J. H., O'Donoghue, P., Campbell, A. G., Schwientek, P., Sczyrba, A., Woyke, T., Söll, D., and Podar, M. (2013) UGA is an additional glycine codon in uncultured SR1 bacteria from the human microbiota. *Proc Natl Acad Sci USA* **110**, 5540-5545

16. Böck, A., and Stadtman, T. C. (1988) Selenocysteine, a highly specific component of certain enzymes, is incorporated by a UGA-directed co-translational mechanism. *Biofactors* **1**, 245-250
17. Berry, M. J., Martin, G. W., 3rd, Tujebajeva, R., Grundner-Culemann, E., Mansell, J. B., Morozova, N., and Harney, J. W. (2002) Selenocysteine insertion sequence element characterization and selenoprotein expression. *Methods Enzymol* **347**, 17-24
18. Bröcker, M. J., Ho, J. M., Church, G. M., Söll, D., and O'Donoghue, P. (2014) Recoding the genetic code with selenocysteine. *Angew Chem Int Ed Engl* **53**, 319-323
19. Schoenmakers, E., Carlson, B., Agostini, M., Moran, C., Rajanayagam, O., Bochukova, E., Tobe, R., Peat, R., Gevers, E., Muntoni, F., Guicheney, P., Schoenmakers, N., Farooqi, S., Lyons, G., Hatfield, D., and Chatterjee, K. (2016) Mutation in human selenocysteine transfer RNA selectively disrupts selenoprotein synthesis. *Journal of Clinical Investigation* **126**, 992-996
20. Kapur, M., and Ackerman, S. L. (2018) mRNA Translation Gone Awry: Translation Fidelity and Neurological Disease. *Trends in Genetics* **34**, 218-231
21. Ishimura, R., Nagy, G., Dotu, I., Zhou, H., Yang, X. L., Schimmel, P., Senju, S., Nishimura, Y., Chuang, J. H., and Ackerman, S. L. (2014) Ribosome stalling induced by mutation of a CNS-specific tRNA causes neurodegeneration. *Science* **345**, 455-459
22. Santos, M., Pereira, P. M., Varanda, A. S., Carvalho, J., Azevedo, M., Mateus, D. D., Mendes, N., Oliveira, P., Trindade, F., Pinto, M. T., Bordeira-Carriço, R., Carneiro, F., Vitorino, R., Oliveira, C., and Santos, M. A. S. (2018) Codon misreading tRNAs promote tumor growth in mice. *RNA Biology* **15**, 773-786
23. Berg, M. D., Hoffman, K. S., Genereaux, J., Mian, S., Trussler, R. S., Haniford, D. B., O'Donoghue, P., and Brandl, C. J. (2017) Evolving Mistranslating tRNAs Through a Phenotypically Ambivalent Intermediate in *Saccharomyces cerevisiae*. *Genetics* **206**, 1865-1879
24. Meyer-Schuman, R., and Antonellis, A. (2017) Emerging mechanisms of aminoacyl-tRNA synthetase mutations in recessive and dominant human disease. *Hum Mol Genet* **26**, R114-R127
25. Bednářová, A., Hanna, M., Durham, I., VanCleave, T., England, A., Chaudhuri, A., and Krishnan, N. (2017) Lost in Translation: Defects in Transfer RNA Modifications and Neurological Disorders. *Frontiers in Molecular Neuroscience* **10**, 135
26. Torres, A. G., Batlle, E., and Ribas de Pouplana, L. (2014) Role of tRNA modifications in human diseases. *Trends in Molecular Medicine* **20**, 306-314
27. Kirchner, S., and Ignatova, Z. (2015) Emerging roles of tRNA in adaptive translation, signalling dynamics and disease. *Nat Rev Genet* **16**, 98-112
28. Abbott, J. A., Francklyn, C. S., and Robey-Bond, S. M. (2014) Transfer RNA and human disease. *Frontiers in Genetics* **5**, 158
29. Yasukawa, T., Suzuki, T., Ishii, N., Ohta, S., and Watanabe, K. (2001) Wobble modification defect in tRNA disturbs codon-anticodon interaction in a mitochondrial disease. *EMBO J* **20**, 4794-4802
30. Agris, P. F., Vendeix, F. A. P., and Graham, W. D. (2007) tRNA's Wobble Decoding of the Genome: 40 Years of Modification. *Journal of Molecular Biology* **366**, 1-13
31. Joshi, K., Bhatt, M. J., and Farabaugh, P. J. (2018) Codon-specific effects of tRNA anticodon loop modifications on translational misreading errors in the yeast *Saccharomyces cerevisiae*. *Nucleic Acids Res* **46**, 10331-10339

32. Pavlov, M. Y., and Ehrenberg, M. (2018) Substrate-Induced Formation of Ribosomal Decoding Center for Accurate and Rapid Genetic Code Translation. *Annu Rev Biophys* **47**, 525-548
33. O'Donoghue, P., Prat, L., Heinemann, I. U., Ling, J., Odoi, K., Liu, W. R., and Söll, D. (2012) Near-cognate suppression of amber, opal and quadruplet codons competes with aminoacyl-tRNA^{Pyl} for genetic code expansion. *FEBS Lett* **586**, 3931-3937
34. Crick, F. H. C. (1966) Codon--anticodon pairing: the wobble hypothesis. *J Mol Biol* **19**, 548-555
35. Söll, D., Jones, D. S., Ohtsuka, E., Faulkner, R. D., Lohrmann, R., Hayatsu, H., and Khorana, H. G. (1966) Specificity of sRNA for recognition of codons as studied by the ribosomal binding technique. *J Mol Biol* **19**, 556-573
36. Agris, P. F., Narendran, A., Sarachan, K., Vare, V. Y. P., and Eruysal, E. (2017) The Importance of Being Modified: The Role of RNA Modifications in Translational Fidelity. *Enzymes* **41**, 1-50
37. Gustilo, E. M., Vendeix, F. A., and Agris, P. F. (2008) tRNA's modifications bring order to gene expression. *Curr Opin Microbiol* **11**, 134-140
38. Tukenmez, H., Xu, H., Esberg, A., and Bystrom, A. S. (2015) The role of wobble uridine modifications in +1 translational frameshifting in eukaryotes. *Nucleic Acids Res* **43**, 9489-9499
39. Lin, C. A., Ellis, S. R., and True, H. L. (2010) The Sua5 protein is essential for normal translational regulation in yeast. *Mol Cell Biol* **30**, 354-363
40. Jaffe, J. D., Stange-Thomann, N., Smith, C., DeCaprio, D., Fisher, S., Butler, J., Calvo, S., Elkins, T., FitzGerald, M. G., Hafez, N., Kodira, C. D., Major, J., Wang, S., Wilkinson, J., Nicol, R., Nusbaum, C., Birren, B., Berg, H. C., and Church, G. M. (2004) The complete genome and proteome of *Mycoplasma mobile*. *Genome Res* **14**, 1447-1461
41. Chatterjee, K., Nostramo, R. T., Wan, Y., and Hopper, A. K. (2018) tRNA dynamics between the nucleus, cytoplasm and mitochondrial surface: Location, location, location. *Biochim Biophys Acta Gene Regul Mech* **1861**, 373-386
42. Goodenbour, J. M., and Pan, T. (2006) Diversity of tRNA genes in eukaryotes. *Nucleic Acids Research* **34**, 6137-6146
43. Chan, P. P., and Lowe, T. M. (2009) GtRNADB: a database of transfer RNA genes detected in genomic sequence. *Nucleic Acids Research* **37**, D93-D97
44. Bour, T., Mahmoudi, N., Kapps, D., Thiberge, S., Bargieri, D., Menard, R., and Frugier, M. (2016) Apicomplexa-specific tRip facilitates import of exogenous tRNAs into malaria parasites. *Proc Natl Acad Sci USA* **113**, 4717-4722
45. Umu, S. U., Langseth, H., Bucher-Johannessen, C., Fromm, B., Keller, A., Meese, E., Lauritzen, M., Leithaug, M., Lyle, R., and Rounge, T. B. (2018) A comprehensive profile of circulating RNAs in human serum. *RNA Biology* **15**, 242-250
46. Canella, D., Praz, V., Reina, J. H., Cousin, P., and Hernandez, N. (2010) Defining the RNA polymerase III transcriptome: Genome-wide localization of the RNA polymerase III transcription machinery in human cells. *Genome Research* **20**, 710-721
47. Gogakos, T., Brown, M., Garzia, A., Meyer, C., Hafner, M., and Tuschl, T. (2017) Characterizing Expression and Processing of Precursor and Mature Human tRNAs by Hydro-tRNAseq and PAR-CLIP. *Cell Rep* **20**, 1463-1475
48. Dittmar, K. A., Goodenbour, J. M., and Pan, T. (2006) Tissue-Specific Differences in Human Transfer RNA Expression. *PLoS Genetics* **2**, e221

49. Mele, M., Ferreira, P. G., Reverter, F., DeLuca, D. S., Monlong, J., Sammeth, M., Young, T. R., Goldmann, J. M., Pervouchine, D. D., Sullivan, T. J., Johnson, R., Segre, A. V., Djebali, S., Niarchou, A., Consortium, G. T., Wright, F. A., Lappalainen, T., Calvo, M., Getz, G., Dermitzakis, E. T., Ardlie, K. G., and Guigo, R. (2015) Human genomics. The human transcriptome across tissues and individuals. *Science* **348**, 660-665
50. Grote, A., Hiller, K., Scheer, M., Munch, R., Nortemann, B., Hempel, D. C., and Jahn, D. (2005) JCat: a novel tool to adapt codon usage of a target gene to its potential expression host. *Nucleic Acids Res* **33**, W526-531
51. Betat, H., Long, Y., Jackman, J. E., and Morl, M. (2014) From end to end: tRNA editing at 5'- and 3'-terminal positions. *Int J Mol Sci* **15**, 23975-23998
52. Wilusz, J. E. (2015) Controlling translation via modulation of tRNA levels: Controlling translation via modulation of tRNA levels. *Wiley Interdisciplinary Reviews: RNA* **6**, 453-470
53. Wilusz, J. E., Whipple, J. M., Phizicky, E. M., and Sharp, P. A. (2011) tRNAs marked with CCACCA are targeted for degradation. *Science* **334**, 817-821
54. Chakraborty, P. K., Schmitz-Abe, K., Kennedy, E. K., Mamady, H., Naas, T., Durie, D., Campagna, D. R., Lau, A., Sendamarai, A. K., Wiseman, D. H., May, A., Jolles, S., Connor, P., Powell, C., Heeney, M. M., Giardina, P. J., Klaassen, R. J., Kannengiesser, C., Thuret, I., Thompson, A. A., Marques, L., Hughes, S., Bonney, D. K., Bottomley, S. S., Wynn, R. F., Laxer, R. M., Minniti, C. P., Moppett, J., Bordon, V., Geraghty, M., Joyce, P. B., Markianos, K., Rudner, A. D., Holcik, M., and Fleming, M. D. (2014) Mutations in TRNT1 cause congenital sideroblastic anemia with immunodeficiency, fevers, and developmental delay (SIFD). *Blood* **124**, 2867-2871
55. Lorenz, C., Lunse, C. E., and Morl, M. (2017) tRNA Modifications: Impact on Structure and Thermal Adaptation. *Biomolecules* **7**, 35
56. Heinemann, I. U., Nakamura, A., O'Donoghue, P., Eiler, D., and Söll, D. (2012) tRNA^{His}-guanylyltransferase establishes tRNA^{His} identity. *Nucleic Acids Res* **40**, 333-344
57. Gu, W., Hurto, R. L., Hopper, A. K., Grayhack, E. J., and Phizicky, E. M. (2005) Depletion of *Saccharomyces cerevisiae* tRNA(His) guanylyltransferase Thg1p leads to uncharged tRNA^{His} with additional m(5)C. *Mol Cell Biol* **25**, 8191-8201
58. Preston, M. A., D'Silva, S., Kon, Y., and Phizicky, E. M. (2013) tRNA^{His} 5-methylcytidine levels increase in response to several growth arrest conditions in *Saccharomyces cerevisiae*. *RNA* **19**, 243-256
59. Martinez, A., Yamashita, S., Nagaike, T., Sakaguchi, Y., Suzuki, T., and Tomita, K. (2017) Human BCDIN3D monomethylates cytoplasmic histidine transfer RNA. *Nucleic Acids Res* **45**, 5423-5436
60. Tomita, K., and Liu, Y. (2018) Human BCDIN3D Is a Cytoplasmic tRNA(His)-Specific 5'-Monophosphate Methyltransferase. *Front Genet* **9**, 305
61. Saikia, M., Fu, Y., Pavon-Eternod, M., He, C., and Pan, T. (2010) Genome-wide analysis of N1-methyl-adenosine modification in human tRNAs. *RNA* **16**, 1317-1327
62. Schimmel, P. (2017) The emerging complexity of the tRNA world: mammalian tRNAs beyond protein synthesis. *Nature Reviews Molecular Cell Biology* **19**, 45-58
63. Towns, W. L., and Begley, T. J. (2012) Transfer RNA Methyltransferases and Their Corresponding Modifications in Budding Yeast and Humans: Activities, Predications, and Potential Roles in Human Health. *DNA and Cell Biology* **31**, 434-454

64. Hopper, A. K. (2013) Transfer RNA post-transcriptional processing, turnover, and subcellular dynamics in the yeast *Saccharomyces cerevisiae*. *Genetics* **194**, 43-67
65. Dedon, P. C., and Begley, T. J. (2014) A System of RNA Modifications and Biased Codon Use Controls Cellular Stress Response at the Level of Translation. *Chemical Research in Toxicology* **27**, 330-337
66. Endres, L., Dedon, P. C., and Begley, T. J. (2015) Codon-biased translation can be regulated by wobble-base tRNA modification systems during cellular stress responses. *RNA Biology* **12**, 603-614
67. Rapino, F., Delaunay, S., Rambow, F., Zhou, Z., Tharun, L., De Tullio, P., Sin, O., Shostak, K., Schmitz, S., Piepers, J., Ghesquière, B., Karim, L., Charlotiaux, B., Jamart, D., Florin, A., Lambert, C., Rorive, A., Jerusalem, G., Leucci, E., Dewaele, M., Vooijs, M., Leidel, S. A., Georges, M., Voz, M., Peers, B., Büttner, R., Marine, J.-C., Chariot, A., and Close, P. (2018) Codon-specific translation reprogramming promotes resistance to targeted therapy. *Nature* **558**, 605-609
68. Ibbá, M., and Söll, D. (2000) Aminoacyl-tRNA Synthesis. *Annual Review of Biochemistry* **69**, 617-650
69. Giege, R., Sissler, M., and Florentz, C. (1998) Universal rules and idiosyncratic features in tRNA identity. *Nucleic Acids Research* **26**, 5017-5035
70. Payea, M. J., Sloma, M. F., Kon, Y., Young, D. L., Guy, M. P., Zhang, X., De Zoysa, T., Fields, S., Mathews, D. H., and Phizicky, E. M. (2018) Widespread temperature sensitivity and tRNA decay due to mutations in a yeast tRNA. *RNA* **24**, 410-422
71. Kessler, A. C., Silveira d'Almeida, G., and Alfonzo, J. D. (2018) The role of intracellular compartmentalization on tRNA processing and modification. *RNA Biol* **15**, 554-566
72. Hopper, A. K., Pai, D. A., and Engelke, D. R. (2010) Cellular dynamics of tRNAs and their genes. *FEBS Lett* **584**, 310-317
73. Kwon, N. H., Lee, M. R., Kong, J., Park, S. K., Hwang, B. J., Kim, B. G., Lee, E.-S., Moon, H.-G., and Kim, S. (2018) Transfer-RNA-mediated enhancement of ribosomal proteins S6 kinases signaling for cell proliferation. *RNA Biology* **15**, 635-648
74. Lee, Y. S., Shibata, Y., Malhotra, A., and Dutta, A. (2009) A novel class of small RNAs: tRNA-derived RNA fragments (tRFs). *Genes & Development* **23**, 2639-2649
75. Schwartz, M. H., and Pan, T. (2017) Function and origin of mistranslation in distinct cellular contexts. *Crit Rev Biochem Mol Biol* **52**, 205-219
76. Zimmerman, S. M., Kon, Y., Hauke, A. C., Ruiz, B. Y., Fields, S., and Phizicky, E. M. (2018) Conditional accumulation of toxic tRNAs to cause amino acid misincorporation. *Nucleic Acids Res* **46**, 7831-7843
77. Alvarez, A., Barisone, G. A., and Diaz, E. (2014) Focus formation: a cell-based assay to determine the oncogenic potential of a gene. *J Vis Exp*
78. Hou, Y.-M., Francklyn, C., and Schimmel, P. (1989) Molecular dissection of a transfer RNA and the basis for its identity. *Trends in Biochemical Sciences* **14**, 233-237
79. Sun, L., Gomes, A. C., He, W., Zhou, H., Wang, X., Pan, D. W., Schimmel, P., Pan, T., and Yang, X.-L. (2016) Evolutionary Gain of Alanine Mischarging to Noncognate tRNAs with a G4:U69 Base Pair. *Journal of the American Chemical Society* **138**, 12948-12955
80. Kuncha, S. K., Mazeed, M., Singh, R., Kattula, B., Routh, S. B., and Sankaranarayanan, R. (2018) A chiral selectivity relaxed paralog of DTD for proofreading tRNA mischarging in Animalia. *Nat Commun* **9**, 511

81. Pezo, V., Metzgar, D., Hendrickson, T. L., Waas, W. F., Hazebrouck, S., Doring, V., Marliere, P., Schimmel, P., and De Crecy-Lagard, V. (2004) Artificially ambiguous genetic code confers growth yield advantage. *Proc Natl Acad Sci USA* **101**, 8593-8597
82. Netzer, N., Goodenbour, J. M., David, A., Dittmar, K. A., Jones, R. B., Schneider, J. R., Boone, D., Eves, E. M., Rosner, M. R., Gibbs, J. S., Embry, A., Dolan, B., Das, S., Hickman, H. D., Berglund, P., Bennink, J. R., Yewdell, J. W., and Pan, T. (2009) Innate immune and chemically triggered oxidative stress modifies translational fidelity. *Nature* **462**, 522-526
83. Moghal, A., Mohler, K., and Ibba, M. (2014) Mistranslation of the genetic code. *FEBS Lett* **588**, 4305-4310
84. Wu, J., Fan, Y., and Ling, J. (2014) Mechanism of oxidant-induced mistranslation by threonyl-tRNA synthetase. *Nucleic Acids Res* **42**, 6523-6531
85. Lee, J. Y., Kim, D. G., Kim, B. G., Yang, W. S., Hong, J., Kang, T., Oh, Y. S., Kim, K. R., Han, B. W., Hwang, B. J., Kang, B. S., Kang, M. S., Kim, M. H., Kwon, N. H., and Kim, S. (2014) Promiscuous methionyl-tRNA synthetase mediates adaptive mistranslation to protect cells against oxidative stress. *Journal of Cell Science* **127**, 4234-4245
86. Gomes, A. C., Kordala, A. J., Strack, R., Wang, X., Geslain, R., Delaney, K., Clark, W. C., Keenan, R., and Pan, T. (2016) A dual fluorescent reporter for the investigation of methionine mistranslation in live cells. *RNA* **22**, 467-476
87. Fechter, P., Rudinger-Thirion, J., Tukalo, M., and Giege, R. (2001) Major tyrosine identity determinants in *Methanococcus jannaschii* and *Saccharomyces cerevisiae* tRNA(Tyr) are conserved but expressed differently. *Eur J Biochem* **268**, 761-767
88. Torres, A. G., Pineyro, D., Rodriguez-Escriba, M., Camacho, N., Reina, O., Saint-Leger, A., Filonava, L., Batlle, E., and Ribas de Pouplana, L. (2015) Inosine modifications in human tRNAs are incorporated at the precursor tRNA level. *Nucleic Acids Res* **43**, 5145-5157
89. Biddle, W., Schmitt, M. A., and Fisk, J. D. (2016) Modification of orthogonal tRNAs: unexpected consequences for sense codon reassignment. *Nucleic Acids Res* **44**, 10042-10050
90. Biddle, W., Schmitt, M. A., and Fisk, J. D. (2015) Evaluating Sense Codon Reassignment with a Simple Fluorescence Screen. *Biochemistry* **54**, 7355-7364
91. Thornlow, B. P., Hough, J., Roger, J. M., Gong, H., Lowe, T. M., and Corbett-Detig, R. B. (2018) Transfer RNA genes experience exceptionally elevated mutation rates. *Proc Natl Acad Sci USA* **115**, 8996-9001
92. Jinks-Robertson, S., and Bhagwat, A. S. (2014) Transcription-associated mutagenesis. *Annu Rev Genet* **48**, 341-359
93. Shoffner, J. M., Lott, M. T., Lezza, A. M., Seibel, P., Ballinger, S. W., and Wallace, D. C. (1990) Myoclonic epilepsy and ragged-red fiber disease (MERRF) is associated with a mitochondrial DNA tRNA(Lys) mutation. *Cell* **61**, 931-937
94. Jia, Z., Wang, X., Qin, Y., Xue, L., Jiang, P., Meng, Y., Shi, S., Wang, Y., Qin Mo, J., and Guan, M.-X. (2013) Coronary heart disease is associated with a mutation in mitochondrial tRNA. *Human Molecular Genetics* **22**, 4064-4073
95. Li, H., Geng, J., Yu, H., Tang, X., Yang, X., and Xue, L. (2018) Mitochondrial tRNA^{Thr} 15909A>G mutation associated with hypertension in a Chinese Han pedigree. *Biochem. Biophys. Res. Commun.* **495**, 574-581

96. Ding, Y., Xia, B.-H., Zhang, C.-J., and Zhuo, G.-C. (2018) Mitochondrial tRNA^{Leu}(UUR) C3275T, tRNA^{Gln} T4363C and tRNA^{Lys} A8343G mutations may be associated with PCOS and metabolic syndrome. *Gene* **642**, 299-306
97. Meng, F., He, Z., Tang, X., Zheng, J., Jin, X., Zhu, Y., Ren, X., Zhou, M., Wang, M., Gong, S., Mo, J. Q., Shu, Q., and Guan, M.-X. (2018) Contribution of the tRNA^{Ile} 4317A→G mutation to the phenotypic manifestation of the deafness-associated mitochondrial 12S rRNA 1555A→G mutation. *J. Biol. Chem.* **293**, 3321-3334
98. O'Neill, V. A., Eden, F. C., Pratt, K., and Hatfield, D. L. (1985) A human opal suppressor tRNA gene and pseudogene. *J Biol Chem* **260**, 2501-2508
99. Santesmasses, D., Mariotti, M., and Guigo, R. (2017) Computational identification of the selenocysteine tRNA (tRNA^{Sec}) in genomes. *PLoS Comput Biol* **13**, e1005383
100. Iben, J. R., and Maraia, R. J. (2014) tRNA gene copy number variation in humans. *Gene* **536**, 376-384
101. Wei, F.-Y., Suzuki, T., Watanabe, S., Kimura, S., Kaitsuka, T., Fujimura, A., Matsui, H., Atta, M., Michiue, H., Fontecave, M., Yamagata, K., Suzuki, T., and Tomizawa, K. (2011) Deficit of tRNA^{Lys} modification by Cdkal1 causes the development of type 2 diabetes in mice. *Journal of Clinical Investigation* **121**, 3598-3608
102. Kutter, C., Brown, G. D., Gonçalves, Â., Wilson, M. D., Watt, S., Brazma, A., White, R. J., and Odom, D. T. (2011) Pol III binding in six mammals shows conservation among amino acid isotypes despite divergence among tRNA genes. *Nature Genetics* **43**, 948-955
103. Kirchner, S., Cai, Z., Rauscher, R., Kastelic, N., Anding, M., Czech, A., Kleizen, B., Ostedgaard, L. S., Braakman, I., Sheppard, D. N., and Ignatova, Z. (2017) Alteration of protein function by a silent polymorphism linked to tRNA abundance. *PLOS Biology* **15**, e2000779
104. Rauscher, R., and Ignatova, Z. (2018) Timing during translation matters: synonymous mutations in human pathologies influence protein folding and function. *Biochemical Society Transactions* **46**, 937-944
105. Kimchi-Sarfaty, C., Oh, J. M., Kim, I. W., Sauna, Z. E., Calcagno, A. M., Ambudkar, S. V., and Gottesman, M. M. (2007) A "Silent" Polymorphism in the MDR1 Gene Changes Substrate Specificity. *Science* **315**, 525-528
106. Fernández-Calero, T., Cabrera-Cabrera, F., Ehrlich, R., and Marín, M. (2016) Silent Polymorphisms: Can the tRNA Population Explain Changes in Protein Properties? *Life* **6**, 9
107. Horjales, S., Cota, G., Señorale-Pose, M., Rovira, C., Román, E., Artagaveytia, N., Ehrlich, R., and Marín, M. (2007) Translational machinery and protein folding: Evidence of conformational variants of the estrogen receptor alpha. *Archives of Biochemistry and Biophysics* **467**, 139-143
108. Foreman, M. G., Kong, X., DeMeo, D. L., Pillai, S. G., Hersh, C. P., Bakke, P., Gulsvik, A., Lomas, D. A., Litonjua, A. A., Shapiro, S. D., Tal-Singer, R., and Silverman, E. K. (2011) Polymorphisms in Surfactant Protein-D Are Associated with Chronic Obstructive Pulmonary Disease. *American Journal of Respiratory Cell and Molecular Biology* **44**, 316-322
109. Pavon-Eternod, M., Gomes, S., Rosner, M. R., and Pan, T. (2013) Overexpression of initiator methionine tRNA leads to global reprogramming of tRNA expression and increased proliferation in human epithelial cells. *RNA* **19**, 461-466

110. Huang, S. Q., Sun, B., Xiong, Z. P., Shu, Y., Zhou, H. H., Zhang, W., Xiong, J., and Li, Q. (2018) The dysregulation of tRNAs and tRNA derivatives in cancer. *J Exp Clin Cancer Res* **37**, 101
111. Mahlab, S., Tuller, T., and Linial, M. (2012) Conservation of the relative tRNA composition in healthy and cancerous tissues. *RNA* **18**, 640-652
112. Gingold, H., Tehler, D., Christoffersen, Nanna R., Nielsen, Morten M., Asmar, F., Kooistra, Susanne M., Christophersen, Nicolaj S., Christensen, L. L., Borre, M., Sørensen, Karina D., Andersen, Lars D., Andersen, Claus L., Hulleman, E., Wurdinger, T., Ralfkiær, E., Helin, K., Grønbaek, K., Ørntoft, T., Waszak, Sebastian M., Dahan, O., Pedersen, Jakob S., Lund, Anders H., and Pilpel, Y. (2014) A Dual Program for Translation Regulation in Cellular Proliferation and Differentiation. *Cell* **158**, 1281-1292
113. Hatfield, D. L., Yoo, M.-H., Carlson, B. A., and Gladyshev, V. N. (2009) Selenoproteins that function in cancer prevention and promotion. *Biochimica et Biophysica Acta (BBA) - General Subjects* **1790**, 1541-1545
114. Quax, T. E., Claassens, N. J., Söll, D., and van der Oost, J. (2015) Codon Bias as a Means to Fine-Tune Gene Expression. *Mol Cell* **59**, 149-161
115. Frumkin, I., Lajoie, M. J., Gregg, C. J., Hornung, G., Church, G. M., and Pilpel, Y. (2018) Codon usage of highly expressed genes affects proteome-wide translation efficiency. *Proc Natl Acad Sci U S A* **115**, E4940-E4949
116. Alexandrov, A., Chernyakov, I., Gu, W., Hiley, S. L., Hughes, T. R., Grayhack, E. J., and Phizicky, E. M. (2006) Rapid tRNA Decay Can Result from Lack of Nonessential Modifications. *Molecular Cell* **21**, 87-96
117. Boccaletto, P., Machnicka, M. A., Purta, E., Piątkowski, P., Bagiński, B., Wirecki, T. K., de Crécy-Lagard, V., Ross, R., Limbach, P. A., Kotter, A., Helm, M., and Bujnicki, J. M. (2018) MODOMICS: a database of RNA modification pathways. 2017 update. *Nucleic Acids Research* **46**, D303-D307
118. Schweizer, U., and Fradejas-Villar, N. (2016) Why 21? The significance of selenoproteins for human health revealed by inborn errors of metabolism. *FASEB J* **30**, 3669-3681
119. Carlson, B., Yoo, M.-H., Tsuji, P., Gladyshev, V., and Hatfield, D. (2009) Mouse Models Targeting Selenocysteine tRNA Expression for Elucidating the Role of Selenoproteins in Health and Development. *Molecules* **14**, 3509-3527
120. Songe-Moller, L., van den Born, E., Leihne, V., Vagbo, C. B., Kristoffersen, T., Krokan, H. E., Kirpekar, F., Falnes, P. O., and Klungland, A. (2010) Mammalian ALKBH8 possesses tRNA methyltransferase activity required for the biogenesis of multiple wobble uridine modifications implicated in translational decoding. *Mol Cell Biol* **30**, 1814-1827
121. Goodarzi, H., Nguyen, H. C. B., Zhang, S., Dill, B. D., Molina, H., and Tavazoie, S. F. (2016) Modulated Expression of Specific tRNAs Drives Gene Expression and Cancer Progression. *Cell* **165**, 1416-1427
122. Nedialkova, Danny D., and Leidel, Sebastian A. (2015) Optimization of Codon Translation Rates via tRNA Modifications Maintains Proteome Integrity. *Cell* **161**, 1606-1618
123. Masoud, G. N., and Li, W. (2015) HIF-1alpha pathway: role, regulation and intervention for cancer therapy. *Acta Pharm Sin B* **5**, 378-389
124. Josefson, R., Andersson, R., and Nystrom, T. (2017) How and why do toxic conformers of aberrant proteins accumulate during ageing? *Essays Biochem* **61**, 317-324
125. de Toda, I. M., Vida, C., Ortega, E., and De La Fuente, M. (2016) Hsp70 basal levels, a tissue marker of the rate of aging and longevity in mice. *Exp Gerontol* **84**, 21-28

126. Bates, G. P., Dorsey, R., Gusella, J. F., Hayden, M. R., Kay, C., Leavitt, B. R., Nance, M., Ross, C. A., Scahill, R. I., Wetzel, R., Wild, E. J., and Tabrizi, S. J. (2015) Huntington disease. *Nat Rev Dis Primers* **1**, 15005
127. Parisien, M., Wang, X., and Pan, T. (2013) Diversity of human tRNA genes from the 1000-genomes project. *RNA Biology* **10**, 1853-1867
128. Chan, P. P., and Lowe, T. M. (2016) GtRNADB 2.0: an expanded database of transfer RNA genes identified in complete and draft genomes. *Nucleic Acids Research* **44**, D184-D189
129. Casper, J., Zweig, A. S., Villarreal, C., Tyner, C., Speir, M. L., Rosenbloom, K. R., Raney, B. J., Lee, C. M., Lee, B. T., Karolchik, D., Hinrichs, A. S., Haeussler, M., Guruvadoo, L., Navarro Gonzalez, J., Gibson, D., Fiddes, I. T., Eisenhart, C., Diekhans, M., Clawson, H., Barber, G. P., Armstrong, J., Haussler, D., Kuhn, R. M., and Kent, W. J. (2018) The UCSC Genome Browser database: 2018 update. *Nucleic Acids Res* **46**, D762-D769
130. Hrabeta-Robinson, E., Marcus, E., Cozen, A. E., Phizicky, E. M., and Lowe, T. M. (2017) High-Throughput Small RNA Sequencing Enhanced by AlkB-Facilitated RNA de-Methylation (ARM-Seq). *Methods Mol Biol* **1562**, 231-243
131. Gerstein, M. B., Kundaje, A., Hariharan, M., Landt, S. G., Yan, K. K., Cheng, C., Mu, X. J., Khurana, E., Rozowsky, J., Alexander, R., Min, R., Alves, P., Abyzov, A., Addleman, N., Bhardwaj, N., Boyle, A. P., Cayting, P., Charos, A., Chen, D. Z., Cheng, Y., Clarke, D., Eastman, C., Euskirchen, G., Fietze, S., Fu, Y., Gertz, J., Grubert, F., Harmanci, A., Jain, P., Kasowski, M., Lacroute, P., Leng, J. J., Lian, J., Monahan, H., O'Geen, H., Ouyang, Z., Partridge, E. C., Patacsil, D., Pauli, F., Raha, D., Ramirez, L., Reddy, T. E., Reed, B., Shi, M., Slifer, T., Wang, J., Wu, L., Yang, X., Yip, K. Y., Zilberman-Schapira, G., Batzoglou, S., Sidow, A., Farnham, P. J., Myers, R. M., Weissman, S. M., and Snyder, M. (2012) Architecture of the human regulatory network derived from ENCODE data. *Nature* **489**, 91-100
132. Wang, J., Zhuang, J., Iyer, S., Lin, X., Whitfield, T. W., Greven, M. C., Pierce, B. G., Dong, X., Kundaje, A., Cheng, Y., Rando, O. J., Birney, E., Myers, R. M., Noble, W. S., Snyder, M., and Weng, Z. (2012) Sequence features and chromatin structure around the genomic regions bound by 119 human transcription factors. *Genome Res* **22**, 1798-1812
133. Wang, J., Zhuang, J., Iyer, S., Lin, X. Y., Greven, M. C., Kim, B. H., Moore, J., Pierce, B. G., Dong, X., Virgil, D., Birney, E., Hung, J. H., and Weng, Z. (2013) Factorbook.org: a Wiki-based database for transcription factor-binding data generated by the ENCODE consortium. *Nucleic Acids Res* **41**, D171-176
134. Parmeggiani, A., Krab, I. M., Watanabe, T., Nielsen, R. C., Dahlberg, C., Nyborg, J., and Nissen, P. (2006) Enacyloxin IIa pinpoints a binding pocket of elongation factor Tu for development of novel antibiotics. *J Biol Chem* **281**, 2893-2900
135. Hohn, M. J., Park, H. S., O'Donoghue, P., Schnitzbauer, M., and Söll, D. (2006) Emergence of the universal genetic code imprinted in an RNA record. *Proc Natl Acad Sci USA* **103**, 18095-18100
136. Roberts, E., Eargle, J., Wright, D., and Luthey-Schulten, Z. (2006) MultiSeq: unifying sequence and structure data for evolutionary analysis. *BMC Bioinformatics* **7**, 382
137. Guindon, S., Dufayard, J. F., Lefort, V., Anisimova, M., Hordijk, W., and Gascuel, O. (2010) New algorithms and methods to estimate maximum-likelihood phylogenies: assessing the performance of PhyML 3.0. *Syst Biol* **59**, 307-321
138. Shimodaira, H., and Hasegawa, M. (1999) Multiple comparisons of log-likelihoods with applications to phylogenetic inference. *Mol. Biol. Evol.* **16**, 1114-1116

139. Sprinzl, M., and Vassilenko, K. S. (2005) Compilation of tRNA sequences and sequences of tRNA genes. *Nucleic Acids Res* **33**, D139-140

1.8 Supplemental information

1.8.1 Supplemental tables

Table S1.1 Human tRNA variants that introduce a G4:U69 base pair

tRNA	variant	effect	MAF (%) ^a	variant count ^a	MAF (%) ^b	variant count ^b	tRNA Score ^c	Expression ARM ^d CHIP ^e	
Cys-GCA-2-3	C69U	G4:U69	0.02	1	0.00004	5	81.9	+	+
Cys-GCA-9-3	C69U	G4:U69	18.9	948	0.1329	16689	77.2	+	-
Cys-GCA-9-4	C69U	G4:U69	1.5	76	0.0166	2090	77.2	+	+
Cys-GCA-14-1	C69U	G4:U69	0.02	1	-	-	71.6	+	+
Ser-AGA-2-3	C69U	G4:U69	0.02	1	0.00002	2	89.6	+	+
Ser-CGA-2-1	C69U	G4:U69	0.02	1	0.000008	1	94.0	+	+
Ser-GCT-1-1	C69U	G4:U69	-	-	0.00002	2	91.9	+	-
Ser-GCT-4-2	C69U	G4:U69	0.02	1	0.00003	4	88.4	+	+
Ser-GCT-4-1	C69U	G4:U69	0.02	1	0.0003	37	88.4	+	+
Ser-GCT-2-1	C69U	G4:U69	0.02	1	0.0002	21	91	+	+
Ser-TGA-2-1	C69U	G4:U69	0.06	3	0.0002	21	90.4	+	+
iMet-CAT-1-1	A4G	G4:U69	0.02	1	-	-	60.4	+	+
iMet-CAT-1-3	A4G	G4:U69	-	-	0.00005	6	60.4	+	+
iMet-CAT-1-4	A4G	G4:U69	0.5	25	0.0015	185	60.4	+	+
iMet-CAT-1-6	A4G	G4:U69	0.02	1	0.0005	67	60.4	+	+
Phe-GAA-1-4	C69U	G4:U69	-	-	0.00003	4	88.9	+	+
Phe-GAA-1-2	C69U	G4:U69	-	-	-	-	88.9	+	+
Phe-GAA-2-1	C69U	G4:U69	-	-	0.00007	9	87.9	+	+
Phe-GAA-3-1	C69U	G4:U69	-	-	0.00006	7	88.3	+	+
Cys-GCA-23-1	Reference genome = G4:U69						59.1	+	-
Thr-AGT-1-1	Reference genome = G4:U69						82.6	+	+
Thr-AGT-1-2	Reference genome = G4:U69						82.6	+	+
Thr-AGT-1-3	Reference genome = G4:U69						82.6	+	+
Thr-AGT-5-1	Reference genome = G4:U69						80.1	+	-
Thr-CGT-2-1	Reference genome = G4:U69						79.6	+	+
Thr-CGT-4-1	Reference genome = G4:U69						78.3	+	+
Val-AAC-6-1	Reference genome = G4:U69						69.9	+	+

MAF; minor allele frequency. _##N; inserted nucleotide. ^aData from 1000 genomes project (1,2); ^bData from TOPMED sequencing project (2,3); ^ctRNA score was calculated using tRNA-Scan

SE (2); ^dARM = ARM-seq data suggesting expression (2,4); ^eCHIP = CHIP-seq hits for at least 3 of 4 core transcription proteins (RPC155, POLR3G, BRF1, BDP1) (3,5-8).

Table S1.2. List of tRNA counts in selected genomes.

Species	Number of tRNA genes	Number of tRNA genes (high confidence)
<i>E. coli K12</i>	89	86
<i>S. cerevisiae</i>	275	275
<i>M. musculus</i>	471	468
<i>H. sapiens</i>	596	417
<i>C. elegans</i>	596	596
<i>A. thaliana</i>	700	684
<i>G. max</i> (soybean)	738	738
<i>O. sativa</i> (rice)	764	738
<i>S. purpuratus</i> (sea urchin)	1068	1065
<i>Z. mays</i> (maize)	1202	1198
<i>G. morhua</i> (atlantic cod)	1502	1490
<i>P. marinus</i> (lamprey)	2491	2484
<i>X. tropicalis</i> (frog)	2653	2638
<i>Danio rerio</i> (zebrafish)	12292	12244
<i>C. milii</i> (elephant shark)	13758	13724

1.8.2 Supplementary references

1. Parisien, M., Wang, X., and Pan, T. (2013) Diversity of human tRNA genes from the 1000-genomes project. *RNA Biology* **10**, 1853-1867
2. Chan, P. P., and Lowe, T. M. (2016) GtRNAdb 2.0: an expanded database of transfer RNA genes identified in complete and draft genomes. *Nucleic Acids Research* **44**, D184-D189
3. Casper, J., Zweig, A. S., Villarreal, C., Tyner, C., Speir, M. L., Rosenbloom, K. R., Raney, B. J., Lee, C. M., Lee, B. T., Karolchik, D., Hinrichs, A. S., Haeussler, M., Guruvadoo, L., Navarro Gonzalez, J., Gibson, D., Fiddes, I. T., Eisenhart, C., Diekhans, M., Clawson, H., Barber, G. P., Armstrong, J., Haussler, D., Kuhn, R. M., and Kent, W. J. (2018) The UCSC Genome Browser database: 2018 update. *Nucleic Acids Res* **46**, D762-D769

4. Hrabeta-Robinson, E., Marcus, E., Cozen, A. E., Phizicky, E. M., and Lowe, T. M. (2017) High-Throughput Small RNA Sequencing Enhanced by AlkB-Facilitated RNA de-Methylation (ARM-Seq). *Methods Mol Biol* **1562**, 231-243
5. Canella, D., Praz, V., Reina, J. H., Cousin, P., and Hernandez, N. (2010) Defining the RNA polymerase III transcriptome: Genome-wide localization of the RNA polymerase III transcription machinery in human cells. *Genome Res* **20**, 710-721
6. Gerstein, M. B., Kundaje, A., Hariharan, M., Landt, S. G., Yan, K. K., Cheng, C., Mu, X. J., Khurana, E., Rozowsky, J., Alexander, R., Min, R., Alves, P., Abyzov, A., Addleman, N., Bhardwaj, N., Boyle, A. P., Cayting, P., Charos, A., Chen, D. Z., Cheng, Y., Clarke, D., Eastman, C., Euskirchen, G., Fietze, S., Fu, Y., Gertz, J., Grubert, F., Harmanci, A., Jain, P., Kasowski, M., Lacroute, P., Leng, J. J., Lian, J., Monahan, H., O'Geen, H., Ouyang, Z., Partridge, E. C., Patacsil, D., Pauli, F., Raha, D., Ramirez, L., Reddy, T. E., Reed, B., Shi, M., Slifer, T., Wang, J., Wu, L., Yang, X., Yip, K. Y., Zilberman-Schapira, G., Batzoglou, S., Sidow, A., Farnham, P. J., Myers, R. M., Weissman, S. M., and Snyder, M. (2012) Architecture of the human regulatory network derived from ENCODE data. *Nature* **489**, 91-100
7. Wang, J., Zhuang, J., Iyer, S., Lin, X., Whitfield, T. W., Greven, M. C., Pierce, B. G., Dong, X., Kundaje, A., Cheng, Y., Rando, O. J., Birney, E., Myers, R. M., Noble, W. S., Snyder, M., and Weng, Z. (2012) Sequence features and chromatin structure around the genomic regions bound by 119 human transcription factors. *Genome Res* **22**, 1798-1812
8. Wang, J., Zhuang, J., Iyer, S., Lin, X. Y., Greven, M. C., Kim, B. H., Moore, J., Pierce, B. G., Dong, X., Virgil, D., Birney, E., Hung, J. H., and Weng, Z. (2013) Factorbook.org: a Wiki-based database for transcription factor-binding data generated by the ENCODE consortium. *Nucleic Acids Res* **41**, D171-176

Chapter 2

2. Visualizing tRNA-dependent mistranslation in human cells¹

2.1 Introduction

A highly accurate proteome is not required for life. In the years preceding and immediately following the elucidation of the genetic code^{1,2}, it was argued that mis-interpretation of the genetic code and the resulting mistranslation would lead to an error catastrophe³ in the proteome that could not support life. Crick used the same logic to argue that the code could not evolve further or tolerate significant errors because modern proteomes are composed of “*so many highly evolved protein molecules that any change to these would be highly disadvantageous unless accompanied by many simultaneous mutations to correct the ‘mistakes’ produced by altering the code*”⁴. There is now ample evidence that the code does indeed continue to evolve through codon reassignments, codon recoding, and natural genetic code expansion in species representing the complete diversity of life⁵.

In contrast to the concept of a highly accurate proteome, diverse organisms show robustness to genetic code changes and mistranslation. A series of landmark studies, in *Escherichia coli*⁶, yeast⁷, and mammalian cells⁸ reshaped our view of the level of accuracy required to produce a functional proteome. Errors in protein synthesis are estimated to occur at a rate of 1 mis-incorporated amino acid in 10^4 to 10^5 codons^{9,10}, which suggests that between 0.01 and 0.001% of codons are misread in the human proteome. *E. coli* can tolerate remarkably high levels of mistranslation. Indeed, Ruan et al.⁶ showed that *E. coli* grow similarly to wildtype even when 10% of genetically encoded asparagine residues were mistranslated as aspartic acid. The heat-shock response, and the expression of cellular proteases were essential to maintain wild-type like growth in these cells despite proteome-wide mistranslation⁶.

In *Saccharomyces cerevisiae*, we selected a mutant tRNA that suppressed a stress-sensitive phenotype by inducing proline to alanine mistranslation at a rate of ~6%¹¹. Yeast cells tolerated this tRNA-dependent mistranslation by inducing heat-shock, again without a significant growth defect. In the mistranslating yeast strain, we also observed synthetic slow growth with a deletion of a gene (*rpn4*) encoding a transcription factor that regulates proteasome gene expression,

²Work in this chapter was published in: Lant, J.T., Berg, M.D. Sze, D.H.W., Hoffman, K.S., Akinpelu, I.C., Turk, M., Heinemann, I.U., Duennwald, M.L., Brandl, C.J., and O’Donoghue, P. (2017) Visualizing tRNA-dependent mistranslation in human cells. *RNA Biology*.

implicating the proteasome and protein degradation as critical mechanisms the cell uses to tolerate mistranslation¹¹. In mammalian cells, tyrosine limitation leads to proteome-wide mistranslation of tyrosine codons with phenylalanine at a rate of ~1%, again without a significant impact on cellular viability¹².

Not only can cells tolerate mistranslation robustly, but mistranslation may also be advantageous in conditions of stress. Mistranslation in bacteria¹³ and mammalian cells^{14, 15} protects cells from reactive oxygen species. In an *E. coli* strain with a ribosomal protein mutant (RpsD) that enhances mistranslation, a stop codon suppression assay indicated ~5-fold increase in translation errors above the basal level. This mistranslation increased expression of a general stress response activator (RpoS) that in turn up-regulated antioxidant gene expression, making the cell more resistant to peroxide treatment¹³. In HEK 293T cells, mis-aminoacylation of tRNA^{Glu} with methionine accounts for a ~0.5% basal level of mistranslation¹⁶. Immune or chemical induction of oxidative stress increased this rate up to 10-fold¹⁷. The current model suggests that oxidative stress leads to extracellular signal-regulated kinase (ERK) dependent phosphorylation of the methionine-tRNA synthetase, which makes the enzyme more promiscuous for non-cognate tRNAs¹⁸. The additional methionine incorporated in the proteome at non-methionine positions is thought to act as a ‘sink’ for ROS, and methionine mistranslation increased resistance to ROS in cell culture¹⁷. These studies demonstrate that cells are capable not only of tolerating proteome-wide mistranslation, but can derive a selective advantage from mistranslation under certain stress conditions.

We recently devised a selection in yeast that requires mistranslation at proline codons for the organism to survive under stress. The selection relied on a stress-sensitive allele of the PIK kinase chaperon, Tti2^{11, 19, 20}. Single base mutations in tRNA^{Pro} were selected that resulted in a C70U mutation in the acceptor stem of the tRNA, yielding the essential G3:U70 identity element for alanyl-tRNA synthetase (AlaRS). Unlike many tRNA synthetases, AlaRS does not recognize the anticodon of its cognate tRNA (Fig 2.1). Rather it establishes critical interactions with both major and minor groove sides of the G3:U70 base pair in the acceptor stem of tRNA^{Ala}²¹. These interactions orient the 5’ amino acid accepting CCA-end of the tRNA in the AlaRS active site (Fig 2.1). Although AlaRS does not tolerate the reverse U:G pair or other mutations at this position²², the human AlaRS shows significant activity with tRNAs that encode a G4:U69 pair²³, of which there are several in the human reference genome. Taken together, these studies suggest that

because of its minimal identity requirements, the generation of tRNA mutations that are mischarged with Ala may be more prevalent in nature, including in humans, than previously assumed.

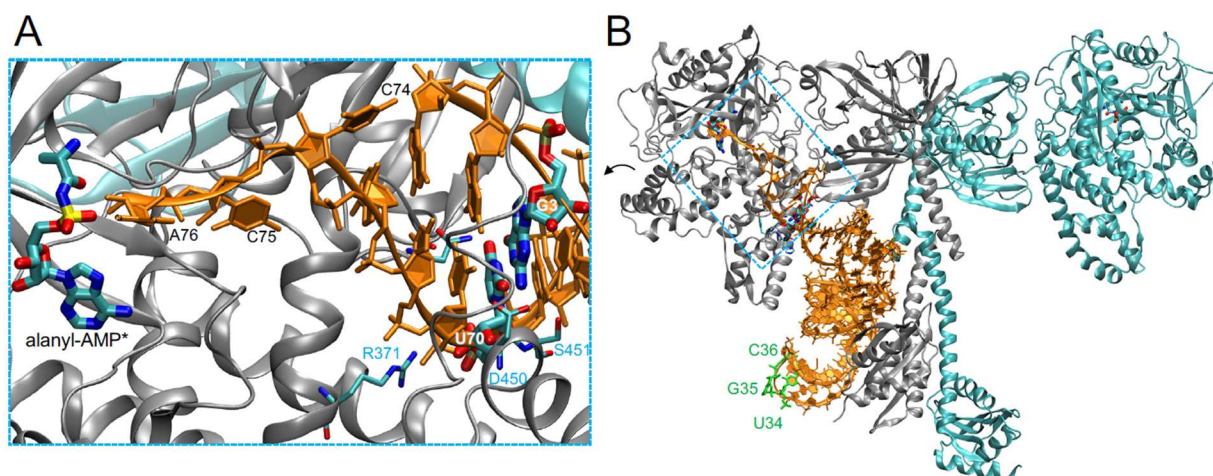


Figure 2.1. Structure of AlaRS and tRNA^{Ala} complex. The zoomed in view (A) focuses on the interaction of the tRNA^{Ala} acceptor stem with the AlaRS active site (PDB code 3WQY²¹). The 3' terminal CCA bases of the tRNA are labeled. An alanyl-adenylate analog (*) is also shown. The major AlaRS identity element G3:U70 is highlighted. AlaRS residues (R371, N359, D450, S451) form a hydrogen bond network (gray dashes) that contacts and ‘reads’ the GU pair from both the major and minor groove sides of the tRNA are annotated. The complete dimeric AlaRS is shown in complex with tRNA^{Ala} (B). The three bases of the anticodon (U34, G35, C36; green) are not recognized by the AlaRS.

Here we produced and characterized a mutant human tRNA^{Pro} with the G3:U70 base pair (Fig 2.2A). With biochemical experiments and live cell imaging, we quantified and visualized tRNA-dependent mistranslation in human cells, finding that the mutant tRNA^{Pro} is an efficient alanine acceptor that promotes mistranslation in human cells in culture.

2.2 Materials and methods

2.2.1 Plasmids and strains.

Plasmid manipulations were performed with *E. coli* DH5 α cells (Invitrogen, Carlsbad, CA, USA). For *in vitro* amino-acylation assays, tRNA genes were ordered as single stranded DNA oligomers from Sigma-Aldrich (Darmstadt, Germany) with overhangs to BamHI/XbaI sites. Single-stranded oligomers were phosphorylated using T4 polynucleotide kinase (New England Biolabs (NEB), Ipswich, MA, USA) and annealed by gradual cooling from 95°C to 55°C. Annealed oligomers were cloned into pUC19 BamHI/XbaI sites using BamHI, XbaI, and T4 DNA ligase (NEB). pUC19-derived plasmids were purified by mini-prep (GeneAid, New Taipei City, Taiwan) and used as template for *in vitro* transcription. For expression in human cell culture, EGFP D129A or D129P genes were cloned into pcDNA3.1 HindIII/EcoRI sites. Transfer RNA genes were fused to a human U6 promoter sequence and 6x thymidine termination sequence by overlap extension PCR (pfu polymerase, Agilent Technologies), then ligated into pcDNA3.1 at the NruI site. Plasmid DNA was isolated from 100 ml *E. coli* cultures by midi-prep (GeneAid) followed by phenol chloroform extraction and ethanol precipitation, then re-suspended in sterile Milli-Q water. All plasmids were diluted to equimolar (\pm 20 ng/ μ l) concentrations before transfection.

2.2.2 *In vitro* tRNA transcription and radiolabeling.

In vitro transcription and radiolabeling of tRNAs for *in vitro* aminoacylation experiments was performed as previously described²⁴ (see Supporting Information for tRNA sequences and details).

2.2.3 *In vitro* tRNA aminoacylation.

For the aminoacylation assays we purchased recombinant human AlaRS (Abcam, ab73442, Cambridge, UK) and human glutamyl-prolyl-tRNA synthetase (EPRS, Origene, TP317559, Rockville, MD). 50 μ l reactions with 5 μ M tRNA, 300 nM ³²P-labelled tRNA, 10 mM amino acid (Ala or Pro as indicated), 5 mM ATP and 1 μ M tRNA synthetase were incubated at 37°C for 0, 20 and 40 minutes. Reactions were digested with nuclease P1, spotted on a polyethyleneimine-cellulose thin layer chromatography (TLC) plate (EMD Millipore, Billerica, MA, USA) and

chromatographed in 5% acetic acid and 100 mM ammonium acetate. TLC plates were exposed to a phosphor screen, which was imaged using a Storm 860 Phosphorimager (GE Healthcare Life Science, Little Chalfont, UK).

2.2.4 HEK 293T cell transfection.

Transfections were performed in 24-well or 6-well plates using 1.25 μg or 2.5 μg of DNA, respectively. Cells were cultured in high glucose Dulbecco's modified Eagle medium (DMEM, 4.5 g/L glucose) containing penicillin, streptomycin (P/S), and 10% fetal bovine serum (FBS) (Gibco by Life Technologies, Carlsbad, MA). At 70-80% cell confluency, media was replaced with standard DMEM (no FBS, P/S) and cells transfected with pcDNA3.1-derived plasmids using lipofectamine 2000 (Invitrogen). Cells were returned to +P/S, +10% FBS media to recover for at least 1 day before analysis. Cell fluorescence was quantitated daily as described below. For experiments in low serum, low glucose media, after 'day 1' quantitation, media was replaced with 1% FBS, 1 g/L glucose DMEM (Corning Cellgro, Corning, NY, USA). Geneticin selections were maintained in DMEM (4.5 g/L glucose, 10% serum, P/S) containing 500 $\mu\text{g}/\text{ml}$ geneticin (G418; Gibco by Life Technologies).

2.2.5 Fluorescence quantitation of enhanced GFP (EGFP) reporter.

To quantify EGFP fluorescence, images were captured using an EVOS FL auto fluorescent microscope (Thermo Fisher Scientific, Waltham, MA, USA) at 20X magnification and GFP foci outlined using the ellipse measurement tool. The EVOS microscope measures GFP fluorescence with 470/525 nm excitation/emission wavelengths. Our negative control and experimental cultures (EGFP D129P) were exposed for 163 ms with a 65 unit light setting and our positive (EGFP D129A) was exposed for 163 ms with a 23 unit light setting. In each field of view, the 15 brightest foci were outlined and data collected as a mean pixel intensity within each ellipse. At least 135 foci were measured from each experiment daily across three biological replicates and three fields-of-view per replicate. On the final day, an additional two fields-of-view were collected per transfection, totaling 225 foci. The average of five empty space measurements was subtracted from all values in each field of view to account for inconsistencies in light scattering between fields. Percentage mistranslation was estimated using the means of each data set and p-values were calculated pairwise using single-factor ANOVA with Microsoft Excel.

2.2.6 Western blotting.

Cells were harvested by pipetting and centrifuged in 1.5 ml microcentrifuge tubes at 1500 \times g for 3 min at 4°C. Supernatant was removed and cells washed with ice cold Phosphate Buffered Saline (1 \times PBS pH 7.4; Corning Cellgro) and centrifuged again. PBS was aspirated off and cells were suspended in 50 μ l of ice-cold Lysis buffer: 50 mM Tris-HCl (pH 7.4), 1% Triton X-100, 150 mM NaCl, 0.1% sodium dodecyl sulfate (SDS), and 1 mM Phenylmethylsulfonyl fluoride. The re-suspended cells were incubated on ice for 5 min then centrifuged at 4°C, 30,000 \times g for 10 minutes. Lysates were separated on standard SDS-polyacrylamide gel electrophoresis (PAGE) (15% acrylamide) and transferred to Polyvinylidene fluoride membranes using a Trans-Blot Turbo Transfer System (BioRad, Hercules, CA, USA). Membranes were cut horizontally according to protein standards to enable multiple antibodies to be assayed in parallel. Membranes were incubated for 1 hr in blocking solution (3% bovine serum albumin (BSA), 0.1% Tween 20, 1% PBS) before adding primary antibodies at a 1:5000 final dilution (α -HSP70, Invitrogen, MA3-006; α -HSP90, Protein Tech, Rosemont, IL, USA, 13171-1-AP; α -GFP, abcam, ab32146; α -GAPDH, Sigma-Aldrich, MAB374). Membranes were incubated overnight at 4°C, washed for 3 \times 10 min in washing solution (1% BSA, 0.1% Tween 20, 1% PBS), then incubated with anti-mouse (Thermo Fisher Scientific, MA1-21315) or anti-rabbit (Sigma, GENA9340) horse radish peroxidase-linked secondary antibodies for 2 hr at 1:2000 final dilution. Membranes were then washed with 1 \times PBS with 0.1% Tween 20 three times for 10 minutes, followed one wash for 10 minute in 1 \times PBS. Protein markers were visualized using Clarity Western enhanced chemiluminescence (ECL) Substrates (Bio-Rad) following the manufacturer's instructions and imaged with a ChemiDoc XRS+ System (Bio-Rad).

2.2.7 Cell viability assay.

HEK 293T cell cultures were seeded at equivalent cell densities and grown overnight in high glucose DMEM, then transfected in triplicate and assayed either one day post-transfection or switched to low serum, low glucose DMEM for 4 days. Cellular viability was determined using a CellTiter-Glo Luminescent Cell Viability Assay following the manufacturer's instructions (Promega, Madison, WI). Each transfection was assayed in triplicate, totaling three biological and nine technical replicates per experiment.

2.3 Results

2.3.1 Biochemical characterization of a mistranslating human tRNA^{Pro} (G3:U70).

We first investigated human tRNA^{Pro} G3:U70 for mis-acylation activity with Ala (Fig 2.2). We produced and purified human tRNA^{Pro}, tRNA^{Ala}, and tRNA^{Pro} G3:U70 by *in vitro* transcription using recombinant T7 RNA polymerase. Recombinant human AlaRS (Abcam) and human glutamyl-prolyl-tRNA synthetase (GluProRS, Origene) were purchased. The ProRS activity in human cells is encoded as a single polypeptide fused to GluRS. We performed aminoacylation assays according to standard protocols (see Methods) as previously²⁴. The level of aminoacyl-tRNA formed at specific time points was measured using ³²P radiolabeled tRNA variants (see SI Methods). Following nuclease P1 digestion, unreacted tRNA and aminoacylated-tRNA product were separated by thin layer chromatography and visualized by autoradiography (Fig 2.2B). The aminoacylation assays confirmed significant activity of human GluProRS in Pro-tRNA^{Pro} formation, and efficient aminoacylation by human AlaRS of tRNA^{Ala} with Ala (Fig 2.2B). Like our previous findings with the homologous yeast AlaRS and ProRS¹¹, ProRS activity is weaker than that observed with AlaRS. Pro accepting activity was not detected with the tRNA^{Pro} G3:U70 mutant and human GluProRS, indicating that the single base pair mutation is a sufficient anti-determinant for GluProRS. In the presence of AlaRS and Ala, however, a gain-of-function was observed as the mutant tRNA was charged with Ala, though to a lesser extent than tRNA^{Ala} (Fig. 2.2B). These results demonstrate tRNA^{Pro} (G3:U70) is an efficient Ala acceptor *in vitro* and the mutation is sufficient to disable ProRS activity.

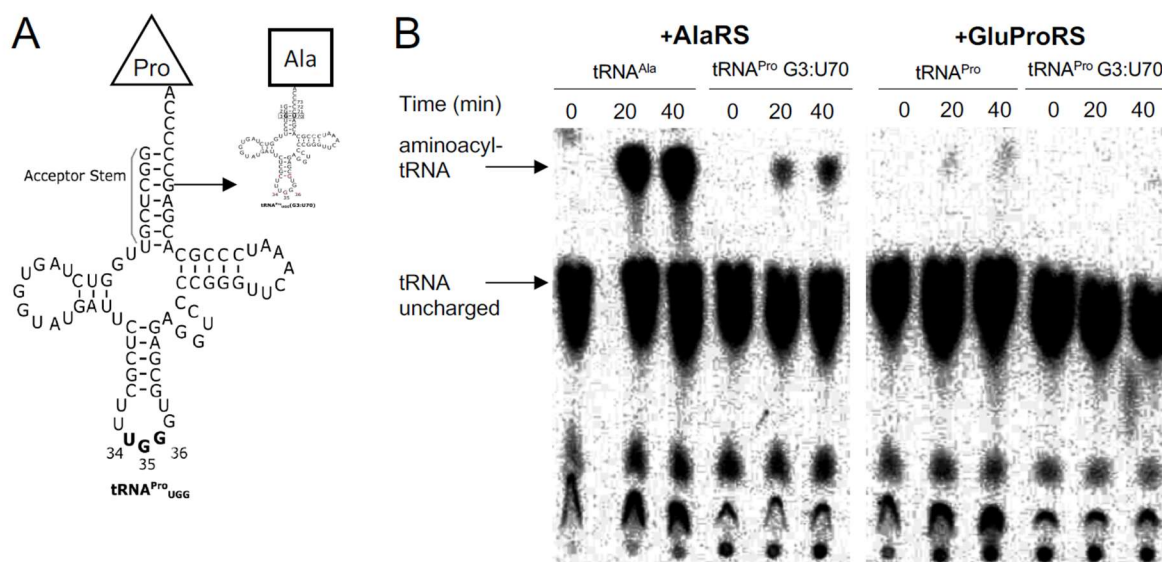


Figure 2.2. *In vitro* amino-acylation of tRNA^{Pro} (G3:U70). Cloverleaf diagrams (A) of human tRNA^{Pro}_{UGG} WT and G3:U70. Mutations in the acceptor stem are outlined with a rectangle. Purified ³²P-radiolabeled tRNAs were aminoacylated with Ala by human AlaRS or Pro by human GluProRS as indicated in Methods. The autoradiographs show reaction progress (accumulation of aminoacylated-tRNA) for each reaction over a 40-minute time course.

2.3.2 GFP reporter illuminates mistranslation in living cells.

We recently established a novel EGFP mistranslation reporter in yeast¹¹. The GFP reporter contains a mutation, D129P, which is thought to cause a kink in the backbone of GFP's β -barrel structure¹¹. When the Pro codon at position 129 in the EGFP reporter is translated accurately as Pro, the resulting EGFP, although stably produced, lacks fluorescence. The mutant D129A, however, fluoresces similarly to wild type EGFP. In our studies in yeast, this reporter was a sensitive measure of mistranslation activity in live cells. We reported a level of ~6% mistranslation of the critical Pro129 codon to Ala in a yeast strain that co-expressed the mistranslating tRNA^{Pro} (G3:U70)¹¹.

To define how human cells in culture respond to mistranslation, we conducted a series of transient transfection experiments in HEK 293T cells. Each cell line harbored a pCDNA3.1 plasmid containing separate EGFP and tRNA expression cassettes. Our EGFP reporter (D129A or

D129P) was expressed under the control of a pCMV constitutive promoter. We chose to test a CCA codon for mistranslation by tRNA^{Pro}_{UGG} G3:U70, consistent with our study in yeast¹¹. The tRNA expression cassette was designed to include an upstream U6 constitutive promoter and followed by a downstream poly-T terminator sequence (see Methods).

Having established our Pro-codon sensitive EGFP mistranslation reporter for use in human cells, we transfected HEK 293T cells in triplicate with plasmids co-expressing EGFP D129P or D129A and the wild type (C3:G70) or mistranslating (G3:U70) human tRNA^{Pro} (Figs 2.3, S2.3). Based on 3 biological replicates, transfection efficiencies were initially ~50-60% as determined from the number of cells fluorescing in our EGFP D129A positive control, but declined to ~20-40% by the end of our multi-day experiment due to plasmid dilution by cell division. Mistranslation was quantified by fluorescence microscopy (Fig. 2.3, see Methods).

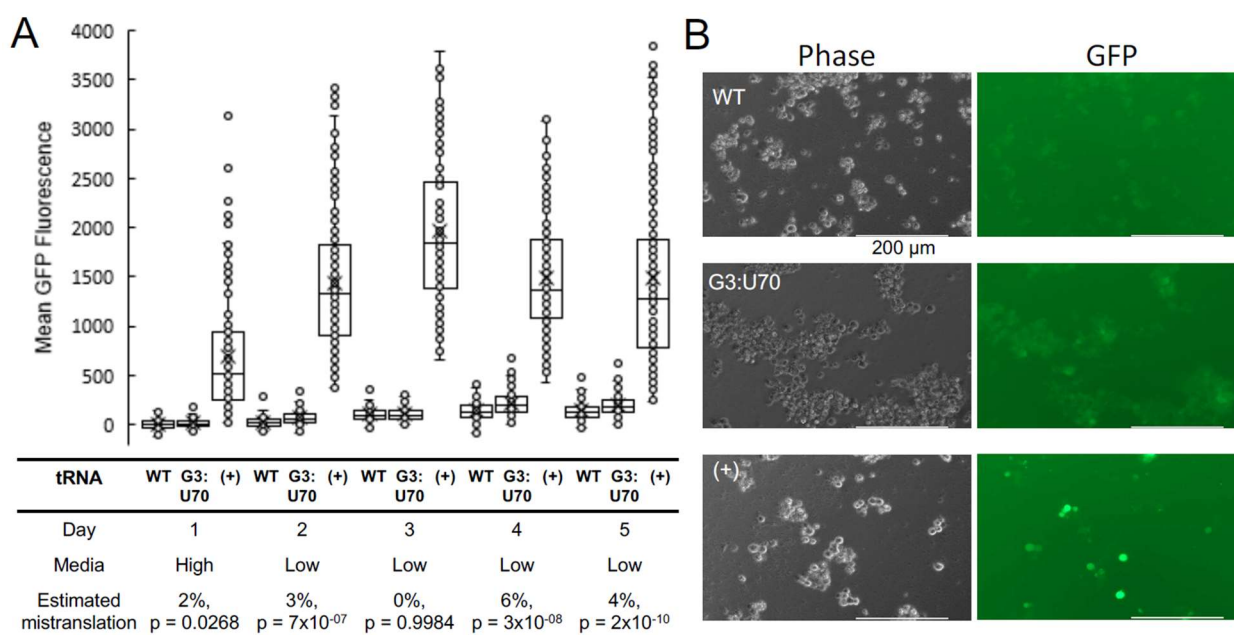


Figure 2.3. tRNA-dependent mistranslation increases under glucose and serum starvation.

HEK 293T cell cultures were transfected in triplicate with plasmid harboring tRNA^{Pro} and EGFP D129P (WT); tRNA^{Pro} G3:U70 and EGFP D129P (G3:U70); or tRNA^{Pro} and EGFP D129A (+). Cells were grown for 1 day post-transfection in high glucose media (high), then media was replaced with low serum, low glucose (low) and fluorescence was measured daily by fluorescence microscopy (see Methods). Box and whisker plots (A) of EGFP foci intensity.

Horizontal demarcations depict quartiles with median centered. Means are depicted with an X. Dots represent the general distribution of at least 135 foci measured in each plot across 3 biological and at least 9 technical replicates. Mistranslation levels were estimated based on means of the three populations on each day and the p-value of a difference between the WT and G3:U70 populations is reported based on single-factor ANOVA. Representative images (B) of mistranslating cells. HEK 293T cell images were captured at 20X magnification using light (phase) or fluorescence (GFP; ex/em = 470/525 nm) microscopy. Scale bars depict 200 μ m.

In standard, high glucose media, we did not detect a significant difference in EGFP D129P fluorescence between cells expressing tRNA^{Pro} versus tRNA^{Pro} (G3:U70). We reasoned, based on the literature (e.g.,¹³⁻¹⁵), that mistranslation would be enhanced in conditions of stress. Therefore, the transfected cell lines were transferred to a low serum and low glucose medium and monitored daily. For cells expressing wild type and mutant tRNA^{Pro}, we analyzed GFP fluorescence up to 5 days following transfection. Under glucose and serum starvation, a trend of accumulating mistranslation was observed in cells expressing the mutant tRNA^{Pro} over the course of the experiment. The estimate of mistranslation was calculated based on the relative fluorescence of EGFP D129P and D129A expressing controls (Figs 2.3, S2.4). Following recovery (~1 day after switching media), we observed a reproducible, and statistically significant, 4-6% (p-value < 10⁻⁸) increased rate of mistranslation on days 4 and 5 in the cells expressing tRNA^{Pro} (G3:U70). Equivalent GFP expression in all cell lines was confirmed by immunoblotting and compared to a glyceraldehyde 3-phosphate dehydrogenase loading control (Fig 2.4). The mistranslation-dependent effect began to taper on day 5 due to gradual plasmid loss. Cells were lysed at this stage for further analysis by western blotting.

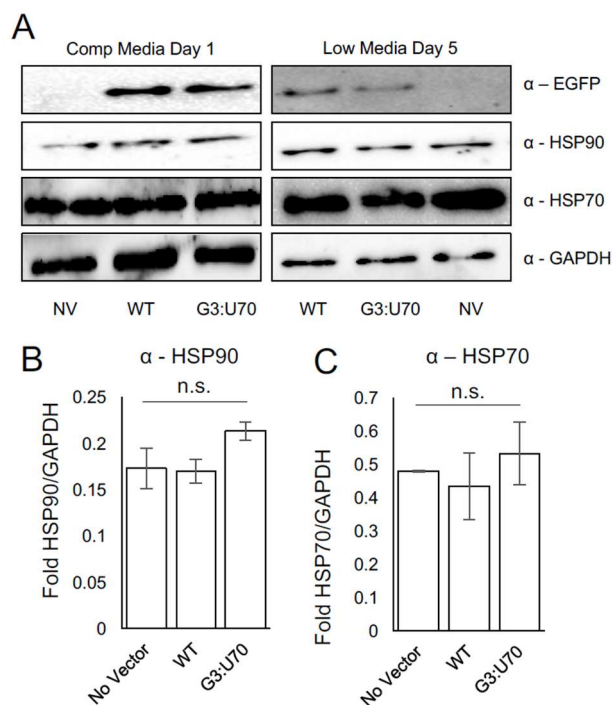


Figure 2.4. Mistranslation caused no detectable induction of heat shock response. Western blotting of HEK 293T cell lysates (A) with antibodies detecting EGFP, heat shock markers (HSP70, HSP90), and a GAPDH loading control. Lysates were harvested after one day incubation in high glucose media (A, left panel) or changed to low serum, low glucose media (A, right panel) for four days before harvesting. Lysates were separated by SDS-PAGE; loading quantities were balanced according to triplicate Bradford assays. Densitometry based on triplicate western blots of HSP90 (B) and HSP70 (C) levels normalized to the GAPDH control. Error bars indicated 1 standard deviation of the mean. (B, C) Lysates harvested on day 5 low serum, low glucose media from three independent transfections. None of the values reported were statistically significantly different (ANOVA).

2.3.3 Mistranslation following antibiotic selection.

In an attempt to control for transfection efficiency in these experiments, we also observed elevated mistranslation in cells following selection on geneticin. The selected cells maintained the pCDNA plasmid bearing the GFP reporter and either the wild type or mistranslating tRNA^{Pro}. Following selection, there was no obvious change in morphology when the tRNA^{Pro} (G3:U70) mutant was expressed compared to tRNA^{Pro}, though morphological heterogeneity could be seen in both cell lines (Fig S2.1). Since geneticin inhibits bacterial growth by interfering with ribosome

function, and similar aminoglycosides decrease ribosome fidelity in bacterial²⁵ and mammalian²⁶ translation systems, we anticipated the potential for elevated mistranslation in these cells. Although we did not observe elevated mistranslation in cells expressing the wild type tRNA^{Pro}, analysis by fluorescence microscopy suggested that GFP D129P fluorescence was restored at a low level (~3%, p-value = 1.2×10^{-8}) by tRNA^{Pro} (G3:U70)-dependent mistranslation with Ala (Fig S2.2). This result is concordant with our observations in nutrient deprived cells (Fig 2.3) as the cells under antibiotic selection are also undergoing stress.

2.3.4 Mistranslation by tRNA^{Pro} (G3:U70) does not induce a heat-shock response.

In our previous studies of mistranslation induced by tRNA^{Pro} (G3:U70) in yeast, the heat-shock response was observed in mistranslating cells¹¹. Here, HEK 293T cells were harvested following 4 days of growth on low serum and low glucose medium where mistranslation was observed. Using GAPDH as a loading control, we immunoblotted to detect markers for the heat shock response (HSP70, HSP90). Despite the fact that cells were mistranslating Pro codons with Ala at a rate of ~5%, we were unable to detect significant differences in the levels of HSP70 or HSP90 in comparison to cells expressing the wild type tRNA^{Pro} (Fig 2.4).

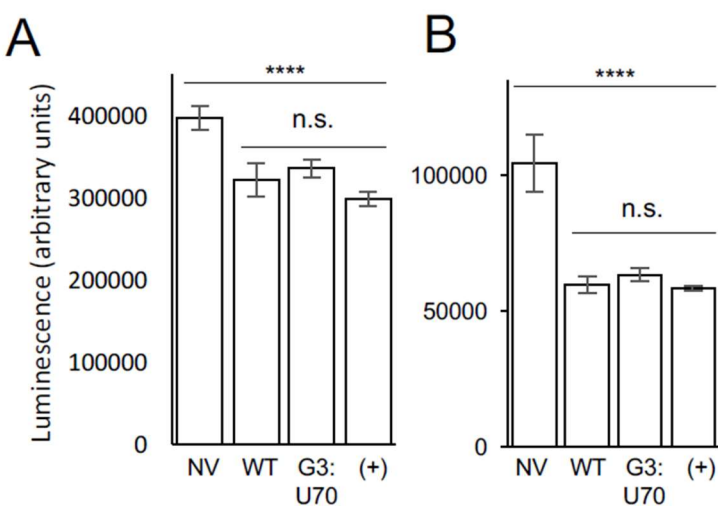


Figure 2.5. Viability of mistranslating cells. HEK 293T cell cultures were transfected in triplicate with lipofectamine only (No Vector, NV), or plasmid harboring tRNA^{Pro} and EGFP D129P (WT); tRNA^{Pro} G3:U70 and EGFP D129P (G3:U70); or tRNA^{Pro} and EGFP D129A (+).

Transfected cells were assayed one day post-transfection (A) or after four days incubation in low serum, low glucose media (B). Viability assays were performed following manufacturer's instructions (see Methods) using three technical replicates per transfection. Plots show mean luminescence, which correlates with cellular ATP levels. Error bars indicated 1 standard deviation of the mean. Stars depict the indicated statistically significant differences according to single-factor ANOVA (**** = $p < 0.0001$; *** = $p < 0.001$; n.s. = $p > 0.05$).

2.3.5 Viability of mistranslating cells.

Using a standard assay for cell viability, based on the production of ATP in metabolically active cells (see Methods), we determined the impact of tRNA^{Pro} and tRNA^{Pro} G3:U70 expression on the viability of HEK 293T cells in culture. Cells were transfected with the indicated EGFP and tRNA^{Pro} expressing pCDNA 3.1 plasmids (Fig 2.5) and grown in rich media or in low nutrient conditions. Expression of the EGFP protein reduced cell viability marginally in comparison to the un-transfected control cells ($p < 0.0001$, Fig 2.5A). In agreement with our measurements of the mistranslation as indicated by the GFP reporter, cell viability in rich media was unaffected by expression of tRNA^{Pro} in comparison to the mistranslating tRNA^{Pro} G3:U70 mutant (Fig 2.5A). In low serum, low glucose medium, the viability of all cultures decreased, yet cells expressing tRNA^{Pro} G3:U70 were equally as viable as cells expressing the wildtype tRNA^{Pro} (Fig 2.5B).

2.4 Discussion

2.4.1 Transfer RNA genes occur in excess.

Translation of the 61 sense codons in the genetic code table requires a theoretical minimum of 32 tRNAs to translate all 20 amino acids²⁷. There are examples of organelles (human mitochondria, 22 tRNAs), parasites (*Borrelia burgdorferi*, 32 tRNAs; *Mycoplasma pulmonis*, 28 tRNAs), and obligate symbiotic microbes (*Sulcia muelleri*, 31 tRNAs) with a small number of tRNA genes, some of which fall below the 'theoretical' limit based on wobble decoding²⁸. In the case of organelles, a complete set of tRNAs for protein synthesis is achieved via tRNA import from nuclear encoded tDNAs²⁹ or perhaps super-wobbling (i.e., one tRNA reading 4 codons) as demonstrated with tRNA^{Gly} in tobacco plants³⁰. The fact that no free-living organisms has less than 32 tRNAs already indicates that the coding problem is more complex or more elaborate than

the simple mechanics of matching codon to anticodon and wobble decoding. In free living microbes, the smallest sets of tRNA genes are found in the model minimal genome of *Mycoplasma genitalium* (36 tRNA genes), while the hyperthermophile *Methanopyrus kandleri* encodes just 34 tRNAs genes.

The number and diversity of tRNA genes expands in correlation with the complexity of the organism³¹. For example, yeast encodes 275 tRNAs whereas humans have 610 tRNA genes²⁸. None of the human tRNA genes are predicted as pseudogenes²⁸. Most human tRNA genes are expressed in some cells or tissues²⁸, and tRNA genes show tissue³² and cell-line specific expression patterns³³. Even individual tissues express a large number of these tRNA genes. For example, in human primary liver tissue, 223 tRNA genes are actively transcribed³⁴. The reason for the overabundance of tRNA genes in human and higher eukaryotes has remained a mystery.

2.4.2 A single tRNA mutant induces mistranslation in human cells.

Among the human population, tRNA mutations are common. Based on sequence data from the 1000-genomes project, more than half of individuals (54%) contain at least 1 mutant tRNA and 20% of individuals harbor two or more mutant tRNAs³⁵. Fascinatingly, tRNA gene copy number also varies even among a small group of individuals³⁶.

Mistranslating tRNAs are present in the reference human genome. Recent work demonstrated tRNA variants with a G4:U69 pair enable aminoacylation with Ala. G4:U69 mutants are common in eukaryotic genomes and 1 of the 30 copies of tRNA^{Cys} in the human genome contains such a GU pair. The mutation confers Ala accepting identity on this tRNA^{Cys} variant in vitro and in HEK 293T cells in culture²³.

Given the complexity of the human tRNAome and its diversity in the human population, we set out to determine if a single tRNA mutant would induce mistranslation in human cells in culture, and to characterize the consequences of this mistranslation. In our previous studies in yeast, expression of a mutant tRNA caused ~6% mis-incorporation at Pro codons in cells grown in nutrient rich conditions¹¹. Here we expressed a homologous mistranslating tRNA^{Pro} mutant in human cells in culture, and we were unable to detect mistranslation in rich media. Only upon subjecting the cells to stresses, including nutrient deprivation or antibiotic selection, did we observe a similar level of mistranslation (5%) induced by the tRNA^{Pro} G3:U70 mutant. The results suggest that the human cell is potentially more resistant to mistranslation caused by a single tRNA

gene. However, under conditions of stress or nutrient deprivation, mis-made protein could be readily detected. We speculate that under stress conditions human cells are either less able to degrade mis-made protein, deacylate mis-charged tRNAs^{37,38} at a lower frequency, or more readily use the mis-aminoacylated tRNA in translation.

2.4.3 tRNA-dependent mistranslation linked to disease.

There is growing evidence connecting mistranslation to disease^{19,39-41}. Many efforts focus on AARSs, either affected by mutations or oxidative damage¹³, that promote mis-aminoacylation of their cognate tRNAs^{12, 42} or of non-cognate tRNAs⁴³, both of which can then lead to mistranslation. The relevance of analyzing the role of tRNA mutants in disease was highlighted by a recent study that identified a mutation in a single tRNA gene specifically expressed in the central nervous system. The tRNA mutation caused a synthetic neurodegenerative phenotype in mice also lacking the gene GTPB2, which is involved in ribosome recycling⁴⁴. In agreement with our findings, the impact of the tRNA mutation alone, in the absence of stress or a synthetic defect, was not sufficient to cause significant mistranslation. This recently established link between tRNA mutations and disease suggests that further studies will uncover a greater role for human tRNA variants in health and disease.

2.4.4 Detecting tRNA-dependent mistranslation in live cells.

A key difference between our work and previous work with editing defective tRNA synthetases is that the AARS mutants mis-aminoacylate (to some level) all tRNA isoacceptors for the cognate amino acid. In our experiments, we expressed a single tRNA^{Pro} mutant. Although this tRNA is specifically mis-aminoacylated with Ala, it then competes with properly aminoacylated tRNA^{Pro} isoacceptors expressed from 46 genetic loci in the diploid human genome. This contrasts with our previous studies in yeast, where mistranslating tRNA^{Pro} competes with only 10 tRNA^{Pro} genes. This difference in tRNA copy number may explain why the tRNA^{Pro} G3:U70 readily mistranslates in yeast cells in rich media, whereas in human cells, stress was required to enhance tRNA^{Pro} G3:U70 induced mistranslation. It may be that the large number of human tRNA genes serves as a ‘buffer’ against mistranslation induced by single gene tRNA mutants.

In this work, we demonstrated the use of a novel mistranslation reporter that is specifically sensitive to mistranslation at Pro codons in human cells. Given the sensitivity of GFP to mutations

at key positions, a number of other groups have developed GFP-based reporters for different types of mistranslation. GFP (M72Q) has been used extensively in mammalian cells to detect natural levels of methionine mis-incorporation, which increases 10-fold in response to oxidative stress^{16, 43}. GFP (E222Q)⁴⁵ and GFP (T65V)⁴⁶ are examples of reporters that detect mistranslation of glutamine and valine codons, respectively. Our GFP (D129P) reporter extends the range of GFP-based reporters for use in live human cells to include a new type of mistranslation.

A complementary approach involves using quantitative mass spectrometry to identify mistranslation in a GFP reporter⁴⁷. In this approach, the fluorescence output of GFP was not used to detect mistranslation, rather a particular residue in GFP was chosen such that tryptic peptides that include the site are ideal for detection by MS. The technique, referred to as MS-READ, is unbiased as it can detect any type of mistranslation event, including detection of exceedingly low levels of amino acid mis-incorporation. Although this quantitative method cannot be applied in live cell imaging, it can be used in a kinetic mode to chart mistranslation in cells at specified time points. Taken together, these mistranslation reporters provide the opportunity to comprehensively identify mistranslation induced by natural and disease-linked tRNA variants.

2.4.5 Cellular adaptation to mistranslation.

In yeast, tRNA^{Pro} G3:U70 induces a heat shock response¹¹. Robust proteasomal activity was also required to maintain wild-type like growth with this proteome-wide mistranslation¹¹. In the current study, we were unable to detect a significant impact of tRNA-dependent mistranslation on the heat shock response or on cell viability in HEK 293T cells. In contrast to the view of a highly accurate proteome, there are many examples in bacteria and eukaryotic cells (see Introduction), where levels of mistranslation of 5-10% have a negligible impact on cell growth and viability. For example, yeast cells expressing an editing defective phenylalanyl-tRNA synthetase (PheRS) in complete media showed no phenotypic defect, despite mis-incorporation of tyrosine at phenylalanine codons⁷. When these mistranslating yeast cells were grown under conditions of amino acid stress, i.e., in media containing a 1/400 ratio of Phe/Tyr, ~5% of phenylalanine codons were mistranslated, which resulted in viable cells with a 50% reduction in growth rate. The strain failed to mount a heat shock response despite proteome wide mistranslation. The growth defect resulted from the fact that the PheRS editing defective yeast strain was ineffective in activating amino acid and protein stress response pathways to this particular type of mistranslation⁷. These

striking observations reveal the complex and varied cellular responses that manifest as a result of distinct types of mistranslation, and highlight the need for a greater understanding of mistranslation in the context of cellular physiology and disease.

2.5 Conclusion

All cells have an inherent level of mistranslation^{8, 14}. Cells, from bacteria to humans, have evolved mechanisms to cope with not only this inherent level of mistranslation, but, also elevated levels resulting from a variety sources including oxidative and nutrient stress as well as AARS and tRNA mutations. The study noted above⁷ and similar studies (reviewed in⁴⁸) are beginning to shed light on the pathways activated in response to mistranslation, and of particular interest is the interaction of mistranslation with cell stress. These advances are motivating our on-going work to further characterize the mammalian cellular response to Pro codon mistranslation in stress conditions and cellular models of disease. In addition, our approach represents a feasible high-throughput cell-based screen for tRNA function. We anticipate that the GFP reporter we developed here will have application in mapping the function of human tRNA variants in the natural population and in elucidating tRNA mutations implicated as drivers or perhaps suppressors of disease.

2.6 References

1. Söll D, Ohtsuka E, Jones DS, Lohrmann R, Hayatsu H, Nishimura S, et al. Studies on polynucleotides, XLIX. Stimulation of the binding of aminoacyl-sRNA's to ribosomes by ribotrinucleotides and a survey of codon assignments for 20 amino acids. *Proc Natl Acad Sci U S A* 1965; 54:1378-85.
2. Brimacombe R, Trupin J, Nirenberg M, Leder P, Bernfield M, Jaouni T. RNA codewords and protein synthesis, 8. Nucleotide sequences of synonym codons for arginine, valine, cysteine, and alanine. *Proc Natl Acad Sci U S A* 1965; 54:954-60.
3. Orgel LE. The maintenance of the accuracy of protein synthesis and its relevance to ageing. *Proc Natl Acad Sci U S A* 1963; 49:517-21.
4. Crick FH. The origin of the genetic code. *J Mol Biol* 1968; 38:367-79.
5. Ling J, O'Donoghue P, Söll D. Genetic code flexibility in microorganisms: novel mechanisms and impact on physiology. *Nat Rev Microbiol* 2015; 13:707-21.
6. Ruan B, Palioura S, Sabina J, Marvin-Guy L, Kochhar S, Larossa RA, et al. Quality control despite mistranslation caused by an ambiguous genetic code. *Proc Natl Acad Sci U S A* 2008; 105:16502-7.
7. Mohler K, Mann R, Bullwinkle TJ, Hopkins K, Hwang L, Reynolds NM, et al. Editing of misaminoacylated tRNA controls the sensitivity of amino acid stress responses in *Saccharomyces cerevisiae*. *Nucleic Acids Res* 2017; 45:3985-96.

8. Schwartz MH, Pan T. Function and origin of mistranslation in distinct cellular contexts. *Crit Rev Biochem Mol Biol* 2017; 52:205-19.
9. Drummond DA, Wilke CO. The evolutionary consequences of erroneous protein synthesis. *Nat Rev Genet* 2009; 10:715-24.
10. Kramer EB, Vallabhaneni H, Mayer LM, Farabaugh PJ. A comprehensive analysis of translational missense errors in the yeast *Saccharomyces cerevisiae*. *RNA* 2010; 16:1797-808.
11. Hoffman KS, Berg MD, Shilton BH, Brandl CJ, O'Donoghue P. Genetic selection for mistranslation rescues a defective co-chaperone in yeast. *Nucleic Acids Res* 2017; 45:3407-21.
12. Raina M, Moghal A, Kano A, Jerums M, Schnier PD, Luo S, et al. Reduced amino acid specificity of mammalian tyrosyl-tRNA synthetase is associated with elevated mistranslation of Tyr codons. *J Biol Chem* 2014; 289:17780-90.
13. Fan Y, Wu J, Ung MH, De Lay N, Cheng C, Ling J. Protein mistranslation protects bacteria against oxidative stress. *Nucleic Acids Res* 2015; 43:1740-8.
14. Wang X, Pan T. Stress Response and Adaptation Mediated by Amino Acid Misincorporation during Protein Synthesis. *Adv Nutr* 2016; 7:773S-9S.
15. Ling J, Söll D. Severe oxidative stress induces protein mistranslation through impairment of an aminoacyl-tRNA synthetase editing site. *Proc Natl Acad Sci U S A* 2010; 107:4028-33.
16. Gomes AC, Kordala AJ, Strack R, Wang X, Geslain R, Delaney K, et al. A dual fluorescent reporter for the investigation of methionine mistranslation in live cells. *RNA* 2016; 22:467-76.
17. Netzer N, Goodenbour JM, David A, Dittmar KA, Jones RB, Schneider JR, et al. Innate immune and chemically triggered oxidative stress modifies translational fidelity. *Nature* 2009; 462:522-6.
18. Lee JY, Kim DG, Kim BG, Yang WS, Hong J, Kang T, et al. Promiscuous methionyl-tRNA synthetase mediates adaptive mistranslation to protect cells against oxidative stress. *J Cell Sci* 2014; 127:4234-45.
19. Hoffman KS, O'Donoghue P, Brandl CJ. Mistranslation: from adaptations to applications. *Biochim Biophys Acta* 2017; doi: 10.1016/j.bbagen.2017.01.031.
20. Berg MD, Hoffman KS, Genereaux J, Mian S, Trussler RS, Haniford DB, et al. Evolving Mistranslating tRNAs Through a Phenotypically Ambivalent Intermediate in *Saccharomyces cerevisiae*. *Genetics* 2017; 206:1865-79.
21. Naganuma M, Sekine S, Chong YE, Guo M, Yang XL, Gamper H, et al. The selective tRNA aminoacylation mechanism based on a single G•U pair. *Nature* 2014; 510:507-11.
22. Park SJ, Hou YM, Schimmel P. A single base pair affects binding and catalytic parameters in the molecular recognition of a transfer RNA. *Biochemistry* 1989; 28:2740-6.
23. Sun L, Gomes AC, He W, Zhou H, Wang X, Pan DW, et al. Evolutionary Gain of Alanine Mischarging to Noncognate tRNAs with a G4:U69 Base Pair. *J Am Chem Soc* 2016; 138:12948-55.
24. O'Donoghue P, Sheppard K, Nureki O, Söll D. Rational design of an evolutionary precursor of glutamyl-tRNA synthetase. *Proc Natl Acad Sci U S A* 2011; 108:20485-90.
25. Ling J, Cho C, Guo LT, Aerni HR, Rinehart J, Söll D. Protein aggregation caused by aminoglycoside action is prevented by a hydrogen peroxide scavenger. *Mol Cell* 2012; 48:713-22.
26. Manuvakhova M, Keeling K, Bedwell DM. Aminoglycoside antibiotics mediate context-dependent suppression of termination codons in a mammalian translation system. *RNA* 2000; 6:1044-55.
27. Crick FH. Codon--anticodon pairing: the wobble hypothesis. *J Mol Biol* 1966; 19:548-55.

28. Chan PP, Lowe TM. GtRNAdb 2.0: an expanded database of transfer RNA genes identified in complete and draft genomes. *Nucleic Acids Res* 2016; 44:D184-9.
29. Schneider A. Mitochondrial tRNA import and its consequences for mitochondrial translation. *Annu Rev Biochem* 2011; 80:1033-53.
30. Rogalski M, Karcher D, Bock R. Superwobbling facilitates translation with reduced tRNA sets. *Nat Struct Mol Biol* 2008; 15:192-8.
31. Goodenbour JM, Pan T. Diversity of tRNA genes in eukaryotes. *Nucleic Acids Res* 2006; 34:6137-46.
32. Dittmar KA, Goodenbour JM, Pan T. Tissue-specific differences in human transfer RNA expression. *PLoS Genet* 2006; 2:e221.
33. Pavon-Eternod M, Gomes S, Geslain R, Dai Q, Rosner MR, Pan T. tRNA over-expression in breast cancer and functional consequences. *Nucleic Acids Res* 2009; 37:7268-80.
34. Kutter C, Brown GD, Goncalves A, Wilson MD, Watt S, Brazma A, et al. Pol III binding in six mammals shows conservation among amino acid isotypes despite divergence among tRNA genes. *Nat Genet* 2011; 43:948-55.
35. Parisien M, Wang X, Pan T. Diversity of human tRNA genes from the 1000-genomes project. *RNA Biol* 2013; 10:1853-67.
36. Iben JR, Maraia RJ. tRNA gene copy number variation in humans. *Gene* 2014; 536:376-84.
37. Ruan LL, Zhou XL, Tan M, Wang ED. Human cytoplasmic ProX edits mischarged tRNA^{Pro} with amino acid but not tRNA specificity. *Biochem J* 2013; 450:243-52.
38. Vargas-Rodriguez O, Musier-Forsyth K. Exclusive use of trans-editing domains prevents proline mistranslation. *J Biol Chem* 2013; 288:14391-9.
39. Schimmel P, Guo M. A tipping point for mistranslation and disease. *Nat Struct Mol Biol* 2009; 16:348-9.
40. Ribas de Pouplana L, Santos MA, Zhu JH, Farabaugh PJ, Javid B. Protein mistranslation: friend or foe? *Trends Biochem Sci* 2014; 39:355-62.
41. Lu J, Bergert M, Walther A, Suter B. Double-sieving-defective aminoacyl-tRNA synthetase causes protein mistranslation and affects cellular physiology and development. *Nat Commun* 2014; 5:5650.
42. Liu Y, Satz JS, Vo MN, Nangle LA, Schimmel P, Ackerman SL. Deficiencies in tRNA synthetase editing activity cause cardioproteinopathy. *Proc Natl Acad Sci USA* 2014; 111:17570-5.
43. Wang X, Pan T. Methionine Mistranslation Bypasses the Restraint of the Genetic Code to Generate Mutant Proteins with Distinct Activities. *PLoS Genet* 2015; 11:e1005745.
44. Ishimura R, Nagy G, Dotu I, Zhou H, Yang XL, Schimmel P, et al. RNA function. Ribosome stalling induced by mutation of a CNS-specific tRNA causes neurodegeneration. *Science* 2014; 345:455-9.
45. Su HW, Zhu JH, Li H, Cai RJ, Ealand C, Wang X, et al. The essential mycobacterial amidotransferase GatCAB is a modulator of specific translational fidelity. *Nat Microbiol* 2016; 1:16147.
46. Nangle LA, Motta CM, Schimmel P. Global effects of mistranslation from an editing defect in mammalian cells. *Chem Biol* 2006; 13:1091-100.
47. Mohler K, Aerni HR, Gassaway B, Ling J, Ibba M, Rinehart J. MS-READ: Quantitative measurement of amino acid incorporation. *Biochim Biophys Acta* 2017; doi: 10.1016/j.bbagen.2017.01.025.

48. Moghal A, Mohler K, Ibba M. Mistranslation of the genetic code. FEBS Lett 2014; 588:4305-10.

2.7 Supplemental information

2.7.1 Supporting methods

Production of T7 RNA polymerase.

T7 RNA polymerase (6xHis-tagged T7 RNAP) was expressed from pT7-911 vector in 1L *E. coli* culture at 37°C in LB + 100 µg/mL ampicillin. Cultures were induced with 1 mM Isopropyl β-D-1-thiogalactopyranoside at OD₆₀₀ = 0.6 and incubated for 3 hours at 20°C before harvesting cells by centrifugation. Recombinant T7 RNAP was purified by Ni-NTA affinity chromatography. The column was washed with 20 column volumes wash buffer (10 mM imidazole, 50 mM Tris-HCl pH 8.0, 100 mM NaCl, 5% glycerol, 5 mM β-mercaptoethanol) and eluted with 10 column volumes elution buffer (500 mM imidazole, 50 mM Tris-HCl pH 8.0, 100 mM NaCl, 5% glycerol, 5 mM β-mercaptoethanol). Elution fractions were analyzed by coomassie-stained SDS-PAGE and fractions containing T7 RNA polymerase at the correct molecular weight were pooled for dialysis. Pooled elution fractions were dialyzed overnight at 4°C in storage buffer (20 mM HEPES-KOH pH 8.0, 1 mM EDTA, 100 mM NaCl, 3 mM dithiothreitol, 50% glycerol) and stored at -20°C.

In vitro tRNA transcription and radiolabeling.

Transcription reactions were performed as previously¹ in a reaction containing 200 ng/µl DNA template in the presence 40 mM HEPES-KOH pH 8.0, 22 mM MgCl₂, 5 mM dithiothreitol, 1 mM spermidine, 4 mM of NTPs (ATP, GTP, CTP, and UTP), and 30 nM T7 RNAP. Samples were run on 12% urea (7M) polyacrylamide gels at 40 W. Correct-sized bands were visualized with a UV transilluminator and excised. Gel plugs were vortexed and dissolved in 10 ml of 3 M sodium acetate (pH 5.2) at 4°C for 2 hours or overnight. The solubilized tRNAs solution was then filter sterilized (2 µm). Filtrates from three reactions (2 × 2-hour, 1 × overnight incubation in 3 M sodium acetate pH 5.2) were pooled together and precipitated with an equal volume of 100% isopropanol at -80°C overnight. Samples were centrifuged at 10,000 × g for one hour, supernatant was decanted, and the pellet was washed with 70% ethanol. Centrifugation was then repeated, supernatant was removed and pellets were air-dried before re-suspension in sterile milli-Q water.

Folding and radiolabeling of tRNA.

tRNAs were denatured in a 95°C water bath for 5 min then cooled gradually to room temperature. At 65°C, MgCl₂ was added to a final concentration of 10 mM to assist with folding. 50 µl reactions were prepared with 1 µM tRNA, 100 mM Tris-HCl pH 8.0, 10 mM dithiothreitol, 40 mM MgCl₂, 10 µM NaPPi, 200 nCi of α-³²[P]-ATP (PerkinElmer) and 5 µl of CCA adding enzyme (produced as previously¹). The reaction was incubated at 37°C for 1 hour. Radio-labelled tRNAs were purified using Biospin30 column (Bio-Rad).

2.7.2 Supporting tables

Table S2.1. Sequences of tRNA construct oligos

	Sequence (5' to 3')
tRNA^{Ala} Watson strand	CTAGATAATACGACTCACTATAGGGGGTATAGCTCAGTGG TAGAGCGCGTGCTTAGCATGCACGAGGTCCTGGGTTCGA TCCCCAGTACCTCCACCATGCATG
tRNA^{Ala} Crick strand	GATCCATGCATGGTGGAGGTAAGGATCGAACCCAGG ACCTCGTGCATGCTAAGCACGCGCTCTACCACTGAGCTAT ACCCCTATAGTGAGTCGTATTAT
tRNA^{Pro} Watson strand	CTAGATAATACGACTCACTATAGGCTCGTTGGTCTAGTGG TATGATTCTCGCTTTGGGTGCGAGAGGTCCCGGGTTCAA ATCCCGGACGAGCCCCCATGCATG
tRNA^{Pro} Crick strand	GATCCATGCATGGGGGCTCGTCCGGGATTTGAACCCGGG ACCTCTCGCACCCAAAGCGAGAATCATACCACTAGACCA ACGAGCCTATAGTGAGTCGTATTAT
tRNA^{Pro} mutant Watson strand	CTAGATAATACGACTCACTATAGGCTCGTTGGTCTAGTGG TATGATTCTCGCTTTGGGTGCGAGAGGTCCCGGGTTCAA ATCCCGGACGATCCCCCATGCATG
tRNA^{Pro} mutant Crick strand	GATCCATGCATGGGGGATCGTCCGGGATTTGAACCCGGG ACCTCTCGCACCCAAAGCGAGAATCATACCACTAGACCA ACGAGCCTATAGTGAGTCGTATTAT

Table S2.2. Sequences of primers for template PCR

	Sequence (5' to 3')
Upstream T7 promoter forward	GTTGGGAAGGGCGATCGGTG
tRNA^{Ala} forward	CTAGATAATACGACTCACTATAGGGGG
tRNA^{Ala} reverse	TGGTGGAGGTACTGGGGAT
tRNA^{Pro} forward	CTAGATAATACGACTCACTATAGGC
tRNA^{Pro} reverse	TGGGGGCTCGTCCGGGA
tRNA^{Pro} mutant forward	TAATACGACTCACTATAGGGTCG
tRNA^{Pro} mutant reverse	TGGGGGATCGTCCGGGA

2.7.3 Supporting figures

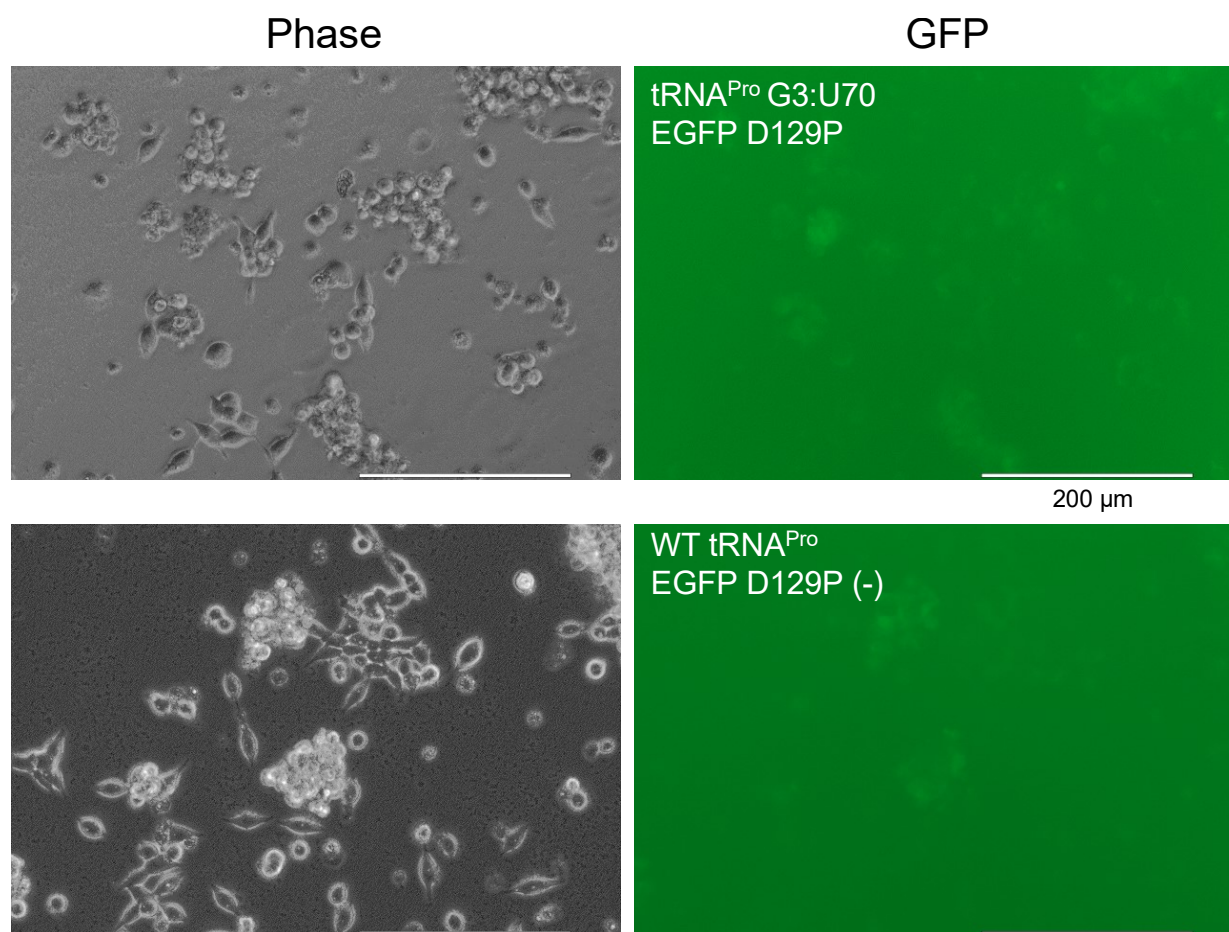


Figure S2.1. Overexpression of tRNA^{Pro} G3:U70 had no obvious effect on cell morphology compared to wild-type tRNA^{Pro}. Images captured by light (phase) or fluorescence (GFP; ex/em = 470/525 nm) microscopy on day three low serum, low glucose media (see main text, Fig. 2.3). Scale bars depict 200 μm distance.

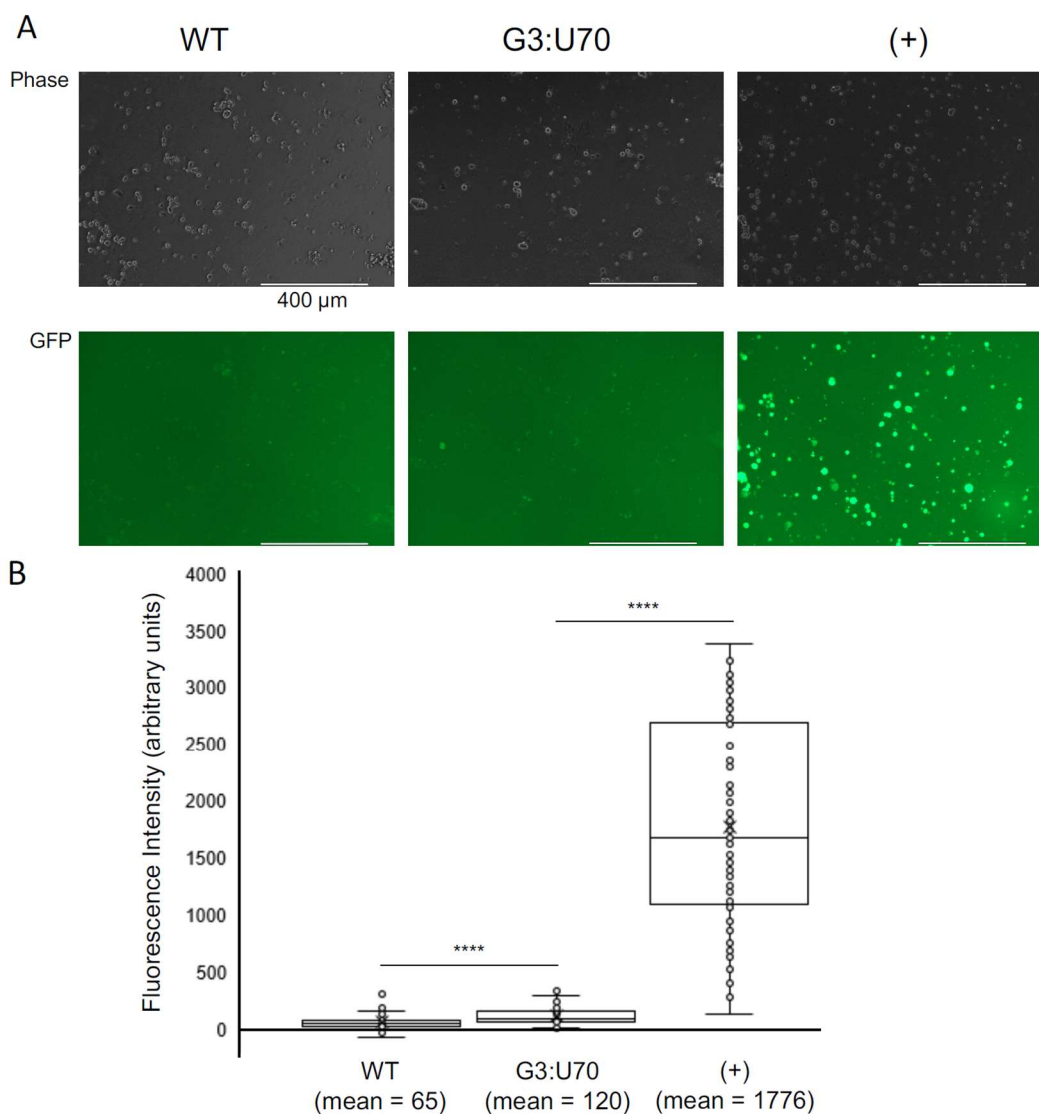


Figure S2.2. Visualizing mistranslation after selection in Geneticin. HEK 293T cell cultures were transfected with plasmid harboring tRNA^{Pro} and EGFP D129P (WT); tRNA^{Pro} G3:U70 and EGFP D129P (G3:U70); or tRNA^{Pro} and EGFP D129A (+). All plasmids have a pCDNA 3.1 (+) backbone containing the bacterial NeoR gene. Selection cultures were maintained in Geneticin (G418) containing media for 25 days prior to quantification. (A) representative images captured by light (phase) or fluorescence (GFP; ex/em = 470/525) microscopy at 4 \times magnification. Scale bars represent 400 μ m distance. (B) Box and whisker plots of EGFP foci intensity. Horizontal demarcations depict quartiles with median centered. Dots represent the general distribution of 100 foci measured in each plot. Stars indicate statistically significant differences according to single-factor ANOVA (**** = $p < 0.0001$). Means are noted below each blot.

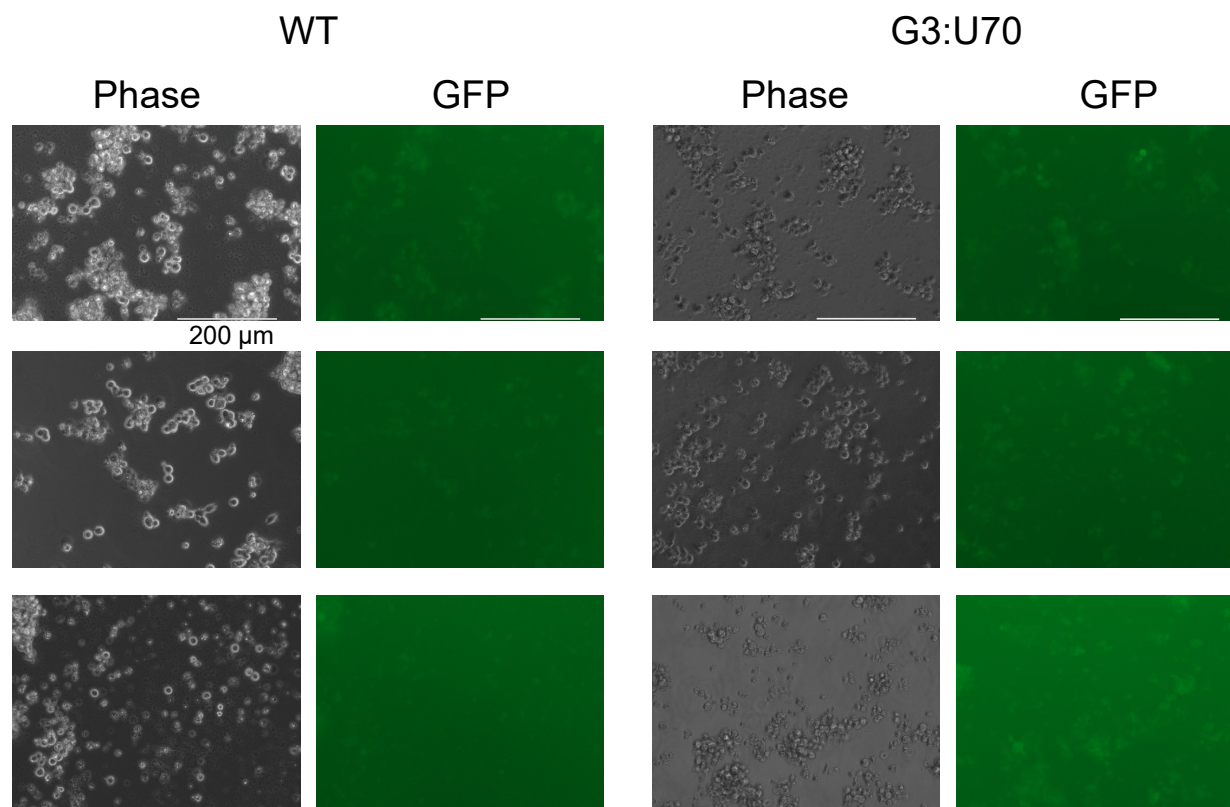


Figure S2.3. Additional images from low serum low glucose growth, experiment day 5. HEK 293T cell cultures were transfected with plasmid harboring tRNA^{Pro} and EGFP D129P (WT); or tRNA^{Pro} G3:U70 and EGFP D129P (G3:U70). Images captured by light (phase) or fluorescence (GFP; ex/em = 470/525) microscopy at 20 × magnification. Scale bars represent 200 μm distance. See main text (Fig. 2.3 and methods) for experimental details.

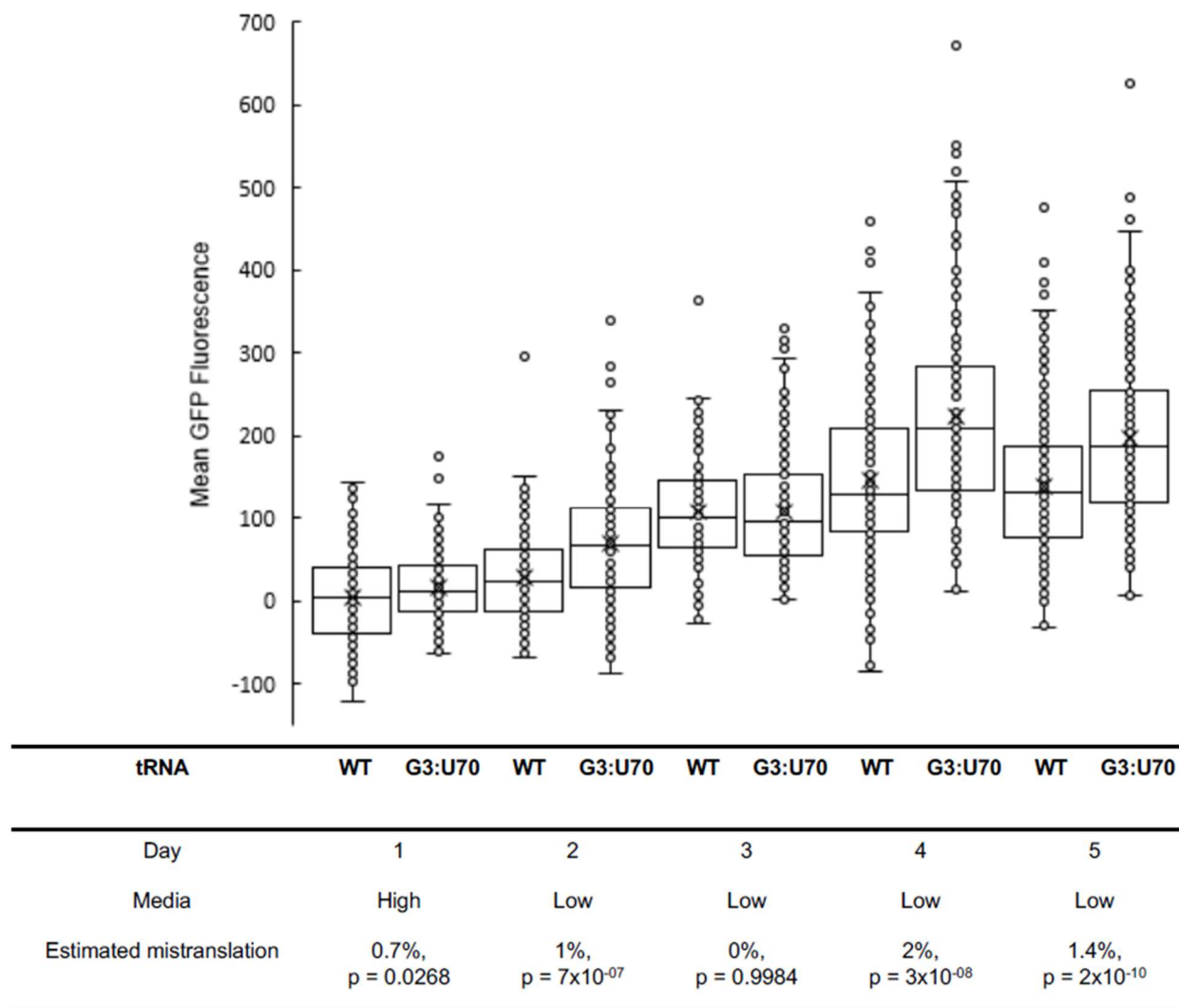


Figure S2.4. Mistranslation under glucose and serum starvation. Box and whisker plots showing data from figure 2.3 (main text) with EGFP D129A data set removed and vertical axis zoomed in to more clearly show differences caused by mistranslating tRNA in comparison to the wild type tRNA. HEK 293T cell cultures were transfected with plasmid harboring tRNA^{Pro} and EGFP D129P (WT); or tRNA^{Pro} G3:U70 and EGFP D129P (G3:U70). See main text (Fig. 2.3 and methods) for experimental details.

2.7.4 Supplemental references

1. O'Donoghue P, Sheppard K, Nureki O, Soll D. Rational design of an evolutionary precursor of glutamyl-tRNA synthetase. Proc Natl Acad Sci USA 2011; 108:20485-90.

Chapter 3

3. Formation and persistence of polyglutamine aggregates in mistranslating cells¹

3.1 Introduction

High-fidelity translation of messenger RNAs (mRNAs) was considered essential for life by assuring the functional reproduction of ‘*so many highly evolved protein molecules*’ (1). In fact, translation of mRNAs is the most erroneous step on the path from gene expression to protein synthesis in cells (2-5). Errors in protein synthesis can result from ribosome stalling or pausing, frameshifting, and amino acid mis-incorporation. Error rates in cells are normally considered low, with 1 mis-incorporation event occurring for every 1,000 to 10,000 codons translated (6,7). Cells can tolerate or even derive a selective advantage from elevated mistranslation rates as a result of stress (8-11), chemical treatment (12-14), or mutations in the protein synthesis machinery (15-18).

The conserved sequence and structure of transfer RNAs (tRNAs) are a major determinant of proteome fidelity. Consequently, single nucleotide substitutions in individual tRNA genes can lead to proteome-wide mistranslation in bacteria (19,20), yeast (18), and mammalian cells (17,21,22). The relevance of tRNA mutations to human disease is becoming more evident since the discovery that cytoplasmic tRNA variants, including those likely to cause errors in translation, are more common in the human population than previously recognized (23). Sequencing efforts, such as the 1000 Genomes Project and our own work (24), confirm that mistranslating tRNA mutants occur in individuals as both rare and common variants with some found in 1-5% of the population.

Mutations in protein coding genes that cause mistranslation, such as aminoacyl-tRNA synthetases, are associated with neurodegeneration in mice (25) and *Drosophila* (26). Mutant tRNAs that lead to a loss of tRNA function were linked to neurodegenerative disease and neuronal phenotypic defects in mice (27,28) and a genetic disorder in humans (29). Mitochondrial tRNA variants have long been associated with human diseases, including neurodegeneration (30). MELAS (mitochondrial myopathy, encephalopathy, lactic acidosis, and stroke-like episodes) (31) and MERRF (myoclonus epilepsy associated with ragged red fibers) (32) are two major

¹Work in this chapter was published in: Lant, J.T., Kiri, R., Duennwald, M.L., O’Donoghue, P. (2021). Formation and persistence of polyglutamine aggregates in mistranslating cells. *Nucleic Acids Research*

neurodegenerative diseases caused by mutations in mitochondrial tRNAs. In both cases, the mutant tRNAs, which occur at different locations in the tRNA body, cannot be properly post-transcriptionally modified at position 34 of the anticodon. Single mitochondrial tRNA mutants lacking the base 34 taurine modification are less efficient in decoding their cognate codons, resulting in reduced protein synthesis in the mitochondria. The tRNA^{Leu} variants lacking U34 modification can read UUA but not UUG Leu codons (33).

Cytoplasmic tRNAs that specifically cause amino acid mis-incorporation, however, have not been assessed for their contribution to neurodegenerative disease. Recently, loss-of-function cytoplasmic tRNA variants emerged with connections to neurodegeneration (23). The n-Tr20 mutant is a tRNA^{Arg}_{CTC} with a C50T substitution in the T-arm of the tRNA (27). The mutation leads to a processing defect and the mature tRNA is not produced. Although there are five nearly identical tRNA^{Arg}_{CTC} genes in the genome, the affected tRNA gene normally shows high expression in the cerebellum where the n-Tr20 gene product accounts for 60% of the tRNA^{Arg}_{CUC} pool (27). In a screen for neurodegeneration in mice, this tRNA mutant was found to be causative when co-incident with a mutation in the ribosome recycling factor GTPBP2. Together both mutants act to stall the ribosome and reduce the rate of protein synthesis. Mice with these mutations displayed multiple neurodegenerative phenotypes, locomotor defects, and died at 8 to 9 weeks (27). Further studies of this tRNA^{Arg} mutant found altered synaptic transmission and increased susceptibility to seizures in mice (28).

Mistranslation is also associated with proteotoxic stress and neurodegeneration in mice (25) and patient-derived cell lines (34). Many studies have focused on tRNA synthetase mutants, particularly those defective in editing mis-charged amino acids. One example involves an editing defective AlaRS that mis-charges tRNA^{Ala} with Ser, causing increased levels of misfolded proteins in neurons. Mice expressing the mutant AlaRS displayed reduced body weight and a neurodegenerative phenotype resulting from cell loss and ataxia of Purkinje cells in the cerebellum (25). Another AlaRS editing-defective mutation caused cardioproteinopathy in mice, characterized by protein aggregation in cardiomyocytes, cardiac fibrosis and dysfunction (35). AlaRS mutants are also associated with additional diseases of the nervous system, including Charcot-Marie-Tooth (CMT) disease (36) and early-onset epileptic encephalopathy (37).

Inspired by these studies, we hypothesized that a tRNA variant that also caused mistranslation will act to modify the progression of neurodegenerative disease at the molecular level by affecting

protein homeostasis and protein aggregation. We investigated the disease-modifying potential of mistranslating tRNA variants in combination with multiple mammalian cellular models of Huntington's disease (HD). HD, like many other neurodegenerative diseases (38), is characterized by the misfolding and aggregation of specific proteins. Protein misfolding typically has the greatest impact on post-mitotic cells such as those found in the heart, brain, and eye (25,39). Since these cells cannot readily divide or undergo apoptosis, misfolded proteins and protein aggregates accumulate over time, leading to dysregulation of the proteome, cytotoxicity, and eventually cell death (39).

Disorders characterized by protein folding stress or by impaired protein quality control may be particularly susceptible to the effects of mistranslating tRNAs, since mistranslation increases the synthesis of misfolded proteins to further burden the cellular protein folding stress responses (17,21,40). In the case of HD, proteinopathy is triggered by an expanded CAG (Gln) codon repeat in exon1 of the HTT gene encoding the huntingtin protein. Pathogenicity results primarily from a region corresponding to the first exon of the HTT gene (mHTT_{exon1}), which can generate a polyQ expanded Htt protein either by mRNA splicing or proteolysis (41,42). CAG repeats of > 38 glutamine residues are associated with disease risk (43). CAG repeat length thereafter correlates with age of onset and severity, but the relationship is highly variable (44). Indeed, some patients with the same CAG repeat length differ by over 20 years in age of onset (44). Further, the severity of symptoms can differ greatly between individuals with a similar age of onset (45). The discrepancies imply the existence of genetic modifiers of Huntington's disease, and several protein-coding genes have been proposed (44). Searches for genetic modifiers, thus far, have relied on whole exome sequencing and single nucleotide polymorphism (SNP) arrays which do not capture tRNA or other non-protein coding RNA gene variants. In addition, whole genome sequencing approaches lack the depth of coverage, read length, and mapping strategy required to confidently identify all tRNA variants in a human genome (24). In this study, we demonstrate that a naturally occurring tRNA variant has significant potential to act as a genetic modifier to Huntington's disease and conceivably other forms of neurodegenerative disease.

3.2 Materials and Methods

3.2.1 Plasmids and strains.

Expression constructs, cloning procedures, and primers (Table S3.1) are described in supplemental methods. Plasmid DNA for transfection in mammalian cells was purified by Midi-Prep (GeneAid, New Taipei City, Taiwan) from 100 ml *Escherichia coli* DH5 α cultures according to manufacturers' instructions. For all tRNA genes used in our study, we collected data on the folding predictions of the wild-type and mutant tRNAs (gtRNAdb (46)), and available expression data from human cells (gtRNAdb (46), UCSC genome browser (47)). All tRNAs used were predicted to be expressed and fold into a canonical tRNA structure in human cells (Table 3.1).

3.2.2 Cell culture and transfection.

Experiments were performed in murine Neuro2a Neuroblastoma (N2a; ATCC #CCL-131), human SH-SY5Y neuroblastoma (SH-SY5Y; ATCC #CRL-226), or rat pheochromocytoma (PC12; parent cells: ATCC #CRL-1721)-derived cells. PC12-derived cell lines containing HTTexon1 fused to EGFP with 23Q or 74Q polyQ under doxycycline promoter (48) were a gift from David Rubinsztein (University of Cambridge, U.K.). All cell lines were grown at 37°C with humidity and 5% CO₂. N2a and SHSY5Y cells were cultured in high glucose Dulbecco's modified Eagle medium (DMEM, 4.5 g/L glucose; Gibco by Life Technologies, Carlsbad, CA) containing penicillin (100 IU/mL), streptomycin (100 μ g/ml; P/S; Wisent Bioproducts, Montreal, QC, Canada), and 10% fetal bovine serum (FBS; Gibco). PC12-derived cell lines were cultured in high glucose DMEM containing P/S, 10% horse serum (Gibco), 5% FBS (Gibco), 50 μ g/ml G418 (Gibco), and 150 μ g/ml hygromycin B (Invitrogen, Carlsbad, CA, USA). All transfections were performed using Lipofectamine 2000 transfection reagent (Invitrogen) with 2 μ g/ml plasmid DNA, following the manufacturer's instructions.

3.2.3 Small molecules and peptides.

Carbobenzoxy-L-leucyl-L-leucyl-L-leucinal (MG132; Sigma-Aldrich 474790, Darmstadt, Germany) and integrated stress response inhibitor (ISRIB; Sigma-Aldrich SML0843) were dissolved in DMSO and cells were treated with final concentrations as described.

3.2.4 Cellular viability and toxicity assays.

Cellular viability was assessed using a CelltiterGlo 2.0 Luminescent Viability Assay (Promega, Madison, WI) in at least three biological replicates following the manufacturer's instructions. Cytotoxicity was assayed with a CytotoxGlo luminescent cytotoxicity assay (Promega) in at least four biological replicates, following the manufacturer's instructions. Cells were assayed 48 hours post-transfection. For assays containing the proteasome inhibitor, cells were treated with MG132 (0.1 to 10 μ M as indicated) or vehicle (DMSO) for 4 hours immediately before assay.

3.2.5 Western blotting.

Detailed western blotting procedures are described in supplemental methods. The following primary antibodies were used in this work: α -GFP, Abcam, Cambridge, UK, ab32146; α -GAPDH, Sigma-Aldrich, Darmstadt, Germany, MAB374m; α -HSP70, Invitrogen, MA3-006; α -HSP90, Protein Tech, Rosemont, IL, USA, 13171-1-AP; α -Phospho-eIF2 α Ser52, ThermoFisher Scientific, 44-728G; α -eIF2 α , ThermoFisher Scientific, AHO0802; α -eEF2, Cell Signaling Technology, Danvers, MA, USA, 2332; α -Phospho-eEF2 (Thr56), Cell Signaling Technology, 2331.

3.2.6 Mass spectrometry.

Detailed mass spectrometry protocols are described in the supplemental methods. Briefly, mCherry protein and wild-type or mistranslating tRNA^{Ser} were co-expressed in N2a cells and mCherry protein was purified using RFP-trap agarose bead immunoprecipitation (Chromotek, Munich, Germany). Immunoprecipitated mCherry was visualized on SDS-PAGE and bands at the correct molecular weight were excised from the gel for MS/MS following tryptic digest of the protein samples. Hits representing Ser misincorporation at Phe codons were curated to include only peptides with a peptide score ($-10\log P$) of > 50 .

3.2.7 Fluorescence microscopy.

Detailed fluorescence microscopy methods are described in supplemental methods. Briefly, Fluorescent microscopy images were captured on an EVOS FL auto fluorescent

microscope (Thermo Fisher Scientific). GFP (470 ± 22 nm excitation, 510 ± 42 nm emission) and RFP (531 ± 40 nm excitation, 593 ± 40 nm emission) filter cubes were used to capture green or red fluorescence. An EVOS onstage incubator was used for live cell experiments and images were quantitated using ImageJ/Fiji (49,50) (see supplemental methods, supplemental appendix).

3.2.8 Cycloheximide chase protein degradation assays.

N2a cells were transfected for 48 hr before the experiment in 96-well plates with three biological and six technical replicates. Cells were washed once with Hank's buffered salt solution (HBSS; Gibco by Life Technologies), then media was replaced with DMEM (10% FBS, P/S) containing 50 μ g/ml cycloheximide (Sigma-Aldrich) and either 10 μ M MG132 or equivalent concentration of DMSO. The plate was immediately transferred to the EVOS FL environment chamber pre-heated to 37°C with 5% CO₂ and humidity. After acclimatizing the plate for 1 hr, images were captured every 30 min for 12 hr. Fluorescence was quantitated using a semi-automated approach in ImageJ (see supplemental information). Initially, increasing concentrations of cycloheximide (0, 50, 250, and 500 μ g/mL) were also assessed with single fluorescent images with the same approach after 24 hr incubation (see supplemental information). All concentrations resulted in a similar reduction in fluorescence after 24 hours, so the lowest concentration (50 μ g/ml) was selected for the kinetic assay.

3.2.9 Semi-denaturing detergent agarose gel electrophoresis (SDD-AGE).

N2a cells were transfected as above. In one experiment (Fig. S3.6A), cells were incubated with DNA and lipofectamine 2000 for 24 hr. In another experiment (Fig. 3.5C,D,E), cells were incubated for 48 hr with lipofectamine 2000 and DNA, then cells were treated for 4 hr with either 10 μ M MG132 dissolved in DMSO or an equal volume of DMSO. Cell lysates were prepared as above (see Western blotting) and protein concentrations were measured with the BCA assay following manufacturer's instructions. SDD-AGE assays were performed similarly to published approaches (51). Lysate volumes containing 40 μ g protein were diluted in 3 \times loading dye (0.5 M Tris-HCl, pH 6.8; 1.12 M sucrose; 0.025% bromophenol blue; 3.8% SDS) with sterile milliQ H₂O, loaded and separated on 1.5% agarose gels containing 0.1% SDS. Proteins were transferred to a nitrocellulose membrane by capillary electrophoresis overnight using Tris-acetate-EDTA buffer (40 mM Tris-base, 20 mM acetic acid, 1 mM EDTA) with 0.1% SDS. EGFP-tagged polyQ

aggregates were visualized by western blotting with α -GFP antibody (see supplemental information).

3.2.10 Protein aggregation clearance assay.

PC12-derived cells were transfected using lipofectamine 2000 and transfectants expressing wild-type or mutant tRNAs were identified by red fluorescence from a plasmid-encoded mCherry protein. 48 hrs post-transfection, mHTT_{Exon1 74Q}-EGFP expression was induced with 2 μ g/ml doxycycline (doxycycline hydrochloride; Sigma-Aldrich) as before (48). After 96 hrs, cells were washed once with doxycycline-free medium and thereafter maintained in doxycycline-free medium. Images were captured daily in RFP (531 \pm 40 nm excitation, 593 \pm 40 nm emission) and GFP (470 \pm 22 nm excitation, 510 \pm 42 nm emission) settings from the time at induction to 72 hrs after doxycycline was removed. To determine the fraction of transfected cells containing aggregates at each time point, the number of transfected cells (red) containing visible aggregates (green) in each image was counted manually by overlaying fluorescent images in ImageJ.

3.3 Results

3.3.1 Transfer RNA variants used in this study.

Transfer RNA variants can elicit several different types of errors in protein synthesis (23). Here we focused on tRNA variants that specifically cause amino acid misincorporation. The cognate aminoacyl-tRNA synthetases (AARS) for Ser, Ala, and to a lesser extent for Leu, do not use the anticodon as an identity or recognition element (52). Thus, nonsynonymous anticodon variants of tRNA^{Ser}, tRNA^{Ala} and tRNA^{Leu} have potential to cause amino acid misincorporation. Seryl-tRNA synthetase is especially flexible in recognizing tRNA^{Ser} with different anticodons (53), since serine is encoded by six codons with no single nucleotide common to all possible sequences. Indeed, engineered tRNA^{Ser} anticodon variants cause mistranslation in mouse and human cells (21), but naturally occurring variants have not been tested.

By searching the genomic tRNA database (46), we found an uncharacterized tRNA^{Ser} anticodon mutant (tRNA-Ser-AGA-2-3 G35A) that occurs in 1.8% of the sequenced population (Fig. 3.1A) (23). The mutant occurs primarily in the tRNA^{Ser}-AGA-2-3 gene and is also found more rarely in the identical tRNA^{Ser}-AGA-2-2 gene (23). In an independent targeted sequencing effort covering

all human tRNA genes, we identified the same mutant in the tRNA^{Ser}-AGA-2-3 gene at a minor allele frequency of 3% in a population of 84 individuals (24). In eukaryotes, tRNA^{Ser}_{AGA} is a substrate for A₃₄-to-I₃₄ editing (54), yielding an IGA anticodon which can decode UCU, UCC, and to a lesser extent UCA codons (55). Hence, assuming canonical A:U pairing in the second anticodon:codon position, the tRNA-AGA-2-3 G35A variant has potential to decode UUU (Phe), UUC (Phe), and UUA (Leu) codons. We also investigated two additional mistranslating tRNA variants that we previously characterized in yeast (18,56) and mammalian cells (22) for their ability to direct amino acid mis-incorporation. One variant is caused by mutation of an identity element such that a different AARS recognizes the tRNA (Fig 3.1B). The resulting Ala-tRNA^{Pro} decodes Pro (CCA/G/U) codons with Ala (18,22). The second variant (tRNA^{Ser} CGA-2-1 C34T, A36G) is a human homolog of a tRNA^{Ser} with a UGG (proline) anticodon that led to mis-incorporation of Ser at Pro codons (CCA/G/U) in yeast (56). Properties of the tRNA genes and variants are noted below (Table 3.1), while additional gene and SNP identifiers as well as sequences for each tRNA gene locus are listed in the supplemental information (Table S3.2).

Table 3.1. tRNA genes and variants

tRNA gene	variants	mistranslation	variant	documented	tRNA score ^f		Expression	
			description	mistranslation	wt	variant	ARM ^g	CHIP ^h
Ser-AGA-2-3	G35A	Ser at Phe (UUU/C), Leu (UUA) codons	natural MAF = 1.8% ^a	N2A cells ^b	89.6	89.6	+	+
Ser-CGA-2-1	C34T, A36G	Ser at Pro codons	synthetic	yeast ^c N2A cells ^b	94.0	94.1	+	+
Pro-TGG-1-1	C3G, G70T	Ala at Pro codons	synthetic	yeast ^d HEK293 ^e cells	74.9	70.8	+	+

^aData from 1000 Genomes Project (46,82); ^bthis study; ^chomolog of Ser-CGA C34T, A36G mistranslation documented in yeast (56,83), ^dhomolog of Pro-TGG-1-1 3G, 70T mistranslation documented in yeast (18), ^ePro-TGG-1-1 C3G, G70T mistranslation documented in HEK293 cells (22), ^ftRNA gene score calculated using tRNA-Scan SE (Infernal score) (46); ^gARM = ARM-seq data suggesting expression (46,84); ^hCHIP = CHIP-seq hits for at least 3 proteins found in RNA Polymerase III holoenzyme or initiation complex (RPC155, POLR3G, BRF1, BDP1, GTF3C2, TBP) (47,85-88).

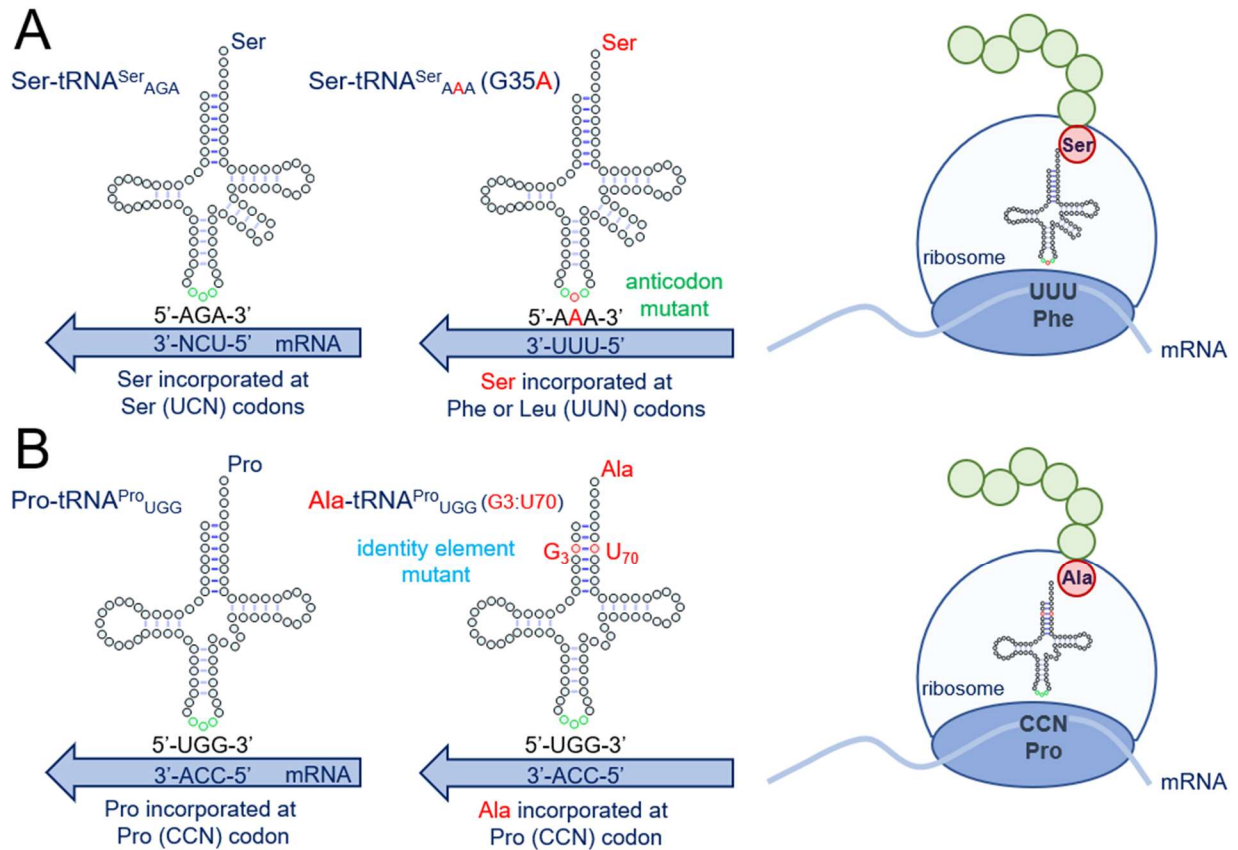


Figure 3.1. Mechanisms of tRNA-dependent mistranslation. Anticodon (A) or identity element (B) mutations in tRNAs can lead to mistranslation. Anticodon mutations in tRNA^{Ser} genes (A) lead to a mutant tRNA that still accepts serine and now decodes other codons. The tRNA^{Ser} G35A mutant decodes phenylalanine or leucine (UUN) codons with serine. We also characterized a tRNA^{Ser}_{UGG} variant (not shown) that decodes proline codons with serine. Mutations in human tRNAs can lead to the acquisition of a G3:U70 base pair, which is a critical identity element for AlaRS (B). The resulting tRNA^{Pro} (G3:U70) is an efficient alanine but not proline acceptor that retains the ability to decode Pro codons.

3.3.2 tRNA^{Ser}_{AAA}-dependent amino acid misincorporation.

To confirm that the tRNA^{Ser}_{AAA} variant causes the expected Ser incorporation at Phe codons in cells, we immunoprecipitated mCherry protein from cells expressing tRNA^{Ser}_{AGA} or tRNA^{Ser}_{AAA} and identified multiple peptides corresponding to Ser misincorporation by mass spectrometry. The mCherry coding sequence contains ten UUC codons that may be mistranslated by tRNA^{Ser}_{AAA}. We detected Ser misincorporation at multiple Phe codons in mCherry from cells expressing tRNA^{Ser}_{AAA}. In addition, we observed potential mistranslated peptide hits, i.e., probability of random hit score (-10logP) ~ 40-60, in both normal (Fig S3.1A) and mistranslating cells (Fig S3.1C, Tables 3.2,3.3). While these lower scoring hits match the full peptide mass, following fragmentation, both hits contain significantly more unidentified peaks and lack multiple y and b ions that cover the site of interest. This is in contrast to the higher scoring hits documenting mistranslation in cells expressing tRNA^{Ser}_{AAA}, where the spectra have multiple ions with a much higher signal to noise ratio confirming misincorporation (Fig S3.1B,D,E, Table 3.2). For an overview of misincorporation in the mCherry reporter, we summarized all peptide hits with -10logP > 50 for Phe or Ser incorporation at each Phe codon in mCherry (Table 3.3). The spectral counts indicate a greater level of mis-incorporation of Ser at Phe codons in mistranslating cells (26 Ser / 266 Phe) compared to the background level (6 Ser / 304 Phe) observed in normal cells. Most of the hits in wild-type cells occur at Phe70 (Fig S3.1A), yet these spectra lack sufficient y and b ion support to confirm these peptides as evidence that mis-incorporation occurs in normal cells.

Table 3.2. Selected observed peptides showing Ser mis-incorporation at Phe codons in mCherry.

Fig.	tRNA ^{Ser} anticodon	Phe codon mCherry	AA change mCherry	Peptide sequence	-10logP	Area
A	AGA	UUC	F70S	GGPLPFAWDILSPQ(+.98) <u>S</u> MYG SKA	58.75	1.7×10 ⁹
B	AAA	UUC	F70S	GGPLPFAWDILSPQ <u>S</u> M(+15.99) YGSK	94.78	3.8×10 ⁷
C	AAA	UUC	F70S	GGPLPFAWDILSPQ(+.98) <u>S</u> MYG SKA	48.50	2.3×10 ⁷
D	AAA	UUC	F104S	VM(+15.99) <u>N</u> SEDGGVVTVTQD SSLQDGEFIYK	88.19	2.0×10 ⁷
E	AAA	UUC	F123S	VM(+15.99) <u>N</u> FEDGGVVTVTQD SSLQDGE <u>S</u> IYK	92.40	2.0×10 ⁷

S indicates Ser misincorporation at Phe codons. Spectra for these peptides are shown in Fig. S3.1.

Table 3.3. Observed spectral counts for Ser or Phe incorporation at Phe codons in mCherry.

Phe codon position in mCherry	tRNA ^{Ser} _{AGA}		tRNA ^{Ser} _{AAA}	
	No. Phe peptides	No. Ser peptides	No. Phe peptides	No. Ser peptides
32	122	1	86	5
61	18	0	15	1
70	14	4	9	9
92	5	0	5	2
96	0	0	0	0
104	54	1	36	4
123	55	0	36	5
134	36	0	42	0
Total:	304	6	229	26

Peptides hits with -10logP score > 50 are shown.

3.3.3 Reduced protein levels in mistranslating cells.

Previous reports established a translation-inhibition response to mistranslating tRNAs expressed in mammalian cells (21,40). Through inhibition of mRNA translation initiation or elongation, general protein synthesis can be downregulated in response to mistranslation or tRNA dysfunction (21,57). Using fluorescence microscopy, we measured red fluorescence (ex. 542 ± 20 nm, em. 593 ± 40 nm) of N2a cells expressing tRNA^{Ser}_{AGA}, tRNA^{Ser}_{AAA}, tRNA^{Ser}_{CGA}, or tRNA^{Ser}_{UGG} and mCherry. We observed a significant reduction in fluorescence of cells expressing either tRNA^{Ser} mutant compared to wild-type tRNA (Fig 3.2A,B). The transfections were repeated with plasmids expressing wild-type tRNA^{Ser}_{AGA} or the tRNA^{Ser}_{AAA} variant for western blotting analysis of GFP (S65F)-mCherry expression (see supplementary methods). Compared to a GAPDH control, the GFP-mCherry protein levels were reduced > 3.6-fold in mistranslating cells (Fig. 3.2C). We captured images of HEK239 cells expressing wild-type and mistranslating tRNA^{Pro} G3:U70 with an EGFP reporter as before (22). Analysis of these images confirmed that tRNA^{Pro} G3:U70 does not elicit the translation suppression response (Fig. S3.2A) that we observed with the anticodon variants of tRNA^{Ser}.

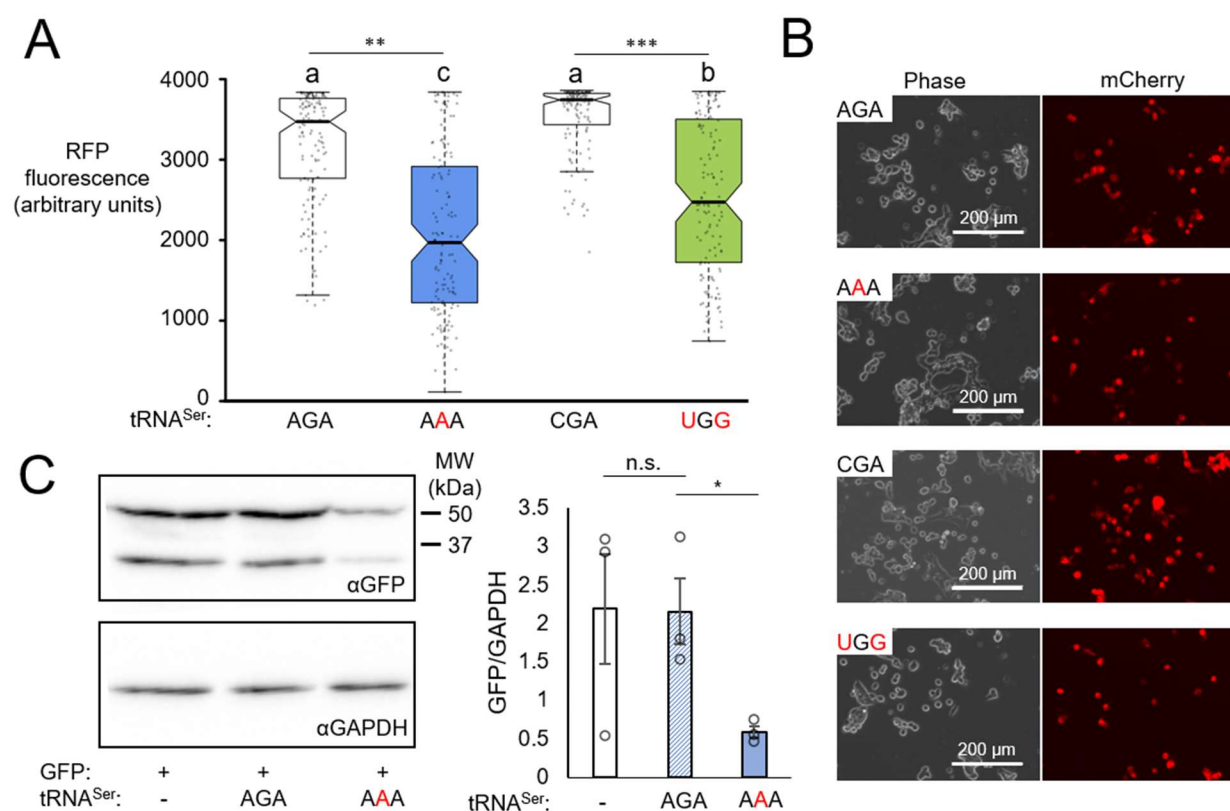


Figure 3.2. Fluorescence and expression of mCherry protein in mistranslating cells. N2a cells were transfected with a plasmid encoding human tRNA^{Ser}_{AGA} or G35A variant tRNA^{Ser}_{AAA}; or tRNA^{Ser}_{CGA} or the C34G, A36G variant tRNA^{Ser}_{UGG} and fluorescently dead GFP (S65F or P) fused to an active mCherry transfection marker. Fluorescence of cells was measured by fluorescence microscopy (RFP, ex 531 nm, em 593 nm). Each box represents data from 135 cells from three biological and nine technical replicates (A). Midline represents the median, boxes represent quartiles, and whiskers represent 1.5× the interquartile range. Representative images were captured under 20× magnification with phase or RFP settings (B). Cell lysates were harvested and western blotted for fluorescent protein expression with anti-GFP and anti-GAPDH antibodies as a loading control (C). Anti-GFP blots were quantitated in three biological replicates by densitometry normalized to GAPDH. Stars indicate p-values from independent sample t-tests (n.s. = no significant difference, * = $p < 0.05$, ** = $p < 0.01$, *** = $p < 0.001$) and letters indicate significantly different groups determined by Tukey's Honestly Significant Different (HSD) test, where groups sharing a letter are not significantly different and groups not sharing a letter are significantly different ($\alpha = 0.05$).

3.3.4 tRNA-dependent toxicity in human and mouse cellular models of HD.

To investigate the viability of cells expressing a known mistranslating tRNA combined with an aggregating polyQ allele, we co-transfected plasmids encoding a wild-type or G3:U70 human tRNA^{Pro} with a non-pathogenic (25Q) or mildly pathogenic (46Q) version of HTT_{Exon1} (58). The experiments were performed in murine N2a and human SHSY5Y cells. Both are neuroblastoma-derived lines that are routinely used as a model for protein misfolding disease, including HD (48,59). Using a luminescent assay for cell viability (Celltiter Glo 2.0), we observed no significant loss of viability from the mutant tRNA alone or from the mildly deleterious HTT-allele co-expressed with a wild-type tRNA. Only the combination of HTT_{Exon1} 46Q expression in mistranslating cells resulted in a significant reduction (1.3 ± 0.05 -fold in SHSY5Y; 1.2 ± 0.06 -fold in N2a) in cellular viability compared to cells expressing wild-type tRNA and 25Q (Fig 3.3A,B). The data demonstrate a synthetic toxic interaction between the Ala accepting tRNA^{Pro} G3:U70 mutant and a deleterious HTT allele. We observed the same result in both mouse (Fig 3.3A) and human cells (Fig 3.3B).

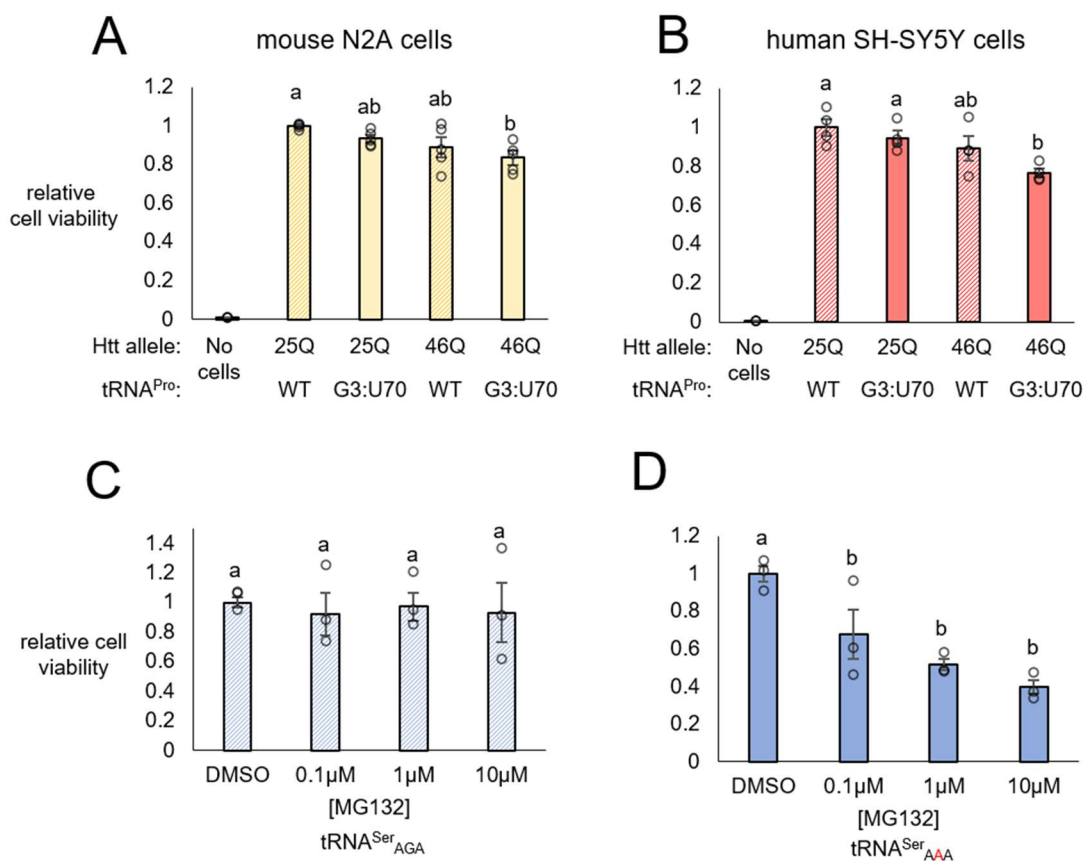


Figure 3.3. Toxic interactions of tRNA variants with a deleterious polyQ allele or proteasome inhibition. N2a (A) or SHSY5Y cells (B) were co-transfected with two plasmids encoding human tRNA^{Pro}_{UGG} or the G3:U70 variant and HTT exon1 containing 25 (25Q) or 46 (46Q) CAG/CAA mixed codon repeats encoding polyQ. Cellular viability was measured 24 hr post-transfection with CellTiterGlo 2.0. Luminescence readings were normalized to the “25Q WT” control. N2a cells were transfected with a plasmid encoding human tRNA^{Ser}_{AGA} (C) or G35A variant tRNA^{Ser}_{AAA} (D) and HTT exon1 containing 23Q fused to EGFP as a transfection marker. Cellular viability was assayed 48 hr post-transfection with the CellTiterGlo 2.0 assay following 4 hr treatment with increasing concentrations of MG132 or equal concentration of DMSO. Luminescence readings were normalized to the DMSO controls. Stars indicate p-values from independent sample t-tests (n.s. = no significant difference, * = $p < 0.05$, ** = $p < 0.01$, *** = $p < 0.001$); letters indicate significantly different groups determined by Tukey’s HSD test ($\alpha = 0.05$). Error bars represent the mean \pm 1 standard deviation of at least three biological replicates.

3.3.5 Interactions of polyQ HTT alleles with tRNA^{Ser} mutants.

We cloned the tRNA-Ser-AGA-2-3 wild type and G35A variant and tRNA-Ser-CGA-2-1 wild type and C34G, A36G double mutant with native genomic context (+/- 300bp) into plasmids containing mCherry fused to a fluorescence-inactivated GFP variant (see supplemental methods). In N2a cells, we co-transfected plasmids with tRNA^{Ser}_{AAA}, tRNA^{Ser}_{UGG} or the respective WT tRNA controls along with the 23Q or 46Q HTT exon1 allele. Unlike our studies with tRNA^{Pro} G3:U70, the tRNA^{Ser} anticodon variants showed no significant loss of cellular viability on their own or in combination with the 46Q HTT exon1 (Fig. S3.3A,B).

For the following experiments, we focused our investigations on tRNA^{Ser}_{AGA} and the G35A variant, since the variant occurs naturally in the human population and leads to phenotypic defects, including inhibited protein synthesis. We cloned the tRNA^{Ser}_{AGA} and the tRNA^{Ser}_{AAA} variant genes into plasmids expressing 23Q or 74Q HTT exon1 allele fused to EGFP. We used a CytotoxGlo assay to measure cellular toxicity. In this assay, the tRNA^{Ser}_{AAA} variant was significantly cytotoxic compared to the wild-type tRNA^{Ser}_{AGA}, but the mutant tRNA showed no apparent additional toxic effect in combination with 74Q HTT exon1 (Fig. S3.3C,D).

We hypothesized that inhibition of the proteasome would increase the toxicity of mistranslating cells because of the accumulation of mistranslated and misfolded proteins. We used increasing concentrations of MG132 in cells expressing 23Q Htt exon1-EGFP and either tRNA^{Ser}_{AGA} (Fig 3.3C) or the tRNA^{Ser}_{AAA} variant (Fig 3.3D) and measured cell viability. We observed a MG132 concentration-dependent decrease in cell viability only in cells expressing the mistranslating tRNA variant, demonstrating a synthetic toxic interaction between the naturally occurring tRNA^{Ser}_{AAA} mutant and proteasome inhibition. MG132 treatments at the same concentrations had no effect on the viability of cells expressing wild-type tRNA (Fig. 3.3C).

Anticipating that proteasome inhibition would exacerbate toxicity of both the mistranslating tRNA and the 74Q allele, we measured the toxicity of cells with or without treatment of MG132. We again confirmed cytotoxicity resulting from the tRNA^{Ser}_{AAA} variant in comparison to wild-type tRNA, however, we observed no additional toxicity with 74Q compared to the 23Q HTT allele in mistranslating cells (Fig. S3.3D). Compared to normal conditions (Fig S3.3C), we note that the addition of MG132 (Fig. S3.3D) resulted in a greater and more significant increase in cytotoxicity for mistranslating cells compared with wild type cells.

3.3.6 Kinetics of polyQ aggregate formation in mistranslating cells.

Using live cell fluorescence microscopy, we captured the formation of EGFP-tagged polyQ aggregates in N2a cells expressing either tRNA^{Ser}_{AGA} or the tRNA^{Ser}_{AAA} variant over an 18 hr time-course. We quantified the fluorescence and number of aggregates in each image series using a semi-automated approach in ImageJ (Fig. S3.4). Mistranslating cells accumulated fewer 74Q aggregates and less overall fluorescence signal over the time-course (Fig. 3.4A, S3.5, Data File S3.1). We normalized the number of aggregates in each image to total fluorescence of the image to account for the reduced fluorescence in mistranslating cells and variability in the number of fluorescing cells between images. In cells expressing the wild-type tRNA, the number of aggregates per unit fluorescence increased over time. In mistranslating cells, the appearance of aggregates proceeded at a slower rate and plateaued earlier at the 10-hour time point (Fig. 3.4B). To further validate that the observed reduction in fluorescence was due to expression of the mutant tRNA, we co-transfected plasmids expressing mCherry and 23Q HTT exon1 allele fused to EGFP, with the mutant tRNA^{Ser}_{AAA} encoded on either one plasmid or the other. Regardless of which plasmid the tRNA was expressed from, 23Q-EGFP fluorescence was significantly and equivalently reduced compared to cells expressing no additional tRNA, and the effect was maintained for at least 48 hrs post-transfection (Fig. S3.2B).

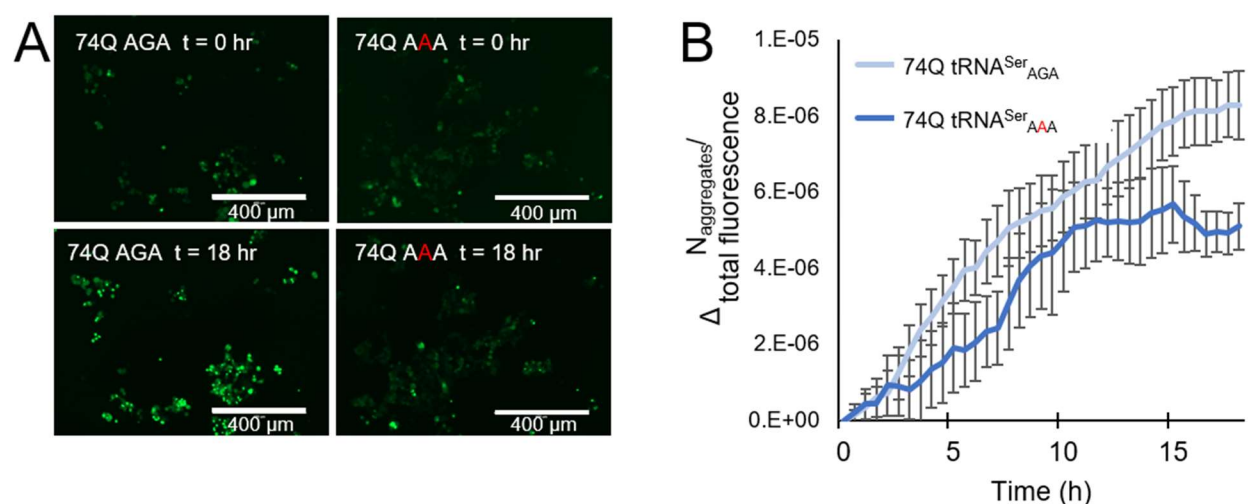


Figure 3.4. Formation of polyQ aggregates in mistranslating cells. N2a cells were transfected with a plasmid encoding human tRNA^{Ser}_{AGA} or G35A variant tRNA^{Ser}_{AAA} and HTT exon1 containing 74Q-EGFP. Images were captured beginning 24 hrs post-transfection by fluorescence microscopy in GFP settings at 10× magnification every 30 min for an 18 hr time course. (A)

Representative images from the beginning ($t = 0$ hr) and end ($t = 18$ hr) of the time course are shown. (B) The number of aggregates in each image was quantitated in ImageJ (see supplemental information). The number of aggregates in each image of the series was then normalized to total fluorescence of the same image ($N_{\text{aggregates}}/\text{total fluorescence}$), and initial values were subtracted ($\Delta N_{\text{aggregates}}/\text{total fluorescence}$). Error bars represent the mean ± 1 standard deviation of six biological replicates.

3.3.7 Mistranslating cells accumulate smaller and fewer polyQ aggregates.

To assess the effects of a mistranslating tRNA on insoluble polyQ aggregate formation, we performed a membrane detergent assay to quantify insoluble EGFP-HTT_{exon1} polyQ aggregates in cells expressing either tRNA^{Ser}_{AGA} or the tRNA^{Ser}_{AAA} variant. Aggregates were allowed to form over a 48 hr transfection period, after which cells were treated with Triton X-100 to permeate the cell membrane. Large, insoluble fluorescent aggregates are retained in the cell, whereas soluble polyQ or small oligomers diffuse into the media (Fig. 3.5A) (60). We used thresholding analysis to assess the number and size of aggregates in images captured before and after Triton X-100 treatment. All fluorescent foci disappeared from cells expressing the non-aggregating 23Q-EGFP following Triton X-100 treatment, while the 74Q foci were clearly visible (Fig. 3.5A). Foci remaining in the mistranslating cells were significantly smaller than cells expressing wild-type tRNA, with a median area of 257 μm^2 compared to 315 μm^2 in the wild-type tRNA-expressing cells (Fig. 3.5B).

different groups determined by Tukey's HSD test, where groups sharing a letter are not significantly different and groups not sharing a letter are significantly different ($\alpha = 0.05$).

We further investigated the effect of the tRNA^{Ser}_{AAA} variant on aggregate formation using semi-denaturing detergent agarose gel electrophoresis (SDD-AGE) (51). SDD-AGE is a semi-quantitative method to visualize insoluble protein aggregates as high molecular weight products after agarose gel electrophoresis and western blotting. We used an α -GFP antibody to detect the EGFP-tagged polyQ proteins. At 24 hrs post-transfection, we observed less aggregated 74Q protein in cells expressing the mistranslating tRNA compared to wild type, and no evidence of aggregated 23Q-EGFP protein in cells expressing either tRNA (Fig. S3.6).

To further promote formation of protein aggregates, we transfected cells for 48 hrs and then treated them for 4 hr with MG132 or DMSO as a control. With 48 hr transfections, high molecular weight aggregates were observed even in 23Q-expressing cells (Fig. 3.5C,D). Comparing the wild-type tRNA^{Ser}_{AGA} and mistranslating tRNA^{Ser}_{AAA}, we observed different effects on 23Q and 74Q aggregation behavior. Cells expressing 23Q with the wild-type tRNA showed a small fraction of aggregated polyQ in the SDD-AGE assay with 13% of the HTT-23Q protein aggregated. In 23Q-expressing cells with the mistranslating tRNA, however, we found a significant increase in the proportion of aggregated protein (33%) compared to cells expressing the wild-type tRNA (Fig. 3.5C,D). The data suggest that mistranslation of the HTT-23Q allele contributes to an increase in aggregation of the non-deleterious HTT allele.

Cells expressing either wild type or mutant tRNA both showed aggregation of the 74Q protein, but mistranslating cells displayed a smaller fraction of high molecular weight 74Q aggregates (Fig. 3.5C,E) in agreement with our Triton-X100 treatments (Fig. 3.5A,B). Proteasome inhibition with MG132 had no significant effect on aggregation of either 23Q or 74Q in mistranslating cells. We observed a greater accumulation of 23Q aggregates in MG132-treated cells expressing wild-type tRNA, which was still significantly less than the level of 23Q aggregates seen in mistranslating cells (Fig 3.5D). MG132-treated cells expressing the wild type tRNA and 74Q showed an intermediate level of protein aggregation, which was not significantly different from either untreated wild-type cells or from cells expressing the mistranslating tRNA (Fig 3.5E). The absence of any change in protein aggregates in mistranslating cells with or without MG132 treatment

suggests that the mistranslating tRNA has a dominant effect on Htt protein aggregation that is independent of proteasome activity.

3.3.8 Heat shock protein levels in mistranslating cells.

Heat shock protein production is a common cellular stress response mounted to mitigate the toxic effects of misfolded proteins in cells and is known to be activated by mistranslating tRNAs in yeast (18,56). Increased heat shock protein levels were also observed in mice expressing editing-defective aminoacyl-tRNA synthetases (25), and mammalian cells expressing mistranslating tRNAs after extended transfection periods of up to 72 hr (21). In a previous study, we observed no change in HSP70 or HSP90 levels in HEK293 cells expressing tRNA^{Pro} G3:U70 (22). Here, we measured the level of heat shock response factors HSP70 and HSP90 24 hrs after transfection in cells expressing tRNA^{Ser}_{AAA} or wild-type tRNA^{Ser}_{AAA}. Consistent with our previous study on tRNA^{Pro} G3:U70, we did not observe any evidence of increased HSP levels at 24 hrs (Fig. S3.7A). We also measured HSP70 levels after more extended transfections periods (24, 48, and 72 hr) and observed no significant differences between wild-type and mistranslating cells (Fig. S3.7B).

3.3.9 Regulation of translation initiation and elongation in mistranslating cells.

Previous studies established that certain tRNA anticodon variants expressed in mammalian cells lead to increased phosphorylation of eIF2 α at Ser52 (21,28,40). Phospho-Ser52 in eIF2 α prevents translation initiation of most cellular mRNAs and is a converging point of the integrated stress response stimulated by numerous cellular stresses. However, p-eIF2 α levels vary substantially depending on the tRNA gene variant expressed (21), and how long cells have been expressing the tRNA variant (40). We used western blotting to measure p-eIF2 α , eIF2 α , and GFP levels from cells expressing all combinations of EGFP-fused Httexon1 23Q and 74Q with wild-type tRNA^{Ser}_{AGA} or the tRNA^{Ser}_{AAA} variant. Despite a reduction in the EGFP-fused HTTExon1 in all mistranslating cells, we did not observe an increase in the level of p-eIF2 α in mistranslating cells, even after longer transfection periods (Fig. S3.8A).

Cells can also down-regulate mRNA translation at the level of elongation. Eukaryotic elongation factor 2 (eEF2) is involved in ribosome repositioning and movement of tRNA from the

A-site to P-site during translation (61). Phosphorylation of the eukaryotic elongation factor 2 (eEF2) by eEF2 kinase (eEF2K) at Thr56 reduces translation elongation rates in conditions of nutrient deprivation or various other forms of cellular stress, including proteasome inhibition with MG132 (62). We used western blotting to measure p-eEF2 and eEF2 levels from cells expressing an mCherry transfection marker and tRNA^{Ser}_{AGA} or the tRNA^{Ser}_{AAA} variant with or without treatment with 10 μ M MG132 (Fig. S3.8B). MG132 treatment stimulated a significant increase in p-eEF2 levels in both cell lines (Fig S3.8), but we did not observe any difference in p-eEF2 levels in the mistranslating cells compared to wild type. In normal cells, MG132 inhibits both protein degradation (see Fig 3.7C) and protein synthesis, leading to no change in the steady state protein levels. Despite the clear induction of p-eEF2 in MG132-treated cells, mistranslating cells show a severely reduced level of protein synthesis in conditions that have high or low p-eEF2 (Fig S3.8C).

3.3.10 Mistranslating cells are resistant to the integrated stress response inhibitor.

To further probe the integrated stress response in cells expressing tRNA^{Ser}_{AAA}, we tested whether the reduction in protein levels could be reversed with a p-eIF2 α antagonist. The integrated stress response inhibitor, ISRIB, relieves translation suppression caused by eIF2 α phosphorylation. ISRIB promotes the formation of active heterodecameric eIF2B complexes to stimulate eIF2B-dependent translation initiation (63). Cells transfected with plasmids expressing EGFP-fused HTTExon1 23Q and no tRNA, wild-type tRNA^{Ser}_{AGA}, or the tRNA^{Ser}_{AAA} variant were treated with 500 nM ISRIB over an 18 hr time-course. Fluorescent images were captured throughout the time course, and a cytotoxicity assay was completed at the final timepoint.

Unlike normal cells, mistranslating cells were unable to increase protein synthesis levels in response to ISRIB. In cells expressing no ectopic tRNA, fluorescence of the EGFP-fused HTT-allele increased significantly from the beginning to end of the time course by 25% in DMSO control and 40% in 500 nM ISRIB. In cells expressing wild-type tRNA^{Ser}_{AGA}, fluorescence increased by 26% in DMSO control and 34% in 500 nM ISRIB. In cells expressing tRNA^{Ser}_{AAA}, ISRIB did not significantly increase protein levels, with only a 6% increase of 23Q-EGFP production in the DMSO control, and a similar 7% increase in 500 nM ISRIB. Hence, the addition of ISRIB did not simulate synthesis of the 23Q-EGFP HTTExon1 alleles in mistranslating cells

(Fig. 3.6A,B). As anticipated, ISRIB also had no effect on the cytotoxicity of the mistranslating tRNA (Fig. 3.6C).

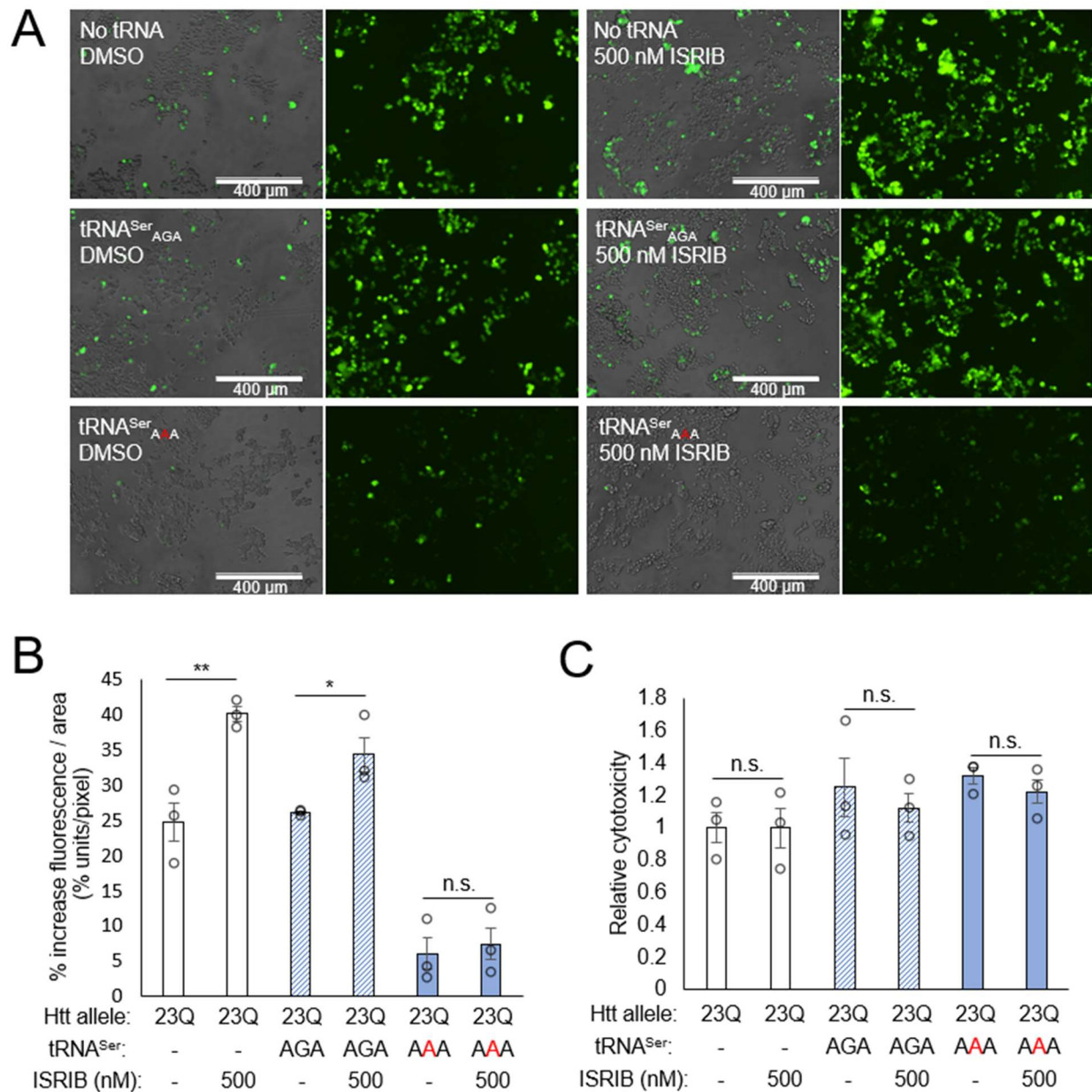


Figure 3.6. Fluorescence and cytotoxicity of mistranslating cells treated with p-eIF2 α antagonist ISRIB. N2a cells were transfected with a plasmid encoding no tRNA, human tRNA^{Ser}_{AGA} or G35A variant tRNA^{Ser}_{AAA} and HTTExon1 23Q-EGFP. Cells were treated for 18 hr with 500 nM ISRIB or equivalent concentration of DMSO. (A) Representative images were capture by fluorescence microscopy in GFP settings after 18 hr ISRIB treatment. (B) Fluorescence intensity per cell area of six technical and three biological replicates was quantitated in ImageJ

(see supplemental methods) before and after treatment. Each bar represents mean (\pm 1 standard deviation) increase in fluorescence intensity per area as a percentage. (C) Cytotoxicity after treatment was measured with CytotoxGlo. Luminescence readings were normalized to the “23Q -/-” control. Stars indicate p-values from independent sample t-tests (n.s. = no significant difference, * = $p < 0.05$, ** = $p < 0.01$, *** = $p < 0.001$).

3.3.11 Defective protein turnover and aggregate clearance in mistranslating cells.

Given the synthetic toxic effect we observed in mistranslating cells treated with MG132, and previous reports of tRNA anticodon variants promoting increased proteasome activity (40), we assayed protein turnover in mistranslating cells. Cycloheximide chase assays (64) were performed on N2a cells expressing no tRNA, wild-type tRNA^{Ser_{AGA}}, or the tRNA^{Ser_{AAA}} variant with EGFP-fused HttExon1 23Q and 74Q (Fig. 3.7A-D). Cycloheximide concentrations of 50, 250 and 500 $\mu\text{g/ml}$ were effective in inhibiting translation and promoting turnover of the 23Q-EGFP protein in N2a cells (Fig. S3.9). Treatment with MG132 to inhibit the proteasome was used as a negative control as described (64). In cells expressing the tRNA^{Ser_{AAA}} variant (Fig. 3.7B,D), we observed a significantly lower rate of protein turnover of both the HttExon1 23Q-EGFP and 74Q-EGFP alleles compared to cells expressing wild-type tRNA^{Ser_{AGA}} (Fig. 3.7B,C). Compared to cells expressing no plasmid-borne tRNA, turnover of the aggregating 74Q-EGFP but not 23Q-EGFP was significantly reduced in mistranslating cells (Fig. 3.7B). In normal cells, MG132 lead to a reduced rate of protein degradation (Fig. 3.7C), while in mistranslating cells MG132 was not able to further slow their already defective rate of protein degradation (Fig. 3.7D).

To assess whether 74Q aggregate clearance was reduced in an independent polyQ model, we used a rat PC12-derived cell line with a stable, genome-integrated HTTExon1 74Q fused to EGFP under control of a doxycycline inducible promoter (48). We transfected either tRNA^{Ser_{AGA}} or the tRNA^{Ser_{AAA}} variant on plasmids with an mCherry transfection marker and monitored the appearance and disappearance of aggregates by induction and removal of doxycycline. Using mCherry to identify tRNA-transfected cells, we counted the number of transfected cells expressing either wild-type or mutant tRNAs containing at least one aggregate (Fig. S3.10). The number of cells containing aggregates was not significantly different during doxycycline treatment, but after doxycycline was removed, aggregates persisted significantly longer in cells expressing the

mistranslating tRNA (Fig. 3.7E). Indeed, cells with wild-type tRNA had a significantly reduced number of polyQ aggregates at 48 and 72 hrs after removal of doxycycline, yet we did not observe any decrease in polyQ aggregates in the mistranslating cells following removal of doxycycline. The data suggest that mistranslating cells are defective in clearing protein aggregates that cause disease.

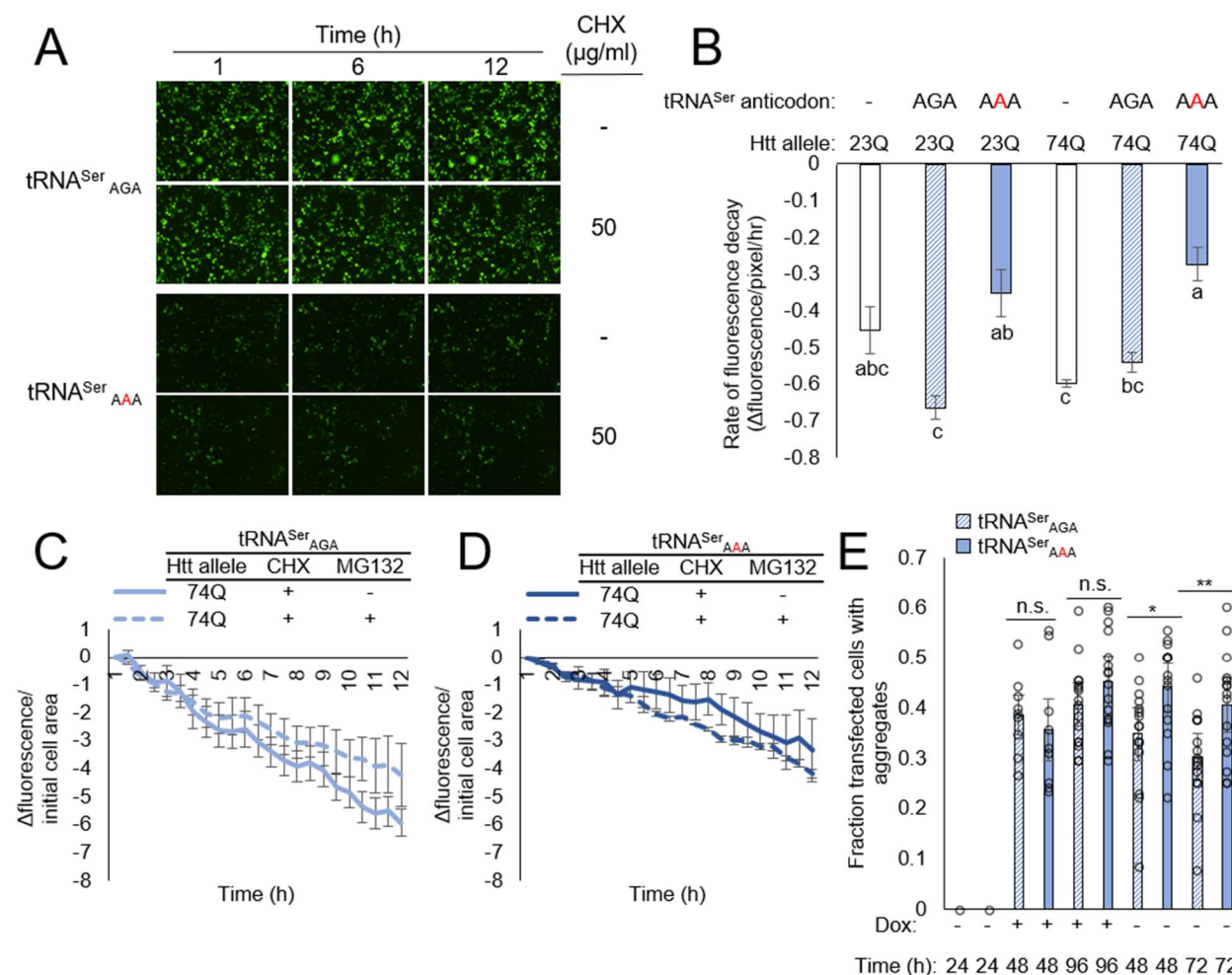


Figure 3.7. Protein turnover and clearance of polyQ aggregates in mistranslating cells. N2a cells were transfected with a plasmid encoding human tRNA^{Ser}_{AGA} or G35A variant tRNA^{Ser}_{AAA} and HTTExon1 containing 23Q or 74Q fused to EGFP for 48 hr before cycloheximide chase assays (A-D). Cells were treated with cycloheximide and/or MG132 and fluorescence was captured by live cell fluorescence microscopy. (A) Representative images of 23Q-EGFP/tRNA^{Ser}_{AGA} and 23Q-EGFP/tRNA^{Ser}_{AAA} expressing cells at the indicated timepoints. Fluorescence was quantitated in ImageJ (see supplemental methods). Average rate of protein decay (B) is shown as a change in fluorescence normalized to initial cell area (C,D) (see

supplemental information). (E) PC12 cells with genomically integrated HTT_{Exon1} 74Q-EGFP under a doxycycline (Dox)-inducible promoter were transfected with a plasmid encoding human tRNA^{Ser}_{AGA} or G35A variant tRNA^{Ser}_{AAA} and mCherry transfection marker. HTT_{Exon1} expression was induced with doxycycline 48 hrs post-transfection and cells were imaged daily by fluorescence microscopy. After 96 hr, Dox was removed and daily imaging was resumed for 72 hr. Aggregate counting is described in methods (see Fig. S3.10). Error bars represent the mean \pm 1 standard deviation of at least three biological replicates and nine technical replicates each. Stars indicate p-values from independent sample t-tests (n.s. = no significant difference, * = $p < 0.05$, ** = $p < 0.01$, *** = $p < 0.001$) and letters indicate significantly different groups determined by Tukey's HSD test ($\alpha = 0.05$).

3.4 Discussion

3.4.1 Huntingtin protein aggregation in mistranslating cells.

Our data show that HTT aggregates form readily in mistranslating cells, but at a slower rate than in wild-type cells. Since cells expressing the 74Q and mistranslating tRNA strongly suppress protein synthesis, polyQ protein concentrations are less likely to reach the threshold required to seed aggregates (65). Consistent with the translation suppression response in mistranslating cells, we observed fewer and smaller aggregates in cells expressing HTT_{Exon1} 74Q and the tRNA^{Ser}_{AAA} variant compared to wild-type tRNA^{Ser}. Further, in N2a cells and in an inducible PC12 cell line of HTT_{Exon1} 74Q, we observed a greater persistence of aggregates in cells expressing tRNA^{Ser}_{AAA} compared to wild-type tRNA^{Ser}. We also found that mistranslating cells were generally defective in their ability to degrade proteins. While mistranslating cells synthesize aggregating proteins more slowly, they are also defective in their ability to degrade HTT-aggregates. In these cellular models of neurodegenerative disease, the data indicate that natural mistranslating tRNA variants have the potential to affect the onset, progression, and severity of HD.

The Ser mis-incorporation at Phe codons we observed in cells expressing tRNA^{Ser}_{AAA} led to the accumulation of misfolded proteins. The label-free MS/MS approach we used is admittedly not ideal for quantifying the mistranslation rate, which will be the subject of future work. The data suggest an estimate for the rate of Ser mis-incorporation at Phe codons could be ~9% per UUC codon, which is 90 to 900 times more than the generally accepted translation error rate of 1 mistake per 1,000 to 10,000 codons (6,7). Even modest levels of mis-incorporation can lead to the

accumulation of mis-made protein as we found. Although mistranslating cells were slower in forming HTTexon1 74Q aggregates, we observed the normally non-aggregating 23Q protein form a significant amount of protein aggregate in mistranslating cells. While 23Q HTTexon1 is less aggregation prone than 74Q, *in vitro* studies have demonstrated that 23Q and shorter HTTexon1 polyQ peptides are capable of aggregation (66). In mistranslating cells, we observed 23Q aggregates at 48 hrs post-transfection. The data suggest that compared to 74Q, higher expression levels and longer times were needed for the 23Q-EGFP protein to aggregate in mistranslating cells. We also observed increased 23Q aggregation in cells treated with the proteasome inhibition. Our observations on HTT protein aggregation suggest mistranslating cells are compromised in their ability to both synthesize and degrade protein aggregates.

3.4.2 Huntingtin protein aggregation and defects in protein quality control.

Our work is the first to explore the interaction between mistranslation and HTT polyQ aggregation. Our studies, focused on mistranslation resulting from a tRNA mutant, suggest that other routes to amino acid mis-incorporation, e.g., editing-defective AARS variants, can also exacerbate polyQ aggregation and HD. Interactions between other factors regulating protein homeostasis and polyQ aggregation represent a continuing theme in yeast and mammalian cell models of polyQ aggregation and toxicity.

For example, work in yeast shows that molecular chaperones (67,68) and protein degradation (69) are critical systems to combat polyQ aggregation. In *Drosophila* S2 cells expressing long 138Q, but not shorter polyQ alleles, protein synthesis is downregulated via the translation regulator Orb2 (70). Studies using N2a cells, as we used, examined production and aggregate formation of HTT alleles with 18Q, 64Q or 150Q. Aggregates were monitored over a 48 hr period, and in agreement with our study, no toxicity from the 64Q or even the 150Q HTT allele was observed (71). In HeLa cells, the same authors used a reporter for nuclear retention of ribosomal protein S2, which signifies inhibition of ribosome biogenesis. Cells expressing a 97Q allele showed a 3-fold increase in nuclear localization of ribosomal protein S2, demonstrating defective ribosome biogenesis in cells expressing an aggregating HTT allele (71). The authors did not directly measure the rate of protein synthesis, but their data suggest dysregulation of protein synthesis in cells expressing long polyQ alleles. Our data suggest that tRNA variants which compromise protein

homeostasis may exacerbate the dysregulation of protein synthesis caused by deleterious and longer polyQ alleles.

3.4.3 Compromised proteostasis in cells expressing mistranslating tRNAs.

We found that cells expressing the naturally occurring tRNA^{Ser}_{AAA} variant were characterized by several phenotypic defects. Using mass spectrometry, we confirmed amino acid misincorporation of Ser at multiple Phe codons. Mistranslating cells were characterized by increased cytotoxicity, general inhibition of protein synthesis, sensitivity to proteasome inhibition, and resistance to the neuroprotective stress response inhibitor ISRIB. Together the data demonstrate that tRNA^{Ser}_{AAA} expression leads to a loss of protein homeostasis.

Despite a mistranslation rate of ~2-3% Ala incorporation at Pro codons, tRNA^{Pro} G3:U70 is not toxic when expressed alone (22). Here we found that toxicity of tRNA^{Pro} G3:U70 is evident in combination with a mildly deleterious 46Q HTT exon1 allele. The data suggest that some mistranslating tRNA variants can exacerbate polyQ toxicity in a model of neurodegenerative disease. Conversely, the naturally occurring tRNA^{Ser}_{AAA} variant was toxic alone, but did not show additional toxicity with aggregating HTT protein. The differences in toxicity may depend on how cells respond to different types of mistranslation. We observed a consistent reduction in protein synthesis in cells expressing the tRNA^{Ser}_{AAA} or tRNA^{Ser}_{UGG} variants, but not in cells expressing tRNA^{Pro} G3:U70. Furthermore, cells mis-incorporating Ser at Phe codons showed a stronger repression of translation than cells mistranslating Pro codons with Ser. The severely inhibited protein synthesis observed in cells with tRNA^{Ser}_{AAA} may indeed protect the cell from the toxicity of the aggregating Htt allele and amino acid mis-incorporation.

A recent study in yeast demonstrated that tRNA variants that result in different types of amino acid change can elicit distinct cellular responses (72). A tRNA^{Ser} mutant that mistranslates Arg and a yeast homolog of the same tRNA^{Pro} G3:U70 variant we tested were found to mistranslate at similar levels. However, in RNA sequencing experiments, each tRNA-expressing strain elicited distinct changes in the transcriptome. For example, down-regulation of genes involved in cell cycle, DNA replication, transcription, and response to stress was observed in cells mistranslating Pro codons with Ala but not in cells mis-incorporating Ser at Arg codons (72).

Phenotypic differences observed from expressing different tRNA variants may also depend on the compatibility of the tRNA in question with a given gain-of-function mutation. For example,

nucleotides in and adjacent to the anticodon sequence are often conserved within tRNA isoacceptor groups (46), and can be modified to ensure optimal fidelity and efficiency in recognizing certain codon sets. This is true for wild-type tRNA^{Phe}, wherein modified guanine bases in position 34 (73) of the anticodon and the anticodon-adjacent position 37 (74) are used to efficiently and accurately decode UUU and UUC codons. Conversely, the tRNA^{Ser}_{AAA} variant we investigated has adenine at 34 and 37, so it is possible that the strong reduction in protein synthesis we observed is due in part to suboptimal codon:anticodon recognition kinetics in the tRNA variant compared to tRNA^{Phe}.

In a previous study of tRNA^{Ser} anticodon variants expressed in HEK293 cells with an EGFP marker, similar to our observations, translation inhibition was recorded for different tRNA^{Ser} anticodon variants (21). For some tRNA^{Ser} variants, translation suppression was attributed to an integrated stress response involving phosphorylation of eIF2 α at Ser52 (21). Phosphorylation of eIF2 α at Ser52 is one mechanism to down-regulate translation initiation. Although tRNA^{Ser} with a Phe anticodon (tRNA^{Ser}_{AAA}) was not tested before, a mutant that decoded Ile codons with Ser showed a strong correlation between increased eIF2 α phosphorylation and depressed protein synthesis (21). Like our observations, mutant tRNAs that decoded His and Lys codons with Ser showed a more muted or little response in p-eIF2 α despite each tRNA mutant causing repression of growth and protein synthesis (21). Another study assayed eIF2 α phosphorylation in stably transfected HEK293 cells expressing tRNA^{Ser} with Ala- and Leu-decoding anticodon mutations (40). In this case, eIF2 α phosphorylation was never observed in cells expressing the Ala anticodon variant and only observed in cells expressing tRNA^{Ser} with a Leu anticodon after aging cells for 30 passages. Compared to normal cells, we did not observe a significant increase in eIF2 α phosphorylation in cells expressing the tRNA^{Ser}_{AAA} variant. The observation was corroborated by our experiments with the inhibitor ISRIB. Treatment of cells expressing wild-type tRNA with ISRIB increased protein synthesis, while treatment of cells expressing tRNA^{Ser}_{AAA} with ISRIB did not increase protein production. Thus, the mistranslating cells were resistant to ISRIB. A previous study demonstrated that ISRIB fails to antagonize excessively high levels of p-eIF2 α induced by arsenite treatment (75). Although eIF2 α is phosphorylated in our mistranslating cells, their lack of response to ISRIB suggests mistranslating cells are defective in translation regulation.

Finally, we found that cells expressing the tRNA^{Ser}_{AAA} variant were sensitive to treatment with the proteasome inhibitor MG132. The synthetic phenotype suggests that mistranslating cells rely critically on protein turnover and activity of the proteasome. We also found that protein turnover

rates were reduced in cells expressing tRNA^{Ser}_{AAA}, consistent with an increased burden on the proteasome caused by amino acid misincorporation. In conditions of nutrient deprivation and various forms of cellular stress (62), cells can also down-regulate elongation through inhibitory phosphorylation of eEF2 (76), which catalyzes ribosomal translocation and repositioning of tRNA from the A-site to P-site of the ribosome (77). While mistranslating cells responded to proteasome inhibition (MG132) by phosphorylated eEF2 similarly to normal cells, expression of tRNA^{Ser}_{AAA} showed a dominant effect on repressing protein synthesis, regardless of stress conditions tested or eEF2 phosphorylation status. Stressors, including MG132, may also alter the activity of the mutant tRNA or the tRNome more broadly, as transcription (78) and modification (79) of tRNAs are regulated in response to stress. Investigating the interaction between mistranslating tRNAs and impact of tRNA processing on protein quality control will form the basis of future investigations.

3.5 Conclusion

Humans encode over 600 tRNA genes. Human cells and tissues are estimated to express between 200 and 400 different tRNA genes (23). While some of these genes may be redundant in function, others are critical for maintaining protein homeostasis. Despite a vast background of tRNA genes, even a single tRNA mutant has the potential to cause amino acid mis-incorporation thus exacerbate protein misfolding diseases at the molecular level. We found that a tRNA^{Ser}_{AAA} gene that occurs in 1.8% of the population indeed directs Ser mis-incorporation at Phe codons and leads to increased cytotoxicity and increased need for protein degradation in mammalian cells. Notably, mistranslating cells exhibit severely inhibited protein synthesis, leading to reduced but effective formation of protein aggregates in cellular models of HD. The mistranslating cells were also defective in clearing huntingtin aggregates and were resistant to the neuroprotective compound ISRIB. Because this compound shows promise as a treatment for neurodegeneration (80), our studies suggest that an active mistranslating tRNA in a patient's genetic background may contribute to drug resistance. Taken together, our data show that naturally occurring tRNA mistranslators have significant potential to disrupt protein homeostasis and act as modifiers of neurodegenerative disease.

3.6 Data availability

Custom imageJ macros are available in the Supplementary Information. For western blots, full size images are included as a supplementary data file. The mass spectrometry data have been deposited to the ProteomeXchange Consortium via the PRIDE (81) repository with the identifier PXD027837 (doi 10.6019/PXD027837).

3.7 References

1. Crick, F.H. (1968) The origin of the genetic code. *J Mol Biol*, **38**, 367-379.
2. Steiner, R.E. and Ibba, M. (2019) Regulation of tRNA-dependent translational quality control. *IUBMB Life*, **71**, 1150-1157.
3. Kunkel, T.A. and Bebenek, K. (2000) DNA replication fidelity. *Annu Rev Biochem*, **69**, 497-529.
4. Rosenberger, R.F. and Foskett, G. (1981) An estimate of the frequency of in vivo transcriptional errors at a nonsense codon in Escherichia coli. *Mol Gen Genet*, **183**, 561-563.
5. Bouadloun, F., Donner, D. and Kurland, C.G. (1983) Codon-specific missense errors in vivo. *EMBO J*, **2**, 1351-1356.
6. Kramer, E.B., Vallabhaneni, H., Mayer, L.M. and Farabaugh, P.J. (2010) A comprehensive analysis of translational missense errors in the yeast *Saccharomyces cerevisiae*. *RNA*, **16**, 1797-1808.
7. Drummond, D.A. and Wilke, C.O. (2009) The evolutionary consequences of erroneous protein synthesis. *Nat Rev Genet*, **10**, 715-724.
8. Evans, C.R., Fan, Y. and Ling, J. (2019) Increased mistranslation protects E. coli from protein misfolding stress due to activation of a RpoS-dependent heat shock response. *FEBS Lett*.
9. Santos, M.A., Cheesman, C., Costa, V., Moradas-Ferreira, P. and Tuite, M.F. (1999) Selective advantages created by codon ambiguity allowed for the evolution of an alternative genetic code in *Candida* spp. *Mol Microbiol*, **31**, 937-947.
10. Wang, X. and Pan, T. (2016) Stress Response and Adaptation Mediated by Amino Acid Misincorporation during Protein Synthesis. *Adv Nutr*, **7**, 773S-779S.
11. Bacher, J.M., Waas, W.F., Metzgar, D., de Crecy-Lagard, V. and Schimmel, P. (2007) Genetic code ambiguity confers a selective advantage on *Acinetobacter baylyi*. *J Bacteriol*, **189**, 6494-6496.
12. Witzky, A., Tollerson, R., 2nd and Ibba, M. (2019) Translational control of antibiotic resistance. *Open Biol*, **9**, 190051.
13. Kohanski, M.A., Dwyer, D.J., Wierzbowski, J., Cottarel, G. and Collins, J.J. (2008) Mistranslation of membrane proteins and two-component system activation trigger antibiotic-mediated cell death. *Cell*, **135**, 679-690.
14. Davis, B.D., Chen, L.L. and Tai, P.C. (1986) Misread protein creates membrane channels: an essential step in the bactericidal action of aminoglycosides. *Proc Natl Acad Sci U S A*, **83**, 6164-6168.

15. Ruan, B., Palioura, S., Sabina, J., Marvin-Guy, L., Kochhar, S., Larossa, R.A. and Soll, D. (2008) Quality control despite mistranslation caused by an ambiguous genetic code. *Proc Natl Acad Sci U S A*, **105**, 16502-16507.
16. Pezo, V., Metzgar, D., Hendrickson, T.L., Waas, W.F., Hazebrouck, S., Doring, V., Marliere, P., Schimmel, P. and De Crecy-Lagard, V. (2004) Artificially ambiguous genetic code confers growth yield advantage. *Proc Natl Acad Sci U S A*, **101**, 8593-8597.
17. Santos, M., Pereira, P.M., Varanda, A.S., Carvalho, J., Azevedo, M., Mateus, D.D., Mendes, N., Oliveira, P., Trindade, F., Pinto, M.T. *et al.* (2018) Codon misreading tRNAs promote tumor growth in mice. *RNA Biol*, **15**, 773-786.
18. Hoffman, K.S., Berg, M.D., Shilton, B.H., Brandl, C.J. and O'Donoghue, P. (2017) Genetic selection for mistranslation rescues a defective co-chaperone in yeast. *Nucleic Acids Res*, **45**, 3407-3421.
19. Carbon, J., Berg, P. and Yanofsky, C. (1966) Missense suppression due to a genetically altered tRNA. *Cold Spring Harb Symp Quant Biol*, **31**, 487-497.
20. Kelly, P., Backes, N., Mohler, K., Buser, C., Kavoor, A., Rinehart, J., Phillips, G. and Ibba, M. (2019) Alanyl-tRNA Synthetase Quality Control Prevents Global Dysregulation of the Escherichia coli Proteome. *mBio*, **10**.
21. Geslain, R., Cubells, L., Bori-Sanz, T., Alvarez-Medina, R., Rossell, D., Marti, E. and Ribas de Pouplana, L. (2010) Chimeric tRNAs as tools to induce proteome damage and identify components of stress responses. *Nucleic Acids Res*, **38**, e30.
22. Lant, J.T., Berg, M.D., Sze, D.H.W., Hoffman, K.S., Akinpelu, I.C., Turk, M.A., Heinemann, I.U., Duennwald, M.L., Brandl, C.J. and O'Donoghue, P. (2018) Visualizing tRNA-dependent mistranslation in human cells. *RNA Biol*, **15**, 567-575.
23. Lant, J.T., Berg, M.D., Heinemann, I.U., Brandl, C.J. and O'Donoghue, P. (2019) Pathways to disease from natural variations in human cytoplasmic tRNAs. *J Biol Chem*, **294**, 5294-5308.
24. Berg, M.D., Giguere, D.J., Dron, J.S., Lant, J.T., Genereaux, J., Liao, C., Wang, J., Robinson, J.F., Gloor, G.B., Hegele, R.A. *et al.* (2019) Targeted sequencing reveals expanded genetic diversity of human transfer RNAs. *RNA Biol*, **16**, 1574-1585.
25. Lee, J.W., Beebe, K., Nangle, L.A., Jang, J., Longo-Guess, C.M., Cook, S.A., Davisson, M.T., Sundberg, J.P., Schimmel, P. and Ackerman, S.L. (2006) Editing-defective tRNA synthetase causes protein misfolding and neurodegeneration. *Nature*, **443**, 50-55.
26. Lu, J., Bergert, M., Walther, A. and Suter, B. (2014) Double-sieving-defective aminoacyl-tRNA synthetase causes protein mistranslation and affects cellular physiology and development. *Nat Commun*, **5**, 5650.
27. Ishimura, R., Nagy, G., Dotu, I., Zhou, H., Yang, X.L., Schimmel, P., Senju, S., Nishimura, Y., Chuang, J.H. and Ackerman, S.L. (2014) RNA function. Ribosome stalling induced by mutation of a CNS-specific tRNA causes neurodegeneration. *Science*, **345**, 455-459.
28. Kapur, M., Ganguly, A., Nagy, G., Adamson, S.I., Chuang, J.H., Frankel, W.N. and Ackerman, S.L. (2020) Expression of the Neuronal tRNA n-Tr20 Regulates Synaptic Transmission and Seizure Susceptibility. *Neuron*, **108**, 193-208 e199.
29. Schoenmakers, E., Carlson, B., Agostini, M., Moran, C., Rajanayagam, O., Bochukova, E., Tobe, R., Peat, R., Gevers, E., Muntoni, F. *et al.* (2016) Mutation in human selenocysteine transfer RNA selectively disrupts selenoprotein synthesis. *J Clin Invest*, **126**, 992-996.
30. Suzuki, T., Nagao, A. and Suzuki, T. (2011) Human mitochondrial diseases caused by lack of taurine modification in mitochondrial tRNAs. *Wiley Interdiscip Rev RNA*, **2**, 376-386.

31. Goto, Y., Nonaka, I. and Horai, S. (1990) A mutation in the tRNA(Leu)(UUR) gene associated with the MELAS subgroup of mitochondrial encephalomyopathies. *Nature*, **348**, 651-653.
32. Shoffner, J.M., Lott, M.T., Lezza, A.M., Seibel, P., Ballinger, S.W. and Wallace, D.C. (1990) Myoclonic epilepsy and ragged-red fiber disease (MERRF) is associated with a mitochondrial DNA tRNA(Lys) mutation. *Cell*, **61**, 931-937.
33. Yasukawa, T., Suzuki, T., Ueda, T., Ohta, S. and Watanabe, K. (2000) Modification defect at anticodon wobble nucleotide of mitochondrial tRNAs(Leu)(UUR) with pathogenic mutations of mitochondrial myopathy, encephalopathy, lactic acidosis, and stroke-like episodes. *J Biol Chem*, **275**, 4251-4257.
34. Nakayama, T., Wu, J., Galvin-Parton, P., Weiss, J., Andriola, M.R., Hill, R.S., Vaughan, D.J., El-Quessny, M., Barry, B.J., Partlow, J.N. *et al.* (2017) Deficient activity of alanyl-tRNA synthetase underlies an autosomal recessive syndrome of progressive microcephaly, hypomyelination, and epileptic encephalopathy. *Hum Mutat*, **38**, 1348-1354.
35. Liu, Y., Satz, J.S., Vo, M.N., Nangle, L.A., Schimmel, P. and Ackerman, S.L. (2014) Deficiencies in tRNA synthetase editing activity cause cardioproteinopathy. *Proc Natl Acad Sci U S A*, **111**, 17570-17575.
36. Latour, P., Thauvin-Robinet, C., Baudalet-Mery, C., Soichot, P., Cusin, V., Faivre, L., Locatelli, M.C., Mayencon, M., Sarcey, A., Broussolle, E. *et al.* (2010) A major determinant for binding and aminoacylation of tRNA(Ala) in cytoplasmic Alanyl-tRNA synthetase is mutated in dominant axonal Charcot-Marie-Tooth disease. *Am J Hum Genet*, **86**, 77-82.
37. Simons, C., Griffin, L.B., Helman, G., Golas, G., Pizzino, A., Bloom, M., Murphy, J.L., Crawford, J., Evans, S.H., Topper, S. *et al.* (2015) Loss-of-function alanyl-tRNA synthetase mutations cause an autosomal-recessive early-onset epileptic encephalopathy with persistent myelination defect. *Am J Hum Genet*, **96**, 675-681.
38. Sweeney, P., Park, H., Baumann, M., Dunlop, J., Frydman, J., Kopito, R., McCampbell, A., Leblanc, G., Venkateswaran, A., Nurmi, A. *et al.* (2017) Protein misfolding in neurodegenerative diseases: implications and strategies. *Transl Neurodegener*, **6**, 6.
39. Rodgers, K.J. (2014) Non-protein amino acids and neurodegeneration: the enemy within. *Exp Neurol*, **253**, 192-196.
40. Varanda, A.S., Santos, M., Soares, A.R., Vitorino, R., Oliveira, P., Oliveira, C. and Santos, M.A.S. (2020) Human cells adapt to translational errors by modulating protein synthesis rate and protein turnover. *RNA Biol*, **17**, 135-149.
41. Kim, Y.J., Yi, Y., Sapp, E., Wang, Y., Cuiffo, B., Kegel, K.B., Qin, Z.H., Aronin, N. and DiFiglia, M. (2001) Caspase 3-cleaved N-terminal fragments of wild-type and mutant huntingtin are present in normal and Huntington's disease brains, associate with membranes, and undergo calpain-dependent proteolysis. *Proc Natl Acad Sci U S A*, **98**, 12784-12789.
42. Wellington, C.L., Ellerby, L.M., Gutekunst, C.A., Rogers, D., Warby, S., Graham, R.K., Loubser, O., van Raamsdonk, J., Singaraja, R., Yang, Y.Z. *et al.* (2002) Caspase cleavage of mutant huntingtin precedes neurodegeneration in Huntington's disease. *J Neurosci*, **22**, 7862-7872.
43. Chen, S., Ferrone, F.A. and Wetzel, R. (2002) Huntington's disease age-of-onset linked to polyglutamine aggregation nucleation. *Proc Natl Acad Sci U S A*, **99**, 11884-11889.

44. GeM-HD_Consortium., G.o.H.s.D. (2019) CAG Repeat Not Polyglutamine Length Determines Timing of Huntington's Disease Onset. *Cell*, **178**, 887-900 e814.
45. Gusella, J.F., MacDonald, M.E. and Lee, J.M. (2014) Genetic modifiers of Huntington's disease. *Mov Disord*, **29**, 1359-1365.
46. Chan, P.P. and Lowe, T.M. (2016) GtRNADB 2.0: an expanded database of transfer RNA genes identified in complete and draft genomes. *Nucleic Acids Res*, **44**, D184-189.
47. Haeussler, M., Zweig, A.S., Tyner, C., Speir, M.L., Rosenbloom, K.R., Raney, B.J., Lee, C.M., Lee, B.T., Hinrichs, A.S., Gonzalez, J.N. *et al.* (2019) The UCSC Genome Browser database: 2019 update. *Nucleic Acids Res*, **47**, D853-D858.
48. Wyttenbach, A., Swartz, J., Kita, H., Thykjaer, T., Carmichael, J., Bradley, J., Brown, R., Maxwell, M., Schapira, A., Orntoft, T.F. *et al.* (2001) Polyglutamine expansions cause decreased CRE-mediated transcription and early gene expression changes prior to cell death in an inducible cell model of Huntington's disease. *Hum Mol Genet*, **10**, 1829-1845.
49. Schneider, C.A., Rasband, W.S. and Eliceiri, K.W. (2012) NIH Image to ImageJ: 25 years of image analysis. *Nat Methods*, **9**, 671-675.
50. Rueden, C.T., Schindelin, J., Hiner, M.C., DeZonia, B.E., Walter, A.E., Arena, E.T. and Eliceiri, K.W. (2017) ImageJ2: ImageJ for the next generation of scientific image data. *BMC Bioinformatics*, **18**, 529.
51. Halfmann, R. and Lindquist, S. (2008) Screening for amyloid aggregation by Semi-Denaturing Detergent-Agarose Gel Electrophoresis. *J Vis Exp*.
52. Giege, R., Sissler, M. and Florentz, C. (1998) Universal rules and idiosyncratic features in tRNA identity. *Nucleic Acids Res*, **26**, 5017-5035.
53. Achsel, T. and Gross, H.J. (1993) Identity determinants of human tRNA(Ser): sequence elements necessary for serylation and maturation of a tRNA with a long extra arm. *EMBO J*, **12**, 3333-3338.
54. Torres, A.G., Pineyro, D., Filonava, L., Stracker, T.H., Batlle, E. and Ribas de Pouplana, L. (2014) A-to-I editing on tRNAs: biochemical, biological and evolutionary implications. *FEBS Lett*, **588**, 4279-4286.
55. Lim, V.I. and Curran, J.F. (2001) Analysis of codon:anticodon interactions within the ribosome provides new insights into codon reading and the genetic code structure. *RNA*, **7**, 942-957.
56. Berg, M.D., Hoffman, K.S., Genereaux, J., Mian, S., Trussler, R.S., Haniford, D.B., O'Donoghue, P. and Brandl, C.J. (2017) Evolving Mistranslating tRNAs Through a Phenotypically Ambivalent Intermediate in *Saccharomyces cerevisiae*. *Genetics*, **206**, 1865-1879.
57. Shcherbakov, D., Teo, Y., Boukari, H., Cortes-Sanchon, A., Mantovani, M., Osinnii, I., Moore, J., Juskeviciene, R., Brilkova, M., Duscha, S. *et al.* (2019) Ribosomal mistranslation leads to silencing of the unfolded protein response and increased mitochondrial biogenesis. *Commun Biol*, **2**, 381.
58. O'Rourke, J.G., Gareau, J.R., Ochaba, J., Song, W., Rasko, T., Reverter, D., Lee, J., Monteys, A.M., Pallos, J., Mee, L. *et al.* (2013) SUMO-2 and PIAS1 modulate insoluble mutant huntingtin protein accumulation. *Cell Rep*, **4**, 362-375.
59. Narain, Y., Wyttenbach, A., Rankin, J., Furlong, R.A. and Rubinsztein, D.C. (1999) A molecular investigation of true dominance in Huntington's disease. *J Med Genet*, **36**, 739-746.

60. Titus, S.A., Southall, N., Marugan, J., Austin, C.P. and Zheng, W. (2012) High-Throughput Multiplexed Quantitation of Protein Aggregation and Cytotoxicity in a Huntington's Disease Model. *Curr Chem Genomics*, **6**, 79-86.
61. Ryazanov, A.G. and Davydova, E.K. (1989) Mechanism of elongation factor 2 (EF-2) inactivation upon phosphorylation. Phosphorylated EF-2 is unable to catalyze translocation. *FEBS Lett*, **251**, 187-190.
62. Moore, C.E., Wang, X., Xie, J., Pickford, J., Barron, J., Regufe da Mota, S., Versele, M. and Proud, C.G. (2016) Elongation factor 2 kinase promotes cell survival by inhibiting protein synthesis without inducing autophagy. *Cell Signal*, **28**, 284-293.
63. Tsai, J.C., Miller-Vedam, L.E., Anand, A.A., Jaishankar, P., Nguyen, H.C., Renslo, A.R., Frost, A. and Walter, P. (2018) Structure of the nucleotide exchange factor eIF2B reveals mechanism of memory-enhancing molecule. *Science*, **359**.
64. Guo, L., Prall, W. and Yang, X. (2016) Assays for the Degradation of Misfolded Proteins in Cells. *J Vis Exp*.
65. Crick, S.L., Ruff, K.M., Garai, K., Frieden, C. and Pappu, R.V. (2013) Unmasking the roles of N- and C-terminal flanking sequences from exon 1 of huntingtin as modulators of polyglutamine aggregation. *Proc Natl Acad Sci U S A*, **110**, 20075-20080.
66. Vieweg, S., Ansaloni, A., Wang, Z.M., Warner, J.B. and Lashuel, H.A. (2016) An InteIn-based Strategy for the Production of Tag-free Huntingtin Exon 1 Proteins Enables New Insights into the Polyglutamine Dependence of Httex1 Aggregation and Fibril Formation. *J Biol Chem*, **291**, 12074-12086.
67. Kumar, J., Kline, N.L. and Masison, D.C. (2018) Human DnaJB6 Antiamyloid Chaperone Protects Yeast from Polyglutamine Toxicity Separately from Spatial Segregation of Aggregates. *Mol Cell Biol*, **38**.
68. Wolfe, K.J., Ren, H.Y., Trepte, P. and Cyr, D.M. (2013) The Hsp70/90 cochaperone, Sti1, suppresses proteotoxicity by regulating spatial quality control of amyloid-like proteins. *Mol Biol Cell*, **24**, 3588-3602.
69. Yang, J., Hao, X., Cao, X., Liu, B. and Nystrom, T. (2016) Spatial sequestration and detoxification of Huntingtin by the ribosome quality control complex. *Elife*, **5**.
70. Joag, H., Ghatpande, V., Desai, M., Sarkar, M., Raina, A., Shinde, M., Chitale, R., Deo, A., Bose, T. and Majumdar, A. (2020) A role of cellular translation regulation associated with toxic Huntingtin protein. *Cell Mol Life Sci*, **77**, 3657-3670.
71. Kim, Y.E., Hosp, F., Frottin, F., Ge, H., Mann, M., Hayer-Hartl, M. and Hartl, F.U. (2016) Soluble Oligomers of PolyQ-Expanded Huntingtin Target a Multiplicity of Key Cellular Factors. *Mol Cell*, **63**, 951-964.
72. Berg, M.D., Zhu, Y., Ruiz, B.Y., Loll-Krippelber, R., Isaacson, J., San Luis, B., Genereaux, J., Boone, C., Villén, J., Brown, G.W. *et al.* (2021) The amino acid substitution affects cellular response to mistranslation. *G3 Genes Genomes Genetics* doi: 10.1093/g1093journal/jkab1218.
73. Guy, M.P., Podyma, B.M., Preston, M.A., Shaheen, H.H., Krivos, K.L., Limbach, P.A., Hopper, A.K. and Phizicky, E.M. (2012) Yeast Trm7 interacts with distinct proteins for critical modifications of the tRNAPhe anticodon loop. *RNA*, **18**, 1921-1933.
74. Fandilolu, P.M., Kamble, A.S., Sambhare, S.B. and Sonawane, K.D. (2018) Conformational preferences and structural analysis of hypermodified nucleoside, peroxywybutosine (o2yW) found at 37(th) position in anticodon loop of tRNA(Phe) and its role in modulating UUC codon-anticodon interactions. *Gene*, **641**, 310-325.

75. Rabouw, H.H., Langereis, M.A., Anand, A.A., Visser, L.J., de Groot, R.J., Walter, P. and van Kuppeveld, F.J.M. (2019) Small molecule ISRIB suppresses the integrated stress response within a defined window of activation. *Proc Natl Acad Sci U S A*, **116**, 2097-2102.
76. Carlberg, U., Nilsson, A. and Nygard, O. (1990) Functional properties of phosphorylated elongation factor 2. *Eur J Biochem*, **191**, 639-645.
77. Kenney, J.W., Moore, C.E., Wang, X. and Proud, C.G. (2014) Eukaryotic elongation factor 2 kinase, an unusual enzyme with multiple roles. *Adv Biol Regul*, **55**, 15-27.
78. Torrent, M., Chalancon, G., de Groot, N.S., Wuster, A. and Madan Babu, M. (2018) Cells alter their tRNA abundance to selectively regulate protein synthesis during stress conditions. *Sci Signal*, **11**.
79. Endres, L., Dedon, P.C. and Begley, T.J. (2015) Codon-biased translation can be regulated by wobble-base tRNA modification systems during cellular stress responses. *RNA Biol*, **12**, 603-614.
80. Krukowski, K., Nolan, A., Frias, E.S., Boone, M., Ureta, G., Grue, K., Paladini, M.S., Elizarraras, E., Delgado, L., Bernales, S. *et al.* (2020) Small molecule cognitive enhancer reverses age-related memory decline in mice. *Elife*, **9**.
81. Perez-Riverol, Y., Csordas, A., Bai, J., Bernal-Llinares, M., Hewapathirana, S., Kundu, D.J., Inuganti, A., Griss, J., Mayer, G., Eisenacher, M. *et al.* (2019) The PRIDE database and related tools and resources in 2019: improving support for quantification data. *Nucleic Acids Res*, **47**, D442-D450.
82. Parisien, M., Wang, X. and Pan, T. (2013) Diversity of human tRNA genes from the 1000-genomes project. *RNA Biol*, **10**, 1853-1867.
83. Berg, M.D., Zhu, Y., Genereaux, J., Ruiz, B.Y., Rodriguez-Mias, R.A., Allan, T., Bahcheli, A., Villen, J. and Brandl, C.J. (2019) Modulating Mistranslation Potential of tRNA(Ser) in *Saccharomyces cerevisiae*. *Genetics*, **213**, 849-863.
84. Hrabeta-Robinson, E., Marcus, E., Cozen, A.E., Phizicky, E.M. and Lowe, T.M. (2017) High-Throughput Small RNA Sequencing Enhanced by AlkB-Facilitated RNA de-Methylation (ARM-Seq). *Methods Mol Biol*, **1562**, 231-243.
85. Canella, D., Praz, V., Reina, J.H., Cousin, P. and Hernandez, N. (2010) Defining the RNA polymerase III transcriptome: Genome-wide localization of the RNA polymerase III transcription machinery in human cells. *Genome Res*, **20**, 710-721.
86. Gerstein, M.B., Kundaje, A., Hariharan, M., Landt, S.G., Yan, K.K., Cheng, C., Mu, X.J., Khurana, E., Rozowsky, J., Alexander, R. *et al.* (2012) Architecture of the human regulatory network derived from ENCODE data. *Nature*, **489**, 91-100.
87. Wang, J., Zhuang, J., Iyer, S., Lin, X., Whitfield, T.W., Greven, M.C., Pierce, B.G., Dong, X., Kundaje, A., Cheng, Y. *et al.* (2012) Sequence features and chromatin structure around the genomic regions bound by 119 human transcription factors. *Genome Res*, **22**, 1798-1812.
88. Wang, J., Zhuang, J., Iyer, S., Lin, X.Y., Greven, M.C., Kim, B.H., Moore, J., Pierce, B.G., Dong, X., Virgil, D. *et al.* (2013) Factorbook.org: a Wiki-based database for transcription factor-binding data generated by the ENCODE consortium. *Nucleic Acids Res*, **41**, D171-176.

3.8 Supplemental information

3.8.1 Supplemental Methods

Plasmids and strains.

Plasmid manipulations were performed with *Escherichia coli* DH5 α cells (Invitrogen). Multiple vectors for HTT_{Exon1} expression were used. The polyQ regions were encoded by mixed CAG/CAA codon repeats. For the pcDNA3.1-derived HTT_{Exon1} (MATLEKLMKAFESLKSF-[polyQ]-P₁₁-QLPQPP) expression plasmids, we subcloned the HTT_{Exon1} fragment into pCDNA3.1 from a plasmid that as a kind gift of Leslie Thompson (UC Irvine) (1). The pEGFP-derived HTT_{Exon1} (MKAFESLKSF-[polyQ]-P₁₁-QLPQPP) expression plasmids were purchased from Addgene (WT-Pan #99638, pEGFP-Q23 #40261, pEGFP-Q74 #40262). tRNA^{Pro} WT and G3:U70 variants were expressed from a U6 promoter with polythymidine terminator as previously described (2). Human tRNA^{Ser} genes (Ser-AGA-2-3, Ser-CGA-2-1) were PCR amplified from HEK293 genomic DNA with ~300 bp flanking sequence. Anticodon variants were introduced in PCR fragments using overlap extension PCR. tRNA expression cassettes inserted at the PciI (New England Biolabs (NEB), Ipswich, MA, USA) restriction site in pWTPAN, pEGFP-Q23, or pEGFP-Q74-derived plasmids. In pWTPAN constructs, which contain mCherry linked to EGFP, the EGFP was reverted to GFP by site-directed mutagenesis: L64F(TTC), T65S(TCT). Previously, we successfully used a EGFP D129P mistranslation sensitive reporter to observe mis-incorporation resulting from the tRNA^{Pro} G3:U70 variant, that rescued fluorescence by incorporation of Ala at residue 129 (2). S65 in GFP was mutated to Phe (TTT) or Pro (CCA) with the intent of generating similar reporters sensitive to mistranslation of UUU or CCA codons with serine. We found wildtype GFP fluorescence (compared to EGFP) was insufficient to detect mistranslation by fluorescence restoration from these tRNA^{Ser} variants tested. These constructs were used to track transfection efficiency of tRNA expression cassettes and measure protein synthesis rates according to the mCherry fluorescence or by Western blotting. Plasmid DNA for transfection in mammalian cells was purified by Midi-Prep (GeneAid) from 100 ml *E. coli* DH5 α cultures grown at 37°C for 16 hrs to an OD₆₀₀ > 1.0. DNA concentrations were measured using a Nanodrop 2000C (ThermoFisher Scientific).

Western blotting.

Cells were lifted in phosphate buffered saline (1 × PBS pH 7.4; Corning Cellgro, Corning, NY, USA) supplemented with 1 mM EDTA, harvested by pipetting, and centrifuged in 1.5 ml microcentrifuge tubes at 900 × g for 3 min at 4°C. Supernatant was removed and cells washed with ice cold PBS (Corning Cellgro) and centrifuged again. Supernatant was removed and cells were suspended in 50 µl of ice-cold lysis buffer: 50 mM Tris-HCl (pH 7.4), 1% Triton X-100, 150 mM NaCl, 0.1% sodium dodecyl sulfate (SDS), and 1 mM phenylmethylsulfonyl fluoride. The re-suspended cells were incubated on ice for 5 min then centrifuged at 4°C, 20,000 × g for 10 minutes. Supernatant was collected and used immediately or flash-frozen and stored at -80°C. Protein concentrations were measured in duplicate using the bicinchoninic acid (BCA) assay (ThermoFisher Scientific) and diluted to equimolar protein concentrations before SDS-polyacrylamide gel electrophoresis (SDS-PAGE). Lysates were separated on SDS-PAGE (10% acrylamide) with protein standards (BioRad, Hercules, CA, USA) for size determination. After SDS-PAGE, proteins were transferred to polyvinylidene fluoride membranes using a Trans-Blot Turbo Transfer System (max 25 V, 2.5 A constant for 7 min; BioRad). Membranes were incubated for 1 hr in blocking solution (3% bovine serum albumin (BSA), 0.1% Tween 20, 1% PBS) before adding primary antibodies at a 1:5000 (α -GFP, Abcam, ab32146; α -GAPDH, Sigma-Aldrich, MAB374m, α -HSP70, Invitrogen, MA3-006; α -HSP90, Protein Tech, Rosemont, IL, USA, 13171-1-AP) or 1:1000 (α -Phospho-eIF2a Ser52, ThermoFisher Scientific, 44-728G; α -eIF2a, ThermoFisher Scientific, AHO0802). Membranes were incubated with primary antibody in blocking solution overnight at 4°C, washed 3 × 10 min in washing solution (1% BSA, 0.1% Tween 20, 1% PBS), then incubated with anti-mouse (Thermo Fisher Scientific, MA1-21315) or anti-rabbit (Sigma, GENA9340) horse radish peroxidase-linked secondary antibodies for 2 hr at room temperature (~22°C) with a 1:2000 final dilution. Membranes were then washed with 1 × PBS with 0.1% Tween 20 for 3 × 10 min, followed by one wash for 10 minutes in 1 × PBS. Proteins were visualized using Clarity Western enhanced chemiluminescence (ECL) Substrates (Bio-Rad) following the manufacturer's instructions and imaged with a ChemiDoc XRS+ System (Bio-Rad).

Mass Spectrometry.

mCherry protein was immunoprecipitated from N2a cells expressing wildtype tRNA^{Ser}_{AGA} or mistranslating tRNA^{Ser}_{AAA} after 48 hr transfection. Three 10 cm plates of transfected cells were harvested for each plasmid and lysed in ice-cold lysis buffer (see Western Blotting). mCherry protein was immunoprecipitated using RFP-trap agarose affinity resin (Chromotek, Munich, Germany) following the manufacturer's instructions. In the final step, mCherry protein was eluted by boiling the affinity beads in SDS loading dye at 95°C for 5 min. Beads were pelleted in a quickspin mini centrifuge, and supernatants were loaded on a 12% SDS-PAGE gel. Gels were stained with Coomassie blue to visualize the mCherry protein.

Bands corresponding to mCherry protein were picked from the SDS-PAGE gel using an Ettan Robotic Spot-Picker and submitted for proteolytic digestion (Trypsin) and peptide extraction at the Functional Proteomics Facility at the University of Western Ontario, Canada. Gel plugs were de-stained with 50 mM ammonium bicarbonate and 50% acetonitrile solution, dehydrated in 100% acetonitrile solution, then reduced with 10 mM DTT at 40°C. Alkylation was performed with 55 mM iodoacetamide at 40°C. Gel plugs were then washed once with 100% acetonitrile, once with 50 mM ammonium bicarbonate and 50% acetonitrile, then twice with 100% acetonitrile. Gel-bound proteins were digested overnight with 4 ng/μl trypsin in 50 mM ammonium bicarbonate at 40°C. Trypsinized proteins were extracted from gel plugs with 2% formic acid and 2% acetonitrile.

The dried sample was reconstituted in 40 μl for sample WT, and in 25 μl or sample VAR, of 0.1% Formic acid in water and 1 μl was injected onto an ACQUITY MClass UPLC system using an ACQUITY UPLC MClass Symmetry C18 trap column (Waters Corporation, Milford, MA), at a flow rate of 5 μl/min for 6 minutes using 99% buffer A (0.1% formic acid) and 1% buffer B (Acetonitrile + 0.1% formic acid). After trapping the peptides were eluted onto the analytical column for separation, using a 90 min run time. Flow was established at 300 nl/min for the ACQUITY UPLC MClass Peptide BEH C18 Column 15K psi, 130A, 1.7 μm x 25mm which was held at 35°C. The gradient initial condition was 1% buffer B. Buffer B then increased to 7.0% over 1 min, then to 23% over 44 min, then to 35% over 15 min, then to 98% over 5 min, then held at 98% for 5 min, before washing and re-equilibration steps. The LC system was directly connected to a NanoFlex (Thermo Electron Corp., Waltham, MA) nanospray ionization source with a source voltage of 2.3 KV and was interfaced to a QExactive Plus mass spectrometer (Thermo Electron

Corp., Waltham, MA). The mass spectrometer was controlled by Xcalibur software (Thermo, v. 2.8.1) and operated in the data-dependent mode using an FT/FT/HCD Top 12 scheme. The MS scan recorded the mass-to-charge ratios (m/z) of ions over the range of 375–1500 with a resolution of 70,000 at m/z 400, positive ion, profile, full MS mode using a lock mass (445.120025 m/z). The 12 most abundant multiply charged ions were automatically selected for subsequent high energy collisional induced dissociation in the HCD cell, (FT/HCD) with an isolation width of 2.00 Da, and a 0.5 Da offset, centroid mode, 17500 resolution in the orbitrap, with charge state filtering allowing only ions of +2, to +6 charged states. Normalized Collision energy was 25, and precursor ions were then excluded from further HCD for 15s.

Raw data files were loaded, processed, and searched using Peaks X+ (Bioinformatics Solutions Inc.), against a custom database, consisting of a group of common contaminants and possible proteoforms of mCherry resulting from Phe-to-Ser, and Leu-to-Ser possible substitutions. An FDR of 0.1% and at least 1 unique peptide were used. A maximum of 3 missed cleavages (MC) were allowed for searching tryptic peptides. Fixed modification of carbamidomethylation (CAM) Cysteine, and variable modifications of deamidation (N/Q), oxidation (M, H, W), sulphone (M), and iodination (YH) with a parent mass error tolerance of 10.0 ppm and fragment mass error tolerance of 0.02 Da were used, allowing non-specific cleavage at one end of peptide. Hits representing Phe-to-Ser misincorporation were curated to include only peptides with area-under-the-curve values $\geq 1 \times 10^7$ and with y and b ion spectra capturing the misincorporation event. Example peptides demonstrating mis-incorporation (Table 3.2, Fig. S3.1) as well as a complete list (Table 3.3) are included.

Fluorescence microscopy.

ImageJ macros are included in the appendix of this file with detailed analysis, descriptions, and line-by-line commentary. Fluorescent microscopy images were captured on an EVOS FL auto fluorescent microscope (Thermo Fisher Scientific). GFP (470 ± 22 nm excitation, 510 ± 42 nm emission) and RFP (531 ± 40 nm excitation, 593 ± 40 nm emission) filter cubes were used to capture green or red fluorescence. In our initial experiments (Fig. 3.2A), fluorescence was quantitated on the EVOS software by drawing ellipses within fluorescing cells as described previously (2). For subsequent fluorescence analyses, we used semi-automated ImageJ macros to annotate cells and measure intensity within regions of interest (ROI; see appendix). For

experiments with ISRIB, 500nM ISRIB dissolved in DMSO or an equivalent volume of DMSO was added to cells after 24 hrs transfection. Images were captured immediately after adding ISRIB and again after 18 hr incubation. For fluorescence-based aggregation experiments, aggregates of EGFP-fused polyQ proteins were visible after 24-48 hrs, and all images of aggregates were captured at least 24 hrs post-transfection unless otherwise stated. To quantify insoluble protein aggregate size, an established membrane detergent assay with Triton X-100 was performed (3). Initial images were captured 48 hrs post-transfection, cells were incubated for 40 min in media containing 0.25% Triton X-100, and images were captured again from the same location using the EVOS microscope. The size of the insoluble aggregates was quantified using ImageJ thresholding analysis (see appendix) similarly to published approaches (4). Scale bars were used to determine the conversion factor of pixels to μm^2 . For live cell imaging, cells were incubated at 37°C with humidity and 5% CO₂ in the EVOS FL auto-fluorescent microscope environment chamber. Images were captured every 30 minutes for an 18 hr time-course, starting 24 hrs post-transfection. Fluorescence and number of aggregates were quantified using a semi-automated approach in ImageJ (see appendix) based on established approaches to quantitate protein aggregation (4).

3.8.2 Supplemental Tables

Table S3.1. Oligonucleotide sequences

Description	Nucleotide sequence
tRNA-Ser-AGA-2-3 genomic PCR (Fwd)	CCTGGAAGTCCGAACACC
tRNA-Ser-AGA-2-3 genomic PCR (Rev)	GTGAACACAAAGATGAGAGACACC
tRNA-Ser-AGA-2-3 nested PCR with PciI cloning site (Fwd)	CAGACTACATGTGTTGGCCATGACTCCCC
tRNA-Ser-AGA-2-3 nested PCR with PciI cloning site (Rev)	CAGACTACATGTGCAATTCCGTGAGGGAAATTCG
tRNA-Ser-AGA-2-3 G35A mutagenesis (Fwd)	GCGATGGACTAAAAATCCATTGGGGTCTCCCC
tRNA-Ser-AGA-2-3 G35A mutagenesis (Rev)	CCAATGGATTTTTAGTCCATCGCCTTAACCACTC
tRNA-Ser-CGA-2-1 nested PCR with PciI cloning site (Fwd)	CAGACTACATGTACATGCACAGCAGCGTTC

tRNA-Ser-CGA-2-1 nested PCR with PciI cloning site (Rev)	CAGACTACATGTTTGCCGTTAGAATCTGTTCG
tRNA-Ser-CGA-2-1 C34T, A36G mutagenesis (Fwd)	CGTTGGACTTGGGAATCCAATGGGGTCTCCCC
tRNA-Ser-CGA-2-1 C34T, A36G mutagenesis (Rev)	CCATTGGATTCCAAGTCCAACGCCTTAACCAC
Replace EGFP in WT-PAN with GFP mutant with EcoRI (Fwd)	CAGACTGAATTCGCCACCATGGTGAGCAAG
Replace EGFP in WT-PAN with GFP mutant with BamHI (Fwd)	CAGACTGGATCCGACTTGTACAGCTCGTCCATG
GFP S65F(UUU) mutagenesis (Fwd)	GACCACCTTCTTTTACGGCGTGCAGTGCTTC
GFP S65F(UUU) mutagenesis (Rev)	GCCGTAAAAGAAGGTGGTCACGAGGGTGG
GFP S65P(CCA) mutagenesis (Fwd)	GACCACCTTCCCATACGGCGTGCAGTGCTTC
GFP S65P(CCA) mutagenesis (Rev)	GCCGTATGGGAAGGTGGTCACGAGGGTGG

Table S3.2. tRNA gene sequences and identifiers

tRNA gene ^a	genomic sequence ^b	locus	variants	dbSNP ID ^c
Ser-AGA-2-3	GTAGTCGTGGCCGAGTGGTTAAGGCGAT GGACTAGAAATCCATTGGGGTCTCCCCG CGCAGGTTCTGAATCCTGCCGACTACG	chr6:27463593 -27463674	G35A	rs14743933 7
Ser-CGA-2-1	GCTGTGATGGCCGAGTGGTTAAGGCGTT GGACTCGAAATCCAATGGGGTCTCCCCG CGCAGGTTCAAATCCTGCTCACAGCG	chr6:27177628 -27177709	C34T, A36G	n.a. ^d
Pro-TGG-1-1	GGCTCGTTGGTCTAGTGGTATGATTCTCG CTTTGGGTGCGAGAGGtCCCGGGTTCAAA TCCCGGACGAGCCC	chr14:2110116 5-21101236	C3G, G70T	n.a. ^d

^aGtRNadb gene symbol from high confidence tRNA gene set (*Human Feb. 2009 GRCh37/hg19*) (5). ^bNone of the listed tRNA genes contain introns compared to the predicted mature tRNA sequence (5). ^cdbSNP is the NCBI database of genetic variation (build 155; released Apr. 9, 2021) (6). ^dSynthetic variants, no associated SNP ID.

3.8.3 Supplemental Figures

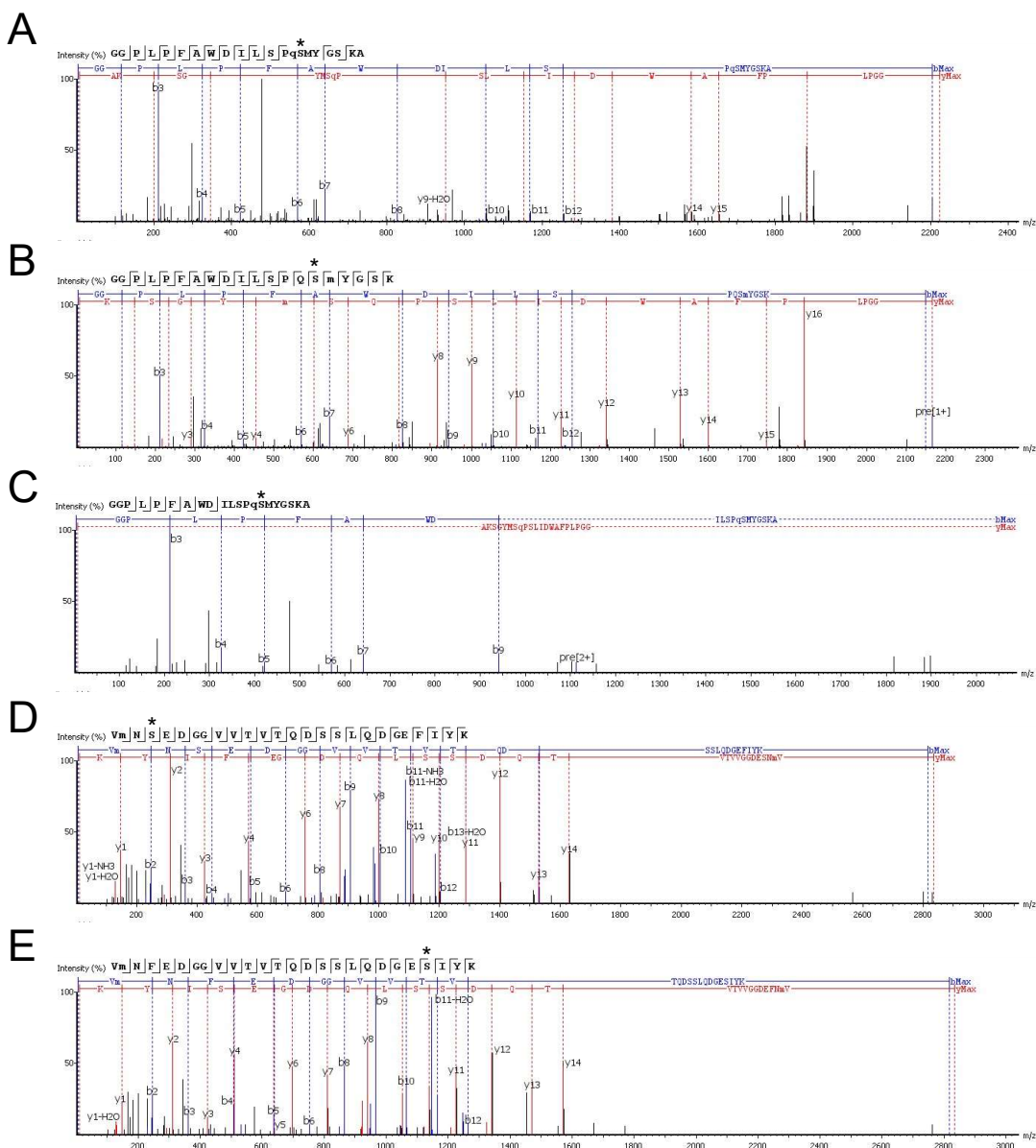


Figure S3.1. Detailed y and b ion spectra of observed Ser mistranslation at Phe codons. MS/MS spectra of high abundance peptides (area > 1×10^7) described in Table 2 are shown. Stars indicate Phe (UUC) codons that were mistranslated as Ser. One low scoring peptide hit ($-10\log P = 58.8$) was observed from cells expressing (A) $tRNA^{\text{Ser}}_{\text{AGA}}$ and a (C) similar low scoring hit ($-10\log P = 48$) was found in mistranslating cells. (B, D, E) Multiple high-quality hits ($-10\log P > 88$) demonstrated Ser mis-incorporation at three different Phe codons in mCherry in cells expressing $tRNA^{\text{Ser}}_{\text{AAA}}$.

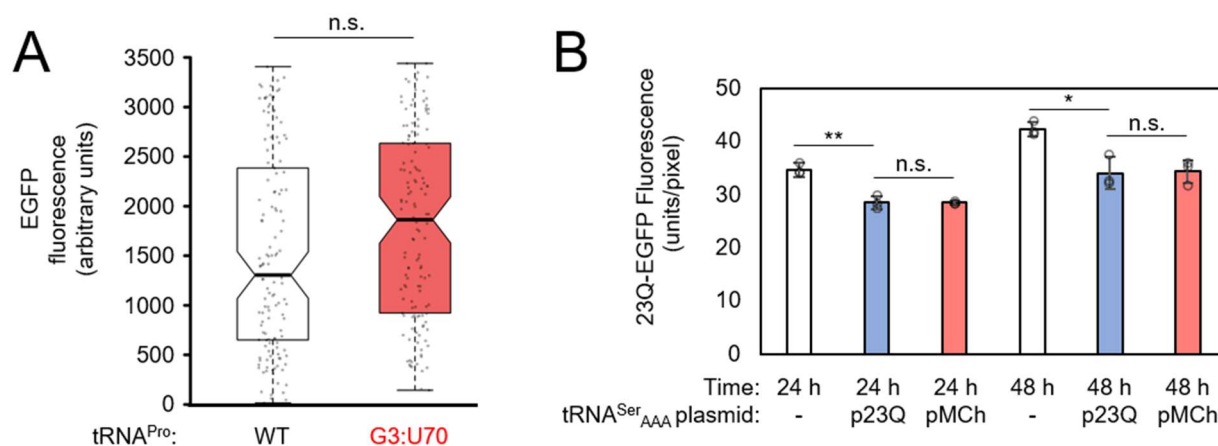


Figure S3.2. HEK293 cells expressing tRNA^{Pro} G3:U70 and cis/trans-plasmid expression tests of N2a cells expressing tRNA^{Ser}_{AAA}. (A) HEK293 cells were transfected with a plasmid encoding human tRNA^{Pro} or the tRNA^{Pro} G3:U70 variant and wild-type EGFP as previously described (2). Fluorescence of cells was measured by fluorescence microscopy in GFP settings. Significant differences (independent sample t-test) of biological means are marked (n.s. = no significant difference). (B) N2a cells were co-transfected with two plasmids: one encoding 23Q-EGFP (p23Q) and another encoding mCherry (pMCh). The tRNA^{Ser}_{AAA} variant was either not included (-) or cloned into the p23Q or the pMCh plasmid as indicated. Cellular fluorescence was captured by fluorescence microscopy in GFP and RFP settings at 24 hr and 48 hr timepoints. Fluorescence per unit area was quantitated in ImageJ. Error bars represent the mean \pm 1 standard deviation of three biological replicates; stars indicate statistically significant differences according to independent sample t-tests (n.s. = no significant difference, * = $p < 0.05$, ** = $p < 0.01$).

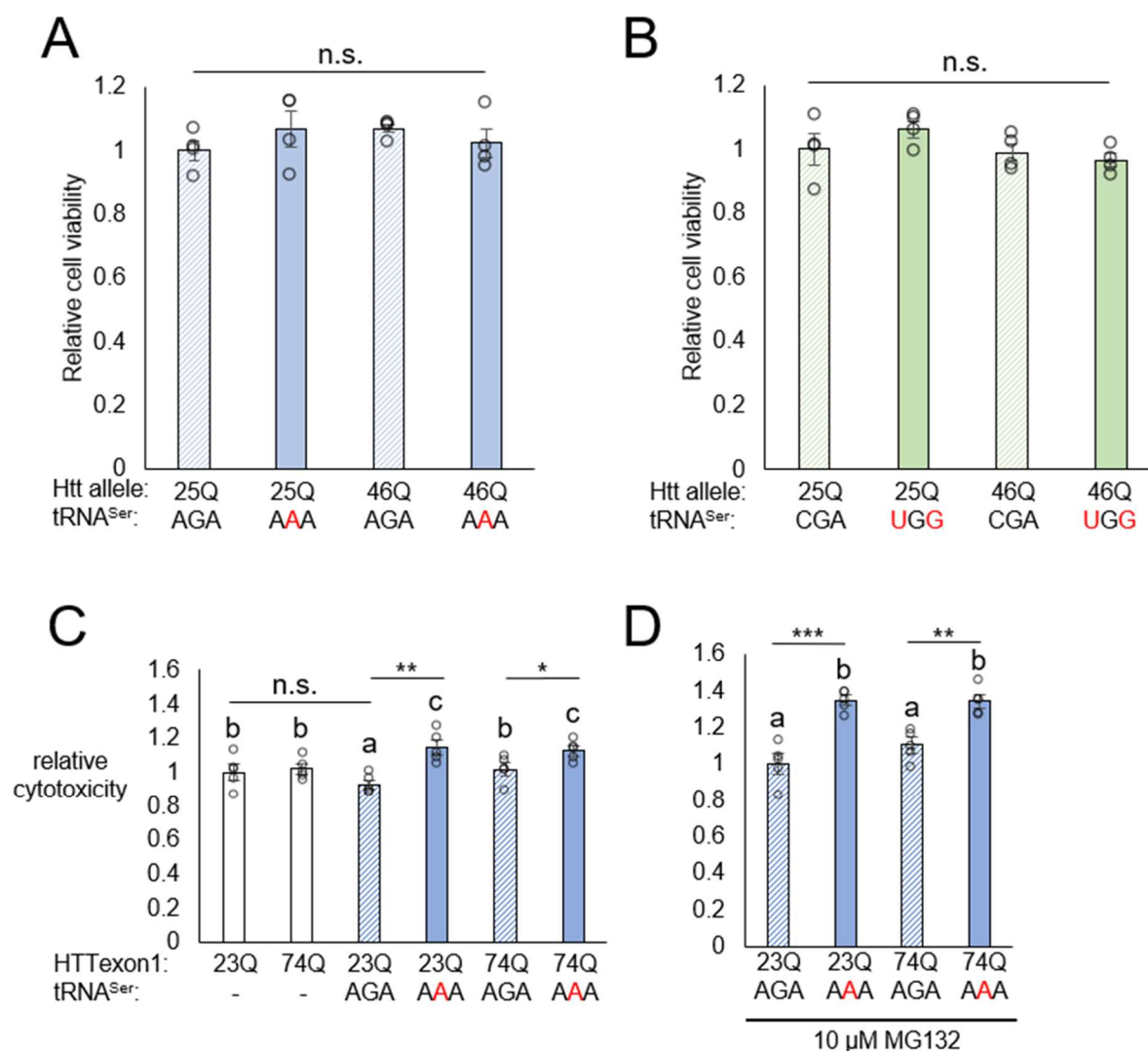


Figure S3.3. Viability of cells mistranslating Phe or Pro codons with Ser and expressing HTTExon1 variants. (A, B) N2a cells were co-transfected with two plasmids encoding HTTExon1 25Q or 46Q and (A) tRNA^{Ser}_{AGA} or G35A variant tRNA^{Ser}_{AAA} or (B) tRNA^{Ser}_{CGA} or C34G, A36G variant tRNA^{Ser}_{UGG}. Cellular viability was assayed 24 hr post-transfection with the CellTiterGlo 2.0 assay. Luminescence readings were normalized to the (A) 25Q/AGA or (B) 25Q/CGA controls. (C, D) N2a cells were transfected with a plasmid encoding human tRNA^{Ser}_{AGA} or G35A variant tRNA^{Ser}_{AAA} and HTTExon1 containing 23Q- or 74Q-EGFP. (C) Cytotoxicity was assayed 48 hr post-transfection with the CytotoxGlo assay. (D) The experiment was repeated with a 4-hour treatment of 10 μM MG132 before assay. Luminescence readings were normalized to the (C) 23Q/no tRNA control or to the (D) 23Q/AGA control. Stars represent p-values from (A,B) ANOVA or (C,D) pairwise independent sample t-tests (n.s. = no significant difference, * = $p < 0.05$, ** = $p < 0.01$, *** = $p < 0.001$); letters represent significantly different groups from Tukey's honestly significant difference tests ($\alpha = 0.05$). Each bar represents the mean \pm 1 standard deviation of four (A,B) or five (C,D) biological replicates.

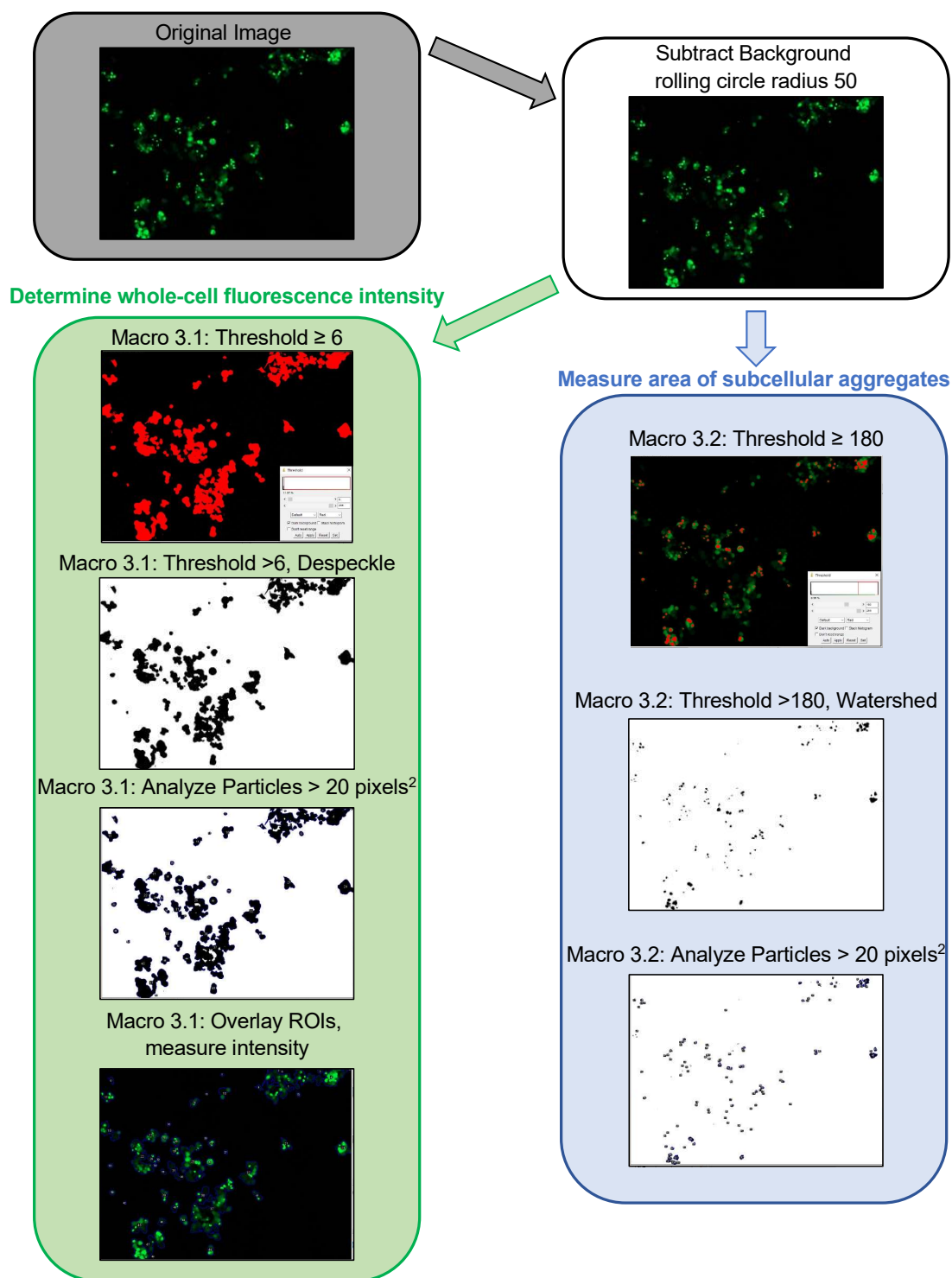


Figure S3.4. Quantitation of aggregate fluorescence and area in ImageJ. Images represent steps in ImageJ macros used to quantitate fluorescent aggregates in live cell data shown in Fig. 3.4. See supplemental methods and appendix for details and ImageJ macros.

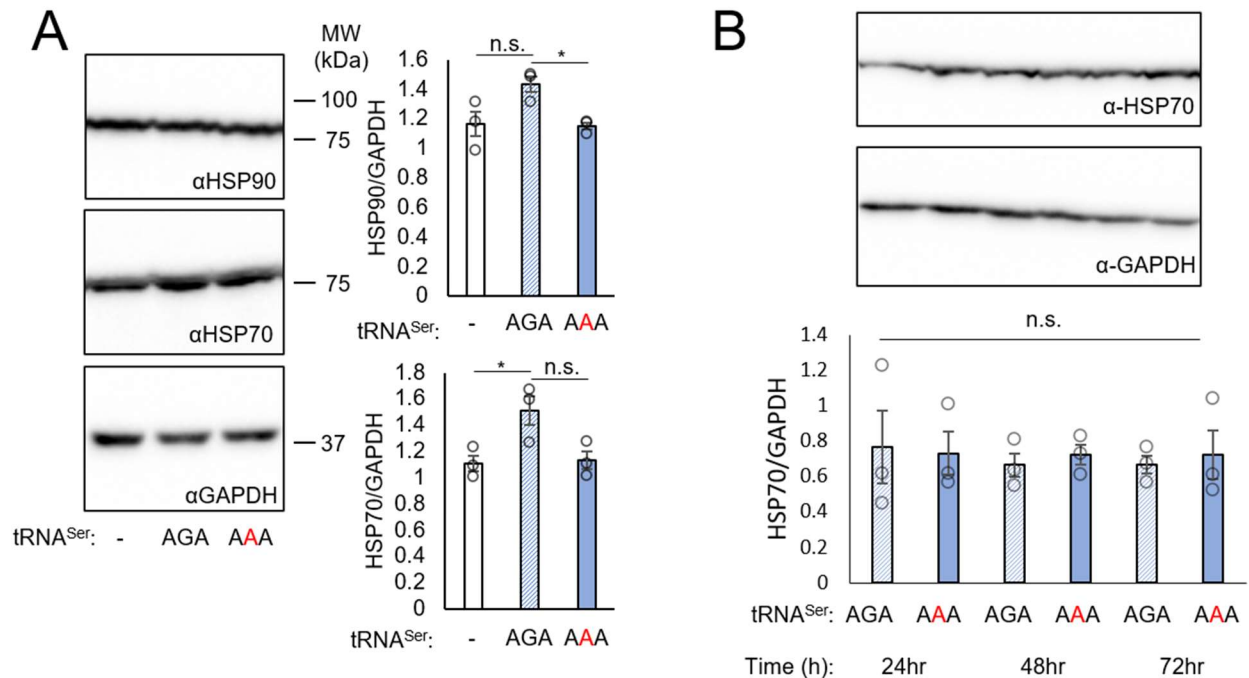


Figure S3.7. Heat shock protein levels in mistranslating cells. N2a cells were transfected with a plasmid encoding human tRNA^{Ser}_{AGA} or G35A variant tRNA^{Ser}_{AAA} and dead GFP(S65F)-mCherry transfection marker. (A) After 24 hr transfections, cell lysates were harvested and western blotted for HSP90, HSP70, and GAPDH loading control. (B) The same transfections were repeated with longer transfection periods and western blotted for HSP70 and GAPDH. Significant differences (independent sample t-test) of three biological replicates are marked with stars (n.s. = no significant difference, * = $p < 0.05$). Error bars represent ± 1 standard deviation.

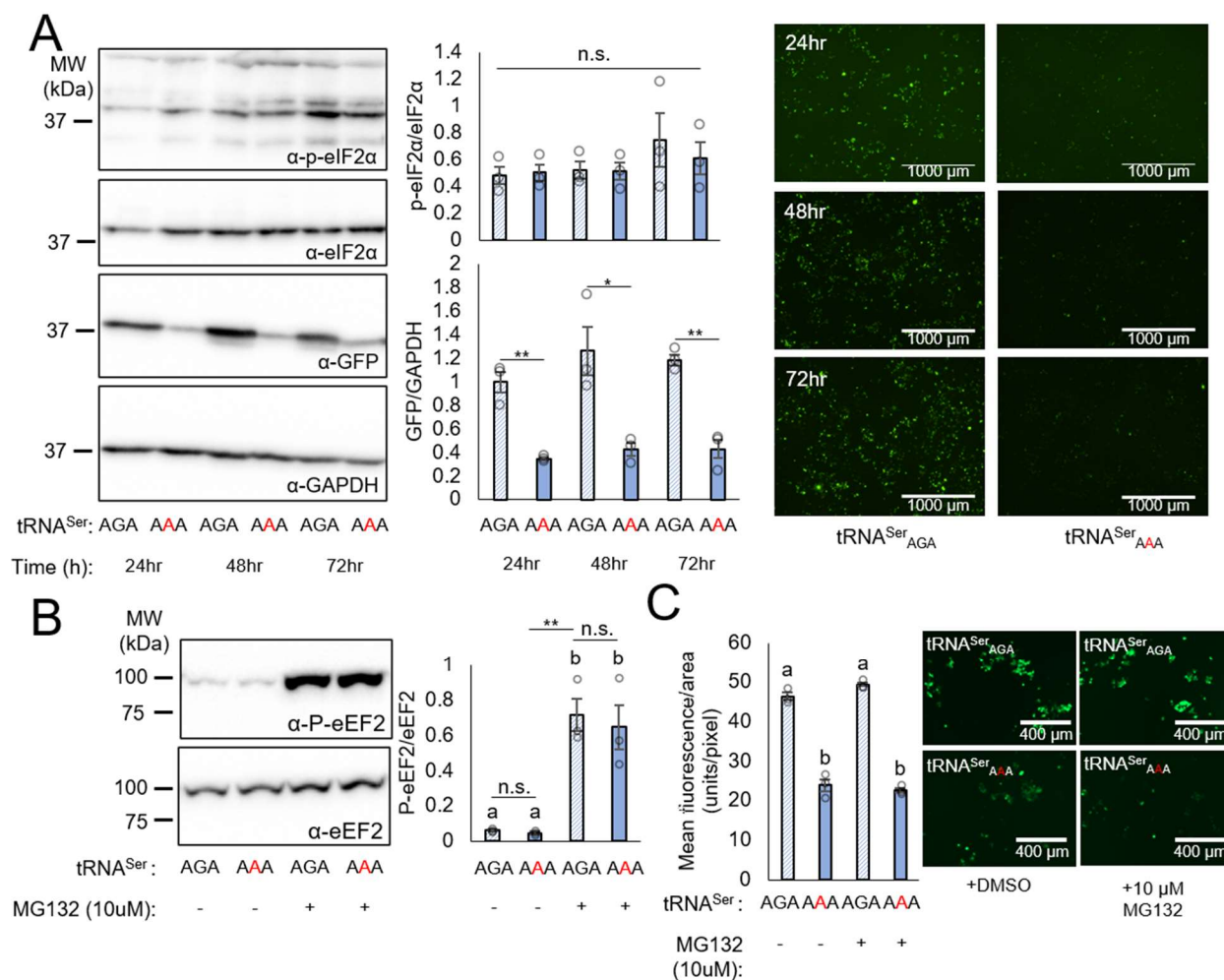


Figure S3.8. Regulation of translation initiation and elongation in mistranslating cells. (A) N2a cells were transfected with a plasmid encoding human tRNA^{Ser}_{AGA} or G35A variant tRNA^{Ser}_{AAA} and HTTexon1 containing 23 (23Q) CAG/CAA mixed codon repeats encoding polyQ fused to EGFP as a transfection marker. Cells were imaged by fluorescence microscopy in GFP settings (A, right panel), harvested, lysed, and western blotted with anti-p-eIF2 α (pSer52), anti-eIF2 α , anti-GFP, and anti-GAPDH antibodies after 24, 48, or 72 hr transfection. (B) N2a cells were transfected with a plasmid encoding human tRNA^{Ser}_{AGA} or G35A variant tRNA^{Ser}_{AAA} and mCherry for 48 hr, treated with MG132 or DMSO for 4 hr, and western blotted with anti-eEF2, anti-p-eEF2 (pThr56). (C) N2a cells were transfected as in (A) and fluorescence was measured after 4 hr treatment with DMSO or MG132. Stars indicate p-values from independent sample t-tests (n.s. = no significant difference, * = $p < 0.05$, ** = $p < 0.01$) and letters indicate significantly different groups determined by Tukey's HSD test ($\alpha = 0.05$).

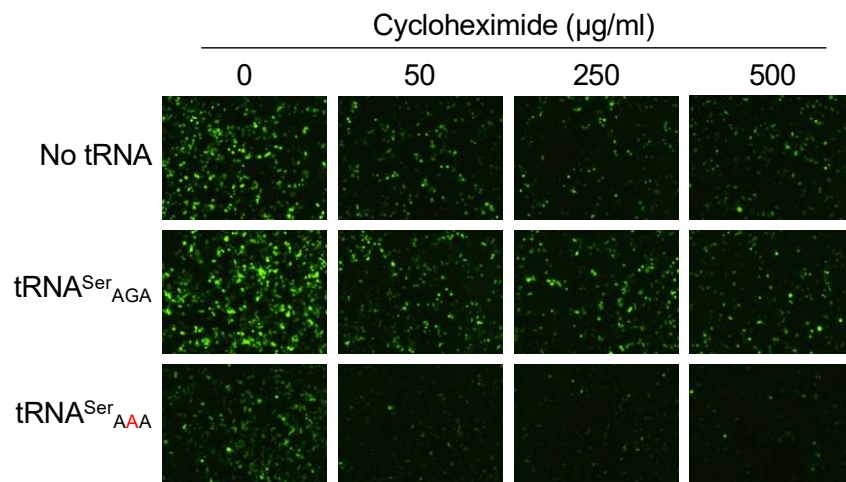


Figure S3.9. Cycloheximide concentration testing. N2a cells were transfected with a plasmid encoding human tRNA^{Ser}_{AGA} or G35A variant tRNA^{Ser}_{AAA} and HTT_{exon1} containing 23Q- or 74Q-EGFP for 48 hr. Cells were washed and treated with indicated concentrations of cycloheximide for 24 hr before capturing images by fluorescence microscopy in GFP settings.

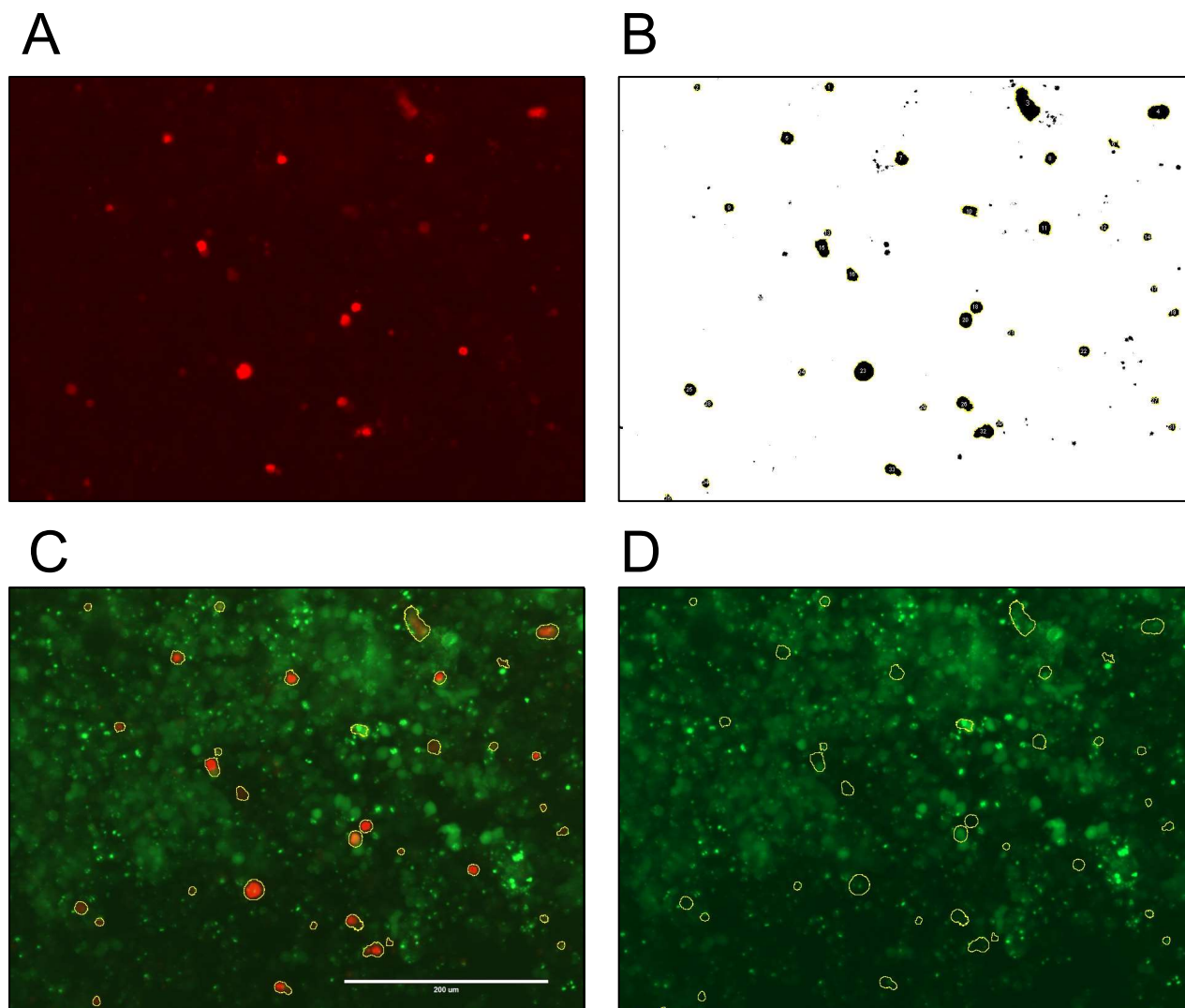


Figure S3.10. Aggregate counting in PC12 cells transfected with mCherry-tRNA plasmids. Mistranslating tRNA^{Ser}_{AAA} and wildtype tRNA^{Ser}_{AGA} were co-expressed with mCherry on plasmids to identify transfected cells. (A) Red channel images were used to generate region of interest markers in ImageJ using (B) threshold and analyze particles functions, then overlaid on (C,D) green channel images to identify cells containing the ectopically expressed tRNA variant and EGFP-tagged polyQ aggregates.

3.8.4 Supporting Data File

Data File S1. Single cell kinetics of polyQ formation in wild type and mistranslating cells.

Image series from live cell fluorescence experiments described in Fig. 3.4 were imported to ImageJ and background fluorescence was subtracted using the rolling circle function. Image series were converted to surface plots using the analyze; surface plot function and saved as .gif files. Peaks represent fluorescent objects in a single field of view. Peak heights represent brightness intensity on a 0-255 scale where zero is black and 255 is maximum pixel intensity.

3.8.5 Supplemental Appendix: ImageJ macros

ImageJ macros and analyses

The following text describes Fiji/ImageJ (7,8) macros used in the manuscript. ImageJ version 1.53c was run on a Windows 10 (64-bit) operating system. Lines beginning with // are commentary describing the line below. See Fig. S3.4 for step-by-step example images showing Macros 3.1.1-3.1.2. Other macros use a similar thresholding approach.

Macros 3.1.1 and 3.1.2: Live cell fluorescence and aggregate count. Live cell image analysis (Fig. 3.4) was done with two split macros on the same image sequences. See Fig. S3.4 for images demonstrating the method. Data sets obtained from ImageJ macros were processed and analyzed in Microsoft Excel. Each image (Fig. 3.4) represented a single time point in one field of view. For each treatment (WT or mutant tRNA), two fields of view were used on three biological replicates, totaling six technical replicates. For fluorescence analysis, image numbers paired to ROIs were copied from the ImageJ ROI manager along with integrated density values from the results window (Macro 3.1.1 and Macro 3.1.2). Using Microsoft Excel, total fluorescence contained within ROIs was calculated for each image (cellular fluorescence).

For aggregate analysis, image numbers paired to ROIs were copied from the ImageJ ROI manager along with area values from the results window (Macro 3.1.2). Using Microsoft Excel, we calculated the sum of area covered by pixels over our aggregation threshold (brightness and size) for each image. We then calculated the average aggregate size across all images. The sum of area covered by aggregates in each image was divided by average aggregate size to estimate the number of aggregates in each image. This approach corrects for clustered objects that cannot be separated by the watershed function. Similar approaches have been used by others to count

fluorescent polyQ protein aggregates in cells (4). For each image sequence (technical replicate), the estimated number of aggregates was plotted against fluorescence (Fig. S3.5). Initial values were subtracted from all data points in each series to exclude fluorescence and aggregates present before the beginning of the time course. Number of aggregates was normalized to image fluorescence for each image series and plotted against time (Fig. 3.4). Error bars represent one standard deviation of the mean for each time point.

Macro 3.1.1.

This macro is to select area containing fluorescing cells from a series of fluorescent cell images, create region of interest (ROI) annotations, and measure fluorescence (integrated density).

```
//Import image sequence. Replace "file" with desired image series location. "number" is the
number of images in the series and "increment" is used to exclude unwanted images in the file
folder.
run("Image Sequence...", "open=[file] number=37 increment=2 sort");
//Subtract background signal using rolling circle method with radius of 50 pixels.
run("Subtract Background...", "rolling=50 stack");
//Set threshold to exclude pixels below chosen cutoff (6 in this case). Fine-tune according to your
image brightness and use same cutoff for all images in one experiment.
setThreshold(6, 255);
//Next two lines convert image to black features (above threshold) on white background (below
threshold)
setOption("BlackBackground", false);
run("Convert to Mask", "method=Default background=Dark");
//Remove noise with despeckle function
run("Despeckle", "stack");
//Create annotations covering area above threshold. Excludes objects under size cutoff of 20
pixels. Size cutoff should be adjusted depending on the magnification of the image and the size
of objects you wish to exclude (noise).
run("Analyze Particles...", "size=20-Infinity display clear summarize add stack");
//Clear results. This macro is only to create ROIs so results meaningless at this point.
run("Clear Results");
//Import unmodified image sequence again. Should be identical to line 1
run("Image Sequence...", "open=[file] number=37 increment=2 sort");
//Subtract background signal using rolling circle method with radius of 50 pixels.
run("Subtract Background...", "rolling=50 stack");
//Set measurements to record integrated density to 3 decimals.
run("Set Measurements...", "integrated redirect=None decimal=3");
//The next three lines overlay the ROIs generated from thresholding steps on the original image
sequence, calculate the intensity within the ROIs, and display the results in the "Results"
window.
```



```
roiManager("Show None");
roiManager("Show All");
roiManager("Measure");
```

Macro 3.1.2.

This macro is to select area containing fluorescing protein aggregates from a series of fluorescent cell images, create region of interest (ROI) annotations, and measure area. The threshold should be fine-tuned to capture only subcellular objects (protein aggregates) and avoid whole fluorescent cells.

```
//import image sequence. Should be identical to line 1 in Macro 3.1.1
run("Image Sequence...", "open=[file] number=37 increment=2 sort");
//Subtract background signal using rolling circle method with radius of 50 pixels.
run("Subtract Background...", "rolling=50 stack");
//Set threshold to exclude pixels below chosen cutoff (180 in this case). Fine-tune according to
your image brightness and use same cutoff for all images in one experiment.
setThreshold(180, 255);
//Next two lines convert image to black features (above threshold) on white background (below
threshold)
setOption("BlackBackground", false);
run("Convert to Mask", "method=Default background=Dark");
//Watershed function separates closely adjacent objects with a line. This is important when
measuring area of objects.
run("Watershed");
//Creates annotations covering area above threshold. Excludes objects under size cutoff of 20
pixels. Size cutoff should be adjusted depending on the magnification of the image and the size
of objects you wish to exclude (noise).
run("Analyze Particles...", "size=20-Infinity display clear summarize add stack");
//Clear results outputting from analyze particles function
run("Clear Results");
//next two lines measure the area of objects above the intensity and size cutoffs and display the
results in the "Results" window.
run("Set Measurements...", "area redirect=None decimal=3");
roiManager("Measure");
```

Macro 3.2.1: Aggregate size and count. The output of this analysis includes the count and size of objects in fluorescent cell images (Fig. 3.5B). Nine images were captured across three biological replicates from each transfected plasmid. Images were captured before and after Triton X-100 treatment. Post-treatment images were used for size analysis. Scale bars was measured in ImageJ

to calculate the conversion factor of pixels to μm^2 . The area values of fluorescent objects (post-Triton X-100) outputted from ImageJ were converted from pixels to μm^2 and all data were plotted as boxplots using R. Outliers exceeding 1.5X the interquartile range of the entire dataset were omitted from plots and statistical analysis. Outlier removal excludes clustered objects that are not properly separated by the watershed function. Statistical differences were calculated with an independent sample t-test based on means of biological replicates.

```
//open image. Replace "file" with desired image location.
open("file");
//Subtract background signal using rolling circle method with radius of 50 pixels.
run("Subtract Background...", "rolling=50");
//Set threshold to exclude pixels below chosen cutoff (100 in this case). Fine-tune according to
your image brightness and use same cutoff for all images in one experiment.
setThreshold(100, 255);
//Next two lines convert image to black features (above threshold) on white background (below
threshold)
setOption("BlackBackground", false);
run("Convert to Mask");
//Remove noise with despeckle function
run("Despeckle");
//Watershed function separates closely adjacent objects with a line.
run("Watershed");
//Set measurements to record object area
run("Set Measurements...", "area redirect=None decimal=3");
//Record measurements and display results summary
run("Analyze Particles...", "display clear summarize add");
```

Macro 3.3.1: % increase fluorescence/area. The “mean” measurement parameter on ImageJ is equal to the integrated density divided by area (pixels) within a region of interest (ROI). ROI annotations were used to select only the area in images covered by fluorescing cells. Mean (fluorescence/area) was measured rather than integrated density to accommodate differences in cell sizes or cell clusters which could not be resolved by the watershed function. Two images were captured from each of three biological replicates, totaling six technical replicates. Images from before (i) and after (f) an 18 hr time course were used in analysis. “% increase fluorescence/area” (Fig. 3.6B) was calculated by the following formula:

$$\% \text{ increase} \frac{\text{fluorescence}}{\text{area}} = 100 \times \left(\frac{\text{fluorescence}_i}{\text{area}_i} - \frac{\text{fluorescence}_f}{\text{area}_f} \right)$$

Statistical differences were calculated with an independent sample t-test based on means of biological replicates.

```
//open image. Replace "file" with desired image location.
open("file");
//Subtract background signal using rolling circle method with radius of 50 pixels.
run("Subtract Background...", "rolling=50");
//Set threshold to exclude pixels below chosen cutoff (6 in this case). Fine-tune according to your
image brightness and use same cutoff for all images in one experiment.
setThreshold(6, 255);
//Next two lines convert image to black features (above threshold) on white background (below
threshold)
setOption("BlackBackground", false);
run("Convert to Mask");
//Remove noise with despeckle function
run("Despeckle");
//Watershed function separates closely adjacent objects with a line.
run("Watershed");
//Analyze particles to generate ROI annotations. Excludes objects under size cutoff of 20 pixels.
Size cutoff should be adjusted depending on the magnification of the image and the size of
objects you wish to exclude (noise).
run("Analyze Particles...", "size=20-Infinity display clear summarize add");
//Clear results
run("Clear Results");
//Reopen the same file from step 1
open("file");
//Subtract background signal using rolling circle method with radius of 50 pixels.
run("Subtract Background...", "rolling=50");
//Overlay ROI markers on reopened image
roiManager("Show None");
roiManager("Show All");
//Set measurements to mean and measure
run("Set Measurements...", "mean redirect=None decimal=3");
roiManager("Measure");
```

Macro 3.4.1: Fluorescence/initial cell area. This macro is to select area containing fluorescing cells from a series of fluorescent cell images, create region of interest (ROI) annotations, and measure fluorescence (integrated density) and area of the ROIs. This was used to quantitate decreasing fluorescence in cycloheximide chase assays (Fig 3.7). A modified analysis was used in this case because cycloheximide-treated cells shrink in size over time. Hence, we found that normalizing fluorescence/area on a per-image basis was ineffective. Therefore, we instead normalized the total fluorescence in each image sequence to the area of fluorescing cells in the first image of the same sequence. We then subtracted the initial values of fluorescence/area for each sequence and calculated the average slope of each data sequence to produce the “Delta Fluorescence/Initial Cell Area” and “Average Slope” plots shown in Fig. 3.7. Six image sequences were captured across three biological replicates for each combination of transfected plasmid and treatment condition.

```
//Import image sequence. Replace “file” with desired image series location. “number” is the
number of images in the series and “increment” is used to exclude unwanted images in the file
folder.
run("Image Sequence...", "open=[file] number=49 starting=2 increment=3 sort");
//Subtract background signal using rolling circle method with radius of 50 pixels.
run("Subtract Background...", "rolling=50 stack");
//Set threshold to exclude pixels below chosen cutoff (6 in this case). Fine-tune according to your
image brightness and use same cutoff for all images in one experiment.
setThreshold(10, 255);
//Next two lines convert image to black features (above threshold) on white background (below
threshold)
setOption("BlackBackground", false);
run("Convert to Mask", "method=Default background=Dark");
//Remove noise with despeckle function
run("Despeckle", "stack");
//Watershed function separates closely adjacent objects with a line.
run("Watershed", "stack");
//Analyze particles to generate ROI annotations. Excludes objects under size cutoff of 100 pixels.
Size cutoff should be adjusted depending on the magnification of the image and the size of
objects you wish to exclude (noise).
run("Analyze Particles...", "size=100-Infinity display clear summarize add stack");
//Clear results
run("Clear Results");
//Reopen the same file from step 1
run("Image Sequence...", "open=[file] number=49 starting=2 increment=3 sort");
//Overlay ROI markers on reopened image
roiManager("Show None");
roiManager("Show All");
```

```
//Set measurements to area and integrated density, then measure
run("Set Measurements...", "area integrated redirect=None decimal=3");
roiManager("Measure");
```

3.8.6 Supplemental References

1. O'Rourke, J.G., Gareau, J.R., Ochaba, J., Song, W., Rasko, T., Reverter, D., Lee, J., Monteys, A.M., Pallos, J., Mee, L. *et al.* (2013) SUMO-2 and PIAS1 modulate insoluble mutant huntingtin protein accumulation. *Cell Rep*, **4**, 362-375.
2. Lant, J.T., Berg, M.D., Sze, D.H.W., Hoffman, K.S., Akinpelu, I.C., Turk, M.A., Heinemann, I.U., Duennwald, M.L., Brandl, C.J. and O'Donoghue, P. (2018) Visualizing tRNA-dependent mistranslation in human cells. *RNA Biol*, **15**, 567-575.
3. Titus, S.A., Southall, N., Marugan, J., Austin, C.P. and Zheng, W. (2012) High-Throughput Multiplexed Quantitation of Protein Aggregation and Cytotoxicity in a Huntington's Disease Model. *Curr Chem Genomics*, **6**, 79-86.
4. Scotter, E.L., Narayan, P., Glass, M. and Dragunow, M. (2008) High throughput quantification of mutant huntingtin aggregates. *J Neurosci Methods*, **171**, 174-179.
5. Chan, P.P. and Lowe, T.M. (2016) GtRNAdb 2.0: an expanded database of transfer RNA genes identified in complete and draft genomes. *Nucleic Acids Res*, **44**, D184-189.
6. Sherry, S.T., Ward, M.H., Kholodov, M., Baker, J., Phan, L., Smigielski, E.M. and Sirotkin, K. (2001) dbSNP: the NCBI database of genetic variation. *Nucleic Acids Res*, **29**, 308-311.
7. Schneider, C.A., Rasband, W.S. and Eliceiri, K.W. (2012) NIH Image to ImageJ: 25 years of image analysis. *Nat Methods*, **9**, 671-675.
8. Rueden, C.T., Schindelin, J., Hiner, M.C., DeZonia, B.E., Walter, A.E., Arena, E.T. and Eliceiri, K.W. (2017) ImageJ2: ImageJ for the next generation of scientific image data. *BMC Bioinformatics*, **18**, 529.

Chapter 4

4. Kinetics of amyotrophic lateral sclerosis-associated protein aggregation in mistranslating cells¹

4.1 Introduction

Transfer RNAs (tRNAs) play an essential role in the translation of messenger RNA (mRNA) into protein. High-fidelity protein synthesis or the accurate translation of the genetic code was considered an essential feature of cells and organisms. Although errors in protein synthesis normally occur rarely with estimates suggesting that every 1 in 1,000 to 10,000 codons is misread (1), diverse cells can survive or tolerate significantly elevated levels of mistranslation of 1-10% per codon (2-4). Mistranslation can result from mutations in tRNAs (5) or the aminoacyl-tRNA synthetases (6) that are responsible for ligating each tRNA with its cognate amino acid (7). In addition, mutations to the ribosome (8), ribosomal proteins ((9)), and other (10) components of the protein quality control machinery can also increase rates of error in protein synthesis.

Mistranslation due to tRNA variants can result from a mutation in the anticodon or in identity element nucleotides (11) that each AARS uses to recognize its cognate tRNA. Anti-codon mutations have great potential to cause loss of tRNA function, yet for certain tRNAs, the cognate AARS does not recognize the anticodon nucleotides. Thus, mutations to the anticodon in alanine (Ala), serine (Ser), and in part leucine (Leu) tRNAs have significant potential to cause amino acid mis-incorporation at different codons in cells. In a distinct mechanism, mutations to tRNA identity elements that inhibit AARS activity may cause loss-of-function (12), while mutations that enable a tRNA to acquire new identity can lead to mis-aminoacylation of tRNAs and mistranslation (3,13). For example, the G3:U70 base pair is the major recognition element for alanyl-tRNA synthetase (AlaRS) (14). Certain variants in the human population (5) create alanine identity elements in other tRNAs that direct alanine mis-incorporation in yeast (13) and cells (3).

There are over 600 tRNA genes in the human genome. In comparison to the reference genome, individuals carry many single nucleotide (15,16) and even multi-site variants in their tRNA genes (17). In a study of 84 individuals, unprecedented variation in tRNAs was uncovered, indicating individuals harbor 60-70 tRNA variants, including mistranslating tRNAs that occur as both rare or more common variants in the population (17). One such mistranslating tRNA is a G35A variant

¹Work in this chapter is preparation for publication. Authorship: Jeremy T. Lant, Farah Hasan, Julia Briggs, and Patrick O'Donoghue.

in the tRNA-Ser-AGA-2-3 gene (tRNA^{Ser}_{AGA}). The resulting tRNA^{Ser}_{AAA} mutant contains a G-to-A substitution in the second position of the anticodon. Because seryl-tRNA synthetase (SerRS) does not recognize the anticodon of tRNA^{Ser} (18), the mutant tRNA causes mis-incorporation of serine at phenylalanine codons in mammalian cells (19).

The tRNA^{Ser}_{AAA} variants, which are found in 2-3% of the population (5,17), have the potential to exacerbate human diseases, including neurodegeneration (19). We recently characterized the impact of tRNA^{Ser}_{AAA} on cytotoxicity, protein synthesis, and in genetic interactions with non-aggregating and aggregating huntingtin alleles. Mistranslating cells expressing the tRNA^{Ser} G35A variant were slow but effective in forming disease-causing huntingtin aggregates, but mistranslating cells were completely deficient in degrading and clearing the same aggregates. The results suggested that natural tRNA variants compromise translation fidelity, which may increase the severity of Huntington's disease caused by protein aggregation. We hypothesized that other neurodegenerative diseases may also be exacerbated by the presence of a mistranslating tRNA in a patient's genetic background. To establish the general potential for mistranslating tRNA variants to modify neurodegenerative disease, we characterized tRNA-dependent mistranslation in a well-established cellular models of Amyotrophic Lateral Sclerosis (ALS)

Protein misfolding and aggregation is characteristic of many neurodegenerative diseases, however, the impact of mistranslation on the molecular pathology of neurodegenerative diseases is unknown aside from the Huntington's Disease model noted above. ALS is a neurodegenerative disease caused by the aggregation of proteins in neurons, leading to muscle wasting, weakness, and eventual death (20). The aggregation of nuclear RNA binding proteins, notably the fused in sarcoma (FUS) protein, is commonly associated with ALS (21). FUS is a DNA and RNA binding protein that is important for transcription and mRNA processing in neurons (22). There are 19 known FUS mutations that are linked to the development of ALS, and FUS mutations are found >4% of patients who present with ALS (23-26). Most FUS mutations are present in the nuclear localization domain at the C-terminus of the protein, which prevents translocation of FUS into the nucleus where it normally regulates transcription and RNA splicing (27,28) through interactions with RNA polymerase II, transcription factor TFIID, and directly with RNA (29,30). FUS also plays important roles in regulating DNA replication kinetics (31).

FUS variants associated with disease mis-localize to the cytoplasm and form insoluble protein aggregates. Disease pathology results from both loss of nuclear function as well as gain of toxic

function in the cytosol (32). The Arg521Cys (R521C) mutation occurs in the C-terminal non-canonical nuclear localization signal (NLS) domain of the FUS protein and leads to decreased trafficking of FUS into the nucleus, increased cytoplasmic FUS concentrations (33), and greater insoluble protein aggregate formation (34). Individuals carrying mutations like R521C tend to develop early onset ALS, with 60% of cases occurring before 40 years of age (28).

Here we tested our hypothesis that compromised translation fidelity will alter FUS aggregation kinetics in neuroblastoma cells and exacerbate FUS toxicity. Using established cellular model of ALS (35,36), we found that mistranslating cells readily formed FUS protein aggregates but at a slower rate compared to cells expressing wild-type tRNA. We observed a synthetic toxic interaction between the FUS R521C mutant and tRNA-dependent mistranslation in mammalian cells. The data further establishes the ability of naturally occurring tRNA mistranslators to impact cell fitness and protein aggregation in a cellular model of neurodegeneration.

4.2 Material and Methods

4.2.1 Plasmids and strains

Plasmid manipulations were performed in *Escherichia coli* DH5 α cells (Invitrogen Canada, Burlington, ON). tRNA^{Pro} WT and G3:U70 variants were expressed from a U6 promoter with polythymidine terminator as previously described (3). Human tRNA^{Ser} genes (Ser-AGA-2-3) were PCR amplified from human embryonic kidney (HEK) 293T genomic DNA with \pm 300 bp flanking sequence. Anticodon variants were introduced in PCR fragments using overlap extension PCR, as previously described (19). The tRNA expression cassettes were inserted at the *Pci*I (New England Biolabs, Ipswich, MA, USA) restriction site in pWTPAN-derived plasmids or at the *Nru*I site in pcDNA3.1-derived plasmids.

Fusions of the FUS gene with fluorescent proteins were created by PCR amplifying the full-length FUS gene (encoding residues 1-526) from a pcDNA3.1 plasmid containing the human FUS gene isoform 1 (a kind gift of Dr. Michael Strong) with a primer-encoded flexible linker sequence (amino acid sequence GGGSGG). EGFP fusions were created by inserting the FUS-linker sequence into *Nhe*I and *Hind*III restriction sites in our previously described pcDNA3.1-EGFP plasmid (3). FUS-mCherry fusion constructs were also created by inserting the FUS-linker PCR product into the *Nhe*I and *Spe*I sites of WT-PAN (37). WT-PAN contains an EGFP-mCherry

fusion protein, and our approach replaced the EGFP segment with the FUS gene and linker sequence.

The R521C variant of the FUS-mCherry protein was created by round-the-horn PCR mutagenesis using primers, including the mutant nucleotide C1561T. Plasmids containing mCherry were created by digesting and cross-ligating the isoschizomeric *NheI* and *SpeI* sites in WT-PAN to remove the EGFP gene. Plasmid DNA for transfection in mammalian cells was purified by Midi-Prep (GeneAid, New Taipei City, Taiwan) from 100 ml *E. coli* DH5 α cultures grown at 37 °C for 16 hrs to an A₆₀₀ > 1.0. DNA concentrations were measured using a Nanodrop 2000C (ThermoFisher Scientific, Waltham, MA).

4.2.2 Cell culture and transfections

Experiments were performed in murine Neuro2a Neuroblastoma (N2a) cells (ATCC #CCL-131) or HEK 293T cells (ATCC #CRL-3216). All cell lines were grown at 37 °C with humidity and 5% CO₂. Cells were cultured in high glucose Dulbecco's modified Eagle medium (DMEM with 4.5 g/L glucose, Gibco by Life Technologies, Carlsbad, CA) containing penicillin (100 IU/mL, Wisent Bioproducts, Montreal, QC, Canada), streptomycin (100 μ g/mL, Wisent Bioproducts), and 10% fetal bovine serum (FBS, Gibco). All transfections were performed using Lipofectamine 3000 transfection reagent (Invitrogen) with 2 μ g/mL plasmid DNA, following the manufacturer's instructions.

4.2.3 Cytotoxicity assay

Cytotoxicity was determined using a dye-exclusion assay with SYTOX Blue Dead Cell Stain (Invitrogen). No tRNA, wild-type tRNA^{Ser}_{AGA}, or the tRNA^{Ser}_{AAA} variant was co-expressed in N2a cells with mCherry, FUS-mCherry or R521C FUS-mCherry in N = 5 biological replicates. After 48 hrs, cells were washed once with Hank's buffered salt solution (HBSS) and the media was replaced with DMEM containing 1 μ M SYTOX Blue Dead Cell Stain. SYTOX Blue fluorescence intensity was measured with a Synergy H1 plate reader with a monochromatic filter set to 444 nm excitation and 480 nm emission. Images were captured using an EVOS FL auto fluorescent microscope using an RFP filter cube (531 \pm 40 nm excitation, 593 \pm 40 nm emission) to measure mCherry fluorescence and CFP filter cube (445 \pm 45 nm excitation, 510 \pm 42 nm emission) to measure SYTOX Blue fluorescence. To establish the total number of cells, 0.25% v/v

Triton X-100 was added to each well and the cells were incubated at 37 °C for 40 min to completely permeate cell membranes and allow SYTOX Blue staining. Images were captured again from the same location using the EVOS microscope and SYTOX Blue fluorescence was measured again with the Synergy H1 after Triton X-100 treatment. Cell death levels were calculated as the ratio SYTOX blue fluorescence before and after Triton X-100 treatment.

4.2.4 Fluorescence microscopy

Green and red fluorescent images were captured on an EVOS FL auto fluorescent microscope using GFP (470 ± 22nm excitation, 510 ± 42nm emission) and RFP (531 ± 40 nm excitation, 593 ± 40 nm emission) filter cubes. Aggregates of FUS begin to form at 24 hrs post-transfection, and all images of cells were taken between 24- and 72-hours post-transfection. For live cell imaging, cells were incubated in the EVOS environment chamber at 37 °C and 5% CO₂ with humidity. Images were captured every 30 min, beginning 24 hrs after the start of transfection for time courses of 18 to 44 hrs as indicated. Before beginning the time course, culture plates were placed in the environment chamber for 1 hr to acclimate before fine-tuning fields of view. Fluorescence per cell and number of aggregates per cell were quantitated using a semi-automated approach in ImageJ (see supplemental information). To further investigate aggregate solubility, an established membrane detergent assay with Triton X-100 was performed (38). Initial images were captured 72 hrs post-transfection, cells were then incubated for 40 min in DMEM containing 0.25% Triton X-100, and images were captured again from the same location using the EVOS microscope, as before (19). We determined the number of aggregates remaining post-triton X-100 with a semi-automated approach in ImageJ (see supplemental information).

4.2.5 Cell harvesting and western blotting

At 48 or 72 hrs post-transfection, as indicated, cells grown in 6-well plates were lifted in phosphate buffered saline (PBS; 137 mM NaCl, 2.7 mM KCl, 10 mM Na₂HPO₄, 1.8 mM KH₂PO₄, pH 7.4) with 10 mM EDTA for 10 min at 37 °C, collected in sterile 1.5 mL microcentrifuge tubes, and pelleted by centrifugation at 300 × g for 3 min at 4 °C. The supernatant was aspirated, and cell pellets were stored at -80 °C. Cell pellets were resuspended in 90 µL of mammalian cell lysis buffer containing 50 mM Na₂HPO₄, 1 mM Na₄P₂O₇, 20 mM NaF, 2 mM EDTA, 2 mM EGTA, 1 mM Triton X-100, 1 mM dithiothreitol, 0.3 mM phenylmethylsulfonyl fluoride, and 1 tablet/10

ml complete mini EDTA-free Protease Inhibitor Cocktail (Roche, Mississauga, ON), incubated for 5 min on ice, and centrifuged at $21,000 \times g$ for 10 min at 4°C . Supernatants were collected in 1.5 mL microcentrifuge tubes and kept on ice or stored at -20°C for up to one week. Protein concentrations in the lysates were determined with a Pierce bicinchoninic acid (BCA) protein assay kit (ThermoFisher Scientific). Lysates were diluted to equal concentrations with sterile milliQ H_2O and $3 \times$ sodium dodecyl sulfate (SDS) loading dye (0.5 M Tris-HCl, pH 6.8; 1.12 M sucrose; 0.025% w/v bromophenol blue; 3.8% w/v SDS). Lysate corresponding to 12 μg total soluble protein was separated by SDS-polyacrylamide gel electrophoresis (10% acrylamide) with protein standards (BioRad, Hercules, CA, USA) for size determination. Proteins were transferred to methanol-activated polyvinylidene fluoride membranes using a Trans-Blot Turbo Transfer System (25 V, 1.3 A for 14 min; BioRad). Blocking and washing solutions were prepared in tris-buffered saline (TBS; 50 mM Tris-HCl, pH 7.5, 150 mM NaCl). Membranes were incubated for 1 hr in blocking solution (3% bovine serum albumin (BSA), 0.1% Tween 20, 1X TBS) before adding primary antibodies at a 1:1000 (α -mCherry, abcam, ab213511) or 1:5000 (α -GAPDH, Sigma-Aldrich, MAB374m) dilution in blocking solution. Membranes were incubated with primary antibody in blocking solution overnight at 4°C , washed 3×10 min in washing solution (1% BSA, 0.1% Tween 20, 1X TBS), then incubated with anti-mouse (Thermo Fisher Scientific, MA1-21315) or anti-rabbit (Sigma, GENA9340) horse radish peroxidase-linked secondary antibodies for 2 hr at room temperature with a 1:2000 final dilution. Membranes were washed with $1 \times$ TBS with 0.1% Tween 20 for 3×10 min, followed by one wash for 10 minutes in $1 \times$ TBS. Proteins were visualized using Clarity Western enhanced chemiluminescence (ECL) Substrates (Bio-Rad) following the manufacturer's instructions and imaged with a ChemiDoc MP System (Bio-Rad).

4.2.6 Semi-denaturing detergent agarose gel electrophoresis (SDD-AGE)

Cell lysates were prepared, and protein concentrations were measured 72 hrs post-transfection as described above. A 1.5% agarose gel and Tris-acetate EDTA (TAE) running buffer containing 40 mM Tris-acetate, 1 mM EDTA, and 0.1% w/v SDS were prepared according to established protocols (39). Lysate samples containing 20 μg of protein were diluted in $3 \times$ loading dye (0.5 M Tris-HCl, pH 6.8, 1.12 M sucrose; 0.025% w/v bromophenol blue; 3.8% w/v SDS) with sterile milliQ H_2O . Lysates were separated on the agarose-SDS gel for at least 3 hours at 20V. Proteins were transferred to a PVDF membrane by capillary gel transfer overnight using TAE with

0.1% SDS as a buffer. mCherry-tagged FUS aggregates were visualized by western blotting with an α -mCherry antibody.

4.2.7 Statistical analysis

Statistical analyses used in each figure are referenced in the figure legends. All statistical analysis was done in Microsoft Excel (2019). Independent sample t-tests were done by pairwise comparison of groups of biological means. Tukey-Kramer multiple comparison tests were computed by first completing an ANOVA single-factor (one-way) test on all groups of biological means from the experiment. Critical q values were found in studentized range tables ($\alpha = 0.05$). Standard error to determine Tukey's significance threshold was calculated for each pairwise comparison when necessary to account for groups of unequal sample size (eg. some microscopy images were poor quality and excluded).

4.3 Results

4.3.1 FUS protein synthesis in mistranslating cells

To monitor the synthesis and aggregation of FUS proteins in mistranslating cells, we cloned wild-type and R521C FUS as fluorescently tagged fusion proteins (Fig. S4.1A) that were expressed from plasmids containing wild-type tRNA genes or variant alleles that cause mistranslation (3,19). We chose to C-terminally-tag FUS proteins with mCherry, since this approach was already established as an appropriate model of FUS protein aggregation associated with ALS (35,36,40,41). Since FUS aggregation is caused by mis-localization of the FUS protein to the cytoplasm, and FUS utilizes a C-terminal nuclear localization signal, C-terminal fluorescent protein fusions both promote aggregation of FUS and provide a means to visualize FUS aggregation in live cells (42). Since the R521C variant is a common mutation in patients with ALS (23-26), we anticipated that it would be more prone to aggregate and that cells expressing the FUS variant would provide an appropriate model of disease pathology at the cellular level.

To validate expression and aggregation of the FUS-mCherry protein from our constructs, we initially transfected all plasmids in HEK293T cells. Thus, we established transiently transfected cell lines expressing all combinations of wild-type FUS-mCherry or FUS(R521C)-mCherry and wild-type tRNA-Ser-AGA-2-3 (tRNA^{Ser}_{AGA}) or G35A variant (tRNA^{Ser}_{AAA}) (Fig. S4.1B,C). In

HEK293T cells we observed production of the FUS-mCherry variants in normal and mistranslating cells within 24 hrs transfection and clear evidence of subcellular aggregate formation (Fig. S4.1B,C). The data suggested that both FUS and FUS R521C variants were produced and that less protein production was observed in cells also expressing the mistranslating tRNA, in agreement with our previous observations (19).

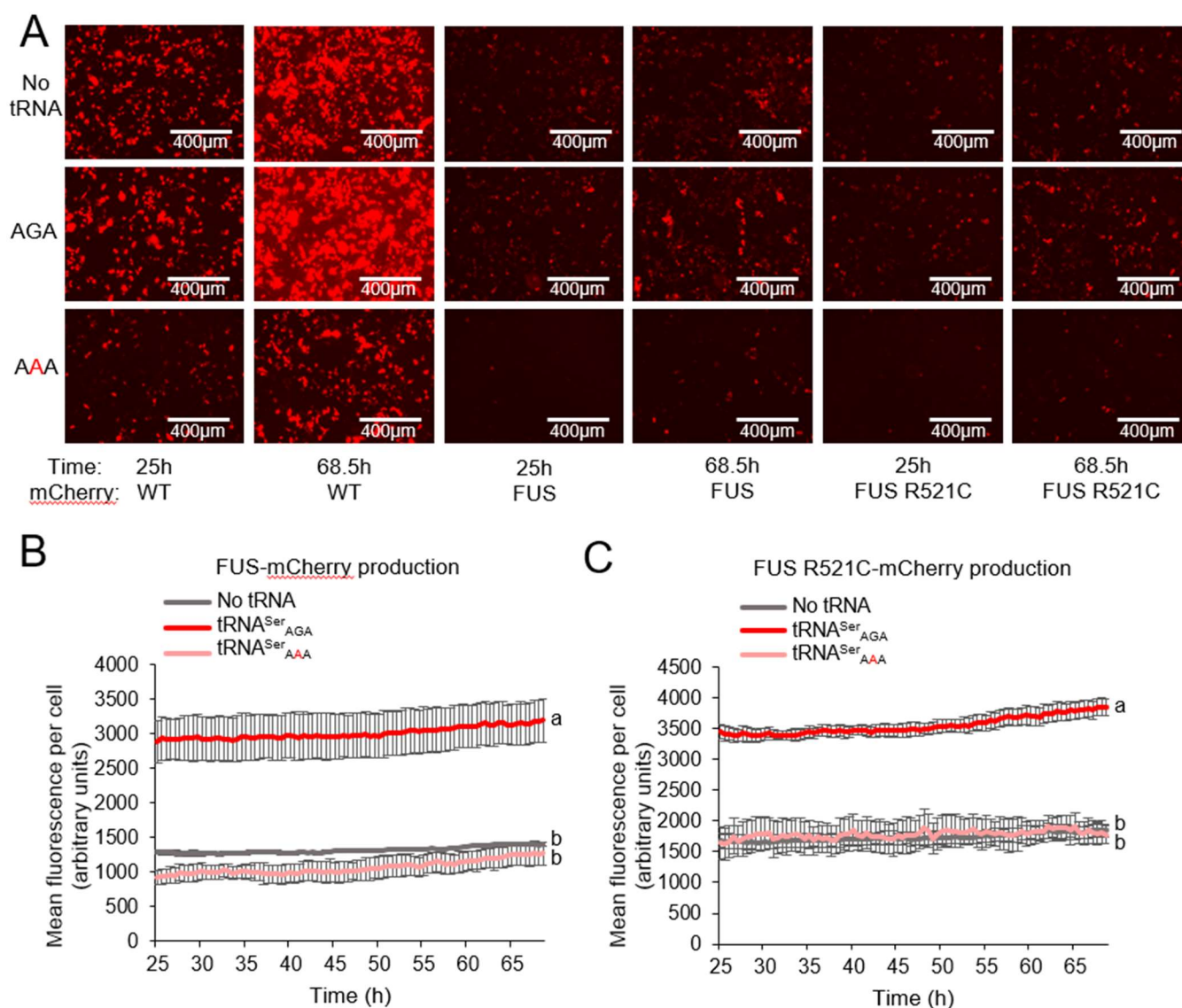


Figure 4.1. Kinetics of FUS protein synthesis in wild-type and mistranslating cells. N2a cells were transfected with a plasmid encoding no tRNA, human $tRNA^{Ser}_{AGA}$ or G35A variant $tRNA^{Ser}_{AAA}$ and mCherry, human FUS-mCherry fusion or R521C variant FUS-mCherry fusion protein. Images of fluorescing cells were captured by live cell fluorescence microscopy (RFP, ex

531 nm, em 593 nm) beginning 24 h after transfection for a 43.5 h timelapse. Representative images at the start and end of the timelapse are shown (A). Fluorescence per cell was quantitated with a custom Fiji/ImageJ macro (see supplemental information) in at least three biological replicates (B,C). Letters indicate significantly different groups determined by Tukey-Kramer tests based on the means across all timepoints, where groups sharing a letter are not significantly different and groups not sharing a letter are significantly different ($\alpha = 0.05$).

To further investigate the synthesis of FUS proteins in normal and mistranslating cells, we employed murine Neuro2A neuroblastoma (N2a) cells that are more accurate models of disease-causing protein aggregation in neuronal cells. In addition to FUS alleles and tRNA variants, we transfected N2a cells with plasmids including mCherry without a FUS allele, as well as plasmids that contained no additional tRNA (Fig. 4.1A). Beginning 25 hr post-transfection, we captured the fluorescence of the mCherry or FUS-mCherry proteins per cell over a 43.5-hr time-course. Strikingly, we observed a significant 2.28 ± 0.24 fold increase in FUS-mCherry and 2.05 ± 0.06 fold increase in FUS(R521C)-mCherry fluorescence of cells expressing the wild-type tRNA^{Ser_{AGA}} compared to no tRNA (Fig 4.1B,C,S4.2A,B). In cells expressing the variant tRNA^{Ser_{AAA}}, we observed fewer living cells with visible FUS-mCherry fluorescence, but surprisingly fluorescence per cell was not reduced significantly compared to cells expressing no tRNA (Fig. 4.1B,C, S4.2A,B).

We found in all cases that FUS-mCherry fluorescence was substantially lower than fluorescence from mCherry alone (Fig. 4.1A). For this reason, quantitative FUS-mCherry and mCherry images could not be obtained at the same exposure settings. To establish effects of the tRNAs on mCherry alone, we transfected the mCherry with no tRNA, tRNA^{Ser_{AGA}}, and tRNA^{Ser_{AAA}} variant separately in N2a cells for 24 hr (Fig. S4.2C). In cells expressing mCherry alone, tRNA^{Ser_{AGA}} caused a significant 1.31 ± 0.05 -fold increase in fluorescence compared to no tRNA, and the tRNA^{Ser_{AAA}} caused a significant 1.28 ± 0.03 -fold reduction in fluorescence compared to no tRNA. Thus, only in cells expressing the FUS-mCherry or FUS(R521C)-mCherry did we not observe a significant reduction in fluorescence when tRNA^{Ser_{AAA}} was expressed compared to no tRNA.

4.3.2 Toxicity of FUS alleles in mistranslating cells

To assess the cytotoxic effects of the tRNA and FUS-mCherry models, we used a dye exclusion assay with Sytox Blue stain to label and count dead cells before and after treatment with a strong membrane detergent (Triton X-100). At 70 hrs post-transfection and following the observation of FUS-mCherry production (Fig. 4.2), the cells were stained with Sytox Blue, and images and fluorescence were captured by fluorescence microscopy and with a microplate reader. Cellular and nuclear membranes were then permeabilized with detergent to establish total cell number and Sytox Blue fluorescence in each well (Fig. 4.2, S4.3). We then calculated the ratio of Sytox blue fluorescence before and after cell permeation to measure the fraction of dead cells in each cell line. In comparing cells expressing the wild-type tRNA, we recorded a significant increase in cell death in cells also expressing the FUS R521C allele compared to cells expressing the wild-type FUS protein or to cells that did not express a FUS allele (Fig. 4.2). While mistranslation resulting from $tRNA^{\text{Ser}}_{\text{AAA}}$ alone did not significantly increase cell death, we found significantly more cell death in mistranslating cells that also expressed the FUS R521C allele. This is the first report of synthetic toxicity between mistranslation caused by a natural tRNA variant and cell death induced by an ALS-associated FUS allele.

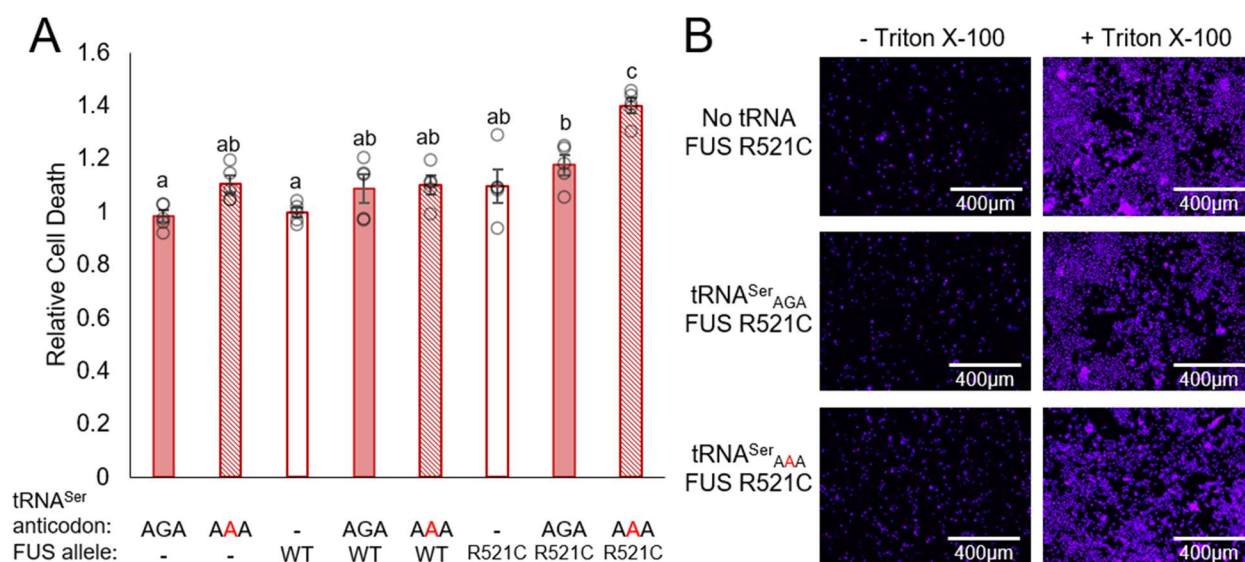


Figure 4.2. Synthetic toxicity of mistranslation and FUS R521C aggregation. N2a cells were transfected with a plasmid encoding no tRNA, human $tRNA^{\text{Ser}}_{\text{AGA}}$ or G35A variant $tRNA^{\text{Ser}}_{\text{AAA}}$ and mCherry, human FUS-mCherry fusion or R521C variant FUS-mCherry fusion protein. After

72hr, cytotoxicity was assayed with a dye exclusion assay using Sytox blue nucleic acid stain. Sytox blue fluorescence was measured in a plate reader (ex 444 nm, em 488 nm) before and after treatment with a cell membrane detergent (Triton X-100) and relative cell death was calculated as the Sytox blue fluorescence ratio before and after detergent. Biological means were normalized to the mean of the wildtype tRNA, mCherry (no FUS) control (**A**). Error bars represent the mean \pm 1 standard deviation of five biological replicates. Letters indicate significantly different groups determined by Tukey's Honestly Significant Difference (HSD) test, where groups sharing a letter are not significantly different and groups not sharing a letter are significantly different ($\alpha = 0.05$). Representative images were captured by fluorescence microscopy (CFP; ex 445 nm, em 510 nm) (**B**; Fig. S4.3).

4.3.3 Aggregation kinetics of FUS in normal and mistranslating cells

Previously, we developed a semi-automated approach based on published methods to quantitate the appearance of fluorescing aggregates of huntingtin poly-glutamine (polyQ) proteins (19). The method employs a dual thresholding strategy, where total cell area is established with a lower intensity threshold that captures all cellular fluorescence, and aggregated protein area is established with a higher intensity threshold which only captures fluorescence emanating from the bright puncta caused by subcellular protein aggregates. Aggregated protein area is then normalized to total cellular fluorescence for a quantitative comparison of the proportion of aggregated protein in live cells. Using this same approach, we first assayed aggregation kinetics of FUS-EGFP fusion protein co-expressed with a synthetic variant of tRNA^{Pro} (G3:U70) which we previously established causes proline to alanine mistranslation in mammalian cells (3). Consistent with our finding on this tRNA and models of huntingtin poly-glutamine proteins (19), we did not observe any significant effects of the tRNA^{Pro} G3:U70 variant on FUS-EGFP aggregation (Fig. S4.4).

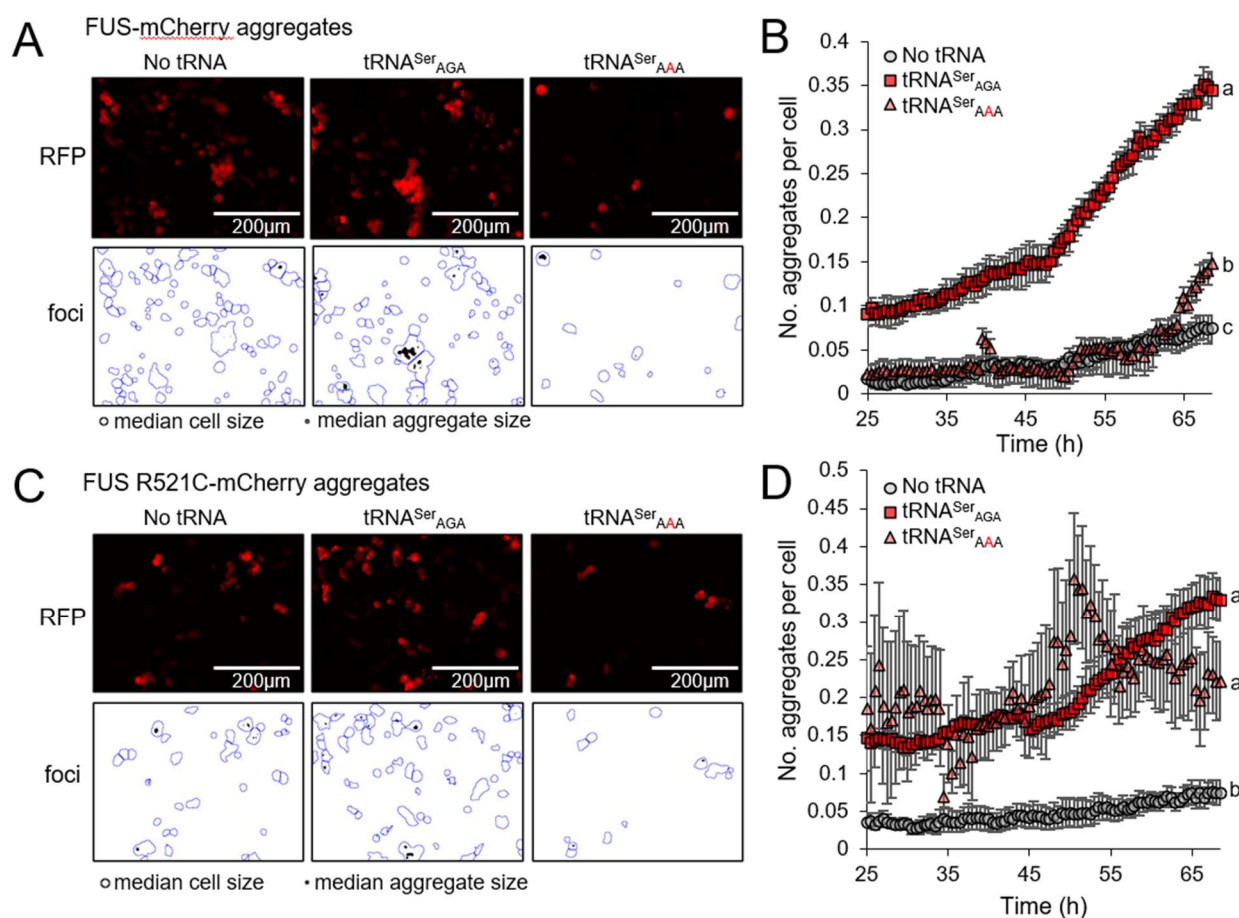


Figure 4.3. Kinetics of FUS protein aggregation in wild-type and mistranslating cells. N2a cells were transfected with a plasmid encoding no tRNA, human tRNA^{Ser}_{AGA} or G35A variant tRNA^{Ser}_{AAA} and mCherry, human FUS-mCherry fusion or R521C variant FUS-mCherry fusion protein. Images of fluorescing cells were captured by live cell fluorescence microscopy (RFP, ex 531 nm, em 593 nm) beginning 24 h after transfection for a 43.5 h timelapse. Fluorescent cell area representing cells and aggregates was determined using a custom Fiji/ImageJ macro and cell and aggregate counts were determined based on correcting object sizes to the median sizes of cells and aggregates (see supplemental information). Representative images of the fluorescing cells and black and white mask images showing aggregate area with blue outlined cell area determined by the macro are shown (A, C). The number of aggregates per cell was plotted against time (B, D). Error bars represent the mean \pm 1 standard deviation of at least four biological replicates. Letters indicate significantly different groups determined by Tukey-Kramer tests based on biological means at the final timepoint, where groups sharing a letter are not significantly different and groups not sharing a letter are significantly different ($\alpha = 0.05$).

To assess aggregation kinetics of our FUS-mCherry and FUS(R521C)-mCherry proteins in the presence of the naturally occurring tRNA^{Ser}_{AAA} variant, we improved on our aggregation analysis by adding a median size adjustment step, where cellular area and aggregate area were normalized to their respective median area values across the entire experiment (Fig. 4.3 A,C, see supplemental information). This allowed us to establish aggregation kinetics on a per-cell rather than per-image basis. Using this approach we measured the number of aggregates per cell over a 43.5 hr time-course (starting 25hr post-transfection) in N2a cells transfected with plasmids encoding FUS-mCherry or FUS(R521C)-mCherry and no tRNA, tRNA^{Ser}_{AGA}, or tRNA^{Ser}_{AAA}.

In cells expressing wild-type tRNA^{Ser}_{AGA} the number of FUS-mCherry aggregates per cell was 5.35 ± 0.76 -fold increased ($p = 0.0004$) at the start of the timecourse and 4.59 ± 0.26 -fold increased ($p = 1.9 \times 10^{-6}$) at the end of the timecourse compared to cells expressing no additional tRNA (Fig. 4A,B, S4.5A). In cells expressing the variant tRNA^{Ser}_{AAA}, the number of aggregates per cell did not differ significantly at the beginning of the timecourse ($p = 0.72$) compared to cells expressing no additional tRNA (Fig. 4.3A,B, S4.5A). However, in the final ~ 5.5 hours of the timecourse, the number of aggregates per cell began increasing rapidly in cells expressing tRNA^{Ser}_{AAA} and FUS-mCherry, to a point where the number of aggregates per cell was 1.97 ± 0.16 -fold increased ($p = 0.0055$) compared to cells expressing no additional tRNA at the end of the timecourse (Fig. 4.3A,B, S5A). While aggregation was still reduced in mistranslating cells compared to cells expressing tRNA^{Ser}_{AGA} (2.38 ± 0.21 -fold, $p = 5.4 \times 10^{-5}$), this suggests that the tRNA^{Ser}_{AAA} variant may promote rapid protein aggregate formation after cells acclimate to the effects of mistranslation.

In cells expressing wild-type tRNA^{Ser}_{AGA}, effects on FUS(R521C)-mCherry aggregation were similar to what we observed for FUS-mCherry, with an initial 4.12 ± 0.29 -fold increase ($p = 1.1 \times 10^{-5}$) in the number of aggregates per cell and 4.59 ± 0.26 -fold increased ($p = 1.8 \times 10^{-5}$) aggregates per cell at the end of the timecourse compared to cells expressing no tRNA (Fig. 4.3C,D, S4.5B). In cells expressing the variant tRNA^{Ser}_{AAA} and FUS(R521C)-mCherry, the increase in cell death (Fig. 4.2) contributed to fewer visibly fluorescing cells. This made aggregation kinetics difficult to quantitate, as dying cells released fluorescent protein into the medium and caused sudden drops in aggregate-per-cell counts (Fig. 4.3D). However, towards the end of the timecourse the variance in aggregates per cell in the tRNA^{Ser}_{AAA} expressing cell population stabilized somewhat and we calculated a significant 2.38 ± 0.89 -fold increase ($p = 0.0172$) in aggregates per cell compared to cells expressing no additional tRNA.

In sum, cells with the additional wild-type tRNA^{Ser} produced FUS and FUS(R521C) more efficiently than cells lacking an additional tRNA, suggesting the added tRNA may provide a more tractable model to study FUS aggregates. Cells with the variant tRNA^{Ser}_{AAA} also promote FUS aggregation compared to cells expressing no tRNA, but the effect is more variable and can be repressed in early stages of tRNA expression. Hence, the tRNA^{Ser}_{AAA} variant caused a discoordination between tRNA expression and protein synthesis, which altered the aggregation kinetics of FUS.

4.3.4 Measuring insoluble FUS aggregates in mistranslating cells

To further assess the effects of mistranslation on FUS aggregation, we attempted a membrane detergent assay (38), which we have used previously to establish the size of huntingtin poly-glutamine aggregates in mistranslating cells compared to wild type. The assay involves mild permeation of cells with Triton X-100, such that diffuse fluorescence dissipates into the medium while insoluble aggregates remain in cells. However, in agreement with our difficulties in quantitating FUS(R521C) in dying cells, we found that FUS aggregates were unstable in permeated cells, and in most cases we could not reliably determine significant differences in the number of aggregates remaining in cells after Triton X-100 treatment (Fig. S4.6).

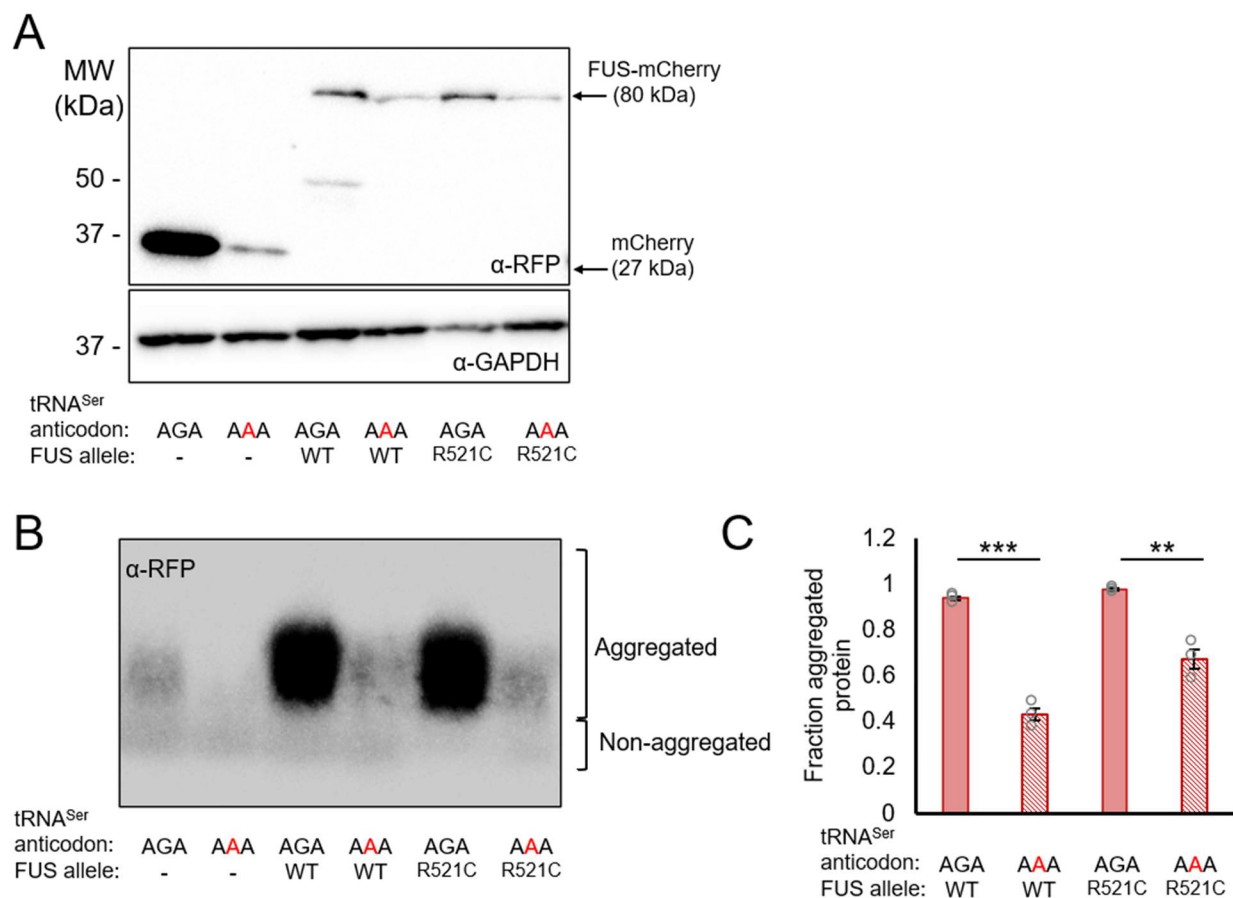


Figure 4.4. FUS protein and aggregate production in wild-type and mistranslating cells. N2a cells were transfected with a plasmid encoding human tRNA^{Ser}_{AGA} or G35A variant tRNA^{Ser}_{AAA} and mCherry, human FUS-mCherry fusion or R521C variant FUS-mCherry fusion protein. Cell lysates were separated on SDS-PAGE (A) or SDD-AGE (B) gels and Western blotted using α -RFP antibody. Percentage aggregated protein in SDD-AGE blots was determined by densitometry (C). Error bars represent the mean \pm 1 standard deviation of three biological replicates. Stars indicate P-values from independent sample t-tests (** P < 0.01, *** P < 0.001).

As an alternative assay of insoluble aggregate abundance, we assayed the levels of FUS-mCherry protein in cells expressing tRNA^{Ser}_{AGA} or tRNA^{Ser}_{AAA} by western blotting and semi-denaturing detergent agarose gel electrophoresis (SDD-AGE; (39)). SDD-AGE is a semi-quantitative approach which utilizes partial denaturation of aggregated proteins and separation by agarose gel electrophoresis. This is followed by western blotting to visual the presence of aggregated proteins from cell lysates as high molecular weight smears. N2a cells were transfected with plasmids encoding mCherry, FUS-mCherry, FUS(R521C)-mCherry, and tRNA^{Ser}_{AGA} or

tRNA^{Ser}_{AAA}. After 72 hr to allow for protein expression, cells were harvested and lysed, and lysates were run on SDS-PAGE or SDD-AGE gels, then western blotted with antibodies against mCherry. The western blots from SDS-PAGE gels revealed discrete bands in all samples corresponding to the molecular weight of the mCherry or FUS-mCherry proteins (Fig. 4.4A). The western blots from SDD-AGE gels revealed a lower band and higher molecular weight smear corresponding to aggregated FUS-mCherry or FUS(R521C)-mCherry protein (Fig. 4.4B). We quantitated the fraction of aggregated protein in each by normalizing the intensity of the aggregate smear to the total band intensity in the lane (Fig. 4.4C). We observed a significant 2.2 ± 0.1 -fold reduction in the amount of aggregated FUS-mCherry and 1.5 ± 0.1 -fold reduction in the amount of aggregated FUS(R521C)-mCherry in mistranslating cells compared to cells expressing wild-type tRNA^{Ser}_{AGA}. Hence, in agreement with our live cell fluorescence experiment, the variant tRNA^{Ser}_{AAA} causes a significant reduction in the aggregation of FUS proteins compared to cells expressing wild-type tRNA.

4.4 Discussion

4.4.1 Protein synthesis de-regulation in ALS models and mistranslating cells

Studies in N2a cells (43), HEK293T cells (44) and mice (45) have demonstrated a down-regulation of mRNA translation in cells expressing mutant human FUS proteins, including the R521C variant tested in this study. Proposed mechanisms overlap but vary, from disruptions to non-sense mediated decay pathways (43), to cellular signaling to inhibit protein synthesis via the mTOR (44) or integrated stress response pathways (45). FUS mutations can also indirectly affect protein synthesis by causing complex dysregulation of transcription (46) and RNA metabolism (47). Likewise, we and others have shown that amino acid mis-incorporation resulting from mutations in tRNA genes (19,48-50) and aminoacyl-tRNA synthetases (51) can cause down-regulation of protein synthesis.

Our work is the first to explore interactions of tRNAs and naturally occurring variants with the ALS-associated FUS protein. First, we found that expression of a wild-type tRNA^{Ser} gene increased protein synthesis in cells expressing FUS or FUS(R521C). Transfer RNA gene supplementation is a common approach to increase protein synthesis in *E. coli* (52), and tRNA upregulation has been shown to promote protein synthesis in human cancer cells (53). Hence, our observation that tRNA^{Ser}_{AGA} expression promoted protein synthesis was not surprising. Alas, the

finding has interesting implications for the potential use of tRNAs in therapy. For example, a recent study demonstrated that tRNA overexpression can rescue peripheral neuropathy in animal and cellular models of Charcot-Marie Tooth disease caused by mutations in glycine-tRNA synthetase (54). In that case, overexpression of tRNA^{Gly} was proposed to promote substrate turnover on a mutated GlyRS which fails to release Gly-tRNA^{Gly} after aminoacylation. Other studies have shown that tRNA expression, however, can more generally enhance cell metabolic activity and proliferation (55,56). While this effect has mainly been viewed as an aberrant gain-of-function in cancer cells (53), it could be used to advantage in cells where protein synthesis is chronically repressed. Indeed, genetic screens in yeast have found that in addition to a multitude of RNA metabolism and transcription-associated factors, some translation initiation factors can suppress toxicity of mutant FUS, and one of these suppressors (eIF4A1) was validated in HEK293T cells (57).

In cells expressing the variant tRNA^{Ser}_{AAA}, which causes Phe to Ser amino acid misincorporation (19), we found a significant reduction in the synthesis of mCherry protein, but not in the synthesis of FUS-mCherry or FUS(R521C)-mCherry compared to cells with no additional tRNA^{Ser}. Hence, expression of FUS-mCherry and FUS(R521C)-mCherry had a dominant effect in reducing protein synthesis in cells, which was not further influenced by expression of the mistranslating tRNA variant. However, given that the tRNA variant causes a reduction in protein synthesis alone, it could contribute to the challenge of “rebooting” protein synthesis in patients with ALS. Indeed, in our study on poly-glutamine models of Huntington’s disease (58), we found that the same tRNA variant expressed in N2a cells caused resistance to the integrated stress response inhibitor (ISRIB), which was designed to stimulate protein synthesis in the cells of neurodegenerative disease patients (59,60).

4.4.2 Influence of tRNAs on FUS aggregation

Compared to our previous work on polyglutamine protein aggregates, lower stability of FUS aggregates and increased death in cells expressing the mutant FUS(R521C) caused higher variability in our quantitation of aggregation kinetics. For example, we found that both FUS and FUS(R521C) aggregates dissipated rapidly in dying cells and in membrane detergent assays developed for poly-glutamine aggregate quantitation (38). By contrast, we found this assay to be a highly effective method for quantitating the size and abundance of poly-glutamine aggregates in

cells (19). The differences in aggregate solubility we observed may be due to differences in the physical properties of FUS aggregates compared to polyglutamine aggregates. Indeed, others have shown that FUS aggregates initially coalesce into liquid-like droplets before maturing into more solid forms (35). Hence, higher solubility of FUS aggregates compared to poly-glutamine aggregates may contribute to their rapid dissolution in membrane-permeated cells. Nonetheless, we found that both wild-type and mutant tRNA expression had modifying effects on FUS aggregation.

Similarly to our previous work on Huntington's disease models, aggregation of FUS-mCherry was reduced in cells expressing the variant tRNA compared to wild-type. However, in this work we followed aggregation kinetics over a longer time-course, finding that aggregates began to form rapidly in mistranslating cells after a long ~63 hour lag of FUS-mCherry expression. Ours and other works on cellular responses to protein folding stress provide clues to why this occurred. Firstly, mistranslation places an increased burden on protein degradation and the unfolded protein response, by constantly generating misfolded proteins (19,48,61) (49). Secondly, cellular stress responses associated with amino acid mis-incorporation cannot be maintained indefinitely. Indeed, chronic activation of the unfolded protein response can result in the toxic accumulation of reactive oxygen species (62) and apoptosis (63). For this reason, cells may mitigate or silence unfolded protein responses in chronically mistranslating cells. Indeed, others have observed this effect in cells expressing ribosomal mutations that cause mistranslation (64). Thus, increased mistranslation caused by natural variants in human tRNAs likely exacerbates the already existing paradox of beneficial and detrimental activation of protein folding stress responses in cells expressing mutant FUS.

This phenomenon was particularly evident in our experiments on aggregates of the FUS(R521C)-mCherry protein in mistranslating cells. Co-expression of the tRNA^{Ser_{AAA}} variant and FUS(R521C) had a potent synthetic toxic effect, and FUS(R521C)-mCherry aggregation kinetics were highly variable compared to cells expressing no tRNA or wild type. Despite the variability, we found that FUS(R521C)-mCherry aggregation was significantly increased in the latter time-points of our assay compared to cells expressing no tRNA. Expression of the wild-type tRNA also promoted FUS-mCherry and FUS(R521C)-mCherry aggregation, but this was expected given that the wild-type tRNA increased expression of the FUS proteins compared to no tRNA. By contrast, the mistranslating tRNA increased aggregation of FUS-mCherry and FUS(R521C)-

mCherry proteins without significantly changing expression. Taken together, our aggregation and cytotoxicity data suggest a highly deleterious interaction between the tRNA and FUS variants.

These results provide further support to our hypothesis that naturally occurring tRNA variants, while tolerable alone, can exacerbate human diseases including neurodegenerative disease (5). While mutations in numerous other mRNA translation-associated factors such as aminoacyl-tRNA synthetases, elongation factors, tRNA modifying enzymes, and more have been linked to neurodegenerative disease (reviewed in (65)), research on tRNA variants in neurodegenerative disease is limited but growing. Including our own work on cellular models of Huntington's disease (19), others researchers identified links between a loss-of-function tRNA mutation and neurodegenerative phenotypes in mice (50), which we reviewed in chapter 1. Briefly, the variant causes ribosome stalling in mice also carrying a mutation in the ribosomal recycling factor GTPBP2 (50). The same group recently expanded on this work, demonstrating that mice harboring the tRNA^{Arg}_{UCU} C50T mutation had defects in synaptic transmission in neuronal cells, and increased seizure susceptibility (66). They also used partial CRISPR genetic knockouts in mouse forebrains to demonstrate that deletion of another tRNA gene, tRNA-Ile-TAT-2-3, stimulated an integrated stress response (66). As with our previous work on Huntington's disease models, we hope that the growing list of associations between tRNA variants and neurodegenerative disease will motivate the greater inclusion of tRNA genes in sequencing studies of patients with neurodegenerative disease.

4.5 References

1. Drummond, D.A. and Wilke, C.O. (2009) The evolutionary consequences of erroneous protein synthesis. *Nat Rev Genet*, **10**, 715-724.
2. Ruan, B., Palioura, S., Sabina, J., Marvin-Guy, L., Kochhar, S., Larossa, R.A. and Soll, D. (2008) Quality control despite mistranslation caused by an ambiguous genetic code. *Proc Natl Acad Sci U S A*, **105**, 16502-16507.
3. Lant, J.T., Berg, M.D., Sze, D.H.W., Hoffman, K.S., Akinpelu, I.C., Turk, M.A., Heinemann, I.U., Duennwald, M.L., Brandl, C.J. and O'Donoghue, P. (2018) Visualizing tRNA-dependent mistranslation in human cells. *RNA Biol*, **15**, 567-575.
4. Rozik, P., Szabla, R., Lant, J.T., Kiri, R., Wright, D.E., Junop, M. and O'Donoghue, P. (2021) A novel fluorescent reporter sensitive to serine mis-incorporation. *RNA Biol*.
5. Lant, J.T., Berg, M.D., Heinemann, I.U., Brandl, C.J. and O'Donoghue, P. (2019) Pathways to disease from natural variations in human cytoplasmic tRNAs. *J Biol Chem*, **294**, 5294-5308.

6. Mohler, K. and Ibba, M. (2017) Translational fidelity and mistranslation in the cellular response to stress. *Nat Microbiol*, **2**, 17117.
7. Rubio Gomez, M.A. and Ibba, M. (2020) Aminoacyl-tRNA synthetases. *RNA*, **26**, 910-936.
8. Hoffer, E.D., Maehigashi, T., Fredrick, K. and Dunham, C.M. (2019) Ribosomal ambiguity (ram) mutations promote the open (off) to closed (on) transition and thereby increase miscoding. *Nucleic Acids Res*, **47**, 1557-1563.
9. Agarwal, D., Gregory, S.T. and O'Connor, M. (2011) Error-prone and error-restrictive mutations affecting ribosomal protein S12. *J Mol Biol*, **410**, 1-9.
10. Reynolds, N.M., Lazizzera, B.A. and Ibba, M. (2010) Cellular mechanisms that control mistranslation. *Nat Rev Microbiol*, **8**, 849-856.
11. Giege, R., Sissler, M. and Florentz, C. (1998) Universal rules and idiosyncratic features in tRNA identity. *Nucleic Acids Res*, **26**, 5017-5035.
12. Kisselev, L.L. (1985) The role of the anticodon in recognition of tRNA by aminoacyl-tRNA synthetases. *Prog Nucleic Acid Res Mol Biol*, **32**, 237-266.
13. Hoffman, K.S., Berg, M.D., Shilton, B.H., Brandl, C.J. and O'Donoghue, P. (2017) Genetic selection for mistranslation rescues a defective co-chaperone in yeast. *Nucleic Acids Res*, **45**, 3407-3421.
14. Hou, Y.M. and Schimmel, P. (1988) A simple structural feature is a major determinant of the identity of a transfer RNA. *Nature*, **333**, 140-145.
15. Parisien, M., Wang, X. and Pan, T. (2013) Diversity of human tRNA genes from the 1000-genomes project. *RNA Biol*, **10**, 1853-1867.
16. Chan, P.P. and Lowe, T.M. (2016) GtRNADB 2.0: an expanded database of transfer RNA genes identified in complete and draft genomes. *Nucleic Acids Res*, **44**, D184-189.
17. Berg, M.D., Giguere, D.J., Dron, J.S., Lant, J.T., Genereaux, J., Liao, C., Wang, J., Robinson, J.F., Gloor, G.B., Hegele, R.A. *et al.* (2019) Targeted sequencing reveals expanded genetic diversity of human transfer RNAs. *RNA Biol*, **16**, 1574-1585.
18. Lenhard, B., Orellana, O., Ibba, M. and Weygand-Durasevic, I. (1999) tRNA recognition and evolution of determinants in seryl-tRNA synthesis. *Nucleic Acids Res*, **27**, 721-729.
19. Lant, J.T., Kiri, R., Duennwald, M.L. and O'Donoghue, P. (2021) Formation and persistence of polyglutamine aggregates in mistranslating cells. *Nucleic Acids Res*.
20. Alsultan, A.A., Waller, R., Heath, P.R. and Kirby, J. (2016) The genetics of amyotrophic lateral sclerosis: current insights. *Degener Neurol Neuromuscul Dis*, **6**, 49-64.
21. Marrone, L., Drexler, H.C.A., Wang, J., Tripathi, P., Distler, T., Heisterkamp, P., Anderson, E.N., Kour, S., Moraiti, A., Maharana, S. *et al.* (2019) FUS pathology in ALS is linked to alterations in multiple ALS-associated proteins and rescued by drugs stimulating autophagy. *Acta Neuropathol*, **138**, 67-84.
22. Wang, X., Schwartz, J.C. and Cech, T.R. (2015) Nucleic acid-binding specificity of human FUS protein. *Nucleic Acids Res*, **43**, 7535-7543.
23. Corrado, L., Del Bo, R., Castellotti, B., Ratti, A., Cereda, C., Penco, S., Soraru, G., Carlomagno, Y., Ghezzi, S., Pensato, V. *et al.* (2010) Mutations of FUS gene in sporadic amyotrophic lateral sclerosis. *J Med Genet*, **47**, 190-194.
24. Kwiatkowski, T.J., Jr., Bosco, D.A., Leclerc, A.L., Tamrazian, E., Vanderburg, C.R., Russ, C., Davis, A., Gilchrist, J., Kasarskis, E.J., Munsat, T. *et al.* (2009) Mutations in the FUS/TLS gene on chromosome 16 cause familial amyotrophic lateral sclerosis. *Science*, **323**, 1205-1208.

25. Vance, C., Rogelj, B., Hortobagyi, T., De Vos, K.J., Nishimura, A.L., Sreedharan, J., Hu, X., Smith, B., Ruddy, D., Wright, P. *et al.* (2009) Mutations in FUS, an RNA processing protein, cause familial amyotrophic lateral sclerosis type 6. *Science*, **323**, 1208-1211.
26. Hou, L., Jiao, B., Xiao, T., Zhou, L., Zhou, Z., Du, J., Yan, X., Wang, J., Tang, B. and Shen, L. (2016) Screening of SOD1, FUS and TARDBP genes in patients with amyotrophic lateral sclerosis in central-southern China. *Sci Rep*, **6**, 32478.
27. Tan, A.Y. and Manley, J.L. (2009) The TET family of proteins: functions and roles in disease. *J Mol Cell Biol*, **1**, 82-92.
28. Shang, Y. and Huang, E.J. (2016) Mechanisms of FUS mutations in familial amyotrophic lateral sclerosis. *Brain Res*, **1647**, 65-78.
29. Lerga, A., Hallier, M., Delva, L., Orvain, C., Gallais, I., Marie, J. and Moreau-Gachelin, F. (2001) Identification of an RNA binding specificity for the potential splicing factor TLS. *J Biol Chem*, **276**, 6807-6816.
30. Ishigaki, S., Masuda, A., Fujioka, Y., Iguchi, Y., Katsuno, M., Shibata, A., Urano, F., Sobue, G. and Ohno, K. (2012) Position-dependent FUS-RNA interactions regulate alternative splicing events and transcriptions. *Sci Rep*, **2**, 529.
31. Jia, W., Kim, S.H., Scaff, M.A., Tonzi, P., Millikin, R.J., Guns, W.M., Liu, L., Mastrocola, A.S., Smith, L.M., Huang, T.T. *et al.* (2021) Fused in sarcoma regulates DNA replication timing and kinetics. *J Biol Chem*, **297**, 101049.
32. Shelkownikova, T.A., Robinson, H.K., Southcombe, J.A., Ninkina, N. and Buchman, V.L. (2014) Multistep process of FUS aggregation in the cell cytoplasm involves RNA-dependent and RNA-independent mechanisms. *Hum Mol Genet*, **23**, 5211-5226.
33. Swetha, R.G., Ramaiah, S. and Anbarasu, A. (2017) R521C and R521H mutations in FUS result in weak binding with Karyopherinbeta2 leading to Amyotrophic lateral sclerosis: a molecular docking and dynamics study. *J Biomol Struct Dyn*, **35**, 2169-2185.
34. Naumann, M., Pal, A., Goswami, A., Lojewski, X., Japtok, J., Vehlow, A., Naujock, M., Gunther, R., Jin, M., Stanslowsky, N. *et al.* (2018) Impaired DNA damage response signaling by FUS-NLS mutations leads to neurodegeneration and FUS aggregate formation. *Nat Commun*, **9**, 335.
35. Patel, A., Lee, H.O., Jawerth, L., Maharana, S., Jahnel, M., Hein, M.Y., Stoyanov, S., Mahamid, J., Saha, S., Franzmann, T.M. *et al.* (2015) A Liquid-to-Solid Phase Transition of the ALS Protein FUS Accelerated by Disease Mutation. *Cell*, **162**, 1066-1077.
36. Schlachetzki, J.C., Saliba, S.W. and Oliveira, A.C. (2013) Studying neurodegenerative diseases in culture models. *Braz J Psychiatry*, **35 Suppl 2**, S92-100.
37. Gomes, A.C., Kordala, A.J., Strack, R., Wang, X., Geslain, R., Delaney, K., Clark, W.C., Keenan, R. and Pan, T. (2016) A dual fluorescent reporter for the investigation of methionine mistranslation in live cells. *RNA*, **22**, 467-476.
38. Titus, S.A., Southall, N., Marugan, J., Austin, C.P. and Zheng, W. (2012) High-Throughput Multiplexed Quantitation of Protein Aggregation and Cytotoxicity in a Huntington's Disease Model. *Curr Chem Genomics*, **6**, 79-86.
39. Halfmann, R. and Lindquist, S. (2008) Screening for amyloid aggregation by Semi-Denaturing Detergent-Agarose Gel Electrophoresis. *J Vis Exp*.
40. McNicoll, F. and Muller-McNicoll, M. (2018) A Quantitative Heterokaryon Assay to Measure the Nucleocytoplasmic Shuttling of Proteins. *Bio Protoc*, **8**, e2472.

41. Bracha, D., Walls, M.T., Wei, M.T., Zhu, L., Kurian, M., Avalos, J.L., Toettcher, J.E. and Brangwynne, C.P. (2018) Mapping Local and Global Liquid Phase Behavior in Living Cells Using Photo-Oligomerizable Seeds. *Cell*, **175**, 1467-1480 e1413.
42. Marrone, L., Poser, I., Casci, I., Japtok, J., Reinhardt, P., Janosch, A., Andree, C., Lee, H.O., Moebius, C., Koerner, E. *et al.* (2018) Isogenic FUS-eGFP iPSC Reporter Lines Enable Quantification of FUS Stress Granule Pathology that Is Rescued by Drugs Inducing Autophagy. *Stem Cell Reports*, **10**, 375-389.
43. Stothard, P. (2000) The sequence manipulation suite: JavaScript programs for analyzing and formatting protein and DNA sequences. *Biotechniques*, **28**, 1102, 1104.
44. Torres, A.G., Pineyro, D., Filonava, L., Stracker, T.H., Batlle, E. and Ribas de Pouplana, L. (2014) A-to-I editing on tRNAs: biochemical, biological and evolutionary implications. *FEBS Lett*, **588**, 4279-4286.
45. Lim, V.I. and Curran, J.F. (2001) Analysis of codon:anticodon interactions within the ribosome provides new insights into codon reading and the genetic code structure. *RNA*, **7**, 942-957.
46. Kamelgarn, M., Chen, J., Kuang, L., Jin, H., Kasarskis, E.J. and Zhu, H. (2018) ALS mutations of FUS suppress protein translation and disrupt the regulation of nonsense-mediated decay. *Proc Natl Acad Sci U S A*, **115**, E11904-E11913.
47. Sevigny, M., Bourdeau Julien, I., Venkatasubramani, J.P., Hui, J.B., Dutchak, P.A. and Sephton, C.F. (2020) FUS contributes to mTOR-dependent inhibition of translation. *J Biol Chem*, **295**, 18459-18473.
48. Lopez-Erauskin, J., Tadokoro, T., Baughn, M.W., Myers, B., McAlonis-Downes, M., Chillon-Marinhas, C., Asiaban, J.N., Artates, J., Bui, A.T., Vetto, A.P. *et al.* (2018) ALS/FTD-Linked Mutation in FUS Suppresses Intra-axonal Protein Synthesis and Drives Disease Without Nuclear Loss-of-Function of FUS. *Neuron*, **100**, 816-830 e817.
49. Yang, L., Gal, J., Chen, J. and Zhu, H. (2014) Self-assembled FUS binds active chromatin and regulates gene transcription. *Proc Natl Acad Sci U S A*, **111**, 17809-17814.
50. Zhou, Y., Liu, S., Ozturk, A. and Hicks, G.G. (2014) FUS-regulated RNA metabolism and DNA damage repair: Implications for amyotrophic lateral sclerosis and frontotemporal dementia pathogenesis. *Rare Dis*, **2**, e29515.
51. Geslain, R., Cubells, L., Bori-Sanz, T., Alvarez-Medina, R., Rossell, D., Marti, E. and Ribas de Pouplana, L. (2010) Chimeric tRNAs as tools to induce proteome damage and identify components of stress responses. *Nucleic Acids Res*, **38**, e30.
52. Varanda, A.S., Santos, M., Soares, A.R., Vitorino, R., Oliveira, P., Oliveira, C. and Santos, M.A.S. (2020) Human cells adapt to translational errors by modulating protein synthesis rate and protein turnover. *RNA Biol*, **17**, 135-149.
53. Ishimura, R., Nagy, G., Dotu, I., Zhou, H., Yang, X.L., Schimmel, P., Senju, S., Nishimura, Y., Chuang, J.H. and Ackerman, S.L. (2014) RNA function. Ribosome stalling induced by mutation of a CNS-specific tRNA causes neurodegeneration. *Science*, **345**, 455-459.
54. Meyer-Schuman, R. and Antonellis, A. (2017) Emerging mechanisms of aminoacyl-tRNA synthetase mutations in recessive and dominant human disease. *Hum Mol Genet*, **26**, R114-R127.
55. Zuko, A., Mallik, M., Thompson, R., Spaulding, E.L., Wienand, A.R., Been, M., Tadenev, A.L.D., van Bakel, N., Sijlmans, C., Santos, L.A. *et al.* (2021) tRNA

- overexpression rescues peripheral neuropathy caused by mutations in tRNA synthetase. *Science*, **373**, 1161-1166.
56. Pavon-Eternod, M., Gomes, S., Rosner, M.R. and Pan, T. (2013) Overexpression of initiator methionine tRNA leads to global reprogramming of tRNA expression and increased proliferation in human epithelial cells. *RNA*, **19**, 461-466.
 57. Kwon, N.H., Lee, M.R., Kong, J., Park, S.K., Hwang, B.J., Kim, B.G., Lee, E.S., Moon, H.G. and Kim, S. (2018) Transfer-RNA-mediated enhancement of ribosomal proteins S6 kinases signaling for cell proliferation. *RNA Biol*, **15**, 635-648.
 58. Zhang, Z., Ye, Y., Gong, J., Ruan, H., Liu, C.J., Xiang, Y., Cai, C., Guo, A.Y., Ling, J., Diao, L. *et al.* (2018) Global analysis of tRNA and translation factor expression reveals a dynamic landscape of translational regulation in human cancers. *Commun Biol*, **1**, 234.
 59. Sun, Z., Diaz, Z., Fang, X., Hart, M.P., Chesi, A., Shorter, J. and Gitler, A.D. (2011) Molecular determinants and genetic modifiers of aggregation and toxicity for the ALS disease protein FUS/TLS. *PLoS Biol*, **9**, e1000614.
 60. Kapur, M., Ganguly, A., Nagy, G., Adamson, S.I., Chuang, J.H., Frankel, W.N. and Ackerman, S.L. (2020) Expression of the Neuronal tRNA n-Tr20 Regulates Synaptic Transmission and Seizure Susceptibility. *Neuron*, **108**, 193-208 e199.
 61. Lee, J.W., Beebe, K., Nangle, L.A., Jang, J., Longo-Guess, C.M., Cook, S.A., Davisson, M.T., Sundberg, J.P., Schimmel, P. and Ackerman, S.L. (2006) Editing-defective tRNA synthetase causes protein misfolding and neurodegeneration. *Nature*, **443**, 50-55.
 62. Santos, C.X., Tanaka, L.Y., Wosniak, J. and Laurindo, F.R. (2009) Mechanisms and implications of reactive oxygen species generation during the unfolded protein response: roles of endoplasmic reticulum oxidoreductases, mitochondrial electron transport, and NADPH oxidase. *Antioxid Redox Signal*, **11**, 2409-2427.
 63. Wang, S. and Kaufman, R.J. (2012) The impact of the unfolded protein response on human disease. *J Cell Biol*, **197**, 857-867.
 64. Shcherbakov, D., Teo, Y., Boukari, H., Cortes-Sanchon, A., Mantovani, M., Osinnii, I., Moore, J., Juskeviciene, R., Brilkova, M., Duscha, S. *et al.* (2019) Ribosomal mistranslation leads to silencing of the unfolded protein response and increased mitochondrial biogenesis. *Commun Biol*, **2**, 381.
 65. Schneider, C.A., Rasband, W.S. and Eliceiri, K.W. (2012) NIH Image to ImageJ: 25 years of image analysis. *Nat Methods*, **9**, 671-675.

4.6 Supplemental information

4.6.1 Supporting Tables

Table S4.1 Oligonucleotide sequences

Description	Nucleotide sequence
FUS cloning in pcDNA3.1 NheI/HindIII sites (Fwd)	CGACTGCTAGCATGGCCTCAAACGATTATACCC
FUS cloning in pcDNA3.1 NheI/HindIII sites (Rev with linker sequence)	CAGACTAAGCTTGCCCTCCAGACCCTCCGCCATAC GGCCTCTCCCTGC
FUS R521C round-the-horn mutagenesis (Fwd)	TGCAGGGAGAGGCCGT
FUS R521C round-the-horn mutagenesis (Rev)	ATCCTGTCTGTGCTCACCC
FUS cloning in WT-Pan NheI/SpeI sites (Fwd)	CGACTGCTAGCATGGCCTCAAACGATTATACCC
FUS cloning in WT-Pan NheI/SpeI sites (Rev with linker sequence)	CAGACTACTAGTGAGCCTCCAGACCCTCCGCCAT ACGGCCTCTCCCTGC

4.6.2 Supporting figures

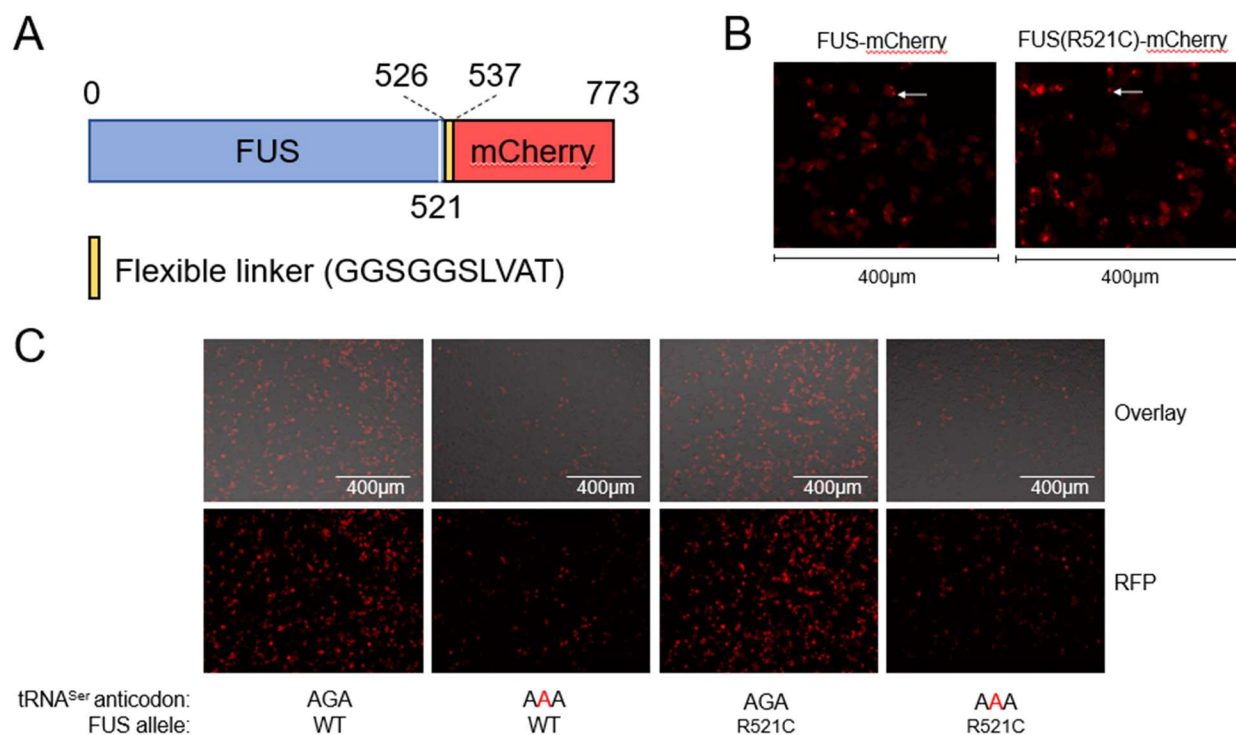


Figure S4.1. FUS-mCherry construct and fluorescence in HEK 293T cells. (A) The human *FUS* gene was fused to the mCherry coding sequence via a flexible linker sequence. Numbers indicate amino acid positions in the fusion protein. (B,C) Representative images of HEK 293T cells 24 hrs post-transfection with a plasmid co-expressing a human tRNA^{Ser}_{AGA} or G35A variant (tRNA^{Ser}_{AAA}) and human FUS-mCherry (WT) or R521C variant FUS-mCherry were captured by

fluorescence microscopy (RFP, ex. 531 nm, em. 593 nm). (B) Cropped and enlarged images of the tRNA^{Ser}_{AGA} transfections with arrows showing subcellular aggregates. (C) Full-size images overlaid with bright field images of the cells.

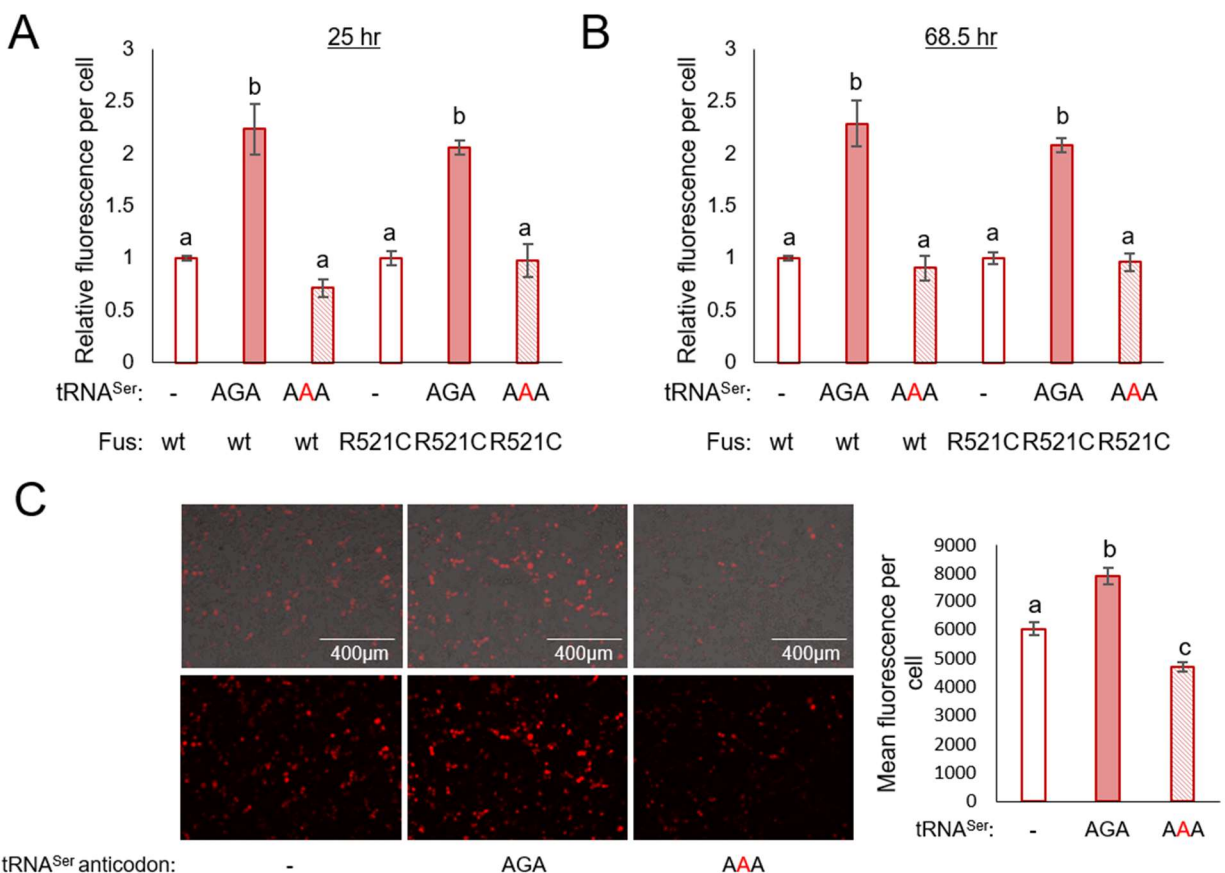


Figure S4.2. FUS-mCherry fluorescence timecourse statistical analysis and mCherry control transfections. (A,B) Tukey-Kramer multiple comparisons test results from initial (A) and final (B) timepoints of FUS-mCherry and FUS(R521C)-mCherry fluorescence timecourse experiments (see Fig. 4.1). Letters indicate significantly different groups based on at least three biological means at the indicated timepoints, where groups sharing a letter are not significantly different and groups not sharing a letter are significantly different ($\alpha = 0.05$). (C) N2a cells were transfected with a plasmid encoding no tRNA, human tRNA^{Ser}_{AGA} or G35A variant tRNA^{Ser}_{AAA} and mCherry. Images of fluorescing cells were captured by fluorescence microscopy (RFP, ex 531 nm, em 593 nm) after 24 hr transfection. Fluorescent images were also overlain with brightfield images of cells. Fluorescence per cell was quantitated with a custom Fiji/ImageJ macro (see appendix) in five biological replicates. Letters represent Tukey-Kramer multiple comparison test results as described above.

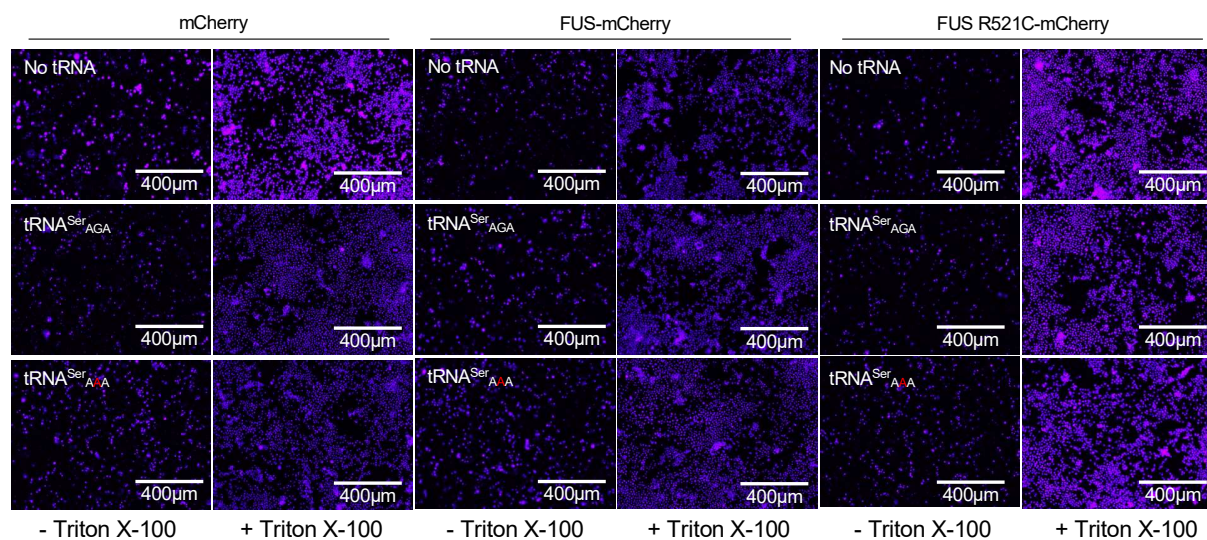


Figure S4.3. Cell death assay for N2a cells co-expressing tRNA^{Ser} variants with mCherry or FUS-mCherry variants. N2a cells were transfected with a plasmid encoding no tRNA, human tRNA^{Ser}_{AGA} or G35A variant tRNA^{Ser}_{AAA}, and mCherry, human FUS-mCherry, or the FUS R521C-mCherry protein. After 72-hr post-transfection, cytotoxicity was assayed with a dye exclusion assay using Sytox blue nucleic acid stain. The images are representative of images from the five biological replicates included in Fig. 4.2A. The images were captured by fluorescence microscopy (CFP ex. 445 nm, em. 510 nm).

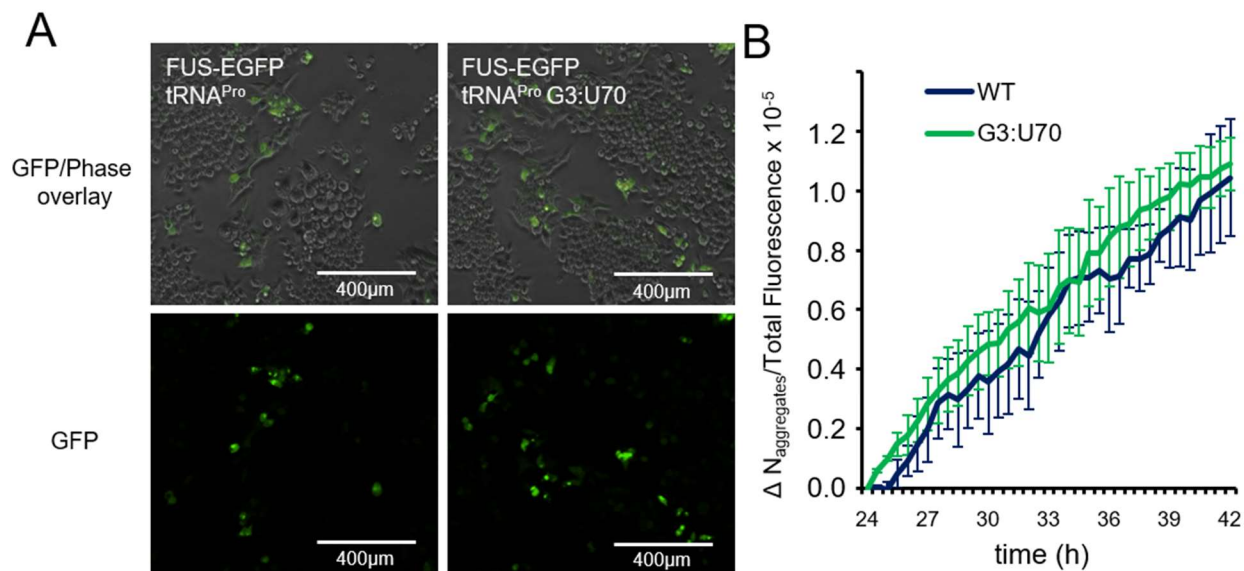


Figure S4.4. FUS aggregate formation in cells expressing wild-type and G3:U70 tRNA^{Pro} variants. N2a cells were transfected with a plasmid encoding human FUS-EGFP fusion protein and wild-type human tRNA^{Pro} or a G3:U70 variant that decodes proline codons with alanine (3). (A) Representative images were captured by fluorescence microscopy (GFP; ex 470 nm, em 510 nm) (bottom) and overlaid with bright field images of the cells (top). (B) Starting 24 hrs post-transfection, the change in number of aggregates over total cell fluorescence was quantified over an 18-hr live cell imaging time-course with a custom Fiji/ImageJ macro (see appendix) as previously described (19).

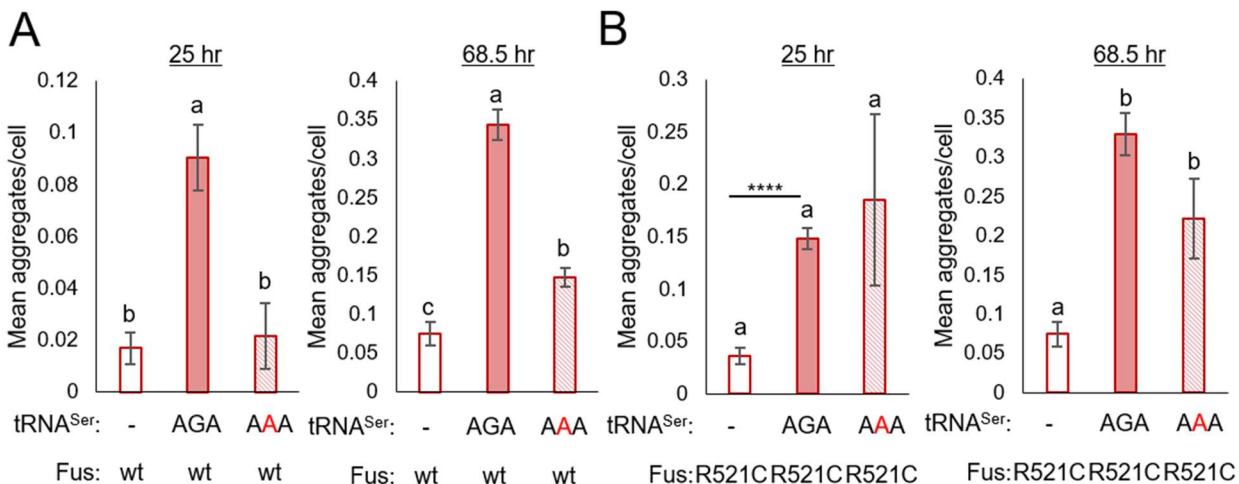


Figure S4.5. FUS-mCherry aggregation timecourse statistical analysis. (A,B) Tukey-Kramer multiple comparisons test results from initial (25 hr) and final (68.5 hr) timepoints of FUS-mCherry (A) and FUS(R521C)-mCherry (B) aggregation timecourse experiments (see Fig. 4.3). Letters indicate significantly different groups based on at least three biological means at the indicated timepoints, where groups sharing a letter are not significantly different and groups not sharing a letter are significantly different ($\alpha = 0.05$). An independent sample t-test comparing the no tRNA and tRNA^{Ser}_{AGA} transfections in (B) 25 hr panel is also shown (**** = $p < 0.0001$).

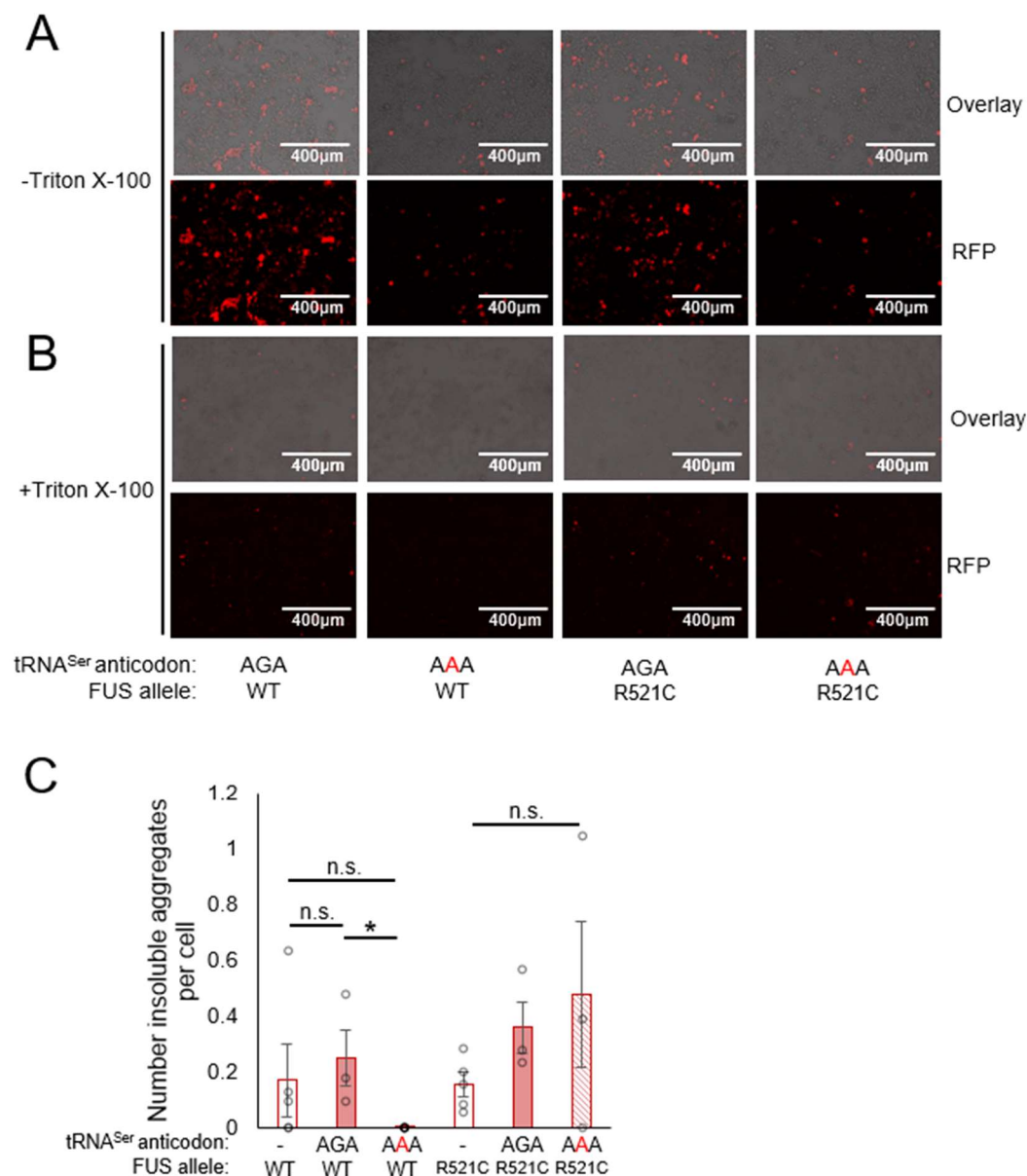


Figure S4.6. Insoluble FUS aggregate levels in wild-type and mistranslating cells. N2a cells were transfected with a plasmid encoding no tRNA, human tRNA^{Ser}_{AGA} or G35A variant tRNA^{Ser}_{AAA} and human FUS-mCherry or FUS R521C-mCherry. After 72 hrs post-transfection, membrane detergent assays were performed using Triton X-100 to permeate cell membranes and reveal insoluble aggregates. Representative images are shown from a series of images captured by fluorescence microscopy (bottom) (RFP; ex 531 nm, em 593 nm) and overlaid with brightfield images (top) both (A) before and (B) after treatment with Triton-X100. The number of aggregates remaining per cell after membrane permeation was quantified using a custom Fiji/ImageJ macro (see Supplemental appendix). Error bars represent the mean \pm 1 standard deviation of N = 5 biological replicates. Stars indicate statistically significant differences determined by pairwise independent sample t-tests (n.s. = no significant difference, * $p < 0.05$).

4.6.3. Appendix: Fiji/ImageJ macros

ImageJ (version 1.53f51 (67); Java version 1.8.0_172 (64-bit)) scripts to measure the fluorescence and analyze images of transfected cells. All macros were run on 16-bit, single-channel images.

Fiji/ImageJ macros used in Figure 4.1 – Mean fluorescence per cell plots. Fluorescence in regions of interest (ROI; fluorescing cells) was measured with the following Macro in Fiji/ImageJ. Since some ROIs capture multiple cells in clusters, ROI areas were weighted in Microsoft Excel by dividing the area of each ROI by median ROI size (i.e., median cell size) for the entire experiment. Hence, all fluorescence measurements underlying the means were weighted to the same fixed area, which approximates median cell size. Standard deviations were calculated based on the means of at least $N = 3$ biological replicates at each timepoint.

```
//Import image sequence. Replace “folder name” with desired image series location. “number” is
the number of images in the series and “increment” is used to exclude unwanted images in the file
folder.
run("Image Sequence...", "open=[“folder name”] number=88 starting=5 increment=3 sort");
//Subtract background signal using rolling circle method with radius of 50 pixels.
run("Subtract Background...", "rolling=50 stack");
//Set threshold to exclude pixels below chosen cutoff (6 in this case). Fine-tune according to your
image brightness and use same cutoff for all images in one experiment.
setThreshold(6, 255);
//Next two lines convert image to black features (above threshold) on white background (below
threshold)
setOption("BlackBackground", false);
run("Convert to Mask", "method=Default background=Dark");
//Remove noise with despeckle function.
run("Despeckle", "stack");
//Create annotations covering area above threshold. Excludes objects of area under chosen size
cut-off (20 pixels in this case). Size cut-off should be adjusted depending on the magnification of
the image and the size of objects you wish to exclude (noise).
run("Analyze Particles...", "size=20-Infinity display clear summarize add stack");
//Clear results. Steps so far to are to create region of interest annotations (ROIs), results will be
collected in following steps.
run("Clear Results");
//Import unmodified image sequence again. Should be identical to line 1
run("Image Sequence...", "open=[“folder name”] number=88 starting=5 increment=3 sort");
//Subtract background signal using rolling circle method with radius of 50 pixels.
run("Subtract Background...", "rolling=50 stack");
```

```
//Set measurements to record area, mean, integrated density to 3 decimal places.
run("Set Measurements...", "area mean integrated redirect=None decimal=3");
//The next three lines overlay the ROIs on the fluorescent cell image sequence, calculate the
intensity within the ROIs, and display the results in the "Results" window.
roiManager("Show None");
roiManager("Show All");
roiManager("Measure");
```

Fiji/ImageJ macros used in Figure 4.3 – Number of aggregates per cell plots. The same ROIs (outlining whole cell area) used in Figure 4.1 fluorescence analysis were used for cell size determination. To determine the size of aggregates, black and white mask images were produced at a higher intensity threshold to select for the brightest foci emanated from protein aggregates. Then the whole cell ROIs were overlaid on the aggregate mask image and “area” and “area fraction” were measured. Aggregate area per ROI was calculated in Microsoft Excel as the product of (Area · Area Fraction). Since some ROIs capture multiple cells or aggregates in clusters, cell and aggregate areas were weighted in Microsoft Excel by dividing the area of each ROI by median cell or aggregate size calculated over the entire experiment. Standard deviation was calculated based on the means of at least N = 3 biological replicates at each timepoint.

```
//Import image sequence. Replace "folder name" with desired image series location. "number" is
the number of images in the series and "increment" is used to exclude unwanted images in the file
folder.
run("Image Sequence...", "open=["folder name"] number=88 starting=5 increment=3 sort");
//Subtract background signal using rolling circle method with radius of 50 pixels.
run("Subtract Background...", "rolling=50 stack");
//Set threshold to exclude pixels below chosen cutoff (6 in this case). Fine-tune according to your
image brightness and use same cutoff for all images in one experiment. In this step, threshold
should be adjusted to capture whole cell area.
setThreshold(6, 255);
//Next two lines convert image to black features (above threshold) on white background (below
threshold).
setOption("BlackBackground", false);
run("Convert to Mask", "method=Default background=Dark");
//Remove noise with despeckle function.
run("Despeckle", "stack");
//Separate closely adjacent objects with watershed function.
run("Watershed", "stack");
//Create annotations covering area above threshold. Excludes objects of area under chosen size
cut-off (100 pixels in this case). Size cut-off should be adjusted depending on the magnification
of the image and the size of objects you wish to exclude (noise).
```

```

run("Analyze Particles...", "size=100-Infinity display clear summarize add stack");
//Clear results. Steps so far to are to create region of interest annotations (ROIs), results will be
collected in following steps.
run("Clear Results");
//Import unmodified image sequence again. Should be identical to line 1
run("Image Sequence...", "open=["folder name"] number=88 starting=5 increment=3 sort");
//Subtract background signal using rolling circle method with radius of 50 pixels.
run("Subtract Background...", "rolling=50 stack");
//Set threshold to exclude pixels below chosen cutoff (100 in this case). Fine-tune according to
your image brightness and use same cutoff for all images in one experiment. In this step, threshold
should be adjusted to capture protein aggregate area only.
setThreshold(100, 255);
//Convert image to black features (above threshold) on white background (below threshold).
run("Convert to Mask", "method=Default background=Dark");
//The next two lines overlay the ROIs from whole cell threshold on the mask image produced from
the aggregate threshold.
roiManager("Show None");
roiManager("Show All");
//Set measurements to record area and area fraction to 3 decimal places. Area will output the whole
cell ROI areas, area fraction will output the fraction of that area containing an aggregate object
from the aggregate mask image. Aggregate area can then be calculated as the product of area x
area fraction.
run("Set Measurements...", "area area_fraction redirect=None decimal=3");
//Measure.
roiManager("Measure");

```

Fiji/ImageJ macros used in Figure S4.4 – Number of aggregates per total fluorescence. Figure S4.4 was analyzed with a previously described ImageJ macro (19). A lower threshold was used to generate ROIs capturing all fluorescence in each image (A, cellular fluorescence) and measure the total fluorescence in each image in the series. A higher threshold was used to generate ROIs capturing only aggregated FUS-EGFP protein (B, aggregate area). Total fluorescence and aggregate area were calculated per image in Microsoft Excel using the SUMIF() function. For each image, total aggregate area was normalized to total transfected cell fluorescence and initial values were subtracted from all datapoints in the series to obtain “ $\Delta N_{\text{aggregates}} / \text{total fluorescence}$ ”. Standard deviation was calculated based on the means of at least three biological replicates at each timepoint.

A) Cellular fluorescence

//Import image sequence. Replace “folder name” with desired image series location. “number” is the number of images in the series and “increment” is used to exclude unwanted images in the file folder.

```
run("Image Sequence...", "open=["folder name"] number=37 starting=2 increment=3 sort");
//Subtract background signal using rolling circle method with radius of 50 pixels.
run("Subtract Background...", "rolling=50 stack");
//Set threshold to exclude pixels below chosen cutoff (6 in this case). Fine-tune according to your
image brightness and use same cutoff for all images in one experiment. In this step, threshold
should be adjusted to capture whole cell area.
setThreshold(6, 255);
//Next two lines convert image to black features (above threshold) on white background (below
threshold).
setOption("BlackBackground", false);
run("Convert to Mask", "method=Default background=Dark");
//Remove noise with despeckle function.
run("Despeckle", "stack");
//Create annotations covering area above threshold. Excludes objects of area under chosen size
cut-off (20 pixels in this case). Size cut-off should be adjusted depending on the magnification of
the image and the size of objects you wish to exclude (noise).
run("Analyze Particles...", "size=20-Infinity display clear summarize add stack");
//Clear results. Steps so far to are to create region of interest annotations (ROIs), results will be
collected in following steps.
run("Clear Results");
//Import unmodified image sequence again. Should be identical to line 1
run("Image Sequence...", "open=["folder name"] number=37 starting=2 increment=3 sort");
//Subtract background signal using rolling circle method with radius of 50 pixels.
run("Subtract Background...", "rolling=50 stack");
//The next two lines overlay the ROIs from the thresholded on the non-thresholded image.
roiManager("Show None");
roiManager("Show All");
//Set measurements to record integrated density to 3 decimal places, then measure.
run("Set Measurements...", "integrated redirect=None decimal=3");
roiManager("Measure");
```

B) Aggregate area

//Import image sequence. Replace “folder name” with desired image series location. “number” is the number of images in the series and “increment” is used to exclude unwanted images in the file folder.

```
run("Image Sequence...", "open=["folder name"] number=37 starting=2 increment=3 sort");
//Subtract background signal using rolling circle method with radius of 50 pixels.
run("Subtract Background...", "rolling=50 stack");
//Set threshold to exclude pixels below chosen cutoff (120 in this case). Fine-tune according to
your image brightness and use same cutoff for all images in one experiment. In this step, threshold
should be adjusted to capture aggregated protein area.
```

```

setThreshold(120, 255);
//Next two lines convert image to black features (above threshold) on white background (below
threshold).
setOption("BlackBackground", false);
run("Convert to Mask", "method=Default background=Dark");
//Create annotations covering area above threshold. Excludes objects of area under chosen size
cut-off (5 pixels in this case). Size cut-off should be adjusted depending on the magnification of
the image and the size of objects you wish to exclude (noise).
run("Analyze Particles...", "size=5-Infinity display clear summarize add stack");
//Set measurements to record area to 3 decimal places, then measure.
run("Set Measurements...", "area redirect=None decimal=3");
roiManager("Measure");

```

4.7.2.4 Fiji/ImageJ macros used in Figure S4.6 – Number of insoluble aggregates per cell.

Images from before and after Triton X-100 treatment were cropped at the edges to account for plate shifting during Triton X-100 addition (3.53% y-shift, 3.85% x-shift in this case). This was done by overlaying images and determining the percentage overhang on each image, then converting the percentage to a 1280 x 960 pixel frame size used in Fiji. This analysis consists of two macros, the first was used to determine cell count before Triton X-100 (A, Cell size pre-Triton X-100) and the second was used to determine insoluble aggregate count after Triton X-100 treatment (B, aggregate size post-Triton X-100). As before, cell and aggregate counts were determined by normalizing ROI areas to median ROI area from all images at the same threshold. Standard deviation was calculated based on the means of at least N = 3 biological replicates at each timepoint. Significant differences were calculated using independent sample t-tests.

A) Cell size pre-Triton X-100.

```

//Open image. Replace "file name" with desired image directory.
open("file name");
//Next two lines crop the image to account for plate shifting during Triton X-100 treatment.
run("Specify...", "width=1178 height=926 x=102 y=0");
run("Crop");
//Subtract background signal using rolling circle method with radius of 50 pixels.
run("Subtract Background...", "rolling=50");
//Set threshold to exclude pixels below chosen cutoff (10 in this case). Fine-tune according to your
image brightness and use same cutoff for all images in one experiment.
setThreshold(10, 255);
//Convert to black on white mask image

```

```
run("Convert to Mask");
//Remove noise with despeckle function.
run("Despeckle");
//Separate closely adjacent objects with watershed function.
run("Watershed");
//Set measurements to area to three decimal places.
run("Set Measurements...", "area redirect=None decimal=3");
//Create annotations covering area above threshold. Excludes objects of area under chosen size
cut-off (100 pixels in this case). Size cut-off should be adjusted depending on the magnification
of the image and the size of objects you wish to exclude (noise).
run("Analyze Particles...", "size=100-Infinity display clear summarize add");
```

B) Aggregate size post-Triton X-100.

```
//Open image. Replace "file name" with desired image directory.
open("file name");
//Next two lines crop the image to account for plate shifting during Triton X-100 treatment.
run("Specify...", "width=1178 height=926 x=0 y=34");
run("Crop");
//Subtract background signal using rolling circle method with radius of 50 pixels.
run("Subtract Background...", "rolling=50");
//Set threshold to exclude pixels below chosen cutoff (10 in this case). Fine-tune according to your
image brightness and use same cutoff for all images in one experiment.
setThreshold(50, 255);
//Convert to black on white mask image
run("Convert to Mask");
//Create annotations covering area above threshold.
run("Analyze Particles...", "size=0-Infinity display clear summarize add");
```


Chapter 5

5. Local DNA sequence context alters the phenotypic potency of identical human tRNA variants¹

5.1 Introduction

Recent studies, including our own work, have demonstrated that transfer RNA (tRNA) variants are more common in the human population than previously thought (1). At the same time, we and others have highlighted the strong potential for tRNA variants to act as disease modifiers (2-4). Indeed, specific tRNA variants cause neurodegenerative phenotypes in mice (5,6) and exacerbate disease in cellular models of cancer (7) and Huntington's disease (8). We anticipate the list will continue to grow, since conceivably many tRNA variants have the potential to modify the development of any human disease. Presently, tRNA genes are not included in the majority of whole exome and genome-wide association studies, so the extent to which tRNA variants associate with disease is not yet known. Thus, very few cause-and-effect relationships have been established between human tRNA variants and disease in real patients (2,9).

Accurately aminoacylated tRNAs and high-fidelity decoding on the ribosome are needed for the faithful production of all proteins in cells. Indeed, tRNAs are essential to ensure the accurate translation of the genetic code into an amino acid sequence. Dysfunctional tRNAs can cause amino acid mis-incorporation, ribosome stalling, or increased reading frame-shifting (2). Further, some tRNAs act outside of their canonical roles in mRNA translation as tRNA-derived fragments (tRFs, tiRNAs), which perform an expanding array of functions in regulating cellular processes (10,11), including protein synthesis (12), stress responses (13), cell proliferation (14), and more. Because proper tRNA activity is important to virtually all cellular functions, tRNA dysfunction has significant potential to modify or exacerbate disease.

Predicting whether a human tRNA variant is deleterious represents a significant challenge. The human genome encodes over 600 tRNA genes and tRNA-like pseudogenes (15). To discriminate real tRNA genes from pseudogenes, tRNAscan-SE was developed, a scoring algorithm that computes the likelihood of tRNA genes being functional (16,17). tRNAscan-SE scores are an assessment of tRNA gene quality which factors in secondary structure predictions

¹Work in this chapter is in preparation for publication. Authorship: Jeremy T. Lant, Farah Hasan, Andrew Seto, Julia Briggs, Patrick O'Donoghue

and conservation of internal promoter sequences found in tRNA genes (A and B box) (16). tRNAscan-SE scores above 50 are considered likely to be functional tRNAs, or “high confidence.” Based on tRNAscan-SE scores, the human genome encodes 416 high confidence tRNA genes (15), and recent estimates predict that over 300 human tRNA genes are actively transcribed in cells (18). Adding to this complexity, healthy individuals commonly harbor ~60-70 tRNA sequence variants in their genome compared to the human reference genome (1). Surprisingly, many of these variants are found in tRNA genes that are known to be expressed and functional in human cells (18,19). Given that many of these variants are found in healthy individuals, the majority of sequenced human tRNA variants are likely benign or have miniscule effects on cellular fitness. The excessive number of tRNA genes and variants in humans, however, provides significant potential for polygenic effects, and we and others have shown that natural tRNA variants can exacerbate or modify human diseases in cellular (5,7,8) and animal (5,6) models.

Significant methodological challenges have also impeded research on tRNAs. One major challenge is the repetitive nature of tRNA genes. Specific iso-decoder tRNAs are found in up to 11 identical copies throughout the human genome (15). Many tRNA families also possess subgroupings which differ by only 1 or 2 nucleotides, making it difficult or impossible to determine which genomic locus a given tRNA was transcribed from using RNA sequencing data. To address this problem, recent efforts developed improved bioinformatic approaches to predict the activity of specific tRNA gene loci based on local sequence context flanking the tRNA gene (18). Even when tRNA gene sequences are identical, the flanking sequence around tRNA genes is often highly divergent (20), and 5' and 3' flanking sequences have long been known to influence eukaryotic tRNA transcription levels (21-23). Transfer RNA genes are somewhat unique in that they harbor internal promoter sequences, referred to as the A and B box, which are sufficient for basal recruitment of the RNA polymerase III transcription initiation complex (24). However, mutational studies on tRNA flanking sequences revealed that local sequence context can alter tRNA gene activity by influencing transcription initiation, termination, and pre-tRNA processing (21,22,25-28). While new sequence-based predictions help to evaluate the likelihood of certain tRNA genes being active, validating the relevance of individual tRNA genes experimentally remains challenging. Inspired by previous work that utilized tRNA anticodon variants to probe elements of the unfolded protein stress response in mammalian cells (29), we hypothesized that anticodon

variants could also be a useful tool in assessing the activity of identical tRNA genes found at distinct genomic loci.

In recent work, we characterized a non-synonymous anticodon variant in the human tRNA-Ser-AGA-2-3 gene which causes mis-incorporation of Serine (Ser) at Phenylalanine (Phe) codons (8). Astoundingly, this variant is found in ~1.8% of the sequenced human population (30-32). The tRNA-Ser-AGA-2-3 gene is one of six identical copies in the human genome, with another five tRNA-Ser genes (AGA-1, AGA-3-1, AGA-4-1, TGA-2-1, TGA-3-1) differing by only 1-2 nucleotides (15). Interestingly, in other copies of the tRNA-Ser-AGA-2-*n* genes, the mistranslating G35A variant is either extremely rare (minor allele frequency > 0.002%) or has never been observed (32). All six copies of the tRNA-Ser-AGA-2-*n* genes are thought to be expressed in human cells based on bioinformatic predictions (18), Chromatin immunoprecipitation (CHIP)-sequencing (33,34), DnaseI hypersensitivity sequencing (34,35), and RNA sequencing data (19). Using the tRNA^{Ser}_{AGA} isodecoders as a proof-of-principle, we developed new assays to investigate the relative importance of identical tRNA genes using a well characterized variant as a genetic probe.

5.2 Materials and Methods

5.2.1 tRNA gene alignments.

tRNA gene sequences were obtained from the human GRCh37/hg19 reference genome using tRNA gene coordinates from the genomic tRNA database (15,36) with added flanking sequence representing regions captured by our genomic PCR primers (Table 5.1, S5.1). Alignments were generated using T-Coffee (37) with ClustalW output format via the EMBL-EBI tools server (38). Results were visualized in Jalview (2.11.14) (39) and colored by sequence identity.

5.2.2 Plasmids and strains.

Plasmid manipulations were performed with *Escherichia coli* DH5 α cells (Invitrogen). All plasmids were derived from WT-Pan (Addgene plasmid #99638; (40)). WT-Pan encodes an EGFP-mCherry fusion protein. To generate mCherry-only plasmids (hereafter referred to as pPan-

Cherry), the EGFP sequence was removed by digestion and ligation of the isoschizomeric *SpeI/NheI* sites flanking EGFP. Human tRNA^{Ser} genes were PCR amplified from human embryonic kidney (HEK) 293T genomic DNA with \pm minimum 300 bp flanking sequence (see Table 5.1, S5.1). This was accomplished with a nested PCR strategy, where larger sequence regions (\pm minimum 400 bp flanking sequence) are first captured with genome-unique primers designed using primer BLAST (41). Inserts for cloning are then re-amplified from the genomic PCR template with primers capturing desired flanking sequence lengths with restriction sites included in 5' tails of the nested PCR primers. Primer sequences are provided (Table S5.1) and human reference genome coordinates of the cloned loci are in Table 5.1. Anticodon variants were introduced in PCR fragments using overlap extension PCR, as described (42). The tRNA expression cassettes were inserted at the *PciI* (New England Biolabs, Ipswich, MA, USA) site of pPan-Cherry. MS-READ (43) peptide-encoding inserts (peptide sequence MSKGPVKVPGAGVPGXGVPGVVGKGGGT; X = L (encoded by TTA or TTG) or F (encoded by TTC or TTT)) were ordered as complimentary DNA oligonucleotides with *BamHI/EcoRI* compatible overhang sequences. Oligonucleotides were phosphorylated *in vitro* using T4 polynucleotide kinase (NEB), then annealed by denaturation for 5 min at 95 °C and gradual cooling to room temperature. The MS-READ peptide encoding sequences were then inserted into *BamHI/EcoRI* sites in WT-Pan, replacing the EGFP sequence. Importantly, WT-Pan harbors a secondary kozak sequence in the linker sequence immediately upstream of the mCherry coding sequence, which allowed us to remove EGFP and its upstream kozak sequence without compromising mCherry expression. Plasmid DNA for transfection in mammalian cells was purified by Midi-Prep (GeneAid) from 100 mL *E. coli* DH5 α cultures grown at 37 °C for 16 hrs to an A₆₀₀ > 1.0. DNA concentrations were measured using a Nanodrop 2000C (ThermoFisher Scientific).

5.2.3 Cell culture and transfection.

Experiments were performed in human embryonic kidney 293T (HEK 293T; American Type Culture Collection (ATCC) #CRL-3216), human K-562 chronic myelogenous leukemia (ATCC #CCL-243), or murine Neuro2a Neuroblastoma (N2a; ATCC #CCL-131) cells. HEK 293T cells were a generous gift from Dr. Ilka Heinemann (University of Western Ontario), K-562 cells were a generous gift from Dr. James Koropatnick and René Figueredo (University of Western

Ontario), and N2a cells were purchased from ATCC. All cell lines were grown at 37 °C with humidity and 5 % CO₂ and cultured in high glucose Dulbecco's modified Eagle medium (DMEM, 4.5 g/L glucose; Gibco by Life Technologies, Carlsbad, CA) containing penicillin (100 IU/mL), streptomycin (100 µg/mL; P/S; Wisent Bioproducts, Montreal, QC, Canada), and 10% fetal bovine serum (FBS; Gibco). Plasmid transfections were performed using Lipofectamine 3000 transfection reagent (Invitrogen) with 2 µg/mL DNA (HEK 293T, N2a cells) or Lipofectamine LTX reagent with PLUS reagent (ThermoFisher Scientific) using 1 µg/mL DNA (K562), following the manufacturer's instructions.

5.2.4 Small molecules and peptides.

Carbobenzoxy-L-leucyl-L-leucyl-L-leucinal (MG132; Sigma-Aldrich 474790, Darmstadt, Germany) was dissolved in DMSO and cells were treated with 10 µM final concentration in all experiments indicated.

5.2.5 Fluorescence microscopy.

Fluorescent microscopy images were captured on an EVOS FL auto fluorescent microscope (Thermo Fisher Scientific). RFP (531 ± 40 nm excitation, 593 ± 40 nm emission) filter cubes were used to capture red fluorescence. For fluorescence analyses, we used semi-automated Fiji/ImageJ (44) macros to annotate cells and measure intensity within regions of interest (ROI), as previously described (8). Fiji/ImageJ macros are included in the supplemental appendix of this chapter with detailed analysis, descriptions, and line-by-line commentary. For live cell imaging (see cell migration assay), cells were incubated at 37 °C with humidity and 5% CO₂ in the EVOS FL auto-fluorescent microscope environment chamber.

5.2.6 tRNA sequencing.

N2a cells were transfected for 48 hrs in biological triplicate on 10 cm plates with plasmids encoding tRNA-Ser-AGA-2-3 or tRNA-Ser-AAA-2-3 variant and mCherry as a transfection marker (Fig. S5.2). We estimated transfection efficiency by manually counting the number of visibly fluorescing cells in images from each transfection. Based on this count, we estimated 50-60% of cells were expressing the transfected plasmids. Cells were harvested by resuspension in TRIzol Reagent (ThermoFisher Scientific), then stored in liquid nitrogen for 1 week before

sending to Arraystar Inc (Rockville, MD, USA) for tRNA sequencing. Samples were sent in an insulated container with dry ice to prevent defrosting during shipment. Detailed descriptions of sample preparation and sequencing methods used by Arraystar Inc. are provided in supplemental information.

5.2.7 Cell harvesting and western blotting.

At 48 hr post-transfection, cells grown in 6-well plates were lifted in phosphate buffered saline (PBS; 137 mM NaCl, 2.7 mM KCl, 10 mM Na₂HPO₄, 1.8 mM KH₂PO₄, pH 7.4) with 10 mM EDTA for 10 min at 37 °C, collected in sterile 1.5 mL microcentrifuge tubes, and pelleted by centrifugation at 300 × g for 3 min at 4 °C. The supernatant was aspirated, and cell pellets were resuspended in 90 µL of mammalian cell lysis buffer containing 50 mM Na₂HPO₄, 1 mM Na₄P₂O₇, 20 mM NaF, 2 mM EDTA, 2 mM EGTA, 1 mM Triton X-100, 1 mM dithiothreitol, 0.3 mM phenylmethylsulfonyl fluoride, and 1 tablet/10 mL complete mini EDTA-free Protease Inhibitor Cocktail (Roche, Mississauga, ON), incubated for 5 min on ice, and centrifuged at 21,000 × g for 10 min at 4 °C. Supernatants were collected in 1.5 mL microcentrifuge tubes and kept on ice for immediate use, or samples were stored at -20°C for up to one week. Protein concentrations in the lysates were determined with a Pierce bicinchoninic acid (BCA) protein assay kit (ThermoFisher Scientific). Lysates were diluted to equal concentrations with sterile milliQ H₂O and 3 × sodium dodecyl sulfate (SDS) loading dye (0.5 M Tris-HCl, pH 6.8; 1.12 M sucrose; 0.025% w/v bromophenol blue; 3.8% w/v SDS). Lysate corresponding to 12 µg total soluble protein was separated by SDS-polyacrylamide gel electrophoresis (10% acrylamide) with protein standards (BioRad, Hercules, CA, USA) for size determination. Proteins were transferred to methanol-activated polyvinylidene fluoride membranes using a Trans-Blot Turbo Transfer System (25 V, 1.3 A for 14 min; BioRad). Blocking and washing solutions were prepared in tris-buffered saline (TBS; 50 mM Tris-HCl, pH 7.5, 150 mM NaCl). Membranes were incubated for 1 hr in blocking solution (3% bovine serum albumin (BSA), 0.1% Tween 20, 1X TBS) before adding primary antibodies at a 1:1000 (α-mCherry, abcam, ab213511) or 1:5000 (α-GAPDH, Sigma-Aldrich, MAB374m) dilution in blocking solution. Membranes were incubated with primary antibody in blocking solution overnight at 4 °C, washed 3 × 10 min in washing solution (1% BSA, 0.1% Tween 20, 1× TBS), then incubated with anti-mouse (Thermo Fisher Scientific, MA1-21315) or anti-rabbit (Sigma, GENA9340) horse radish peroxidase-linked secondary antibodies for 2 hr at room

temperature with a 1:2000 final dilution. Membranes were washed with 1 × TBS with 0.1% Tween 20 for 3 × 10 min, followed by one wash for 10 minutes in 1 × TBS. Proteins were visualized using Clarity Western enhanced chemiluminescence (ECL) Substrates (Bio-Rad) following the manufacturer's instructions and imaged with a ChemiDoc MP System (Bio-Rad).

5.2.8 RFP-trap immunoprecipitation.

HEK 293T cells were transfected for 48 hrs in biological triplicate on 10 cm plates with plasmids encoding tRNA-Ser-AGA-2-5 or tRNA-Ser-AAA-2-5 variant and MS-READ-mCherry proteins with TTA, TTC, TTG, or TTT encoded at the test position in the MS-READ peptide (see Results section 5.3.5). Cells were lifted in phosphate buffered saline (1 × PBS pH 7.4; Corning Cellgro, Corning, NY, USA) supplemented with 1 mM EDTA, harvested by pipetting, and centrifuged in 1.5 mL microcentrifuge tubes at 300 × g for 3 min at 4 °C. Supernatant was removed and cells washed with ice cold PBS (Corning Cellgro) and centrifuged again. The remainder of the protocol, including buffer recipes, was completed according to the RFP-trap agarose manufacturer's instructions (Chromotek). For the elution step, the protein-conjugated RFP-trap beads were boiled in 2× SDS-sample buffer (Laemmli) buffer for 5 min at 95°C to elute. To ensure our protein yields were maximally concentrated, we suspended the beads in 40 µl Laemmli buffer rather than the recommended 80 µL. The beads were then sedimented by centrifugation at 2,500 × g for 2 min at 4 °C, and 30 µL supernatant was loaded on 10% SDS-PAGE gels for gel purification and sample analysis.

SDS-PAGE gels were run at 100-120 V until band fronts reached ~2/3 length of the gel. Gels were stained with Coomassie blue in 10% methanol and 10% acetic acid solution overnight, then de-stained for > 2 hrs in 10% methanol and 10% acetic acid. Bands corresponding to the purified ~29.7 kDa MS-READ-mCherry proteins were picked from the gels using an Ettan Robotic Spot-Picker and submitted for proteolytic digestion (Trypsin) and peptide extraction at the Functional Proteomics Facility at the University of Western Ontario, Canada. Peptide extraction and trypsinization were performed as described (8). LC-MS/MS was performed at the Biological Mass Spectrometry Laboratory at the University of Western Ontario, Canada, as previously described (8).

Raw data files were loaded, processed, and searched using Peaks X+ (Bioinformatics Solutions Inc.) against a custom database consisting of a group of common contaminants and possible proteoforms of MS-READ-mCherry resulting from Phe-to-Ser, and Leu-to-Ser possible substitutions. An FDR of 0.1% and at least 1 unique peptide were used. Spectral count and area-under-the-curve values from liquid chromatogram represent only the exact MS-READ encoded or mistranslated peptides, with no missed cleavages or amino acid modifications. Area-under-the-curve values from mistranslated peptides were normalized to the encoded peptide from the same sample to estimate misincorporation levels (Fig. 5.4D) and account for differences in mCherry yield obtained from the different sample conditions.

5.2.9 Cytotoxicity assays.

Cytotoxicity was measured with CytotoxGlo luminescent cytotoxicity assays (Promega) in at least three biological replicates, following the manufacturer's instructions. Cells were assayed 24 hr or 48 hours post-transfection, as indicated. We also assayed cell death in HEK 293T cells independently using dye exclusion assays with the SYTOX Blue dead cell stain, as described in Chapter 4 (section 4.3.2). For assays involving proteasome inhibition, cells were treated with 10 μ M MG132 or vehicle (DMSO) for 4 hours immediately before assay.

5.2.10 Cell migration assay.

HEK 293T cells were grown to ~80% confluence in a 96-well plate, then deprived of serum by 24 hr incubation in high glucose DMEM containing 1% FBS. Four hours prior to the start of the assay, cells were transfected with plasmids encoding tRNAs and mCherry transfection marker. After 4 hr transfection, the media was replaced with high glucose DMEM containing 20% FBS and either 10 μ M MG132 or DMSO control. The FBS deprivation and spike-in was done to promote *de novo* protein synthesis in the presence of the expressed tRNAs, and MG132 treatment was used to exacerbate phenotypes of mistranslating tRNAs. Immediately after changing the media, wounds were created in the ~90% confluent cell monolayers by scoring each well with a sterile 10 μ l micropipette tip. Live cell fluorescent microscopy time courses were started 1 hr after wound creation, allowing time for plate acclimation and field-of-view focusing in the EVOS environment chamber. Hence, the assay started 5 hrs post-transfection and 1 hr after adding the high serum media with DMSO or 10 μ M MG132. Images were captured every 30 minutes over a

15 hr timecourse. Migration of fluorescing cells was quantitated with the Fiji plugin TrackMate (45) similarly to published approaches (46,47). Briefly, cell migration velocity was approximated as an average of speed measurements for each 30 min capture interval, excluding tracks of duration less than three frames (1.5 hr). Detailed descriptions of TrackMate analysis are included in the supplemental appendix.

5.3 Results

5.3.1 tRNA gene alignments and variant frequencies.

The tRNA variant used in this study is a G35A mutation found in the tRNA-Ser-AGA-2-3 gene in ~1.8% of the sequenced human population (1,30,31). The G35A variant creates an AAA anticodon which causes misincorporation of Ser at Phe codons (UUC and presumably UUU) (8). We previously found that the variant caused a strong reduction in protein synthesis in cells and altered the kinetics of protein aggregation in models of Huntington's disease (8) and ALS (see chapter 4). The human tRNA-Ser-AGA-2-3 gene is one of six identical copies encoded in the human genome, referred to collectively hereafter as tRNA-Ser-AGA-2-*n* genes. We gathered minor allele frequencies for the G35A variant at all tRNA-Ser-AGA-2-*n* loci found in the single nucleotide polymorphism database (dbSNP) (32). According to minor allele frequencies from the largest data source, GnomAD (31), the AGA-2-3 gene is the most frequent site of the G35A variant (Table 5.1). In other tRNA-Ser-AGA-2-*n* genes, the G35A variant is either extremely rare (allele frequency < 0.002%) or has never been observed (Table 5.1).

Transfer RNA genes typically have low sequence conservation immediately flanking the tRNA gene sequence, as noted (20). To assess local flanking sequence contributions on tRNA variant activity, we designed primers to PCR amplify all tRNA-Ser-AGA-2-*n* genes with ~300 bp flanking sequence from HEK 293T genomic DNA (Table S5.1). We used the regions captured by our primers to generate sequence alignments (Fig. S5.1). As expected, sequence conservation was low surrounding the tRNA genes (Fig. S5.1). The only feature which appeared to be conserved outside of the tRNA gene sequence was a T-rich sequence found 5-11 bp downstream of the tRNA genes, which is required for transcription termination (26).

Table 5.1. tRNA-Ser-AGA-2-*n* gene loci and variant frequencies.

tRNA gene	gene coordinates	+upstream ^b	+downstream ^b	Cloned loci coordinates ^c	length	G35A MAF (%) ^d
Ser-AGA-2-1 ^a	chr6:26327817-26327898 (+)	n.a.	n.a.	n.a.	n.a.	0
Ser-AGA-2-2	chr6:27446591-27446672 (+)	320	336	chr6:27446271-27447008 (+)	737	0.0007
Ser-AGA-2-3	chr6:27463593-27463674 (+)	320	308	chr6:27463273-27463982 (+)	709	1.7662
Ser-AGA-2-4	chr6:27470818-27470899 (+)	320	336	chr6:27470498-27471235 (+)	737	0.0014
Ser-AGA-2-5	chr8:96281885-96281966 (-)	323	326	chr8:96281562-96282292 (-)	730	0
Ser-AGA-2-6 ^a	chr17:8129928-8130009 (-)	n.a.	n.a.	n.a.	n.a.	0

^aNot included in experimental work in this study. ^b+upstream and +downstream represent added 5' and 3' sequence lengths respective to the tRNA gene sequence (primer sequences provided in Table S5.1; tRNA gene coordinates from GtRNAdb (15,36)). ^cCloned loci coordinates represent human reference genome GRCh37/hg19 coordinates for complete sequence cloned in our expression plasmids (see Materials and Methods) ^dMinor allele frequency of G35A variant from GnomAD (31) accessed from dbSNP (32) (build 155 released April 9, 2021).

5.3.2 Single nucleotide variants allow detection of tRNA expression by tRNAseq.

Introduction of a single nucleotide variant in a tRNA gene provides a unique sequence feature which we hypothesized could be used to detect expression amidst otherwise identical tRNAs. To test this hypothesis, we conducted tRNA-sequencing of N2a cells expressing the tRNA-Ser-AGA-2-3 or tRNA-Ser-AAA-2-3 genes. We selected N2a cells in this case as we reliably obtain high transfection efficiency, readily detect cytotoxicity from tRNA^{Ser_{AAA}}, and validated Phe to Ser misincorporation in N2a cells expressing the tRNA-Ser-AAA-2-3 variant using mass spectrometry (8).

In addition to having strong tertiary structures (48), tRNAs are among the most densely modified RNAs in cells (49). Hence, custom tRNA sequencing approaches were developed to overcome poor cDNA conversion efficiency by reverse transcriptase enzymes on tRNA genes (50). Cells were sent for a modified version of Hydro-tRNAseq (50) coupled with enzymatic tRNA modification-stripping, similarly to published approaches (19). Sample preparation and sequencing was completed by Arraystar Inc. (Rockville, MD, USA).

Transfer RNA sequencing results can be interpreted by two different read counting strategies, including unique read counts or multi-map-corrected read counts. Unique counts only consider reads which map to a single tRNA sequence, making them preferable for estimating the expression of a specific variant. Multi-map-corrected read counts include reads which map to multiple tRNA gene sequences, considering each unique read as a count of 1 and each multi-mapped read as $1/n$, where n is the number of tRNA sequences which contain the identical sequence. Since tRNAs contain highly repetitive sequence elements and hydro-tRNA sequencing is limited to short 18-40 nt reads, multi-map corrected read counting is essential to estimate expression of most endogenous tRNAs. Indeed, in this case only 8 - 16 % of over five million reads were uniquely mapped from our samples (Table S5.3).

According to the unique read counts, $\text{tRNA}^{\text{Ser}}_{\text{AAA}}$ expression was significantly higher in cells expressing $\text{tRNA}^{\text{Ser}}_{\text{AAA}}$ compared to cells expressing $\text{tRNA}^{\text{Ser}}_{\text{AGA}}$, as expected given that the $\text{tRNA}^{\text{Ser}}_{\text{AAA}}$ sequence is not found endogenously in mouse cells (31.48-fold, $p = 0.0023$; Fig. 5.1). We note that in one of the samples from cells expressing $\text{tRNA}^{\text{Ser}}_{\text{AAA}}$, we did not detect the $\text{tRNA}^{\text{Ser}}_{\text{AAA}}$ sequence (additional samples are in preparation to generate more biological replicates of the sequencing data.). However, in this sample only 237 reads were uniquely mapped to tRNA-Ser sequences in total, compared to 1358 and 2088 in the other samples (Table 5.2). Hence the lack of tRNA-Ser-AAA detection in that sample was likely a false negative due to low read counts. Regardless, $\text{tRNA}^{\text{Ser}}_{\text{AAA}}$ expression was clearly detected in mistranslating cells only. Hence, a single nucleotide variant in a single tRNA gene can be confidently detected by tRNA sequencing.

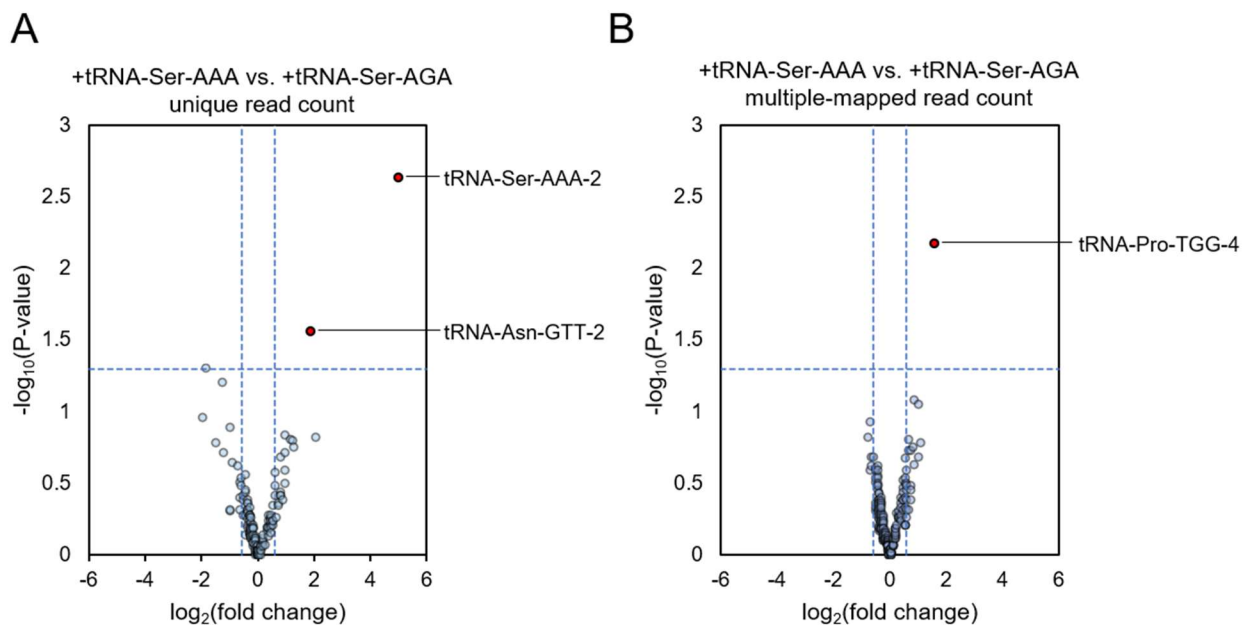


Figure 5.1. tRNA and tRNA variant expression in N2a cells revealed by tRNAseq. N2a cells were transfected with a plasmid encoding wild-type human tRNA^{Ser}_{AGA} or tRNA^{Ser}_{AAA} G35A variants (expressed from human tRNA-Ser-AGA-2-3 gene flanking sequence context) and mCherry (see Materials and Methods). tRNA-sequencing results from the transfected cells are depicted as volcano plots, where x-asymptotes denote a ± 1.5 -fold change and y-asymptote denotes a p-value of 0.05 based on exact tests by negative binomial distribution. Values were calculated based on unique (A) or multi-map-corrected (B) read counts. Significantly differentially expressed genes are highlighted in red and labeled.

Importantly, our results suggest that tRNA^{Ser}_{AAA} was expressed but not over-expressed in our cells transfected with the tRNA^{Ser}_{AAA} plasmid. In the samples where tRNA^{Ser}_{AAA} expression was detected, we observed 19 and 29 unique read counts (Table 5.2). By comparison, we observed hundreds of unique counts for comparable tRNA^{Ser} isodecoder and isoacceptor sequences (Table 5.2) For example, in the same samples where we observed 19 and 29 unique read counts for tRNA^{Ser}_{AAA}, we observed 142 and 290 unique read counts for a comparable tRNA^{Ser}_{GCT} sequence (tRNA-Ser-GCT-3), which differs from three identical copies of the tRNA^{Ser}_{GCT} genes (tRNA-Ser-GCT-4-1, 4-2, 4-3) by only a single nucleotide. While our data is only roughly quantitative from transiently transfected cells, accounting for transfection efficiency estimates of 50-60% implies that tRNA^{Ser}_{AAA} was not expressed more highly than endogenous tRNA-Ser genes.

Table 5.2. tRNAseq unique read counts for all tRNA-Ser isodecoders.

Isodecoder	Sample-replicate ^a					
	AGA-1	AGA-2	AGA-3	AAA-1	AAA-2	AAA-3
tRNA-Ser-AAA	0	1	0	19	0	29
tRNA-Ser-AGA-2	1	2	1	0	0	1
tRNA-Ser-AGA-3	2	2	15	2	0	5
tRNA-Ser-CGA-1	28	162	110	143	15	214
tRNA-Ser-CGA-2	61	1223	716	504	63	807
tRNA-Ser-CGA-3	2	5	4	3	4	5
tRNA-Ser-GCT-1	11	282	149	112	13	146
tRNA-Ser-GCT-2	4	36	64	18	1	27
tRNA-Ser-GCT-3	71	213	354	142	31	290
tRNA-Ser-GCT-4	2	0	2	0	0	2
tRNA-Ser-GCT-5	2	2	2	3	1	4
tRNA-Ser-GGA-1	5	10	12	9	7	7
tRNA-Ser-TGA-1	144	684	448	397	102	542
tRNA-Ser-TGA-2	2	3	6	6	0	9
Total:	335	2625	1883	1358	237	2088
% AAA-2^b:	0	0.04	0	1.4	0	1.4

^aSamples are labelled according to the anticodon of expressed tRNA and biological replicate number. ^bPercentage of unique tRNA^{Ser} mapped reads corresponding to the expressed tRNA^{Ser}_{AAA} variant.

Table 5.3. tRNAseq multi-map-corrected read counts for all tRNA-Ser isodecoders.

Isodecoder	Sample-replicate ^a					
	AGA-1	AGA-2	AGA-3	AAA-1	AAA-2	AAA-3
tRNA-Ser-AAA	299	1131	1030	701	221	912
tRNA-Ser-AGA-1	328	1196	1138	727	228	950
tRNA-Ser-AGA-2	306	1134	1067	682	220	895
tRNA-Ser-AGA-3	4	16	30	4	1	8
tRNA-Ser-CGA-1	63	195	144	168	23	256
tRNA-Ser-CGA-2	63	1224	725	510	63	823
tRNA-Ser-CGA-3	13	18	26	12	12	21
tRNA-Ser-GCT-1	52	380	297	175	41	269
tRNA-Ser-GCT-2	73	966	534	395	73	524
tRNA-Ser-GCT-3	136	1201	882	538	107	817
tRNA-Ser-GCT-4	86	1029	576	424	80	575
tRNA-Ser-GCT-5	9	48	75	30	5	67
tRNA-Ser-GGA-1	24	65	68	44	21	46
tRNA-Ser-TGA-1	146	692	467	407	103	552
tRNA-Ser-TGA-2	328	1185	1151	751	226	970
Total:	1631	7432	6429	4867	1127	6763

^aSamples are labelled according to the anticodon of expressed tRNA and biological replicate number. ^bPercentage of multi-map-corrected tRNA-Ser reads corresponding to the tRNA-Ser-AGA-2 sequence.

Since the human tRNA-Ser-AGA-2-3 sequence is identical to six endogenous mouse tRNA^{Ser} genes, the plasmid based tRNA^{Ser}_{AGA} could not be detected by unique read counts. Indeed, we observed at most 2 uniquely mapped reads corresponding to the tRNA-Ser-AGA-2 sequence (representing all tRNA-Ser-AGA-2-*n* genes), in a sample where 266,903 uniquely mapped reads were obtained in total (Table S5.3). Otherwise, the unique read count-based quantitation suggested a significant change in expression of only one other tRNA when comparing the tRNA-Ser-AAA and tRNA-Ser-AGA samples, tRNA-Asn-GTT-2 (3.61-fold, $p = 0.027$, Fig. 6A).

Based on the multi-map-corrected counts, we detected a significant up-regulation of another single tRNA, tRNA-Pro-TGG-4 (3.04-fold, $p = 0.0067$, Fig. 5.1B). Our ability to interpret expression of the tRNA-Ser-AAA and tRNA-Ser-AGA-2 sequences was limited when considering multi-map-corrected reads (Table 5.3). The expressed human tRNA-Ser-AGA-2-3 gene is identical to six endogenous mouse tRNA genes, so the expressed and endogenous tRNA-Ser-AGA-2-*n* sequences are reported together as “tRNA-Ser-AGA-2”. The tRNA-Ser-AAA sequence expressed in the “AAA” samples differs by a single nucleotide, and another three endogenous mouse tRNA-Ser genes (AGA-1-1, TGA-2-1, TGA-2-2) differ by only 1-2 nucleotides (15). Hence, the majority of reads for the tRNA-Ser-AAA, tRNA-Ser-AGA-1, tRNA-Ser-AGA-2, and tRNA-Ser-TGA-2 sequences would be counted as a conglomerate in the multi-map-corrected read calculation. For these reason we could not logically infer changes in expression of tRNA^{Ser}_{AGA} or tRNA^{Ser}_{AAA} in our samples groups based on the multi-map corrected read counts.

5.3.3 tRNA gene expression predictions.

While identical tRNA copies cannot be distinguished once transcribed, clues to the expression of individual loci can be gathered from DNA sequence-based predictive scores (18) as well as chromatin immunoprecipitation (CHIP) sequencing and DNase hypersensitivity sequencing data available on the UCSC genome browser (34,51).

Recently, a landmark publication assessed a variety of DNA sequence-based predictive factors in evaluating the likelihood of individual tRNA genes being active (18). The authors detailed numerous sequence features which correlate with a higher or lower likelihood of tRNA gene activity. Among the features assessed, CpG density and CpG island scores upstream of the tRNA gene were most strongly predictive of tRNA gene activity (18). To visualize predictions on the tRNA-Ser-AGA-2-*n* loci, we plotted CpG island scores against CpG density from the human dataset (high confidence tRNA genes only; available at gtRNADB.ucsc.edu/tRAP/) as scatter plots and highlighted all tRNA genes containing the AGA anticodon. In general, all of the tRNA-Ser-AGA-2-*n* genes had moderate CpG island and CpG density scores compared to the other high confidence human tRNA genes. Among the tRNA-Ser-AGA-2-*n* loci, the 2-3, 2-4, 2-5, and 2-6 loci scored slightly higher than the 2-1 and 2-2 loci (Fig. 5.2A). Compared to the other three tRNA-Ser-AGA genes (AGA-1-1, -3-1, and -4-1) all of the -2-*n* genes had generally higher CpG density and CpG island scores, except for the -2-1 loci, which scored lower than -4-1 in CpG density.

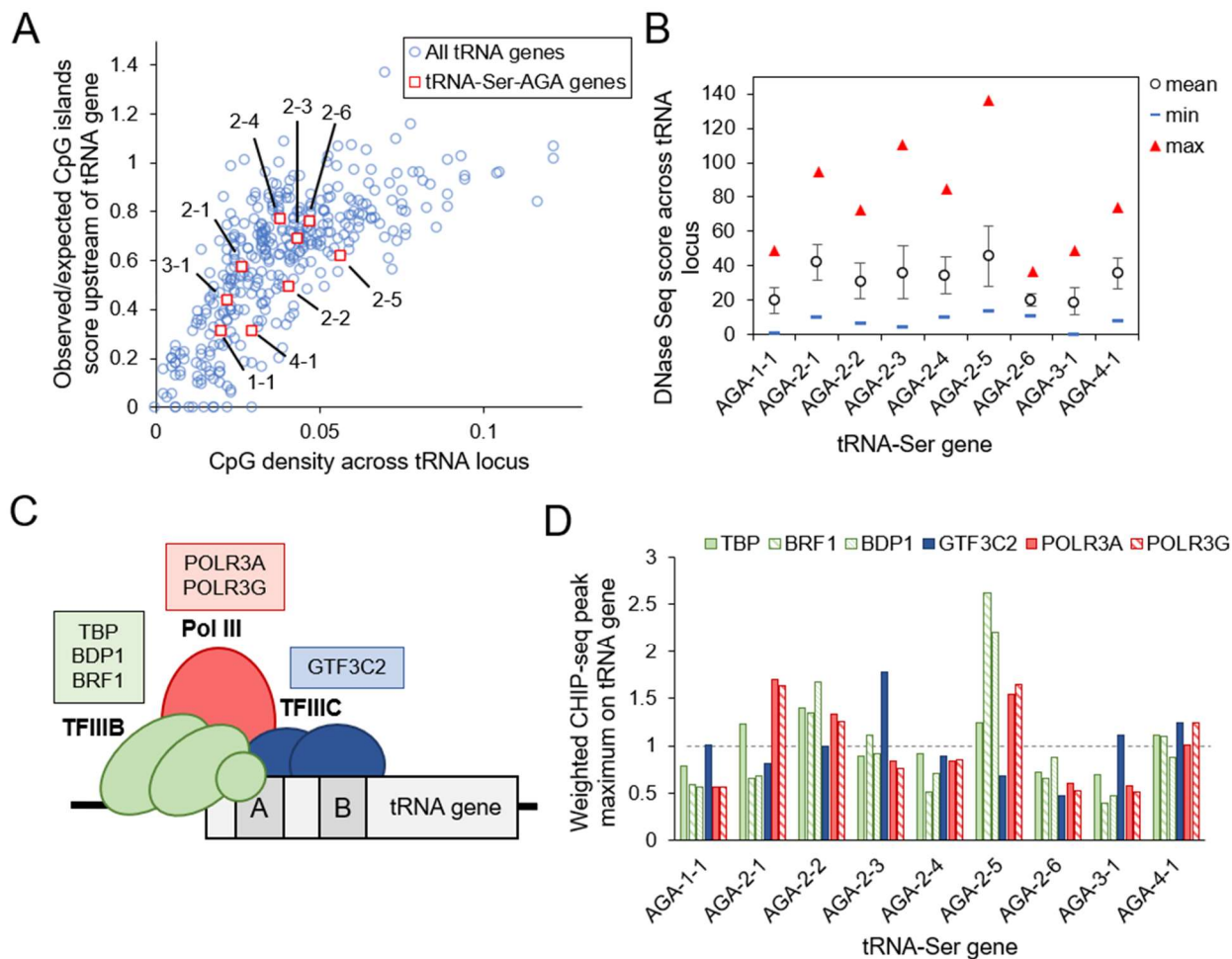


Figure 5.2 tRNA gene expression activity predictions from publicly available datasets. CpG island and CpG density scores reported by Thornlow *et al.* (18) for all high confidence human tRNA genes were plotted as scatter plots (A). All tRNA-Ser genes with AGA anticodon were highlighted with red squares and labeled with standard tRNA gene numbers from GtRNAdb (15,36). DNase I hypersensitivity sequencing (35) scores for all AGA anticodon tRNA-Ser genes with ± 350 bp flanking sequence were gathered from ENCODE human K562 cell data (34) (accessed through the UCSC genome browser (51)), and descriptive statistics were plotted (B). Error bars represent one standard deviation of the mean score in each sequence window. A cartoon depicting RNA polymerase III transcription initiation complex members with associated CHIP-sequencing data is shown (C). Cartoon is based on a review by R.J. White (24). CHIP-sequencing peak maxima from ENCODE human K562 cell data (34) (accessed through the UCSC genome browser (51)) were tabulated for all tRNA-Ser genes with AGA anticodon and plotted (D). For each transcription initiation complex protein, peak maxima were weighted to the mean of all

tRNA-Ser-AGA genes shown, such that a value of 1 represents the mean peak maximum value for each protein across all high confidence human tRNA-Ser-AGA genes (D).

We also tabulated other predictive scores reported by Thornlow *et al.* (18) for all AGA anticodon tRNA-Ser genes (Table 5.4). tRNAscan-SE scores are an assessment of tRNA gene quality which factors in secondary structure predictions and conservation of internal promoter sequences found in tRNA genes (A and B box) (16). Since all of the tRNA-Ser-AGA-2-*n* genes have identical sequence, their tRNAscan-SE scores are identical, with a score of 89.6. tRNAscan-SE scores above 50 are considered likely to be functional tRNAs, so this score suggests that the tRNA-Ser-AGA-2-*n* sequence is functional when expressed. The other scores are all predictive factors associated with likelihood of tRNA genes being active (18). PhyloP scores are a metric of evolutionary conservation of sequences among mammalian phylogenies (52). High PhyloP scores in tRNA gene sequences correlate with higher likelihood of gene activity (18). Interestingly, low PhyloP scores in the 5' flanking sequence adjacent to tRNA genes also correlate with higher likelihood of tRNA gene activity (18), since tRNA genes are subject to high rates of transcription-associated mutagenesis (20). Other predictive factors reported by Thornlow *et al.* included distance to TTTT transcription termination sites and number of tRNA gene copies with the same anticodon sequence (18). Distance to TTTT transcription termination sites correlated negatively with likelihood of expression. The number of tRNA gene copies with the same anticodon correlated with a higher likelihood of the tRNA gene being active, but lower likelihood of the tRNA gene being highly expressed. These factors and the CpG density and island scores all contributed to the calculated probability score.

Comparing the other predictive scores for all tRNA-Ser-AGA genes (Table 5.4), the tRNA-Ser-AGA-2-*n* genes were all predicted to have higher likelihood of activity (>97%) compared to the tRNA-Ser-AGA-1-1, 3-1, and 4-1 genes (83.6 – 93.5%), and compared to the mean score of all high confidence human tRNA-Ser genes (93.9%). Hence, all of the tRNA-Ser-AGA-2-*n* loci are likely active tRNA genes in humans. Comparing within the tRNA-Ser-AGA-2-*n* group, we could not determine any clear indication of which gene might be more active than another. For example, the tRNA-Ser-AGA-2-5 locus scored higher than all other tRNA-Ser-AGA genes in CpG density across the tRNA locus (Fig. 5.2A) and PhyloP score within the tRNA gene sequence (Table 5.4), but also had the longest distance to transcription termination site among the tRNA-Ser-AGA-

2-*n* loci, and highest PhyloP score in the 5' flanking region, which inversely correlates with likelihood of tRNA gene activity (Table 5.4).

Table 5.4. Extended tRNA gene activity prediction scores.

tRNA-Ser Gene Name (suffix)	Total Number of tRNA Genes With Identical Anticodon	tRNAscan-SE General Bit Score	Average PhyloP Score in tRNA Gene Sequence ^a	Distance To Nearest TTTT Transcription Termination Sequence	Average PhyloP Score in 5' Flanking Region ^a	Probability of active tRNA gene ^{a,b}
AGA-1-1	9	90.3	0.850	100	-3.575	0.850
AGA-2-1	9	89.6	0.984	8	-2.709	0.986
AGA-2-2	9	89.6	0.796	5	-3.311	0.984
AGA-2-3	9	89.6	0.649	6	-3.587	0.985
AGA-2-4	9	89.6	0.588	9	-2.552	0.984
AGA-2-5	9	89.6	1.488	11	-0.774	0.973
AGA-2-6	9	89.6	1.418	5	-4.848	0.988
AGA-3-1	9	87.2	0.838	123	-3.564	0.935
AGA-4-1	9	78.8	0.666	7	-1.330	0.836
All human tRNA^{Ser} mean^c	7.08	88.772	0.950	17.88	-2.397	0.939

^aValues were rounded to fit the table. ^bAll tRNA-Ser-AGA genes shown were predicted active in *H. sapiens*. ^cMean values for all high confidence human tRNA-Ser genes characterized by Thornlow B.P. *et al* (18).

As a secondary estimate of tRNA gene expression activity, we tabulated DNase hypersensitivity sequencing and CHIP-sequencing data from encyclopedia of DNA elements (ENCODE) (34) datasets available on the UCSC genome browser (51) First, we downloaded tracks from DNaseI sequencing data ((35) K562, University of Washington) using custom windows representing each tRNA gene sequence \pm 350 bp of flanking sequence (Fig. 5.2B, S5.3B-E). DNase I hypersensitivity sequencing uses partial digestion of chromatin with an endonuclease (DNase I) followed by sequencing to map areas of open and closed chromatin in the genome, since areas of open chromatin are more susceptible to endonucleolytic cleavage (53). Areas of open chromatin also tend to be more transcriptionally active, meaning a high DNase sequencing score is suggestive of higher expression at a given genomic locus. However, since different DNA sequences are more readily detected in sequencing than others, and some sequences may be more

amenable to DNase I activity than others, we report these data as merely a qualitative indicator of tRNA gene expression activity. Based on data collected from human K562 cells, DNase I sequencing peaks (Fig. S5.3) and descriptive statistics (Fig. 5.2B) suggested that expression activity of the tRNA-Ser-AGA-2-*n* loci would occur roughly in order of 2-5 > 2-3 ~ 2-1 > 2-4 ~ 2-2 > 2-6. We also found that most of the tRNA-Ser-AGA-2-*n* loci had generally higher DNase I sequencing scores compared to the tRNA-Ser-AGA-1-1, 3-1, and 4-1 loci, with the exception of tRNA-Ser-AGA-2-6, which had among the lowest scores.

CHIP-sequencing data can also be used to estimate tRNA gene expression activity. CHIP-sequencing uses antibodies against DNA binding proteins to immunoprecipitate and sequence chromatin fragments, giving a semi-quantitative readout of the relative binding propensity of individual proteins based on read counts for the associated DNA sequence (54). By comparing relative CHIP-sequencing scores from components of the RNA polymerase III transcription initiation complex (24) on tRNA genes, qualitative inferences of tRNA gene expression activity can be made. The basal transcription initiation machinery for tRNAs consists of three protein complexes, the TFIIB and TFIIC complexes which bind to internal promoter sequences found within the tRNA sequence (A and B box), and the RNA polymerase III complex (24). We searched for CHIP-sequencing data from the encyclopedia of DNA elements (ENCODE) (34) accessed through the UCSCS genome browser (51). The largest available datasets were gathered from K562 cells, so we limited our search to K562, and excluded any datasets where cells were treated or stimulated, e.g., with growth factors or small molecules. We found high quality CHIP-sequencing peaks for two proteins in the RNA polymerase III complex (gene names POLR3A, POLR3G), three proteins in the TFIIB complex (gene names TBP, BDP1, BRF1), and one protein in the TFIIC complex (gene name GTF3C2) (Fig. 5.2C; Table S5.4).

To compare the relative CHIP-sequencing scores for each transcription factor, we gathered the peak maximum value found within each tRNA sequence for all human tRNA-Ser genes with AGA anticodon. We then normalized the individual score at each tRNA gene locus to the mean score of all the tRNA-Ser-AGA genes, such that a score of one represents the mean value for a given transcription factor (Fig. 5.2D). Based on this analysis, we found the overall highest binding activity for RNA polymerase III transcription initiation complex proteins occurred on the tRNA-Ser-AGA-2-5 locus. We also observed elevated scores on the tRNA-Ser-AGA-2-1, 2-2, and 2-3

loci for certain factors, and generally lower binding activity on the AGA-1-1, -2-4, 2-6, and -3-1 loci. Hence, the CHIP-sequencing data suggest that expression activity of the tRNA-Ser-AGA-2-*n* loci would occur roughly in order of 2-5 > 2-3 ~ 2-1 ~ 2-2 > 2-4 ~ 2-6 in human K562 cells.

Another observation we made based on the CHIP-sequencing data was that the tRNA-Ser-AGA-2-1 and 2-6 genes both had closely neighboring tRNA genes, such that peaks from transcription factors binding to the nearby genes overlapped in the \pm 350 bp windows capturing the genomic loci (Fig. S3). For this reason, we decided to limit the remainder of our study to the tRNA-Ser-AGA-2-2, 2-3, 2-4, and 2-5 loci, which could be more easily isolated with their flanking sequences.

5.3.4 Mistranslating tRNAs reduce protein synthesis to varying degrees depending on local sequence context.

To test the effects of local sequence context on identical tRNA variants expressed in mammalian cells, we PCR amplified a subset of the tRNA-Ser-AGA-2-*n* loci (2-2, -2-3, -2-4, and -2-5) with local sequence context (\pm 300 bp; see Table 5.1) from HEK 293T cell genomic DNA and cloned the tRNA alleles into plasmids that co-express an mCherry transfection marker. In each gene, we created constructs with the corresponding G35A variant, which is naturally found in the tRNA-Ser-AGA-2-3 and 2-2 loci (see Table 5.1).

In previous work, we observed a strong reduction in protein synthesis in cells expressing the tRNA-Ser-AGA-2-3 G35A variant (8), and others have observed this effect from expressing different synthetic anticodon variants of tRNA^{Ser} (29,55). We transfected all plasmids expressing wild-type or G35A tRNA genes and mCherry into K562 (Fig. 5.3A,D), HEK 293T (Fig. 5.3B,E), and N2a cells (Fig. 5.3C,F) and measured mCherry fluorescence per cell using fluorescence microscopy and a custom analysis macro in Fiji/ImageJ (see supplemental information). We also used western blotting against mCherry (α -RFP) from HEK 293T cell lysates to confirm that observed changes in fluorescence were associated with changes in mCherry protein expression (Fig. 5.3G).

In K562 cells, mCherry fluorescence was reduced in cells expressing the variant compared to wild-type tRNA^{Ser} from all sequence contexts except the Ser-AGA-2-4 gene. We observed the strongest reductions in cellular fluorescence when the variant was expressed from the tRNA^{Ser}

AGA-2-3 and AGA-2-5 contexts. Overall, we observed differential reductions in protein synthesis that followed a trend of decreasing inhibition with 2-3 ~ 2-5 > 2-2 > 2-4. The results are in reasonable agreement with the trends we predicted from K562 CHIP-sequencing and DNase sequencing data (Fig. 5.2B,D).

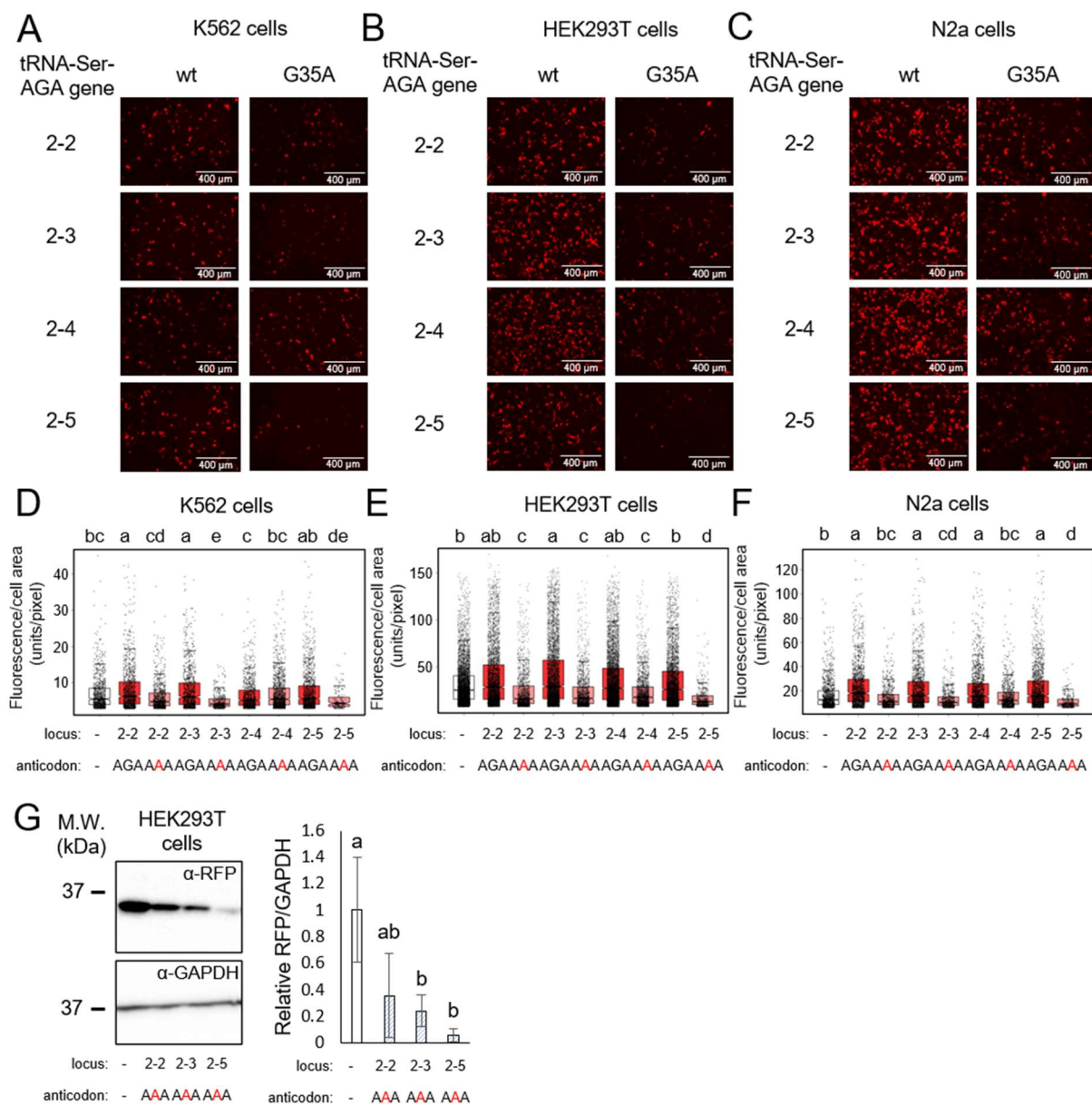


Figure 5.3 Fluorescence of cells expressing tRNA-Ser-AAA-2-*n* variants. Plasmids encoding mCherry and wild-type human tRNA^{Ser}_{AGA} or G35A variant tRNA^{Ser}_{AAA} with different flanking sequence contexts from human tRNA-Ser-AGA-2-*n* genes were transfected in human K562 (A), HEK 293T (B) and murine N2a (C) cells. Representative images were captured by fluorescence

microscopy (A-C) and fluorescence was quantitated using custom Fiji/ImageJ macros (D-F; see supplemental information) as previously described (8). Each box-and-whisker plot represents data from at least $N = 4$ biological replicates (D-E). Midline represents the median, boxes represent quartiles, and whiskers represent $1.5\times$ the interquartile range. Dots show underlying datapoints from individual cells. HEK 293T cell lysates from cells expressing no tRNA, tRNA-Ser-AAA-2-2, 2-3, and 2-5 genes were western blotted with α -RFP and α -GAPDH (G). Letters indicate significantly different groups determined by Tukey's Honestly Significant Different (HSD) tests of biological replicate means, where groups sharing a letter are not significantly different and groups not sharing a letter are significantly different ($\alpha = 0.05$).

In HEK 293T cells, we observed a strong mistranslating tRNA variant-induced reduction in mCherry fluorescence from all AGA-2-*n* sequence contexts (Fig. 5.3B,E), including the AGA-2-4 context which had no effect in K562 cells (Fig. 5.3D). To our knowledge, this is the first known example of identical human cytoplasmic tRNA genes being differentially regulated in different cell types. We also observed in HEK 293T cells that the variant in the 2-5 context had a stronger effect on mCherry fluorescence than in the 2-3 context. In N2a cells, we observed similar effects to HEK 293T cells, where the Ser-AAA-2-5 gene variant caused the strongest reduction in cellular mCherry fluorescence and the other contexts reduced fluorescence compared to their respective wild-type tRNAs but not significantly differently from each other (Fig. 5.3C,F).

5.3.5 Precise detection of tRNA-dependent codon misreading with MS-READ.

Previously we demonstrated by liquid chromatography with tandem mass spectrometry (LC-MS/MS) that the tRNA-Ser-AGA-2-3 G35A variant causes Phe to Ser mis-incorporation at UUC codons in N2a cells (8). We hypothesized that the variant could also mistranslate UUU (Phe) codons, and potentially UUA (Leu) codons, since wild-type tRNA-Ser-AGA tRNAs may be modified at the A34 position to inosine (56), and A34I tRNAs can pair with codons ending in U, C, or A (57-59). Given the strong reduction in protein synthesis that we observed was from expressing the tRNA-Ser-AAA variant in the Ser-AGA-2-5 genetic context in HEK 293T cells, we expected the 2-5 context to cause higher levels of mis-incorporation, allowing us to establish exactly which codons the variant is capable of mis-coding with serine.

We also improved on our previous mass spectrometry approach which involved immunoprecipitation of mCherry as a test protein for misincorporation events (8). In that approach, we expressed wild-type or variant tRNA from the same plasmid as the mCherry test protein. Hence, the timing of tRNA and reporter expression is coupled, and all transfected cells expressing the reporter protein also express the tRNA variant. In this case, we fused a designer peptide sequence (MS-READ) to mCherry to improve detection sensitivity (Fig. 5.4A). MS-READ is an affinity purification combined with mass spectrometry approach which utilizes a designer peptide readily detected in LC-MS/MS to identify all possible amino acid misincorporation events (43). At the test site of the designer peptide, we cloned all UUN codons (UUA, UUC, UUG, and UUU) and fused the peptide sequence to mCherry. The MS-READ-mCherry protein was co-expressed with wild-type tRNA-Ser-AGA-2-5 or variant tRNA-Ser-AAA-2-5 on the same plasmid in HEK 293T cells. After 48hr transfection, we purified the MS-READ-mCherry protein by RFP-trap immunoprecipitation (See Materials and Methods, Fig. S5.4) and analyzed the mCherry samples by LC-MS/MS.

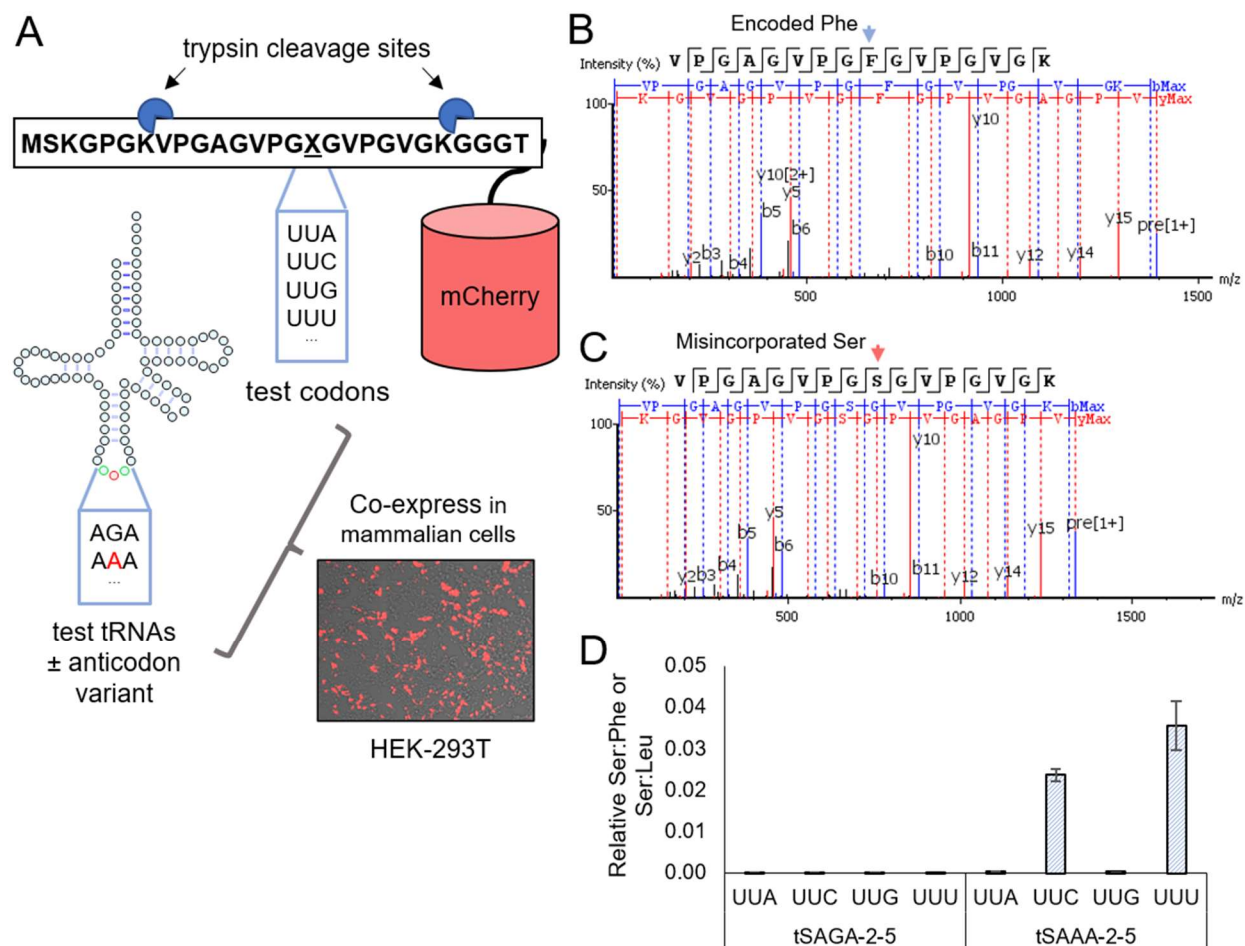


Figure 5.4 tRNA-dependent Phe to Ser misincorporation detected by MS-READ. A cartoon depicting the MS-READ reporter approach is shown (A). The MS-READ peptide-coding sequence was mutagenized to include UUA, UUC, UUG, or UUU codons at the test position, and fused to mCherry in a mammalian expression plasmid. From the same plasmid, we expressed wild-type tRNA^{Ser}_{AGA} or the variant tRNA^{Ser}_{AAA} with flanking sequence context from the human tRNA-Ser-AGA-2-5 gene. High quality y and b ion spectra were obtained pertaining to the encoded Phe (B) and Leu (Fig. S4), and the mistranslated Ser (C) peptide in cells expressing the tRNA variant with UUC and UUU test codons in MS-READ (see also Table 5.5). Area-under-the-curve values from the liquid chromatogram were used for quantitation, where mistranslated Ser peptide values were normalized to the encoded Phe or Leu peptide value from the same sample (D), similarly to published approaches (43). Error bars represent one standard deviation of the means of three biological replicates.

Table 5.5 LC-MS/MS area under the curve and spectral counts for MS-READ peptides.

tRNA anticodon	Test codon	Expected am. Acid ^c	Area ^a			Spectral count ^b		
			Phe ^d	Leu ^d	Ser ^d	Phe ^d	Leu ^d	Ser ^d
AGA	UUA	Leu	1.18E+07	1.30E+10	0	3	45	0
AGA	UUA	Leu	1.30E+09	1.11E+10	1.74E+06	4	5	1
AGA	UUA	Leu	2.32E+06	1.20E+10	0	2	55	0
AAA	UUA	Leu	5.45E+06	1.23E+10	5.97E+05	3	45	0
AAA	UUA	Leu	0	2.45E+09	1.21E+06	0	4	0
AAA	UUA	Leu	6.22E+06	1.26E+10	2.55E+06	3	26	1
AGA	UUG	Leu	5.86E+07	1.43E+10	7.76E+05	4	33	0
AGA	UUG	Leu	1.22E+06	1.98E+10	0	2	54	0
AGA	UUG	Leu	7.65E+08	2.87E+10	1.89E+06	4	44	1
AAA	UUG	Leu	3.09E+06	9.87E+09	3.86E+05	3	23	1
AAA	UUG	Leu	4.49E+06	9.66E+09	2.43E+06	1	33	0
AAA	UUG	Leu	2.44E+06	1.13E+10	2.37E+05	2	42	0
AGA	UUC	Phe	1.21E+10	1.02E+07	0	5	3	0
AGA	UUC	Phe	2.72E+10	1.81E+06	0	20	2	0
AGA	UUC	Phe	1.03E+10	3.10E+08	1.30E+06	56	5	0
AAA	UUC	Phe	1.27E+10	5.05E+06	2.94E+08	38	2	5
AAA	UUC	Phe	1.24E+10	3.86E+06	2.61E+08	38	2	5
AAA	UUC	Phe	6.56E+09	1.57E+06	1.77E+08	33	3	5
AGA	UUU	Phe	1.19E+10	1.32E+08	1.42E+05	4	3	0
AGA	UUU	Phe	1.40E+10	2.66E+08	6.69E+03	5	3	0
AGA	UUU	Phe	1.54E+10	1.27E+08	0	5	3	0
AAA	UUU	Phe	2.69E+09	1.40E+06	1.32E+08	33	0	5
AAA	UUU	Phe	6.11E+09	1.78E+06	1.74E+08	30	2	4
AAA	UUU	Phe	4.74E+09	1.17E+06	1.39E+08	5	2	5

^aArea-under-the-curve values from liquid chromatogram. ^bSpectral counts for number of spectra with area > 1E6 and -10logP value > 50. ^cExpected amino acid refers to the amino acid encoded by the test codon in the MS-READ peptide. ^dAmino acids refer to the detected amino acid in the test position of the MS-READ peptide

Complete area and spectral count results are described in Table 5.5 and exemplary y and b ion spectra for all samples where Ser misincorporation was detected are provided in Fig. S5.5. We observed high quality y and b ion spectra pertaining to the mistranslated Ser residue incorporated at Phe UUC and UUU codons only when the variant tRNA was expressed (Table 5.5, Fig. S5.5), and not in samples from any other tRNA or codon pair. In several other samples we observed a single putative spectral count for Phe:Ser misincorporation (Table 5.5), but in these cases the y and b ion spectra showed poor coverage of the misincorporation site (Fig. S5.5). As expected, in

all samples we identified many high-quality peptide spectra pertaining to the properly encoded Phe or Leu peptides (Fig. 5.4B, Table 5.5). For an estimate of mis-incorporation levels, we normalized the abundance from the area under the chromatographic curves of the Ser peptides to the respective Leu or Phe encoded peptide from the same sample, as others have described for label-free quantitation using the MS-READ peptide (43). According to the estimate, the proportion of Ser : Phe was 0.023 ± 0.002 when the variant tRNA^{Ser}_{AAA} and UUC test peptide were co-expressed and 0.036 ± 0.006 when the variant tRNA^{Ser}_{AAA} and UUU test peptide were co-expressed (Fig. 5.4D). For all other tRNA and codon pairs the Ser : Phe/Leu ratios were effectively zero, since the un-normalized area-under-the-curve values for any putative mis-incorporation hits were below background level ($< 1 \times 10^7$). Hence, the tRNA-Ser-AGA-2-5 G35A variant is capable of mistranslating both UUU and UUC Phe codons in HEK 293T cells, but Ser mistranslation at Leu codons was not detected. These data also represent the first successful adaptation of MS-READ for detecting amino acid misincorporation in mammalian cells.

5.3.6 Cytotoxicity of a mistranslating tRNA variant expressed from different sequence contexts.

In previous work, we demonstrated that the human tRNA-Ser-AGA-2-3 G35A variant is cytotoxic when expressed in N2a cells, and that cytotoxicity is exacerbated by treating cells with the proteasome inhibitor MG132 (8). To assess cytotoxicity of the tRNA variant in other sequence contexts and cell lines, we transfected K562 (Fig. 5.5A), HEK 293T (Fig. 5.5B), and N2a (Fig. 5.5C) cells with wild-type or G35A variant tRNA-Ser-AGA in the 2-2, 2-3, 2-4, and 2-5 sequence contexts expressed from our mCherry plasmids as above. Cytotoxicity was assessed with CytoxGlo2.0 assays, which involved luminescent detection of cellular proteases released into the medium by dying cells. In N2a cells, we observed significant cytotoxicity from the tRNA^{Ser}_{AAA} variants expressed from all sequence contexts, though we could not detect differences in cytotoxicity when comparing the different sequence contexts to each other (Fig. 5.5C). In K562 and HEK 293T cells, we found cytotoxicity results to be highly variable and could not conclude cytotoxic effects from any of the tRNA variants (Fig. 5.5A,B).

To further probe cytotoxicity in HEK 293T cells, we used a dye exclusion assay with SYTOX Blue, a cell-impermeable nucleic acid stain, and subsequent treatment with a membrane detergent (Triton X-100) to establish total cell counts, as previously described (see Chapter 4).

Cells were assayed in the presence (Fig. S5.6B) or absence (Fig. S5.6A) of 10 μ M MG132, and after longer transfection periods (48 hr; Fig. S5.6C). Again, we were unable to detect significant cytotoxic effects from the variant expressed from any of the sequence contexts in HEK 293T cells. Hence, the tRNA-Ser-AGA-2-*n* G35A variants were not significantly cytotoxic to K562 or HEK 293T cells, but cytotoxicity was detected readily in N2a from all sequence contexts.

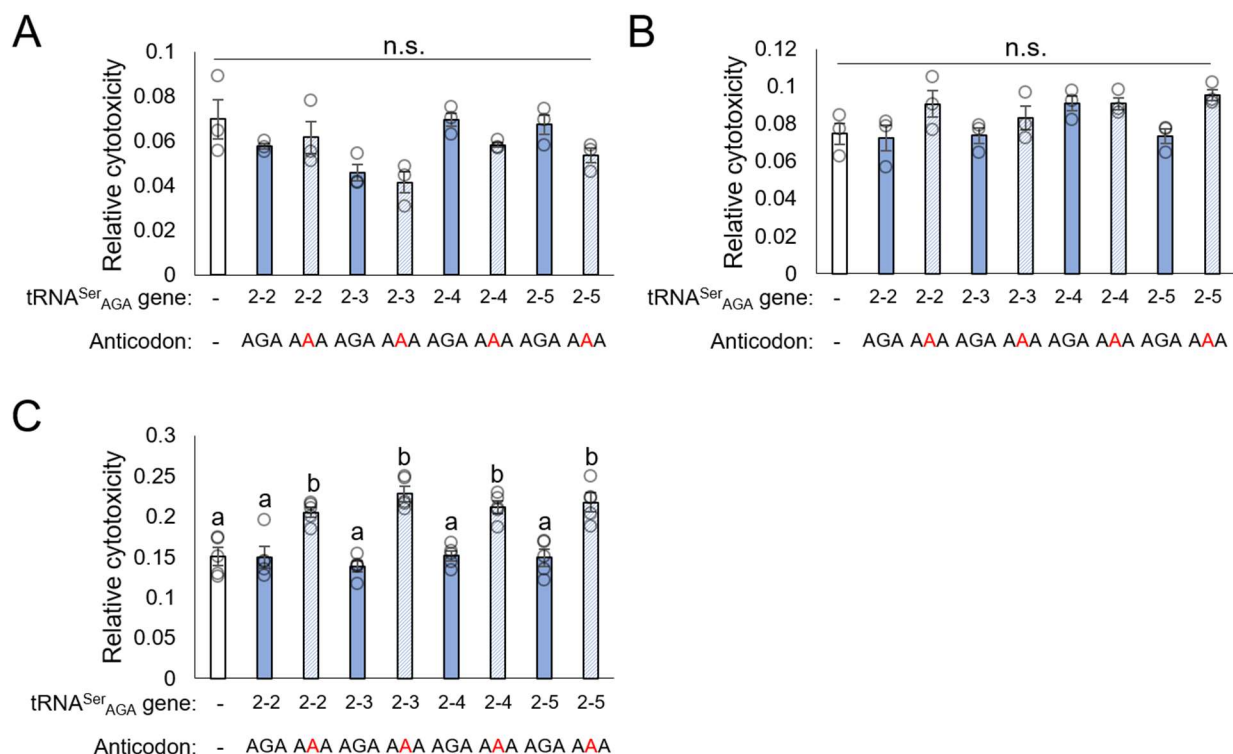


Figure 5.5 Cytotoxicity of tRNA^{Ser}_{AAA} variants in different cell lines and sequence contexts. Plasmids encoding mCherry and wild-type human tRNA^{Ser}_{AGA} or variant tRNA^{Ser}_{AAA} with different flanking sequence contexts from human tRNA-Ser-AGA-2 genes were transfected in human K562 (A), HEK 293T (B) and murine N2a (C) cells. Cytotoxicity was determined after 24 hr transfection using Cytotoxglo assays (see Materials and Methods). Letters indicate significantly different groups determined by Tukey's Honestly Significant Different (HSD) tests of at least three biological replicates, where groups sharing a letter are not significantly different and groups not sharing a letter are significantly different ($\alpha = 0.05$).

5.3.7 Migration kinetics of cells expressing a mistranslating tRNA variant expressed from different sequence contexts.

Given that we could not reliably detect cytotoxicity of the tRNA^{Ser}_{AAA} variant expressed from different sequence contexts in K562 or HEK 293T cells, we sought to test other phenotypic assays which could be used to compare identical tRNA variants in cells. In previous work, we found that the tRNA-Ser-AGA-2-3 G35A variant caused perturbations to protein homeostasis, reducing protein synthesis but also reducing protein turnover rates in N2a cells (2). Others have observed similar perturbations to protein homeostasis in yeast (60) and mammalian cells (7,29,55) that expressed different anticodon variants of tRNA^{Ser}. Since mistranslating tRNAs cause defects in protein synthesis and degradation, we hypothesized that cellular processes that require active protein synthesis and turnover would be sensitive to mistranslation. One such process is cell migration. For example, others have shown that knockdown of ribosomal protein S6 (61) suppresses migration and proliferation of ovarian cancer cells.

To assay cell migration in mistranslating cells, we devised several modifications to standard wound healing assays that would render the assay highly sensitive to the effects of tRNA-dependent mistranslation (see Materials and Methods). To track cell migration we used live cell fluorescence microscopy, capturing images of red fluorescing cells every 30 min over a 15 hr time course. We analyzed the data using a particle tracking software package in Fiji (TrackMate (45)). As others have demonstrated, TrackMate can be used to quantitate migration of fluorescently labeled cells from live-cell imaging data with single-cell resolution (46,47). With this approach, we tracked the movement of individual HEK 293T cells transfected with plasmids expressing mCherry and wild-type tRNA^{Ser}_{AGA} or tRNA^{Ser}_{AAA} from the -2-2, -2-3, or -2-5 sequence contexts (Fig. 5.6A). We also assayed migration in the presence or absence of 10 μ M MG132 to inhibit the proteasome, which exacerbated tRNA^{Ser}_{AAA} cytotoxicity in N2a cells (8).

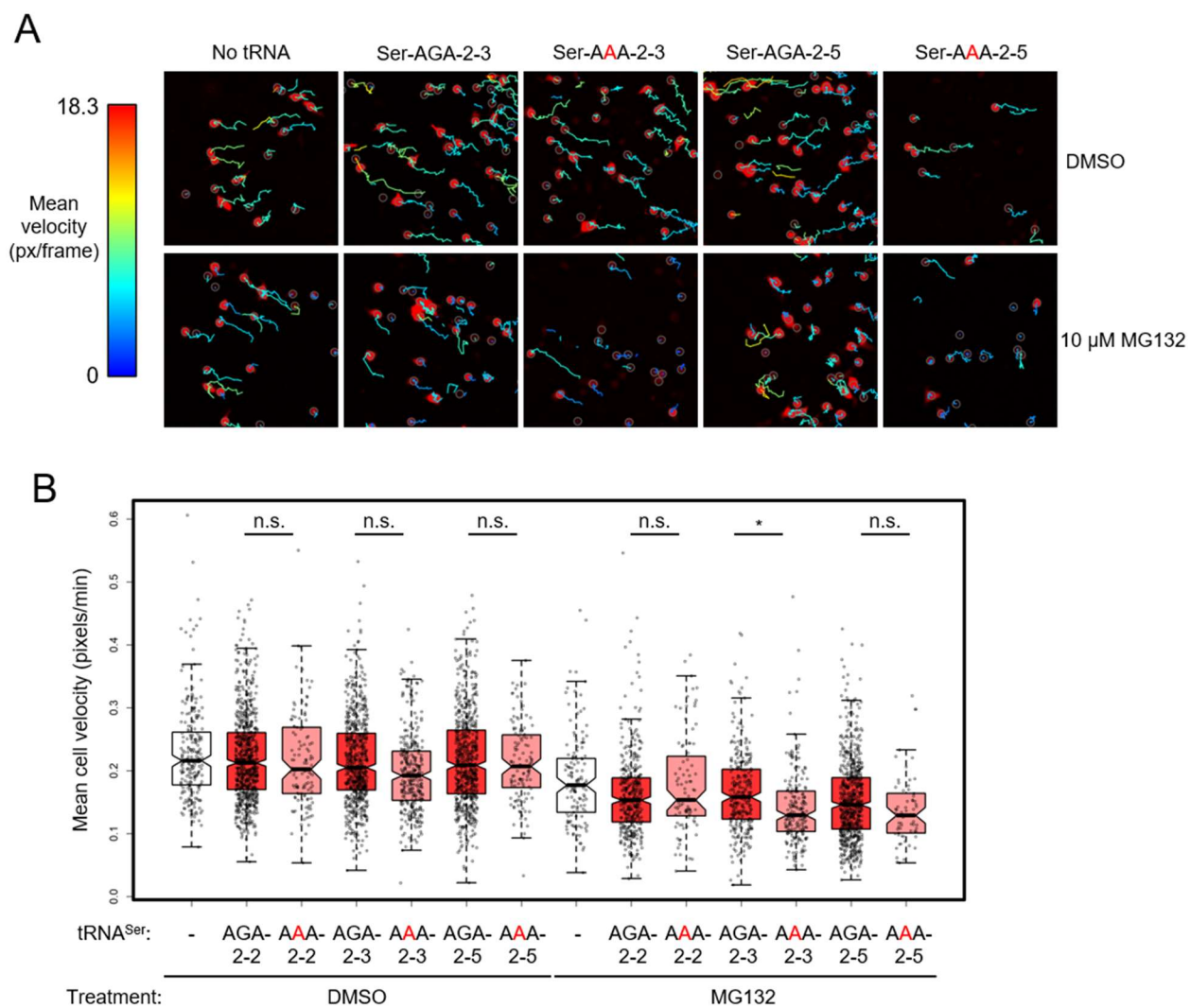


Figure 5.6 Migration kinetics of cells expressing tRNA-Ser-AAA-2-*n* variants. Plasmids encoding mCherry and wild-type human tRNA^{Ser}_{AGA} or variant tRNA^{Ser}_{AAA} with different flanking sequence contexts from human tRNA-Ser-AGA-2 genes were transfected in HEK 293T cells. Migration velocity of fluorescing cells was measured using a wound healing assay combined with cell tracking in Fiji/ImageJ (A; see Materials and Methods, Supplemental appendix). Each box-and-whisker plot represents data from three biological replicates (B). Midline represents the median, boxes represent quartiles, and whiskers represent 1.5× the interquartile range. Dots show underlying datapoints from individual tracks detected with TrackMate. Stars indicate statistically significant differences of biological replicate means determined by independent sample t-tests (n.s. = not significant, * = p-value < 0.05)

In DMSO control, we could not detect significant changes to migration velocity in cells expressing the tRNA variant in any of the tested sequence contexts (Fig. 5.6). In MG132 treated cells, we detected a significant 1.17 ± 0.02 -fold reduction ($p = 0.013$) in cell migration velocity in the tRNA-Ser-AAA-2-3 expressing cells compared to cells expressing tRNA-Ser-AGA-2-3 (Fig. 5.6). Compared to cells expressing no tRNA, tRNA-Ser-AAA-2-3 reduced cell migration by 1.29 ± 0.02 -fold ($p = 0.02$). Hence, in cells treated with a proteasome inhibitor, tRNA-dependent mistranslation suppressed cell migration. To our knowledge, this is the first example of a natural human tRNA variant altering migration kinetics in human cells. In cells expressing the variant from the -2-2 context and 2-5 contexts, we could not detect a significant change in cell migration velocity (Fig. 5.6). We note that our detection sensitivity was limited in the tRNA-Ser-AAA-2-5 + MG132 population as cellular fluorescence was severely reduced (see also Fig. 5.3B). Further refinement of this assay may be required for optimal detection sensitivity. However, we have shown for the first time that human tRNA variants can act as modifiers of cell migration activity in cells treated with a proteasome inhibitor.

5.4 Discussion

5.4.1 tRNA gene copy number does not imply redundancy.

The theoretical minimum number of tRNA genes required for an organism to decode all 61 sense codons is 32, since tRNAs are capable of decoding multiple codons through G:U pairing and modification of nucleotides in the anticodon (57,58). Most eukaryotes far exceed this theoretical minimum, harboring hundreds to thousands of tRNA genes, many of which are predicted to be functional (15). In humans, the most recent estimates suggest 416 functional tRNA genes (15). Excessive tRNA gene counts provide a buffer for the occurrence of variants, which occur commonly in tRNA genes via transcription associated mutagenesis (20). Many of these variants exist in the genomes of healthy individuals, as we and others have revealed in sequencing studies (1,30,31).

Despite the apparent “buffering capacity” of the tRNAome, tRNA copy numbers are not uniform across isodecoder groups (15), so mutations in some tRNA genes with fewer equivalent copies may be more deleterious. The most striking example of this being the single-copy human selenocysteine tRNA gene (15,62), mutation in which has been linked to a rare disease

characterized by abdominal pain, fatigue, muscle weakness and low plasma selenium levels (9). Numerous links to disease have also been established with variants in mitochondrial tRNAs (63,64), which comprise of only 22 tRNA genes (64). Remarkably, human mitochondria use an alternative genetic code to defy the theoretical minimum number of tRNA genes established for the standard genetic code (65). Even in cytosolic tRNA isodecoder groups with higher tRNA gene copy numbers, tissue-specific sensitivities can exist, since some tRNA genes are only transcribed in certain tissues (5). Transfer RNA mutation sensitivities may also arise from changes in tRNA regulation that occur in different cell states. For example, changes in cellular tRNA pools have been reported in differentiating versus proliferating cells (66,67).

Our work expands on our understanding of redundancy in tRNA genes by demonstrating that even identical tRNA genes can be regulated differently in different cell lines, as others have predicted bioinformatically (18). Hence, as our understanding of variation sensitivity in specific human tRNA genes grows, characterization of not only specific tRNA sequences but also their genomic context will be essential. Our work also demonstrates experimentally that data from DNA sequence-based predictions (18), DNase hypersensitivity sequencing (34,35), and CHIP-sequencing (34,54) provide a reasonable but not definitive estimation of tRNA gene activity in human cell lines. For example, our observation that expression of the tRNA^{Ser_{AAA}} variant in K562 cells from the tRNA-Ser-AGA-2-5 gene context had a stronger effect on mCherry fluorescence compared to expression from the tRNA-Ser-AGA-2-4 context was in excellent agreement with our predictions based on the K562 cell DNase hypersensitivity and CHIP sequencing data. However, we had not predicted that expression of the variant from the tRNA-Ser-AGA-2-3 context would have an equivalent effect to expression from the tRNA-Ser-AGA-2-5 context, and a stronger effect than expression from the tRNA-Ser-AGA-2-2 context.

5.4.2 Using variants as tools to detect tRNA expression.

Our tRNA sequencing data demonstrate that tRNA^{Ser_{AAA}} was expressed and detectable against a highly repetitive background of tRNA sequences in murine N2a cells. By contrast, we were unable to discriminate expressed wild-type tRNA^{Ser_{AGA}} from identical endogenous tRNAs, as expected. Hence, the inclusion of a variant in expressed tRNAs could represent a valuable approach to detect expression levels of tRNAs that are encoded at multiple genomic loci. While our ability to make quantitative comparisons was limited in transiently transfected cells, we

anticipate that tRNAseq will be a valuable method to study tRNA variant expression in more homogenous cell populations, such as patient-derived cells or knock-in cell lines created by genome editing. Knowing that the tRNA^{Ser}_{AAA} variant is detectable and elicits clear phenotypes which we have characterized in this and other works (see chapter 4, (8)), genome-integrated cell lines expressing this variant will form the basis of future studies.

5.4.3 Detecting amino acid misincorporation by mass spectrometry.

Detecting low level amino acid mis-incorporation events caused by tRNA variants is not trivial and requires further research. We and others have developed fluorescent reporters for this purpose, which detect amino acid misincorporation by reversing a disabling mutation in a fluorescent protein (29,40,68). In many cases, these fluorescent reporters have proven effective in detecting mistranslation caused by mutant tRNA genes. However, many tRNA variants that cause amino acid misincorporation, including the tRNA^{Ser}_{AAA} variant studied here, also lead to severe reductions in protein synthesis in mammalian cells (8,29,55). This limits the sensitivity of fluorescent mistranslation reporters since higher mistranslation levels result in lower expression of the reporter protein. Some reporters have been developed to account for this phenomenon, by fusing the inactive fluorescent protein to a differently colored, active fluorescent protein (40). This provides a control for reporter expression, where fluorescence of the test protein is normalized to fluorescence of the active protein. We are currently optimizing reporters based on this design, and the mass spectrometry data here will provide a means of validating reporter efficacy.

In this work, we improved upon current mass spectrometry methods for detecting amino acid mis-incorporation in mammalian cells by adapting a technique developed for detecting mistranslation in yeast and *Escherichia coli* (43). MS-READ is an affinity purification combined with LC-MS/MS approach that utilizes a designer peptide optimized for detection by mass spectrometry with any of the proteinogenic amino acids encoded at a central test residue (43). The test peptide is fused to a readily purified fluorescent protein allowing purification in high yields. The advantage of this method is that amino acid misincorporation events can be detected unambiguously, and high sensitivity can be achieved by optimizing reporter purification.

In mammalian cells, large batch protein purifications are often prohibitively expensive, especially for academic laboratories. However, we found in previous work that suitable yields of

mCherry protein for mass spectrometry could be obtained from 20 mL cultures of N2a cells grown on 3 x 10 cm plates (8), by immunoprecipitating mCherry with α -RFP nanobody-conjugated agarose beads (RFP-trap; developed by Chromotek). Here we optimized this approach further, by expressing the tRNAs and reporter in HEK 293T cells and making some adjustments to our protocol such that complete yields could be loaded in a single SDS-PAGE well. HEK 293T cells have been modified from their parental HEK 293 line for high expression of recombinant proteins from plasmids using the Simian Virus 40 (SV40) promoter sequence (69). For this reason, HEK 293T cells are a preferred cell line for high expression of recombinant proteins (70). With our improved expression and purification approach combined with MS-READ reporter proteins, we readily detected Phe to Ser misincorporation from replicates of single 10 cm HEK 293T cell cultures (7 mL volume). Thus, we have demonstrated a more feasible and cost-effective strategy to detect amino acid misincorporation by mass spectrometry in mammalian cells.

5.4.4 Phenotypic assays enable high sensitivity and throughput in tRNA variant testing.

Given the immense number of tRNA genes (15) and variants (1,30,31) in human genomes and populations, the ability to test variants in high throughput will be essential in characterizing which naturally occurring variants have the strongest potential to act as disease modifiers. As we and others have shown here and previously (19,50), the ability to make quantitative inferences about the expression of specific tRNAs and variants is limited by the highly repetitive nature of tRNA sequences. For this reason, tRNA sequencing can only resolve changes in expression of highly unique tRNA sequences, and multi-copy tRNAs must be discussed as a conglomerate or pool of identical or highly similar sequences.

Another challenge associated with the study of tRNA genes is that most popular antibiotics used to establish stably selected mammalian cell lines act on the ribosome (Table 5.6). Hence, the use of selectable markers in tRNA studies is likely to influence physiological observations. Indeed, the only well characterized antibiotic used to select transfected mammalian cell lines that does not act on the ribosome is Zeocin, which others have shown induces DNA cleavage even in resistant human cells (71). Further, selectable markers can significantly influence proteins synthesis rates in mammalian cells (72), making it difficult to compare the effects of tRNA genes on protein synthesis in selected cell lines. For these reasons we have general avoided the use of antibiotic

selection markers in our previous studies on tRNA genes (8), and chose to tailor our investigations in this work to methods which can be done in transiently transfected cells.

Table 5.6. Mechanism of action of common selectable markers used in mammalian cell line selection.

Antibiotic	Mechanism of action	References
Blasticidin	Inhibits peptidyl-tRNA hydrolysis in the ribosome	(73,74)
Puromycin	Integrates into elongating nascent peptides, causing premature termination of translation	(75)
G418 (geneticin)	Interferes with mRNA translation elongation	(76)
Hygromycin B	Interferes with ribosomal translocation and aminoacyl-tRNA recognition	(77)
Zeocin	Intercalates DNA, inducing single and double strand breaks	(78)

In this work, we demonstrated the value of using local flanking sequence from human tRNA genes found in the genome to express a well characterized gain-of-function tRNA mistranslator. This allowed us to probe the contributions of flanking sequence to activity of identical tRNA genes. With this approach, we found that phenotypic effects can be used to compare tRNA gene activity in transiently transfected cells. For example, we found that expressing the tRNA^{Ser}_{AAA} variant from sequence context found around the human tRNA-Ser-AGA-2-4 gene caused a reduction in protein synthesis in human HEK 293T and murine N2a cells, but not in human K562 cells. While behaviors in cell lines are only models of the biology in real human tissues (79), the same approach could be used in transfected primary cells (80) for a more clinically relevant investigation. A major challenge in studies using primary cells and certain disease-model cell lines is that transfection efficiency is typically poor compared to more commonly used cell lines (81). Since the assays we described are fluorescence-based and can be quantitated with automated image analysis software, they can be employed with single cell resolution even in cells where high transfection efficiency cannot be achieved. Thus, our work opens new possibilities for

exploring the biology of natural human tRNA variants in systems with increasing potential for translational discoveries.

5.6 References

1. Berg, M.D., Giguere, D.J., Dron, J.S., Lant, J.T., Genereaux, J., Liao, C., Wang, J., Robinson, J.F., Gloor, G.B., Hegele, R.A. *et al.* (2019) Targeted sequencing reveals expanded genetic diversity of human transfer RNAs. *RNA Biol*, **16**, 1574-1585.
2. Lant, J.T., Berg, M.D., Heinemann, I.U., Brandl, C.J. and O'Donoghue, P. (2019) Pathways to disease from natural variations in human cytoplasmic tRNAs. *J Biol Chem*, **294**, 5294-5308.
3. Kapur, M., Monaghan, C.E. and Ackerman, S.L. (2017) Regulation of mRNA Translation in Neurons-A Matter of Life and Death. *Neuron*, **96**, 616-637.
4. Schaffer, A.E., Pinkard, O. and Collier, J.M. (2019) tRNA Metabolism and Neurodevelopmental Disorders. *Annu Rev Genomics Hum Genet*, **20**, 359-387.
5. Ishimura, R., Nagy, G., Dotu, I., Zhou, H., Yang, X.L., Schimmel, P., Senju, S., Nishimura, Y., Chuang, J.H. and Ackerman, S.L. (2014) RNA function. Ribosome stalling induced by mutation of a CNS-specific tRNA causes neurodegeneration. *Science*, **345**, 455-459.
6. Kapur, M., Ganguly, A., Nagy, G., Adamson, S.I., Chuang, J.H., Frankel, W.N. and Ackerman, S.L. (2020) Expression of the Neuronal tRNA n-Tr20 Regulates Synaptic Transmission and Seizure Susceptibility. *Neuron*, **108**, 193-208 e199.
7. Santos, M., Pereira, P.M., Varanda, A.S., Carvalho, J., Azevedo, M., Mateus, D.D., Mendes, N., Oliveira, P., Trindade, F., Pinto, M.T. *et al.* (2018) Codon misreading tRNAs promote tumor growth in mice. *RNA Biol*, **15**, 773-786.
8. Lant, J.T., Kiri, R., Duennwald, M.L. and O'Donoghue, P. (2021) Formation and persistence of polyglutamine aggregates in mistranslating cells. *Nucleic Acids Res*, **49**, 11883-11899.
9. Schoenmakers, E., Carlson, B., Agostini, M., Moran, C., Rajanayagam, O., Bochukova, E., Tobe, R., Peat, R., Gevers, E., Muntoni, F. *et al.* (2016) Mutation in human selenocysteine transfer RNA selectively disrupts selenoprotein synthesis. *J Clin Invest*, **126**, 992-996.
10. Schimmel, P. (2018) The emerging complexity of the tRNA world: mammalian tRNAs beyond protein synthesis. *Nat Rev Mol Cell Biol*, **19**, 45-58.
11. Magee, R. and Rigoutsos, I. (2020) On the expanding roles of tRNA fragments in modulating cell behavior. *Nucleic Acids Res*, **48**, 9433-9448.
12. Keam, S.P., Sobala, A., Ten Have, S. and Hutvagner, G. (2017) tRNA-Derived RNA Fragments Associate with Human Multisynthetase Complex (MSC) and Modulate Ribosomal Protein Translation. *J Proteome Res*, **16**, 413-420.
13. Thompson, D.M., Lu, C., Green, P.J. and Parker, R. (2008) tRNA cleavage is a conserved response to oxidative stress in eukaryotes. *RNA*, **14**, 2095-2103.
14. Balatti, V., Rizzotto, L., Miller, C., Palamarchuk, A., Fadda, P., Pandolfo, R., Rassenti, L.Z., Hertlein, E., Ruppert, A.S., Lozanski, A. *et al.* (2015) TCL1 targeting miR-3676 is codeleted with tumor protein p53 in chronic lymphocytic leukemia. *Proc Natl Acad Sci U S A*, **112**, 2169-2174.
15. Chan, P.P. and Lowe, T.M. (2016) GtRNADB 2.0: an expanded database of transfer RNA genes identified in complete and draft genomes. *Nucleic Acids Res*, **44**, D184-189.
16. Chan, P.P., Lin, B.Y., Mak, A.J. and Lowe, T.M. (2021) tRNAscan-SE 2.0: improved detection and functional classification of transfer RNA genes. *Nucleic Acids Res*, **49**, 9077-9096.
17. Chan, P.P. and Lowe, T.M. (2019) tRNAscan-SE: Searching for tRNA Genes in Genomic Sequences. *Methods Mol Biol*, **1962**, 1-14.
18. Thornlow, B.P., Armstrong, J., Holmes, A.D., Howard, J.M., Corbett-Detig, R.B. and Lowe, T.M. (2020) Predicting transfer RNA gene activity from sequence and genome context. *Genome Res*, **30**, 85-94.

19. Hrabeta-Robinson, E., Marcus, E., Cozen, A.E., Phizicky, E.M. and Lowe, T.M. (2017) High-Throughput Small RNA Sequencing Enhanced by AlkB-Facilitated RNA de-Methylation (ARM-Seq). *Methods Mol Biol*, **1562**, 231-243.
20. Thornlow, B.P., Hough, J., Roger, J.M., Gong, H., Lowe, T.M. and Corbett-Detig, R.B. (2018) Transfer RNA genes experience exceptionally elevated mutation rates. *Proc Natl Acad Sci U S A*, **115**, 8996-9001.
21. Allison, D.S. and Hall, B.D. (1985) Effects of alterations in the 3' flanking sequence on in vivo and in vitro expression of the yeast SUP4-o tRNA^{Tyr} gene. *EMBO J*, **4**, 2657-2664.
22. Koski, R.A., Clarkson, S.G., Kurjan, J., Hall, B.D. and Smith, M. (1980) Mutations of the yeast SUP4 tRNA^{Tyr} locus: transcription of the mutant genes in vitro. *Cell*, **22**, 415-425.
23. DeFranco, D., Sharp, S. and Soll, D. (1981) Identification of regulatory sequences contained in the 5'-flanking region of Drosophila lysine tRNA² genes. *J Biol Chem*, **256**, 12424-12429.
24. White, R.J. (2011) Transcription by RNA polymerase III: more complex than we thought. *Nat Rev Genet*, **12**, 459-463.
25. Maraia, R.J., Kenan, D.J. and Keene, J.D. (1994) Eukaryotic transcription termination factor La mediates transcript release and facilitates reinitiation by RNA polymerase III. *Mol Cell Biol*, **14**, 2147-2158.
26. Arimbasseri, A.G., Rijal, K. and Maraia, R.J. (2013) Transcription termination by the eukaryotic RNA polymerase III. *Biochim Biophys Acta*, **1829**, 318-330.
27. Hamada, M., Sakulich, A.L., Koduru, S.B. and Maraia, R.J. (2000) Transcription termination by RNA polymerase III in fission yeast. A genetic and biochemically tractable model system. *J Biol Chem*, **275**, 29076-29081.
28. Orioli, A., Pascali, C., Quartararo, J., Diebel, K.W., Praz, V., Romascano, D., Percudani, R., van Dyk, L.F., Hernandez, N., Teichmann, M. *et al.* (2011) Widespread occurrence of non-canonical transcription termination by human RNA polymerase III. *Nucleic Acids Res*, **39**, 5499-5512.
29. Geslain, R., Cubells, L., Bori-Sanz, T., Alvarez-Medina, R., Rossell, D., Marti, E. and Ribas de Pouplana, L. (2010) Chimeric tRNAs as tools to induce proteome damage and identify components of stress responses. *Nucleic Acids Res*, **38**, e30.
30. Parisien, M., Wang, X. and Pan, T. (2013) Diversity of human tRNA genes from the 1000-genomes project. *RNA Biol*, **10**, 1853-1867.
31. Karczewski, K.J., Francioli, L.C., Tiao, G., Cummings, B.B., Alfoldi, J., Wang, Q., Collins, R.L., Laricchia, K.M., Ganna, A., Birnbaum, D.P. *et al.* (2020) The mutational constraint spectrum quantified from variation in 141,456 humans. *Nature*, **581**, 434-443.
32. Sherry, S.T., Ward, M.H., Kholodov, M., Baker, J., Phan, L., Smigielski, E.M. and Sirotkin, K. (2001) dbSNP: the NCBI database of genetic variation. *Nucleic Acids Res*, **29**, 308-311.
33. Consortium, E.P. (2011) A user's guide to the encyclopedia of DNA elements (ENCODE). *PLoS Biol*, **9**, e1001046.
34. Consortium, E.P. (2012) An integrated encyclopedia of DNA elements in the human genome. *Nature*, **489**, 57-74.
35. Meuleman, W., Muratov, A., Rynes, E., Halow, J., Lee, K., Bates, D., Diegel, M., Dunn, D., Neri, F., Teodosiadis, A. *et al.* (2020) Index and biological spectrum of human DNase I hypersensitive sites. *Nature*, **584**, 244-251.
36. Chan, P.P. and Lowe, T.M. (2009) GtRNADB: a database of transfer RNA genes detected in genomic sequence. *Nucleic Acids Res*, **37**, D93-97.
37. Notredame, C., Higgins, D.G. and Heringa, J. (2000) T-Coffee: A novel method for fast and accurate multiple sequence alignment. *J Mol Biol*, **302**, 205-217.
38. Madeira, F., Park, Y.M., Lee, J., Buso, N., Gur, T., Madhusoodanan, N., Basutkar, P., Tivey, A.R.N., Potter, S.C., Finn, R.D. *et al.* (2019) The EMBL-EBI search and sequence analysis tools APIs in 2019. *Nucleic Acids Res*, **47**, W636-W641.
39. Waterhouse, A.M., Procter, J.B., Martin, D.M., Clamp, M. and Barton, G.J. (2009) Jalview Version 2--a multiple sequence alignment editor and analysis workbench. *Bioinformatics*, **25**, 1189-1191.

40. Gomes, A.C., Kordala, A.J., Strack, R., Wang, X., Geslain, R., Delaney, K., Clark, W.C., Keenan, R. and Pan, T. (2016) A dual fluorescent reporter for the investigation of methionine mistranslation in live cells. *RNA*, **22**, 467-476.
41. Ye, J., Coulouris, G., Zaretskaya, I., Cutcutache, I., Rozen, S. and Madden, T.L. (2012) Primer-BLAST: a tool to design target-specific primers for polymerase chain reaction. *BMC Bioinformatics*, **13**, 134.
42. Lant, J.T., Kiri, R., Duennwald, M.L. and O'Donoghue, P. (2021) Formation and persistence of polyglutamine aggregates in mistranslating cells. *Nucleic Acids Res.*
43. Mohler, K., Aerni, H.R., Gassaway, B., Ling, J., Ibba, M. and Rinehart, J. (2017) MS-READ: Quantitative measurement of amino acid incorporation. *Biochim Biophys Acta Gen Subj*, **1861**, 3081-3088.
44. Schneider, C.A., Rasband, W.S. and Eliceiri, K.W. (2012) NIH Image to ImageJ: 25 years of image analysis. *Nat Methods*, **9**, 671-675.
45. Tinevez, J.Y., Perry, N., Schindelin, J., Hoopes, G.M., Reynolds, G.D., Laplantine, E., Bednarek, S.Y., Shorte, S.L. and Eliceiri, K.W. (2017) TrackMate: An open and extensible platform for single-particle tracking. *Methods*, **115**, 80-90.
46. Fazeli, E., Roy, N.H., Follain, G., Laine, R.F., von Chamier, L., Hanninen, P.E., Eriksson, J.E., Tinevez, J.Y. and Jacquemet, G. (2020) Automated cell tracking using StarDist and TrackMate. *F1000Res*, **9**, 1279.
47. DuChez, B.J. (2017) Automated Tracking of Cell Migration with Rapid Data Analysis. *Curr Protoc Cell Biol*, **76**, 12 12 11-12 12 16.
48. Shi, H. and Moore, P.B. (2000) The crystal structure of yeast phenylalanine tRNA at 1.93 Å resolution: a classic structure revisited. *RNA*, **6**, 1091-1105.
49. Saikia, M., Fu, Y., Pavon-Eternod, M., He, C. and Pan, T. (2010) Genome-wide analysis of N1-methyl-adenosine modification in human tRNAs. *RNA*, **16**, 1317-1327.
50. Gogakos, T., Brown, M., Garzia, A., Meyer, C., Hafner, M. and Tuschl, T. (2017) Characterizing Expression and Processing of Precursor and Mature Human tRNAs by Hydro-tRNAseq and PAR-CLIP. *Cell Rep*, **20**, 1463-1475.
51. Haeussler, M., Zweig, A.S., Tyner, C., Speir, M.L., Rosenbloom, K.R., Raney, B.J., Lee, C.M., Lee, B.T., Hinrichs, A.S., Gonzalez, J.N. *et al.* (2019) The UCSC Genome Browser database: 2019 update. *Nucleic Acids Res*, **47**, D853-D858.
52. Pollard, K.S., Hubisz, M.J., Rosenbloom, K.R. and Siepel, A. (2010) Detection of nonneutral substitution rates on mammalian phylogenies. *Genome Res*, **20**, 110-121.
53. Song, L. and Crawford, G.E. (2010) DNase-seq: a high-resolution technique for mapping active gene regulatory elements across the genome from mammalian cells. *Cold Spring Harb Protoc*, **2010**, pdb prot5384.
54. Kharchenko, P.V., Tolstorukov, M.Y. and Park, P.J. (2008) Design and analysis of ChIP-seq experiments for DNA-binding proteins. *Nat Biotechnol*, **26**, 1351-1359.
55. Varanda, A.S., Santos, M., Soares, A.R., Vitorino, R., Oliveira, P., Oliveira, C. and Santos, M.A.S. (2020) Human cells adapt to translational errors by modulating protein synthesis rate and protein turnover. *RNA Biol*, **17**, 135-149.
56. Torres, A.G., Pineyro, D., Filonava, L., Stracker, T.H., Batlle, E. and Ribas de Pouplana, L. (2014) A-to-I editing on tRNAs: biochemical, biological and evolutionary implications. *FEBS Lett*, **588**, 4279-4286.
57. Crick, F.H. (1966) Codon-anticodon pairing: the wobble hypothesis. *J Mol Biol*, **19**, 548-555.
58. Söll, D., Cherayil, J., Jones, D.S., Faulkner, R.D., Hapel, A., Bock, R.M. and Khorana, H.G. (1966) sRNA specificity for codon recognition as studied by the ribosomal binding technique. *Cold Spring Harb Symp Quant Biol*, **31**, 51-61.
59. Lim, V.I. and Curran, J.F. (2001) Analysis of codon:anticodon interactions within the ribosome provides new insights into codon reading and the genetic code structure. *RNA*, **7**, 942-957.

60. Berg, M.D., Zhu, Y., Ruiz, B.Y., Loll-Krippelber, R., Isaacson, J., San Luis, B.J., Genereaux, J., Boone, C., Villen, J., Brown, G.W. *et al.* (2021) The amino acid substitution affects cellular response to mistranslation. *G3 (Bethesda)*, **11**.
61. Yang, X., Xu, L., Yang, Y.E., Xiong, C., Yu, J., Wang, Y. and Lin, Y. (2020) Knockdown of ribosomal protein S6 suppresses proliferation, migration, and invasion in epithelial ovarian cancer. *J Ovarian Res*, **13**, 100.
62. O'Neill, V.A., Eden, F.C., Pratt, K. and Hatfield, D.L. (1985) A human opal suppressor tRNA gene and pseudogene. *J Biol Chem*, **260**, 2501-2508.
63. Webb, B.D., Diaz, G.A. and Prasun, P. (2020) Mitochondrial translation defects and human disease. *J Transl Genet Genom*, **4**, 71-80.
64. Suzuki, T., Nagao, A. and Suzuki, T. (2011) Human mitochondrial tRNAs: biogenesis, function, structural aspects, and diseases. *Annu Rev Genet*, **45**, 299-329.
65. Suzuki, T., Yashiro, Y., Kikuchi, I., Ishigami, Y., Saito, H., Matsuzawa, I., Okada, S., Mito, M., Iwasaki, S., Ma, D. *et al.* (2020) Complete chemical structures of human mitochondrial tRNAs. *Nat Commun*, **11**, 4269.
66. Gingold, H., Tehler, D., Christoffersen, N.R., Nielsen, M.M., Asmar, F., Kooistra, S.M., Christophersen, N.S., Christensen, L.L., Borre, M., Sorensen, K.D. *et al.* (2014) A dual program for translation regulation in cellular proliferation and differentiation. *Cell*, **158**, 1281-1292.
67. Aharon-Hefetz, N., Frumkin, I., Mayshar, Y., Dahan, O., Pilpel, Y. and Rak, R. (2020) Manipulation of the human tRNA pool reveals distinct tRNA sets that act in cellular proliferation or cell cycle arrest. *Elife*, **9**.
68. Lant, J.T., Berg, M.D., Sze, D.H.W., Hoffman, K.S., Akinpelu, I.C., Turk, M.A., Heinemann, I.U., Duennwald, M.L., Brandl, C.J. and O'Donoghue, P. (2018) Visualizing tRNA-dependent mistranslation in human cells. *RNA Biol*, **15**, 567-575.
69. Lebkowski, J.S., Clancy, S. and Calos, M.P. (1985) Simian virus 40 replication in adenovirus-transformed human cells antagonizes gene expression. *Nature*, **317**, 169-171.
70. Thomas, P. and Smart, T.G. (2005) HEK293 cell line: a vehicle for the expression of recombinant proteins. *J Pharmacol Toxicol Methods*, **51**, 187-200.
71. Oliva-Trastoy, M., Defais, M. and Larminat, F. (2005) Resistance to the antibiotic Zeocin by stable expression of the Sh ble gene does not fully suppress Zeocin-induced DNA cleavage in human cells. *Mutagenesis*, **20**, 111-114.
72. Guo, C., Fordjour, F.K., Tsai, S.J., Morrell, J.C. and Gould, S.J. (2021) Choice of selectable marker affects recombinant protein expression in cells and exosomes. *J Biol Chem*, **297**, 100838.
73. Izumi, M., Miyazawa, H., Kamakura, T., Yamaguchi, I., Endo, T. and Hanaoka, F. (1991) Blasticidin S-resistance gene (bsr): a novel selectable marker for mammalian cells. *Exp Cell Res*, **197**, 229-233.
74. Svidritskiy, E., Ling, C., Ermolenko, D.N. and Korostelev, A.A. (2013) Blasticidin S inhibits translation by trapping deformed tRNA on the ribosome. *Proc Natl Acad Sci U S A*, **110**, 12283-12288.
75. Lacalle, R.A., Pulido, D., Vara, J., Zalacain, M. and Jimenez, A. (1989) Molecular analysis of the pac gene encoding a puromycin N-acetyl transferase from *Streptomyces alboniger*. *Gene*, **79**, 375-380.
76. Eustice, D.C. and Wilhelm, J.M. (1984) Mechanisms of action of aminoglycoside antibiotics in eucaryotic protein synthesis. *Antimicrob Agents Chemother*, **26**, 53-60.
77. Cabanas, M.J., Vazquez, D. and Modolell, J. (1978) Dual interference of hygromycin B with ribosomal translocation and with aminoacyl-tRNA recognition. *Eur J Biochem*, **87**, 21-27.
78. Stokowa-Soltys, K., Dzyhovskiy, V., Wiczorek, R. and Jezowska-Bojczuk, M. (2019) Phleomycin complex - Coordination mode and in vitro cleavage of DNA. *J Inorg Biochem*, **195**, 71-82.
79. Kaur, G. and Dufour, J.M. (2012) Cell lines: Valuable tools or useless artifacts. *Spermatogenesis*, **2**, 1-5.

80. Hamm, A., Krott, N., Breibach, I., Blindt, R. and Bosserhoff, A.K. (2002) Efficient transfection method for primary cells. *Tissue Eng*, **8**, 235-245.
81. Maurisse, R., De Semir, D., Enamekhoo, H., Bedayat, B., Abdolmohammadi, A., Parsi, H. and Gruenert, D.C. (2010) Comparative transfection of DNA into primary and transformed mammalian cells from different lineages. *BMC Biotechnol*, **10**, 9.
82. Andrews, S. (2010).
83. Martin, M. (2011) Cutadapt removes adapter sequences from high-throughput sequencing reads. *EMBnet.journal*.
84. Juhling, F., Morl, M., Hartmann, R.K., Sprinzl, M., Stadler, P.F. and Putz, J. (2009) tRNADB 2009: compilation of tRNA sequences and tRNA genes. *Nucleic Acids Res*, **37**, D159-162.
85. Li, H. and Durbin, R. (2009) Fast and accurate short read alignment with Burrows-Wheeler transform. *Bioinformatics*, **25**, 1754-1760.
86. Robinson, M.D., McCarthy, D.J. and Smyth, G.K. (2010) edgeR: a Bioconductor package for differential expression analysis of digital gene expression data. *Bioinformatics*, **26**, 139-140.

5.7 Supplemental information

5.7.1 Supplemental methods

tRNA sequencing.

The following text describes sample prep and tRNA sequencing methods as reported by Arraystar Inc. For transfection and cell harvesting details, see Materials and Methods.

RNA sample QC.

Integrity of total RNA samples was checked using denaturing agarose electrophoresis, in which the 28S and 18S ribosomal bands of samples should be fairly sharpened, intense bands and the intensity of upper 28S bands should be about twice of the lower 18S bands. Quantification of total RNA samples was done using NanoDrop ND-1000 instrument.

tRNA isolation.

tRNA was isolated from total RNA using Denaturing Urea Polyacrylamide Gel Electrophoresis (Urea PAGE) method. Over 2 μ g total RNA was resolved on 7.5% Urea PAGE gels (7M Urea) and recovered within a size window of 60-100 nt for tRNA.

tRNA demethylation.

Reagents: rtStarTM tRF&tRNA Pretreatment Kit (Arraystar, AS-FS-005)

Procedures: ‘Demethylation’ section in rtStarTM tRF&tRNA Pretreatment Kit was used for tRNA m¹A&m³C demethylation treatment. 50 μ L demethylation reaction mixture was prepared according to the manufacturer’s protocol and incubated at 37°C for 2 hr. Then 40 μ L nuclease-free water and 10 μ L 5 \times Stop Buffer were added to terminate the reaction. Demethylated tRNA was purified by phenol-chloroform extraction and ethanol precipitation.

Partial Hydrolysis of tRNA (Hydro-tRNAseq).

Demethylated tRNA was partially hydrolyzed according to Hydro-tRNAseq method with little modification (50). tRNA was subjected to limited alkaline hydrolysis in a 15 μ L buffer of 10mM Na₂CO₃ and 10mM NaHCO₃ (pH 9.7) at 90°C for 7 min. The partially hydrolyzed tRNA was dephosphorylated with 10 U Calf Intestinal Alkaline Phosphatase (CIP; New England Biolabs, M0290L) in a 50 μ l reaction of 100mM NaCl, 50 mM Tris-HCl (pH 7.9), and 10 mM MgCl₂, 1mM DTT, 3mM Na₂CO₃, 3mM NaHCO₃, at 37°C for 1hr. The resulting tRNA was purified with TRIzol reagent and then re-phosphorylated with 10 U T4 polynucleotide kinase (New England Biolabs, M0201L) in a 20 μ l reaction of 70 mM Tris-HCl (pH 7.6), 10 mM MgCl₂, 5 mM DTT, and 1 mM ATP at 37°C for 1 hr. TRIzol reagent purification was performed once more.

Library preparation.

Partially hydrolyzed tRNA fragments were converted to barcoded small RNA sequencing libraries using NEBNext[®] Multiplex Small RNA Library Prep Set for Illumina[®] kit (New England Biolabs, E7300L/E7850L) according to manufacturer’s instructions. The procedures generally included: 1) 3’-adapter ligation; 2) 3’-adapter blocking; 3) 5’-adapter ligation; 4) reverse transcription; 5) PCR amplification; 6) size selection of ~140-155 bp PCR amplified fragments (corresponding to ~19-35nt tRNA fragments) using 6% PolyAcrylamide Gel (PAGE). The completed libraries were qualified and quantified by Agilent 2100 Bioanalyzer. Equal amount of Hydro-tRNAseq libraries were mixed for following sequencing on Illumina NextSeq 500 instrument.

Sequencing.

The DNA fragments in well mixed libraries were denatured with 0.1M NaOH to generate single-stranded DNA molecules, and loaded onto the reagent cartridge (NextSeq 500/550 High-Output v2 kit) at a loading concentration. The sequencing run was performed on Illumina NextSeq 500 system and carried out by running 50 cycles.

Data analysis.

Sequencing quality was examined by FastQC software (82) and trimmed reads (pass Illumina quality filter, trimmed 3'-adaptor bases by cutadapt (83)) were aligned to the cytoplasmic mature-tRNA sequence getting from GtRNAdb (15) and the mitochondrial mature-tRNA sequences getting from mitotRNAdb (84) using BWA (85) software. For tRNA alignment, the maximum mismatch was 2 (50). The tRNAs expression profiling was calculated based on uniquely mapped reads and including mapped reads, respectively. The differentially expressed tRNAs were screened based on the count value with R package edgeR (86).

5.7.2 Supplemental tables

Table S5.1. Oligonucleotide sequences

Description	Nucleotide sequence
tRNA-Ser-AGA-2-2 genomic PCR (Fwd)	AAAATGCCGTGCAAACGAG
tRNA-Ser-AGA-2-2 genomic PCR (Rev)	CAATACCTGCGCTCCGTTG
tRNA-Ser-AGA-2-2 nested PCR with PciI cloning site (Fwd)	CAGACTACATGTGTGTCAGGCCCAGATTTAC
tRNA-Ser-AGA-2-2 nested PCR with PciI cloning site (Rev)	CAGACTACATGTCCCCAAACTGAAAGCAAATATG
tRNA-Ser-AGA-2-3 genomic PCR (Fwd)	CCTGGAAGTCCGAACACC
tRNA-Ser-AGA-2-3 genomic PCR (Rev)	GTGAACACAAAGATGAGAGACACC
tRNA-Ser-AGA-2-3 nested PCR with PciI cloning site (Fwd)	CAGACTACATGTGTTGGCCATGACTCCCC

tRNA-Ser-AGA-2-3 nested PCR with PciI cloning site (Rev)	CAGACTACATGTGCAATTCCGTGAGGGAAATTCG
tRNA-Ser-AGA-2-4 genomic PCR (Fwd)	AGTGGACATCCTTGCATCG
tRNA-Ser-AGA-2-4 genomic PCR (Rev)	CTTTAATCTGCCGCCTAAGC
tRNA-Ser-AGA-2-4 nested PCR with PciI cloning site (Fwd)	CAGACTACATGTTCCACTGCCAGAGCTCAG
tRNA-Ser-AGA-2-4 nested PCR with PciI cloning site (Rev)	CAGACTACATGTCTTGGACCTCTGACTAGGAC
tRNA-Ser-AGA-2-5 genomic PCR (Fwd)	TTATGGCACGGTGGGACTG
tRNA-Ser-AGA-2-5 genomic PCR (Rev)	CTTTTCCCCTCCAATCGCC
tRNA-Ser-AGA-2-5 nested PCR with PciI cloning site (Fwd)	CAGACTACATGTGTTCTGTTCTCTCCTGG
tRNA-Ser-AGA-2-5 nested PCR with PciI cloning site (Rev)	CAGACTACATGTGGGCTCGCGGCAGAGAAC
tRNA-Ser-AGA to G35A mutagenesis (Fwd)	GCGATGGACTAAAAATCCATTGGGGTCTCCCC
tRNA-Ser-AGA to G35A mutagenesis (Rev)	CCAATGGATTTTTAGTCCATCGCCTTAACCACTC
MS-READ (TTA) insert with BamHI/EcoRI overhangs (Fwd)	AATTCGCCACCATGTCTAAAGGGCCAGGTAAAGTT CCAGGAGCCGGAGTTCCTGGATTAGGGGTGCCTGG AGTTGGAAAAGGAGGCGGCACCTCG
MS-READ (TTA) insert with BamHI/EcoRI overhangs (Rev)	GATCCGAGGTGCCGCCTCCTTTTCCAACCTCCAGGC ACCCCTAATCCAGGAACCTCCGGCTCCTGGAACCTT ACCTGGCCCTTTAGACATGGTGGCG
MS-READ (TTC) insert with BamHI/EcoRI overhangs (Fwd)	AATTCGCCACCATGTCTAAAGGGCCAGGTAAAGTT CCAGGAGCCGGAGTTCCTGGATTCCGGGGTGCCTGG AGTTGGAAAAGGAGGCGGCACCTCG
MS-READ (TTC) insert with BamHI/EcoRI overhangs (Rev)	GATCCGAGGTGCCGCCTCCTTTTCCAACCTCCAGGC ACCCCGAATCCAGGAACCTCCGGCTCCTGGAACCTT ACCTGGCCCTTTAGACATGGTGGCG
MS-READ (TTG) insert with BamHI/EcoRI overhangs (Fwd)	AATTCGCCACCATGTCTAAAGGGCCAGGTAAAGTT CCAGGAGCCGGAGTTCCTGGATTGGGGGTGCCTGG AGTTGGAAAAGGAGGCGGCACCTCG
MS-READ (TTG) insert with BamHI/EcoRI overhangs (Rev)	GATCCGAGGTGCCGCCTCCTTTTCCAACCTCCAGGC ACCCCAATCCAGGAACCTCCGGCTCCTGGAACCTT ACCTGGCCCTTTAGACATGGTGGCG

MS-READ (TTT) insert with BamHI/EcoRI overhangs (Fwd)	AATTCGCCACCATGTCTAAAGGGGCCAGGTAAAGTT CCAGGAGCCGGAGTTCCTGGATTTGGGGTGCCTGG AGTTGGAAAAGGAGGCGGCACCTCG
MS-READ (TTT) insert with BamHI/EcoRI overhangs (Rev)	GATCCGAGGTGCCGCCTCCTTTTCCAACCTCCAGGC ACCCCAAATCCAGGAACCTCCGGCTCCTGGAACCTT ACCTGGCCCTTTAGACATGGTGGCG

Table S5.2. tRNAseq RNA yields and purity.

Sample ID	A260/280 Ratio ¹	A260/230 Ratio ²	Conc. (ng/μl)	Quantity (ng)
AGA-1	2.09	2.15	912.02	89378.1
AGA-2	2.1	1.9	655.16	64205.4
AGA-3	2.1	2.05	910.53	89231.8
AAA-1	2.1	2.08	995.49	97558.3
AAA-2	2.09	2.17	908.33	89016.2
AAA-3	2.08	2.17	1329.53	130293.8

¹A = absorbance (optical density). A260/A280 ratio should be close to 2.0 for pure RNA (ratios between 1.8 and 2.1 are acceptable). ²A260/A230 ratio should be more than 1.8.

Table S5.3. tRNAseq read mapping summary

Sample (tRNA-replicate)	Clean Reads	Trimmed Reads	Mapped Reads	Mapped (%)	Unique	Unique (%)
AGA-1	5277545	2987367	626548	20.97	247994	8.3
AGA-2	6934385	1656226	726798	43.88	266903	16.12
AGA-3	7309565	2836550	1211436	42.71	416086	14.67
AAA-1	6109477	2296773	738696	32.16	268425	11.69
AAA-2	5672373	3666402	786928	21.46	337544	9.21
AAA-3	7231950	2495504	1023582	41.02	359828	14.42

Table S5.4. UCSC genome browser data representing basal tRNA transcription initiation complex proteins.

Gene name (track name)¹	Protein full name	Transcription initiation complex	Data source (lab)	Cell line
TBP	TATA-binding protein	TFIIIB	ENCODE (Stanford)	K562
BDP1	Transcription factor TFIIIB component B'' homolog	TFIIIB	ENCODE (Harvard)	K562
BRF1	Transcription factor IIIB 90 kDa subunit	TFIIIB	ENCODE (Harvard)	K562
POLR3A (RPC155)	DNA-directed RNA polymerase III subunit RPC1	Pol III	ENCODE (Harvard)	K562
POLR3G (POL3)	DNA-direscted RNA polymerase III subunit RPC7	Pol III	ENCODE (Stanford)	K562
GTF3C2 (TFIIIC110)	General transcription factor 3C polypeptide 2	TFIIIC	ENCODE (Harvard)	K562

¹ track name displayed on UCSC genome browser if different from standardized gene name.

5.7.3 Supplemental figures

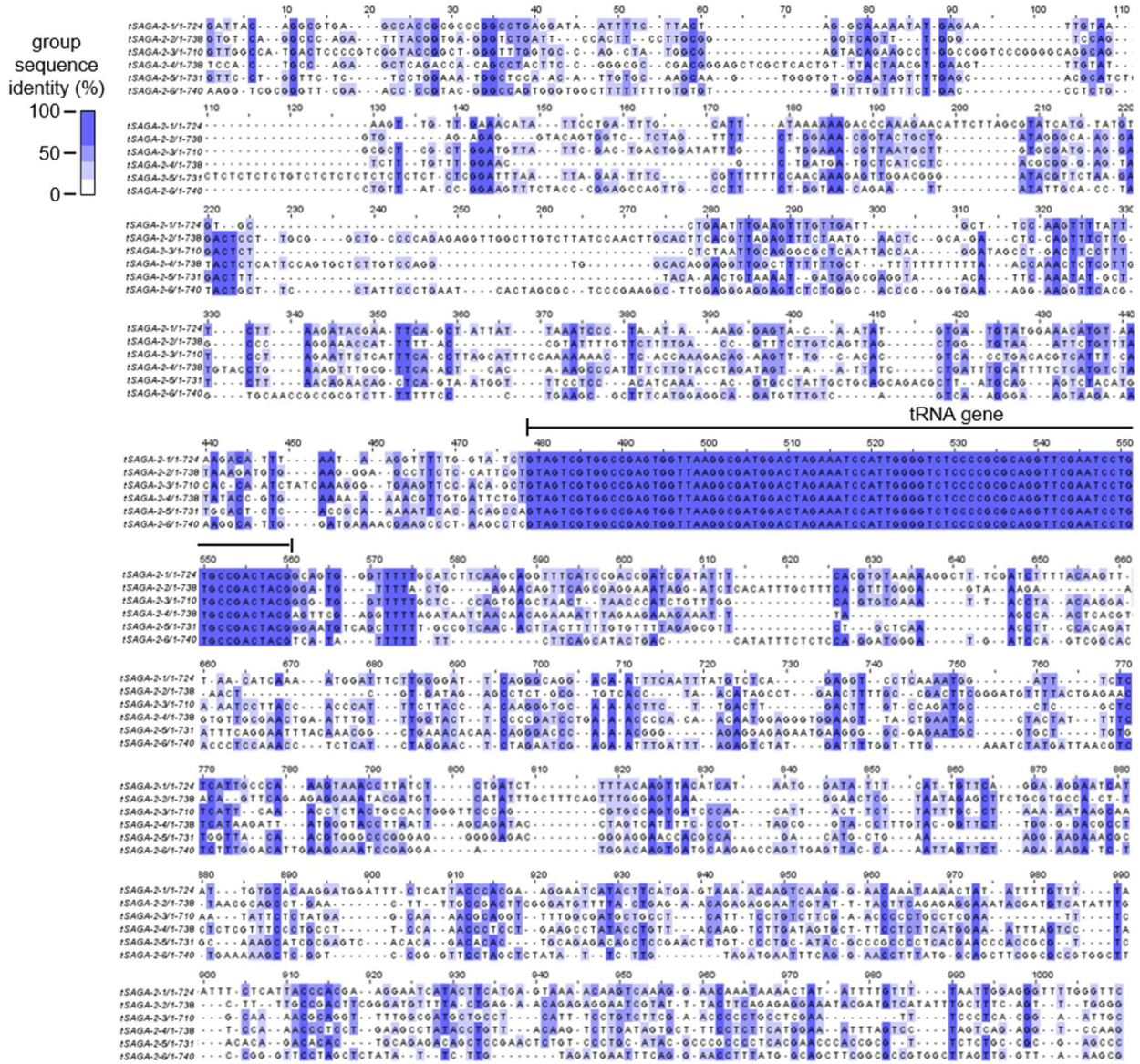


Figure S5.1. tRNA-Ser-AGA-2-n gene alignment. tRNA-Ser-AGA-2-n genes and flanking sequences captured by our genomic PCR primers (Table 5.2, S5.1) were aligned using T-Coffee (see Materials and Methods). Alignments were visualized and colored by sequence identity in Jalview. Sequence encoding the identical tRNA genes is labeled (tRNA gene).

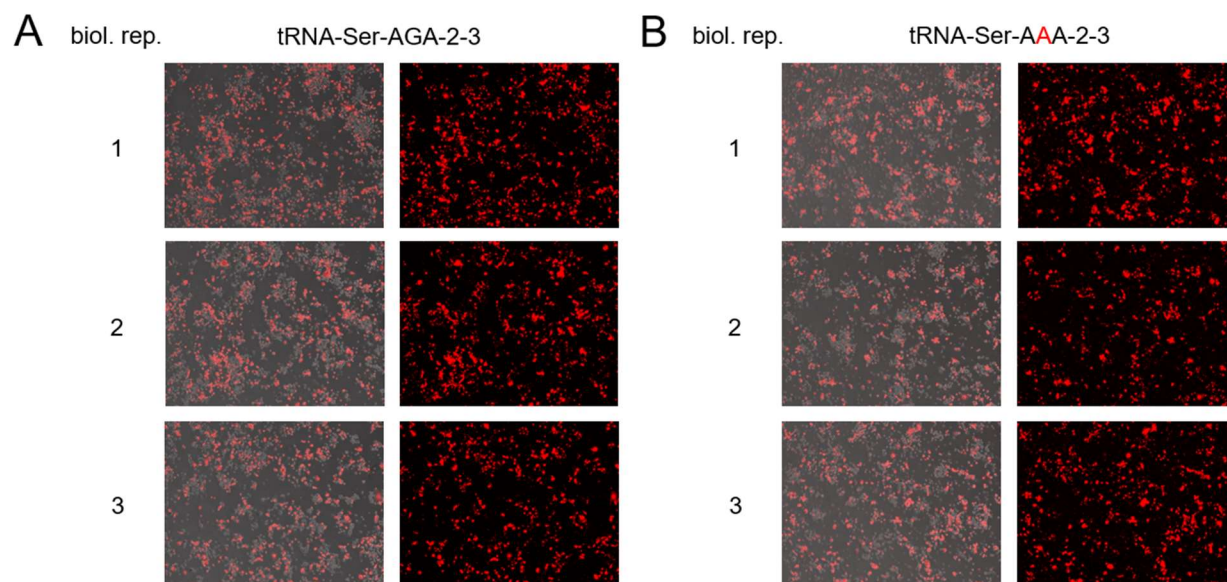


Figure S5.2. tRNAseq transfection images. N2a cells were transfected with a plasmid encoding human wild-type tRNA^{Ser}_{AGA} (A) or tRNA^{Ser}_{AAA} G35A variant (B; expressed from human tRNA-Ser-AGA-2-3 gene flanking sequence context) and mCherry (see Materials and Methods). Representative fluorescent microscopy images used for transfection efficiency counting are shown.

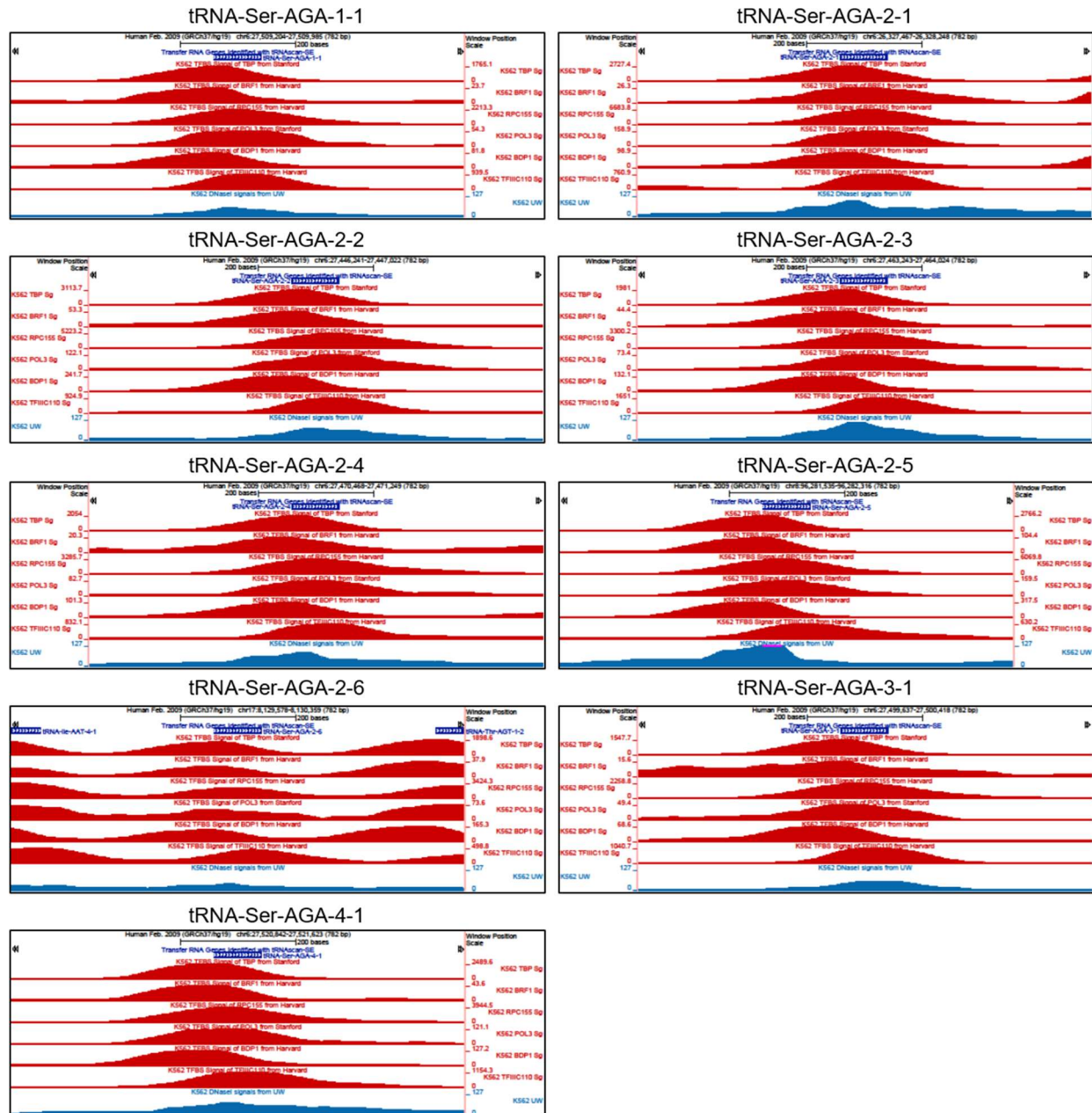


Figure S5.3. CHIP-seq and DNase-seq data for all tRNA-Ser-AGA genes. UCSC genome browser tracks showing K562 cell CHIP-Seq and DNase-seq data from ENCODE datasets for all high confidence human tRNA-Ser-AGA genes with ± 350 bp flanking sequence. See Results section 5.3.3 and Table S5.4 for details on data sources. Transfer RNA gene coordinates were found on GtRNadb.

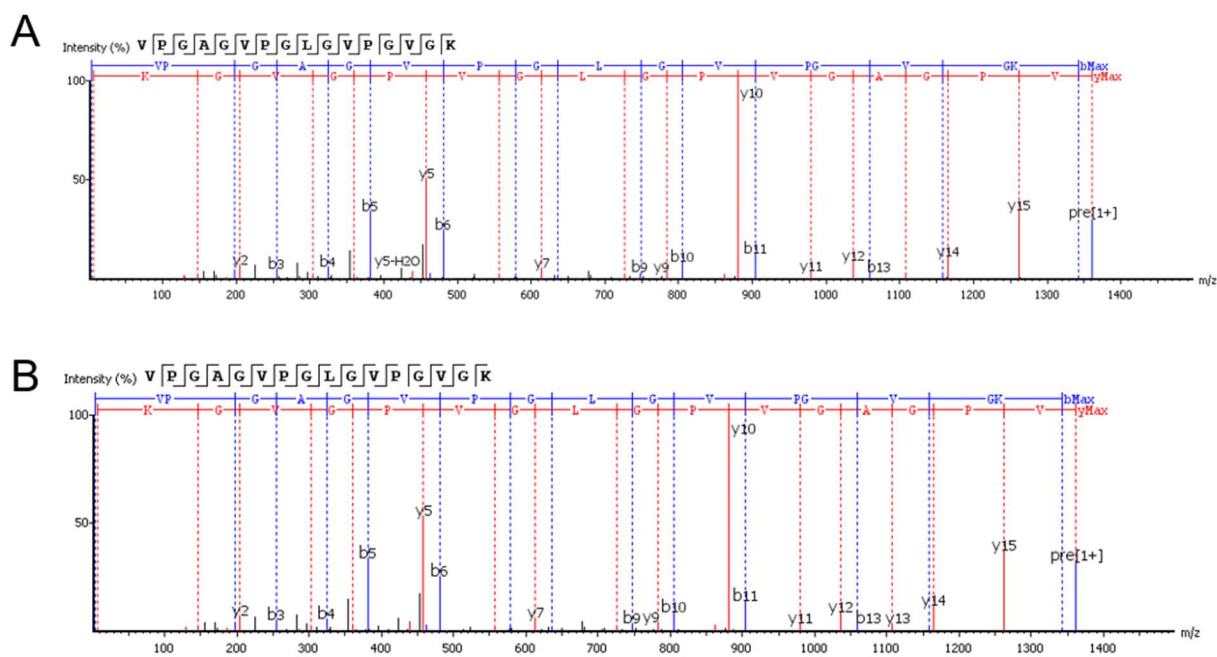


Figure S5.4. Representative y and b ion spectra for Leu containing MS-READ peptides. Detailed y and b ion spectra for MS-READ peptides containing Leu encoded by UUA (A) or UUG (B) codons.

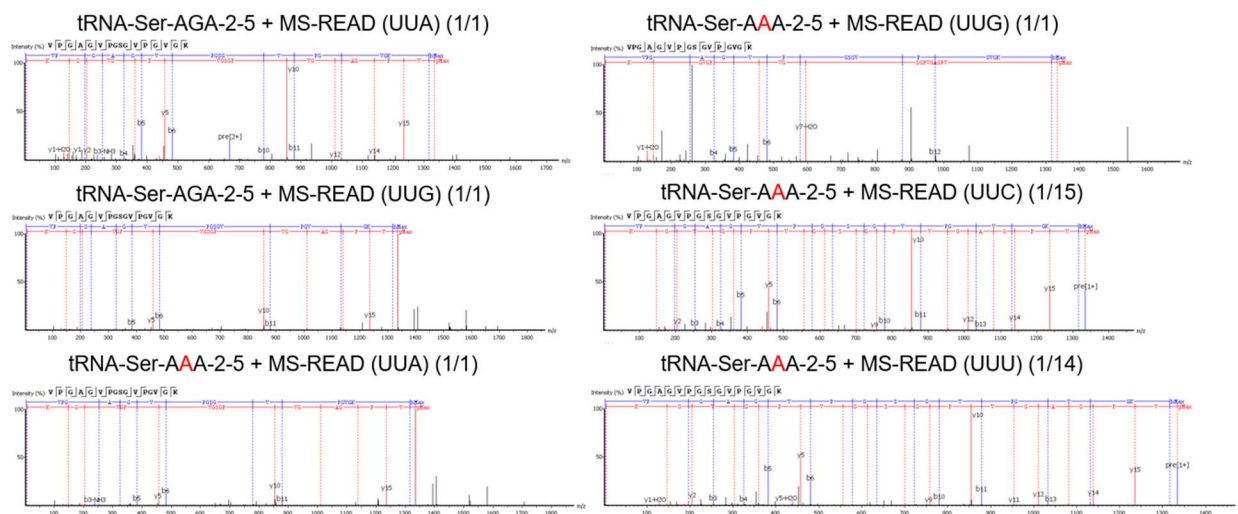


Figure S5.5. Representative y and b ion spectra for Ser-containing MS-READ peptides. The highest quality y and b ion spectra containing putative Ser misincorporation from each tRNA:codon pair tested in MS-READ LC-MS/MS experiment are shown. Expressed tRNA and MS-READ-mCherry reporter proteins are labeled above the spectra. Numbers in brackets indicate spectral counts for total peptides detected from the same tRNA:codon pair (see also Table 5.6).

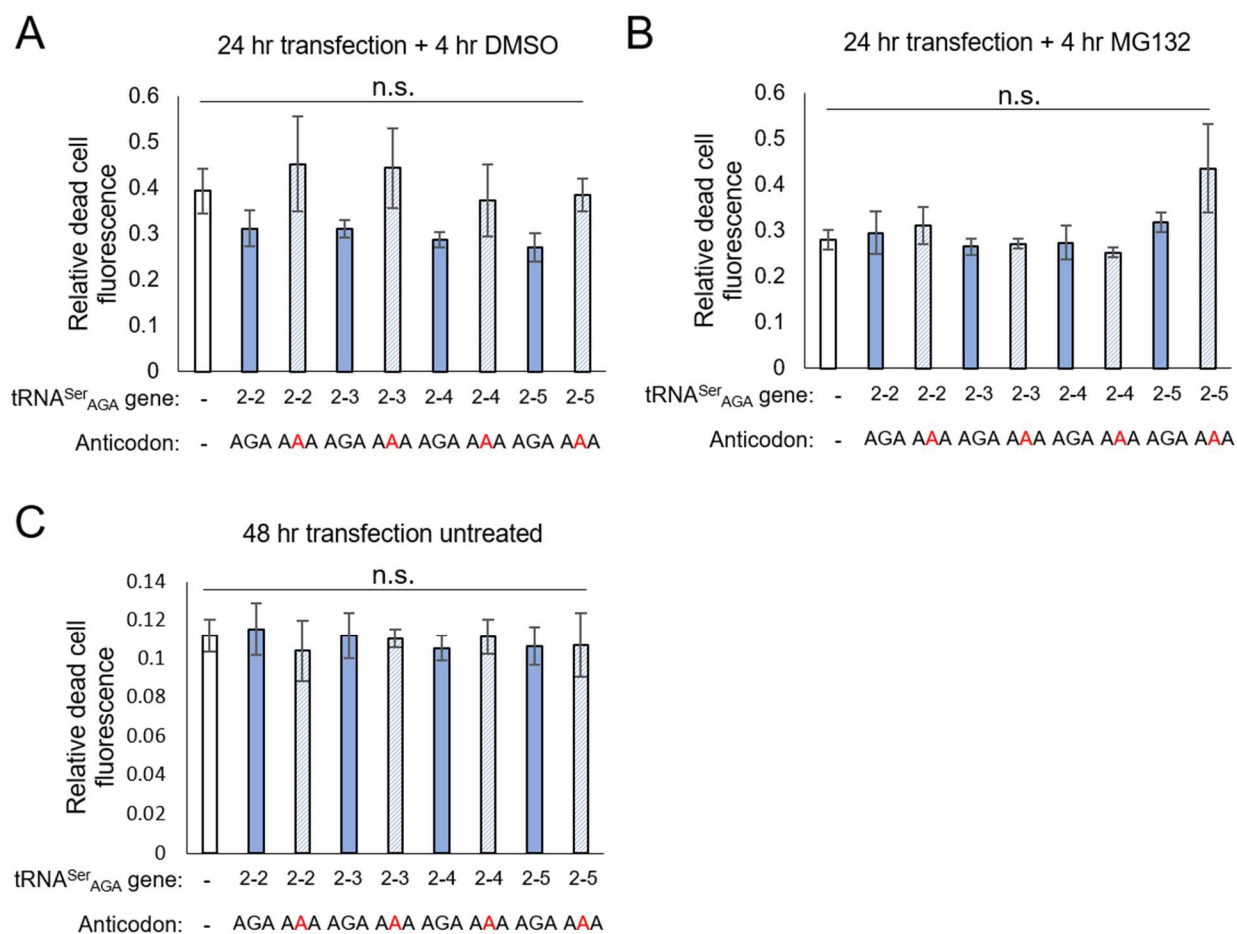


Figure S5.6. Supplemental HEK 293T cell cytotoxicity data. Plasmids encoding mCherry and wild-type human tRNA^{Ser}_{AGA} or variant tRNA^{Ser}_{AAA} with different flanking sequence contexts from human tRNA-Ser-AGA-2 genes were transfected HEK293T cells for 24 hr (A,B) or 48 hr (C). Cells transfected for 24 hr (A,B) were also treated with 10 μ M MG132 or vehicle (DMSO) for 4 hours before assays (see Materials and Methods). Cytotoxicity was measured using dye exclusion assays with SYTOX Blue as previously described (see Chapter 4, Materials and Methods). Statistical significance was determined by Tukey's Honestly Significant difference tests ($\alpha = 0.05$). No statistically significant differences were found (n.s.)

5.7.4 Appendix: Fiji/ImageJ macros and TrackMate analysis

Fiji/Image J macros.

Fiji/ImageJ (version 1.53f51 (44); Java version 1.8.0_172 (64-bit)) scripts to measure the fluorescence and analyze images of transfected cells. All macros were run on 16-bit, single-channel images.

Fiji/ImageJ macros used in Figure 5.3 D-E - Mean fluorescence/cell area plots.

Fluorescence in regions of interest was measured using the following Fiji/ImageJ macro, which is almost identical to our previously described approach (8). Threshold values were tailored slightly to exclude differences in background fluorescence from the different cell line images (K562, HEK293T, N2a), but the same settings were used to analyze all images for a given cell line. Data outputs were processed in Microsoft Excel, where means of biological replicates were calculated and statistical differences were determined using ANOVA followed by Tukey's Honestly Significant Difference tests ($\alpha = 0.05$). Box and whisker plots with strip plot overlays were created in R.

```
//Open image. Replace "file name" with desired image directory.
open("file name");
//Subtract background signal using rolling circle method with radius of 50 pixels.
run("Subtract Background...", "rolling=50");
//Set threshold to exclude pixels below chosen intensity cutoff (6 in this case). Fine-tune according
to your image brightness and use same cutoff for all images in one experiment.
setThreshold(6, 255);
//Next two lines convert to black on white mask image
setOption("BlackBackground", false);
run("Convert to Mask");
//Remove noise with despeckle function.
run("Despeckle");
//Separate closely adjacent objects with watershed function.
run("Watershed");
//Create annotations covering area above threshold. Excludes objects of area under chosen size
cut-off (100 pixels in this case). Size cut-off should be adjusted depending on the magnification
of the image and the size of objects you wish to exclude (noise).
run("Analyze Particles...", "size=100-Infinity display clear summarize add");
```

//Clear results. Steps so far to are to create region of interest annotations (ROIs), results will be collected in following steps.

```
run("Clear Results");
//Import unmodified image again. Should be identical to line 1
open("file name");
//Subtract background signal using rolling circle method with radius of 50 pixels.
run("Subtract Background...", "rolling=50");
//The next two lines overlay the ROIs from the thresholded on the non-thresholded image.
roiManager("Show None");
roiManager("Show All");
//Set measurements to record area, mean, and integrated density to 3 decimal places, then measure.
"Mean" is the quotient of (integrated density) / (area).
run("Set Measurements...", "area mean integrated redirect=None decimal=3");
//Measure.
roiManager("Measure");
```

Fiji/ImageJ analysis of cell migration kinetics using TrackMate.

Image series were imported to Fiji/ImageJ and background-subtracted with the macro below (A). Settings used in the TrackMate user interface for analysis are listed (B). Tracks of duration < 3 frames were excluded (step 7). Mean speed values for each track were processed in Microsoft Excel, where means of biological replicates were calculated and statistical differences were determined using independent sample t-tests. Box and whisker plots with strip plot overlays were created in R.

A) Macro for importing image sequence.

```
//Open image series. Replace "folder name" with desired image series directory.
run("Image Sequence...", "dir=["folder name"] type=16-bit start=2 count=30 step=3 sort");
//Subtract background signal using rolling circle method with radius of 50 pixels.
run("Subtract Background...", "rolling=50 stack");
//Open TrackMate plugin
run("TrackMate");
```

B) TrackMate settings.

- 1) Swap Z and T
- 2) LoG detector
 - 20 pixel
 - 0.3 quality threshold
 - no median filtering
 - do subpixel localization

- 3) Median filtering
skip
- 4) Set filters on spots
skip
- 5) Select a tracker
simple LAP tracker
- 6) Settings for tracker
20.0 pixel linking
20.0 pixel gap-closing max
2 frame gap-closing max
- 7) Set filters on tracks
track duration above 2.91
- 8) Display options
tracks --> click tracks tab on left, export to csv

Chapter 6

6. Conclusions and future perspectives

6.1 Summary and conclusions

The existence of transfer RNAs was first predicted in 1955 (1), and by 1958 the contribution of soluble RNAs in delivering amino acids to translating ribosomes had been demonstrated *in vitro* (2). The first transfer RNA sequence was described in 1965 (3), and in the decades that followed, extensive work would reveal how tRNAs maintain the relationship between the genetic code and amino acid sequences in proteins (4). Despite the long history of tRNA research, their inherent complexity and a series of challenges unique to their study have limited the depth of our understanding of how tRNAs behave (or misbehave) in human cells — especially in models of disease.

The subject of my thesis was inspired by a surprising discovery, where a genetic suppressor screen in yeast revealed a tRNA variant as a suppressor of a toxic loss-of-function mutation in a chaperone protein (Tti2_{L187P}) (5). The tRNA mutation, characterized by Hoffman *et al* in 2017, caused a yeast tRNA^{Pro} to be mis-aminoacylated with alanine by AlaRS. This resulted in low-level (~5%) Pro to Ala amino acid misincorporation, which effectively restored a proportion of the expressed Tti2_{L187P} chaperone protein to a functional Tti2_{L187A} variant. tRNA^{Ala} is a unique case in terms of interaction with its aminoacyl-tRNA synthetase, where a single base-pair in the tRNA acceptor stem (G3:U70) is sufficient for recognition (4,6). Indeed, early studies on the identity determinants of tRNA^{Ala} revealed that introducing a single G3:U70 pair in other tRNAs can be sufficient for mis-aminoacylation by AlaRS (6).

Intrigued by the work of Hoffman *et al*, we tested an equivalent mutation in human tRNA^{Pro} (G3:U70) for mistranslation in mammalian HEK293 cells ((7), Chapter 2). In mammalian cells, we found the levels of mistranslation to be generally lower than in yeast (~2%), but still detectable. We observed this in cells deprived of serum and glucose, which acted to slow cell division and promote accumulation of mis-made proteins. Surprisingly, despite the ~2% amino acid misincorporation, we could not detect a significant loss of cellular viability, or induction of a heat shock response in HEK293 cells expressing the tRNA variant, as had been observed in yeast.

Hence, HEK293 cells tolerated the amino acid misincorporation well. This is in agreement with other studies of tRNA variants in cancerous or embryonic cells, where toxicity of mistranslation is not always evident (8,9), or can vary greatly depending on the type of amino acid misincorporation (10). In Chapter 5, we showed that cell types can also be an important factor in the toxicity of tRNA variants, where tRNA variants that mistranslate Phe to Ser had clear cytotoxic effects in murine neuroblastoma (N2a) cells but not human HEK293 or K562 cells.

Given that human cells can tolerate, at some level, mistranslation caused by mutations in tRNAs, we began investigating the prevalence of human tRNA variants that cause amino acid misincorporation in the human population ((11), Chapter 1). We narrowed our search based on the logic that: 1) most aminoacyl-tRNA synthetases recognize the anticodon during amino acid ligation and 2) most tRNAs make multiple essential contacts with aminoacyl-tRNA synthetases (called identity elements or identity determinants, (4)). This refined our search to several cases where a single nucleotide variant in a tRNA could cause amino acid misincorporation, since many variants would either render the tRNA non-functional, or be insufficient to confer novel identity to a tRNA sequence. Firstly, tRNAs Ser, Ala, and to a lesser extent Leu, do not require specific sequences in the anticodon for recognition by their cognate aminoacyl-tRNA synthetases (4). Hence, non-synonymous anticodon mutations in Ser, Ala, and Leu tRNAs can read noncognate codons without compromising aminoacylation efficiency. The second exception was the case of tRNA^{Ala} and its single identity element, G3:U70. Since only a single base pair is required for AlaRS to recognize tRNAs, any tRNA already possessing a G at position 3 or U at position 70 would require only a single nucleotide variant to become a potential alanine acceptor (5-7).

Our search for mistranslating tRNAs in data from the 1000 genomes project (12,13) bore striking results. While most of the variants we highlighted were rare, some mistranslation-ready anticodon variants were found in allele frequencies as high as 6% ((11), Chapter 1). Some also had the potential to cause remarkably dissimilar amino acid substitutions, including a tRNA^{Ser} variant that mistranslates Phe codons ((14), Chapters 3-5) and is found in ~1.8% of sequenced individuals. We also found several examples of tRNA variants that create G3:U70 pairs in non-alanine tRNAs, the most common of which occurs in ~1.3% of sequenced individuals.

At the same time, we contributed to a DNA sequencing project that would reveal a much greater prevalence of tRNA variants in the human population than previously understood (15). A

major challenge in sequencing tRNA genes is their repetitive nature, with some tRNA genes occurring in as many as 11 identical copies in the human genome (13). This creates a mapping challenge in whole genome sequencing studies, since read lengths typically fall below 50 nucleotides in length (12), and tRNAs are >70 nucleotide sequences. Further, low sequencing coverage in the 1000 genomes project (4x) limited the authors' ability to determine the number of tRNA variants occurring per individual, since many potential variant reads could not be distinguished from sequencing errors (12).

In our study (15), we employed greater depth of coverage (>60x) and a tiled read mapping strategy that used tRNA flanking sequence to more accurately map tRNA sequences to their correct genomic loci. With this approach, we found ~60-70 tRNA variants per individual in a cohort of 84 individuals. Thus, variants in cytoplasmic tRNA genes occur in all individuals. Hence, individuals likely differ in the rate and type of protein synthesis errors that occur in their cells depending on the collection of variants present in their tRNA genes.

Despite the astounding prevalence of tRNA sequence variants in the population, very little was known about how naturally occurring variants in human cytoplasmic tRNA genes affect cellular physiology, especially in models of disease. Indeed, in our 2019 review ((11), Chapter 1), we found only a single proven example of a variant in a human cytoplasmic tRNA acting as a primary driver of disease (16). However, many examples were found of mutations in mitochondrial tRNAs or proteins that interact with cytoplasmic tRNAs (aminoacyl-tRNA synthetases, tRNA-modifying enzymes, ribosome-associated factors, etc.) being implicated in human disease (11). Further, studies on engineered tRNA variants expressed in mammalian cells demonstrated that mistranslating tRNAs can cause protein folding stress (10) and have exacerbating effects in models of cancer (8). Another study demonstrated that in mice, a cytoplasmic tRNA variant was associated with neuronal dysfunction (17).

Based on our review, we hypothesized that human cytoplasmic tRNA variants would be more likely to act as modifiers than primary drivers of disease. To investigate this hypothesis further, we employed mammalian cell-based models of the neurodegenerative diseases Huntington's disease ((14), Chapter 3) and amyotrophic lateral sclerosis (ALS; Chapter 4). We chose to focus on models of neurodegenerative disease since the pathogenesis of most neurodegenerative diseases involves misfolding proteins, which challenge many of the same

protein folding stress responses as mistranslating tRNAs (18). There are also many examples of mutations in mitochondrial tRNAs and proteins that interact with tRNAs being implicated in neurodegenerative disease (11), in addition to the mentioned example of a mouse cytoplasmic tRNA exacerbating a neurodegenerative phenotype (17). For both studies (Chapters 3 and 4), we primarily focused on a naturally occurring non-synonymous anticodon variant in the tRNA-Ser-AGA-2-3 gene which occurs in ~1.8% of sequenced individuals (12,13,15,19). As we demonstrated in Chapters 3 and 5, the tRNA causes Ser amino acid misincorporation at Phe UUC and UUU codons. We expressed the tRNA by encoding it on a plasmid with \pm 300 bp flanking sequence, which was PCR amplified from HEK293 genomic DNA.

In our study on models of Huntington's disease ((14), Chapter 3), we expressed exon 1 sequences from the human HTT gene with extended CAG repeats that encode an aggregation-prone polyglutamine (polyQ) sequence. Conveniently, fusing this protein coding sequence to a fluorescent protein (EGFP) enables real-time monitoring of polyQ aggregation kinetics in live cells (20). Similarly, in the ALS study (Chapter 4), we expressed an mCherry-fused FUS protein or R521C variant. FUS is a frequently mutated protein in ALS (21), and C-terminal fusion to fluorescent proteins allows visualization of aggregate formation in live cells (22).

In cytotoxicity assays where the mistranslating tRNA and extended polyQ proteins were co-expressed, we did not observe synthetic toxic effects ((14), Chapter 3). Rather, the mistranslating tRNA had a dominant effect, exhibiting cytotoxicity in cells expressing either typical (23Q) or disease-length (74Q) polyQ proteins. In our studies co-expressing the mistranslating tRNA and FUS, we observed a synthetic toxic effect with the FUS(R521C) mutant, where expressing both the mistranslating tRNA and FUS mutant had a stronger cytotoxic effect than either component alone (Chapter 4). Further studies may be required to determine why the mutant FUS had an exacerbating effect not seen with mutant polyQ, but it should be noted that toxicity of HTT exon 1 polyQ proteins expressed in cells can be relatively mild (23). Another observation from our cytotoxicity experiments was that proteasome inhibition using the small molecule MG132 was capable of exacerbating toxicity of the mistranslating tRNA ((14), Chapter 3). Hence, we demonstrated the usefulness of MG132 as an exacerbating agent to study mistranslating tRNA toxicity.

In our experiments on aggregation kinetics of polyQ proteins in mistranslating cells, we found that the mistranslating tRNA caused slowed formation of aggregates ((14), Chapter 3). We attributed this to a reduction in protein synthesis which occurred in mistranslating cells. Others have observed a similar effect on protein synthesis when expressing engineered anticodon variants of tRNA^{Ser} in mammalian cells (9,10). We observed a comparable effect in cells expressing the FUS-mCherry proteins (Chapter 4), where expression and aggregation of FUS-mCherry was generally lower in mistranslating cells. However, in our FUS experiments, we monitored cells for a longer time-course, and found that after extended expression of the mistranslating tRNA and FUS-mCherry, the appearance of aggregates began to accelerate rapidly. In cells expressing FUS(R521C)-mCherry, aggregation kinetics were highly sporadic in mistranslating cells and fluctuated above and below aggregation levels in cells expressing wild-type tRNA throughout the timecourse.

Future studies will be required in stable cell lines to assess the more long-term kinetics of protein aggregation in mistranslating cells. However, the data suggest that suppression of protein synthesis in mistranslating cells may be transient or fluctuate over time. Intriguingly, a study on a ribosomal protein mutant that causes chronic amino acid misincorporation showed that protein folding stress responses, which often signal reductions in protein synthesis, can become suppressed in chronically mistranslating cells (24). Another study on tRNA^{Ser} anticodon variants expressed in stably transfected cells demonstrated that protein synthesis rates can vary greatly depending on passage number of the cells and the type of amino acid misincorporation (9). In that study, in cells expressing a tRNA^{Ser} with Ala-decoding anticodon, protein synthesis increased from passages 1 to 15, then fell sharply by passage 30. By contrast, cells expressing a tRNA^{Ser} with Leu-decoding anticodon exhibited reduced protein synthesis at all passages after passage 1. Our observations on FUS-mCherry aggregation (Chapter 4) further demonstrate that protein synthesis rate alterations caused by mistranslating tRNAs can change temporally.

From a mechanistic standpoint, how mistranslating tRNAs elicit reductions in protein synthesis is dependent on a multitude of factors. For example, inhibitory phosphorylation of elongation initiation factor 2 alpha (eIF2 α) is a converging point of numerous stress responses (25) and has been observed in several studies of mistranslating tRNAs expressed in mammalian cells (9,10,26). However, in our studies on the naturally occurring Phe to Ser mistranslating tRNA, we

did not observe phosphorylation of eIF2 α ((14), Chapter 3). Further, cells expressing this tRNA were resistant to effects of the integrated stress response inhibitor (ISRIB), a small molecule designed to promote mRNA translation initiation in cells where eIF2 α is phosphorylated. It should also be noted that this was the first published example (to our knowledge) of a naturally occurring tRNA variant altering small molecule treatment efficacy in mammalian cells. Regarding eIF2 α , others have found that phosphorylation is not always evident in cells expressing mistranslating tRNAs (9), and levels can vary greatly depending on the type of amino acid misincorporation (10), and cell passage number (9). We also did not observe phosphorylation of eukaryotic elongation factor 2 (eEF2), another major regulatory point of protein synthesis (27,28). Studies in our lab are ongoing to better understand the mechanism of translation inhibition in cells expressing the Phe to Ser mistranslating tRNA variant.

In our study on polyQ aggregation in mistranslating cells ((14), Chapter 3), we also measured effects on protein turnover. Cells expressing the mistranslating tRNA exhibited reduced turnover of polyQ protein. Thus, while polyQ aggregates formed more slowly initially, they were also slower to degrade in mistranslating cells. This was supported by our observation that proteasome inhibition can exacerbate mistranslation toxicity (Chapter 3). Given that mistranslating tRNAs lead to the production of misfolded proteins, they place an increased burden on protein turnover. The implications of this finding in patients with neurodegenerative disease are complex. Robust protein turnover is required for cells to tolerate protein folding stress caused by misfolding proteins (29,30). However, in aging cells, reduced protein turnover can also be beneficial, as it helps to compensate for age-related reductions in protein synthesis (31).

Altogether, our studies on Huntington's and ALS disease models were the first to explore naturally occurring human cytoplasmic tRNA gene variants as modifiers of disease. Our work demonstrates that tRNA variants have significant potential to alter disease progression since mistranslation and the signaling events it elicits can alter the expression and degradation of proteins, as well as alter the efficacy of small molecules designed to treat disease. These discoveries shed new light on a potentially vast and understudied source of variability in human disease.

Given that the human genome encodes ~400 functional tRNA genes and ~210 tRNA-like pseudogenes (12,13,32), and each individual harbors ~60-70 variants in these genes (15),

characterizing which variants have potential to affect disease progression represents a significant challenge. While some tRNA variants that cause amino acid misincorporation can be functionally predicted based on knowledge of tRNA identity elements, many more variants can have complex effects that are harder to predict. For example, others have shown that mutations in the T-stem of different tRNAs can compromise tRNA function. In one case, a C65G mutation in human tRNA^{Sec} resulted in changes to stress-dependent modifications in the anticodon (16). Hence, mutations in one location in the tRNA body can affect other sites in the tRNA by changing interactions with tRNA modifying enzymes. In another case, a C50T mutation in a mouse tRNA^{Arg} gene caused ribosome stalling, but only in the central nervous system where the tRNA gene is exclusively expressed (17). Thus, understanding tissue-specific differences in tRNA gene expression is critical to predict the consequences of variants in the tRNA sequence. These examples highlight how the relationship between tRNA sequence and function is complex. Even when mutations occur in well characterized nucleotides in the tRNA body, it is difficult to predict how a given mutation will alter the path of a tRNA from transcription and processing to mRNA translation. Therefore, the rational approach of predicting tRNA variant functions has limitations.

Another tool to classify the disease-modifying potential of tRNA gene variants is to evaluate the loci at which tRNAs are encoded (33). Individual tRNA genes vary greatly in expression activity, and tRNA genes can be activated or silenced depending on tissue (34) or cell states (eg. proliferation versus differentiation) (35). Hence, classifying expression activity of individual tRNA genes could be a valuable approach to predict variants-of-concern and what tissues might be most affected by a given tRNA variant.

Transfer RNA gene expression activity can be roughly predicted based on publicly available gene expression data such as CHIP-sequencing (36,37) and DNase sequencing (36,38), or based on bioinformatic scoring algorithms (33,39). In Chapter 5, we explored the use of a well-characterized tRNA variant as a tool to test tRNA gene activity experimentally. The Phe-to-Ser mistranslating tRNA we characterized in Chapters 3-4 represented an interesting case to explore the effects of loci-of-origin on tRNA gene activity. The variant is a G35A mutation in the tRNA-Ser-AGA-2-3 gene. Intriguingly, the tRNA-Ser-AGA-2-3 is one of the six identical copies of the same tRNA sequence (named tRNA-Ser-AGA-2-1, -2-2, ..., -2-6) (13). Yet, the variant occurs much more commonly in the -2-3 locus than any other site. In the -2-3 locus, the variant is found

in ~1.8% of sequenced individuals. In the other tRNA-Ser-AGA-2 genes, the variant has either not been observed, or is exceedingly rare (allele frequency < 0.0015%) (12,19,40). Given that the genes are identical, it is not possible to compare their expression activity at the RNA level with methods like RNA sequencing or quantitative reverse-transcription polymerase chain reaction (qRT-PCR). Interestingly, while the sequences encoding tRNA-Ser-AGA-2 are identical, the sequences flanking the tRNAs are highly divergent. Indeed, in Chapter 5 I aligned all six tRNA gene loci with ± 300 bp flanking sequence and the only conserved feature outside of the tRNA gene was a short poly-thymidine transcription termination sequence downstream of each tRNA sequence. It has long been known that tRNA flanking sequences can alter the regulation and processing efficiency of tRNA genes (33,41,42). Hence, we expected that the identical tRNA-Ser-AGA-2 loci would be expressed at different levels, and potentially in a tissue-dependent manner.

To test the functional activity of the tRNA gene in its different sequence contexts, we took advantage of the reliable reduction in fluorescence we observed when co-expressing the Phe-to-Ser mistranslating tRNA with fluorescent proteins ((14), Chapters 3-4). We encoded the tRNA variant or wild type on plasmids with flanking sequences (± 300 bp) taken from four different loci at which copies of the gene is encoded in the human genome. With this approach, we found that expressing the tRNA variant from different sequence contexts altered its phenotypic potency in a cell-line dependent manner (Chapter 5). For example, expressing the tRNA variant from the tRNA-Ser-AGA-2-4 gene context caused a significant reduction in fluorescence in two of the tested cell lines (HEK293T and N2a), but no effect in the other cell line (K562). We also found that the effects on fluorescence correlated well with our gene expression predictions based on CHIP-sequencing (36,37) and DNase sequencing (36,38) data from K562 cells. Hence, our approach could be useful for validating tRNA gene expression predictions from publicly available datasets.

We also used our plasmids to test the cytotoxicity of the tRNA variant expressed from different sequence contexts in different cell lines. We could not readily detect cytotoxic effects from the tRNA variant expressed from any context in HEK293T or K562 cells, but in N2a cells we observed a significant cytotoxic effect from the tRNA expressed in all contexts (Chapter 5). Hence, N2a cells may be more sensitive to tRNA-dependent mistranslation than HEK293T or K562 cells. As discussed earlier, we and others have found that some mammalian cell lines

(including HEK293) are robust to amino acid misincorporation, so it was not surprising that the tRNA variants had no detectable cytotoxic effects in HEK293T and K562 cells.

To probe phenotypic effects further, we employed a single-cell resolution cell migration assay. The assay uses fluorescence from transfected cells and particle tracking software to track and measure cell migration speed. With this assay we found that, in the presence of MG132 proteasome inhibitor, the mistranslating tRNA expressed in the tRNA-Ser-AGA-2-3 context caused a significant reduction in cell migration speed compared to cells expressing wild type (Chapter 5). To our knowledge, this is the first demonstration that a naturally occurring tRNA variant can alter mammalian cell migration kinetics. Further studies will be required to determine the detailed mechanism of this phenomenon. One likely explanation is that increased errors in mRNA translation and the reduced protein synthesis rate in mistranslating cells impede cytoskeletal dynamics required for migration. Indeed, genetic interaction screens in yeast using mistranslating tRNAs (43) and amino acids that misincorporate in proteins (44) have shown that actin cytoskeleton regulation is often altered in mistranslating yeast cells.

Another observation we made in our sequence context experiments (Chapter 5) was that one of the sequence contexts (tRNA-Ser-AGA-2-5) had an exceptionally strong effect on fluorescence compared to the other expression contexts in HEK293T cells. We saw this as an opportunity to improve on our methods for detection of amino acid misincorporation with a strong mistranslating tRNA. In Chapter 3, we demonstrated that the tRNA-Ser-AGA-2-3 G35A variant caused Phe-to-Ser amino acid misincorporation by immunoprecipitating a co-expressed mCherry protein from cells and identifying peptides containing misincorporated amino acids by liquid chromatography with tandem mass spectrometry (LC-MS/MS). One limitation of this approach was that we were limited to the codons already present in the mCherry coding sequence, and the peptides containing misincorporated amino acids varied in size and sequence composition, making it difficult to quantitatively compare misincorporation at different codons. To improve on our approach, we used MS-READ (45), a designer peptide-based mass spectrometry method that was developed to quantitatively detect amino acid misincorporation events in yeast. The MS-READ peptide was designed to have optimal characteristics for detection by LS-MS/MS with a broad range of amino acids encoded at a central test position (45).

To adapt MS-READ for use in mammalian cells, we fused the MS-READ peptide sequence containing custom test codons to mCherry and co-expressed the MS-READ-mCherry protein with wild-type or mistranslating tRNA expressed from the tRNA-Ser-AGA-2-5 gene sequence context. We then purified the MS-READ-mCherry proteins from HEK293T cells by immunoprecipitation with anti-RFP nanobody conjugated agarose beads. Lastly, we digested the MS-READ-mCherry proteins with trypsin and analyzed the samples by LC-MS/MS. With this approach, we demonstrated that the tRNA-Ser-AGA-2-5 G35A variants misincorporates Ser at Phe UUU and UUC codons, but not Leu UUA or UUG codons. Thus, we demonstrated a highly sensitive and codon-specific method to characterize tRNA-dependent amino acid misincorporation in mammalian cells. We anticipate that this approach will become a valuable tool in characterizing other human tRNA genes with anticodon and identity element mutations.

In sum, the work described in Chapter 5 demonstrated that identical tRNA gene variants can differ in phenotypic potency and affected cell types depending on local sequence context. We also demonstrated novel methods for phenotypic comparison of tRNA variants and detection of amino acid misincorporation that could significantly improve our ability to study the astounding number of tRNA variants in the human population.

6.2 Future outlook

6.2.1 Mechanisms of protein synthesis inhibition in mistranslating cells

One major outstanding question from my thesis work is how the tRNA-Ser-AGA-2-3 G35A variant causes a reduction in protein synthesis in cells. In Chapter 3, we used western blotting to test for several markers of protein folding stress and protein synthesis inhibition that others had observed in mistranslating yeast (43) and mammalian cells (9,10,26). Surprisingly, we could not establish any of these responses in cells expressing the tRNA-Ser-AGA-2-3 G35A variant (tRNA^{Ser}_{AAA}). Our laboratory is currently working to better answer this question using methods that more broadly assay for changes in the proteome (reverse-phase protein array). I also initiated some investigations into immunofluorescence as a method to assay both signaling changes and changes to physiological features of mistranslating cells.

At the same time, I have initiated investigations into a working hypothesis of anticodon loop compatibility. My hypothesis of anticodon loop compatibility is that tRNAs bearing non-

cognate anticodons would in some cases exhibit sub-optimal decoding kinetics in the ribosome. Since tRNA anticodon variants did not co-evolve with their anticodon sequence, they may or may not be able to orient the anticodon for efficient pairing and unpairing with codons. If true, slowed kinetics in the ribosome could in part reduce protein synthesis rates by physically slowing ribosomal translocation. This would also explain why we found that the integrated stress response inhibitor was unable to restore protein synthesis activity in cells expressing the tRNA^{Ser}_{AAA} variant (Chapter 3).

Interestingly, the AAA anticodon does not occur naturally in human tRNA^{Phe} genes (13,46). Instead tRNA^{Phe} in humans and almost all eukaryotes exclusively utilize a GAA anticodon to decode UUU codons (13,46). tRNA^{Phe} also harbors a highly conserved guanine in the anticodon-adjacent position 37 (46). These guanine bases are modified post-transcriptionally and ensure accurate and efficient pairing with U-rich Phe codons (47-49). By contrast, the tRNA^{Ser}_{AAA} variant harbors five consecutive adenosine nucleotides spanning from the first position of the anticodon to the first pair of the anticodon stem (positions 34-38). Others have postulated that A:U-rich codon:anticodon pairs are prone to frameshifting and inefficient conformational sampling at the decoding center (50,51), which could limit decoding kinetics. Thus, the variant may reduce protein synthesis partly through physical impediment of the ribosome, which would explain the lack of signaling associated with protein synthesis reduction. To investigate this hypothesis, I have done some preliminary investigations introducing G34 or G37 mutations into the tRNA to better mimic the anticodon loop sequence of tRNA^{Phe}. I hope that these investigations will help to better understand the mechanism of protein synthesis inhibition in cells expressing the tRNA^{Ser}_{AAA} variant, as well as provide insight to mechanistic studies of tRNA anticodon variants in general.

6.2.2 Fluorescent reporters of amino acid misincorporation

In Chapter 2, we used a fluorescent reporter protein to monitor Pro to Ala amino acid misincorporation in live cells. Recently, we developed and characterized a similar reporter in *E. coli* that can be used to detect mistranslation caused by tRNA^{Ser} anticodon variants (52). I have developed a version of this reporter for monitoring Ser misincorporation in mammalian cells, and work with this reporter is ongoing in our laboratory. Given that tRNA^{Ser} anticodon variants are especially capable of causing amino acid misincorporation, I anticipate that this reporter will prove valuable in characterizing other tRNA^{Ser} anticodon variants found in the human population.

6.2.3 Sequencing tRNA genes in disease cohorts

As noted in section 6.1, the repetitive nature of tRNA genes has contributed to a lack of reliable sequencing data on tRNA variant frequencies in the human population, especially in disease cohorts. Further, tRNA genes are not typically included in whole exome or genome-wide association sequencing arrays. With increasing examples of tRNAs acting as genetic modifiers in models of disease (8,14,17,26), promoting the further inclusion of tRNA genes in sequencing studies will be critical to determine if our findings in cell culture-based models of disease hold true in real patients. With sequencing data to validate disease associations of tRNA variants, tRNA genes may become valuable markers in predicting the age of onset and severity of diseases in humans.

6.3 Conclusion

In my thesis work, I contributed to revealing a greater prevalence of tRNA gene sequence variants in the human population than previously understood and highlighted how many of these variants have potential to cause amino acid misincorporation and act as modifiers of disease. As proof-of-principle, I demonstrated in mammalian cell-based models of Huntington's disease and ALS that a naturally occurring tRNA variant can alter the cytotoxicity, synthesis, and degradation of aggregation-prone proteins associated with neurodegenerative disease. Finally, I developed novel methodological approaches to study highly similar and identical tRNA genes found in the human population, using a well characterized naturally occurring tRNA variant as a genetic tool. I hope that this work will draw greater attention to tRNA variants as potential modifiers of human disease, refining our ability to predict progression and treatment. Finally, the methodological approaches described should inspire new approaches to characterize the astounding number of tRNA sequence variants found in the human population.

6.4 References

1. Crick, F. (1955), *A note for the RNA Tie Club*, pp. 1-17.
2. Hoagland, M.B., Stephenson, M.L., Scott, J.F., Hecht, L.I. and Zamecnik, P.C. (1958) A soluble ribonucleic acid intermediate in protein synthesis. *J Biol Chem*, **231**, 241-257.
3. Holley, R.W., Everett, G.A., Madison, J.T. and Zamir, A. (1965) Nucleotide Sequences in the Yeast Alanine Transfer Ribonucleic Acid. *J Biol Chem*, **240**, 2122-2128.
4. Giege, R., Sissler, M. and Florentz, C. (1998) Universal rules and idiosyncratic features in tRNA identity. *Nucleic Acids Res*, **26**, 5017-5035.
5. Hoffman, K.S., Berg, M.D., Shilton, B.H., Brandl, C.J. and O'Donoghue, P. (2017) Genetic selection for mistranslation rescues a defective co-chaperone in yeast. *Nucleic Acids Res*, **45**, 3407-3421.
6. Hou, Y.M., Francklyn, C. and Schimmel, P. (1989) Molecular dissection of a transfer RNA and the basis for its identity. *Trends Biochem Sci*, **14**, 233-237.
7. Lant, J.T., Berg, M.D., Sze, D.H.W., Hoffman, K.S., Akinpelu, I.C., Turk, M.A., Heinemann, I.U., Duennwald, M.L., Brandl, C.J. and O'Donoghue, P. (2018) Visualizing tRNA-dependent mistranslation in human cells. *RNA Biol*, **15**, 567-575.
8. Santos, M., Pereira, P.M., Varanda, A.S., Carvalho, J., Azevedo, M., Mateus, D.D., Mendes, N., Oliveira, P., Trindade, F., Pinto, M.T. *et al.* (2018) Codon misreading tRNAs promote tumor growth in mice. *RNA Biol*, **15**, 773-786.
9. Varanda, A.S., Santos, M., Soares, A.R., Vitorino, R., Oliveira, P., Oliveira, C. and Santos, M.A.S. (2020) Human cells adapt to translational errors by modulating protein synthesis rate and protein turnover. *RNA Biol*, **17**, 135-149.
10. Geslain, R., Cubells, L., Bori-Sanz, T., Alvarez-Medina, R., Rossell, D., Marti, E. and Ribas de Pouplana, L. (2010) Chimeric tRNAs as tools to induce proteome damage and identify components of stress responses. *Nucleic Acids Res*, **38**, e30.
11. Lant, J.T., Berg, M.D., Heinemann, I.U., Brandl, C.J. and O'Donoghue, P. (2019) Pathways to disease from natural variations in human cytoplasmic tRNAs. *J Biol Chem*, **294**, 5294-5308.
12. Parisien, M., Wang, X. and Pan, T. (2013) Diversity of human tRNA genes from the 1000-genomes project. *RNA Biol*, **10**, 1853-1867.
13. Chan, P.P. and Lowe, T.M. (2016) GtRNAdb 2.0: an expanded database of transfer RNA genes identified in complete and draft genomes. *Nucleic Acids Res*, **44**, D184-189.
14. Lant, J.T., Kiri, R., Duennwald, M.L. and O'Donoghue, P. (2021) Formation and persistence of polyglutamine aggregates in mistranslating cells. *Nucleic Acids Res*, **49**, 11883-11899.
15. Berg, M.D., Giguere, D.J., Dron, J.S., Lant, J.T., Genereaux, J., Liao, C., Wang, J., Robinson, J.F., Gloor, G.B., Hegele, R.A. *et al.* (2019) Targeted sequencing reveals expanded genetic diversity of human transfer RNAs. *RNA Biol*, **16**, 1574-1585.
16. Schoenmakers, E., Carlson, B., Agostini, M., Moran, C., Rajanayagam, O., Bochukova, E., Tobe, R., Peat, R., Gevers, E., Muntoni, F. *et al.* (2016) Mutation in human selenocysteine transfer RNA selectively disrupts selenoprotein synthesis. *J Clin Invest*, **126**, 992-996.
17. Ishimura, R., Nagy, G., Dotu, I., Zhou, H., Yang, X.L., Schimmel, P., Senju, S., Nishimura, Y., Chuang, J.H. and Ackerman, S.L. (2014) RNA function. Ribosome stalling induced by mutation of a CNS-specific tRNA causes neurodegeneration. *Science*, **345**, 455-459.

18. Kapur, M., Monaghan, C.E. and Ackerman, S.L. (2017) Regulation of mRNA Translation in Neurons-A Matter of Life and Death. *Neuron*, **96**, 616-637.
19. Karczewski, K.J., Francioli, L.C., Tiao, G., Cummings, B.B., Alfoldi, J., Wang, Q., Collins, R.L., Laricchia, K.M., Ganna, A., Birnbaum, D.P. *et al.* (2020) The mutational constraint spectrum quantified from variation in 141,456 humans. *Nature*, **581**, 434-443.
20. Narain, Y., Wyttenbach, A., Rankin, J., Furlong, R.A. and Rubinsztein, D.C. (1999) A molecular investigation of true dominance in Huntington's disease. *J Med Genet*, **36**, 739-746.
21. Shang, Y. and Huang, E.J. (2016) Mechanisms of FUS mutations in familial amyotrophic lateral sclerosis. *Brain Res*, **1647**, 65-78.
22. Marrone, L., Poser, I., Casci, I., Japtok, J., Reinhardt, P., Janosch, A., Andree, C., Lee, H.O., Moebius, C., Koerner, E. *et al.* (2018) Isogenic FUS-eGFP iPSC Reporter Lines Enable Quantification of FUS Stress Granule Pathology that Is Rescued by Drugs Inducing Autophagy. *Stem Cell Reports*, **10**, 375-389.
23. Kim, Y.E., Hosp, F., Frottin, F., Ge, H., Mann, M., Hayer-Hartl, M. and Hartl, F.U. (2016) Soluble Oligomers of PolyQ-Expanded Huntingtin Target a Multiplicity of Key Cellular Factors. *Mol Cell*, **63**, 951-964.
24. Shcherbakov, D., Teo, Y., Boukari, H., Cortes-Sanchon, A., Mantovani, M., Osinnii, I., Moore, J., Juskeviciene, R., Brilkova, M., Duscha, S. *et al.* (2019) Ribosomal mistranslation leads to silencing of the unfolded protein response and increased mitochondrial biogenesis. *Commun Biol*, **2**, 381.
25. Pakos-Zebrucka, K., Koryga, I., Mnich, K., Ljujic, M., Samali, A. and Gorman, A.M. (2016) The integrated stress response. *EMBO Rep*, **17**, 1374-1395.
26. Kapur, M., Ganguly, A., Nagy, G., Adamson, S.I., Chuang, J.H., Frankel, W.N. and Ackerman, S.L. (2020) Expression of the Neuronal tRNA n-Tr20 Regulates Synaptic Transmission and Seizure Susceptibility. *Neuron*, **108**, 193-208 e199.
27. Ryazanov, A.G. and Davydova, E.K. (1989) Mechanism of elongation factor 2 (EF-2) inactivation upon phosphorylation. Phosphorylated EF-2 is unable to catalyze translocation. *FEBS Lett*, **251**, 187-190.
28. Moore, C.E., Wang, X., Xie, J., Pickford, J., Barron, J., Regufe da Mota, S., Versele, M. and Proud, C.G. (2016) Elongation factor 2 kinase promotes cell survival by inhibiting protein synthesis without inducing autophagy. *Cell Signal*, **28**, 284-293.
29. Jackson, M.P. and Hewitt, E.W. (2016) Cellular proteostasis: degradation of misfolded proteins by lysosomes. *Essays Biochem*, **60**, 173-180.
30. Ciechanover, A. and Kwon, Y.T. (2015) Degradation of misfolded proteins in neurodegenerative diseases: therapeutic targets and strategies. *Exp Mol Med*, **47**, e147.
31. Basisty, N., Meyer, J.G. and Schilling, B. (2018) Protein Turnover in Aging and Longevity. *Proteomics*, **18**, e1700108.
32. Chan, P.P. and Lowe, T.M. (2009) GtRNAdb: a database of transfer RNA genes detected in genomic sequence. *Nucleic Acids Res*, **37**, D93-97.
33. Thornlow, B.P., Armstrong, J., Holmes, A.D., Howard, J.M., Corbett-Detig, R.B. and Lowe, T.M. (2020) Predicting transfer RNA gene activity from sequence and genome context. *Genome Res*, **30**, 85-94.
34. Dittmar, K.A., Goodenbour, J.M. and Pan, T. (2006) Tissue-specific differences in human transfer RNA expression. *PLoS Genet*, **2**, e221.

35. Gingold, H., Tehler, D., Christoffersen, N.R., Nielsen, M.M., Asmar, F., Kooistra, S.M., Christophersen, N.S., Christensen, L.L., Borre, M., Sorensen, K.D. *et al.* (2014) A dual program for translation regulation in cellular proliferation and differentiation. *Cell*, **158**, 1281-1292.
36. Consortium, E.P. (2012) An integrated encyclopedia of DNA elements in the human genome. *Nature*, **489**, 57-74.
37. Kharchenko, P.V., Tolstorukov, M.Y. and Park, P.J. (2008) Design and analysis of ChIP-seq experiments for DNA-binding proteins. *Nat Biotechnol*, **26**, 1351-1359.
38. Meuleman, W., Muratov, A., Rynes, E., Halow, J., Lee, K., Bates, D., Diegel, M., Dunn, D., Neri, F., Teodosiadis, A. *et al.* (2020) Index and biological spectrum of human DNase I hypersensitive sites. *Nature*, **584**, 244-251.
39. Chan, P.P., Lin, B.Y., Mak, A.J. and Lowe, T.M. (2021) tRNAscan-SE 2.0: improved detection and functional classification of transfer RNA genes. *Nucleic Acids Res*, **49**, 9077-9096.
40. Sherry, S.T., Ward, M.H., Kholodov, M., Baker, J., Phan, L., Smigielski, E.M. and Sirotkin, K. (2001) dbSNP: the NCBI database of genetic variation. *Nucleic Acids Res*, **29**, 308-311.
41. DeFranco, D., Sharp, S. and Soll, D. (1981) Identification of regulatory sequences contained in the 5'-flanking region of Drosophila lysine tRNA₂ genes. *J Biol Chem*, **256**, 12424-12429.
42. Allison, D.S. and Hall, B.D. (1985) Effects of alterations in the 3' flanking sequence on in vivo and in vitro expression of the yeast SUP4-o tRNA^{Tyr} gene. *EMBO J*, **4**, 2657-2664.
43. Berg, M.D., Zhu, Y., Ruiz, B.Y., Loll-Krippleber, R., Isaacson, J., San Luis, B.J., Genereaux, J., Boone, C., Villen, J., Brown, G.W. *et al.* (2021) The amino acid substitution affects cellular response to mistranslation. *G3 (Bethesda)*, **11**.
44. Berg, M.D., Zhu, Y., Isaacson, J., Genereaux, J., Loll-Krippleber, R., Brown, G.W. and Brandl, C.J. (2020) Chemical-Genetic Interactions with the Proline Analog L-Azetidine-2-Carboxylic Acid in *Saccharomyces cerevisiae*. *G3 (Bethesda)*, **10**, 4335-4345.
45. Mohler, K., Aerni, H.R., Gassaway, B., Ling, J., Ibba, M. and Rinehart, J. (2017) MS-READ: Quantitative measurement of amino acid incorporation. *Biochim Biophys Acta Gen Subj*, **1861**, 3081-3088.
46. Lin, B.Y., Chan, P.P. and Lowe, T.M. (2019) tRNAviz: explore and visualize tRNA sequence features. *Nucleic Acids Res*, **47**, W542-W547.
47. Ashraf, S.S., Guenther, R.H., Ansari, G., Malkiewicz, A., Sochacka, E. and Agris, P.F. (2000) Role of modified nucleosides of yeast tRNA(Phe) in ribosomal binding. *Cell Biochem Biophys*, **33**, 241-252.
48. Fandilolu, P.M., Kamble, A.S., Sambhare, S.B. and Sonawane, K.D. (2018) Conformational preferences and structural analysis of hypermodified nucleoside, peroxywybutosine (o₂yW) found at 37(th) position in anticodon loop of tRNA(Phe) and its role in modulating UUC codon-anticodon interactions. *Gene*, **641**, 310-325.
49. Carlson, B.A., Kwon, S.Y., Chamorro, M., Oroszlan, S., Hatfield, D.L. and Lee, B.J. (1999) Transfer RNA modification status influences retroviral ribosomal frameshifting. *Virology*, **255**, 2-8.
50. Kim, Y., Opron, K. and Burton, Z.F. (2019) A tRNA- and Anticodon-Centric View of the Evolution of Aminoacyl-tRNA Synthetases, tRNAomes, and the Genetic Code. *Life (Basel)*, **9**.

51. Lim, V.I. and Curran, J.F. (2001) Analysis of codon:anticodon interactions within the ribosome provides new insights into codon reading and the genetic code structure. *RNA*, **7**, 942-957.
52. Rozik, P., Szabla, R., Lant, J.T., Kiri, R., Wright, D.E., Junop, M. and O'Donoghue, P. (2022) A novel fluorescent reporter sensitive to serine mis-incorporation. *RNA Biol*, **19**, 221-233.

Copyright permissions

Co-authors

All listed co-authors consented to use of their work as attributed in this thesis.

Chapter 1

This chapter was originally published in the Journal of Biological Chemistry:

Lant, J.T., Berg, M.D., Heinemann, I.U., Brandl, C.J., O'Donoghue, P. Pathways to disease from natural variations in human cytoplasmic tRNAs. *J Biol Chem.* 2019. 294(14):5294-5308.

The Journal of Biological Chemistry does not request permission for reuse of material in academic theses (<https://www.elsevier.com/journals/journal-of-biological-chemistry/0021-9258/guide-for-authors>).

Chapter 2

A version of this chapter was published in RNA Biology:

Lant, J.T., Berg, M.D. Sze, D.H.W., Hoffman, K.S., Akinpelu, I.C., Turk, M., Heinemann, I.U., Duennwald, M.L., Brandl, C.J., and O'Donoghue, P. Visualizing tRNA-dependent mistranslation in human cells. 2017. *RNA Biology.* 15(4-5): 567-575.

The version appearing in this thesis is the accepted manuscript version. Authors in Taylor and Francis journals retain the right to reproduce accepted manuscript versions in thesis and deposit them to open thesis repositories provided that the article is not under embargo. The embargo period for RNA Biology is 0 months. Hence, permission was not required to reproduce this article version in this thesis.

(<https://authorservices.taylorandfrancis.com/research-impact/sharing-versions-of-journal-articles/>).

Chapter 3

This chapter was originally published in *Nucleic Acids Research*:

Lant, J.T., Kiri, R., Duennwald, M.L., O'Donoghue, P. Formation and persistence of polyglutamine aggregates in mistranslating cells. 2021. *Nucleic Acids Research*. 49(20): 11883-11899.

Oxford University Press (<https://global.oup.com/academic/>) grants full permission for reuse of published works in academic thesis.

Curriculum Vitae

Jeremy Thomas Lant

Post-secondary Education and Degrees:

University of Western Ontario
London, ON, Canada
2012-2016 BMSc

Honours and Awards:

Nucleic Acids Research Breakthrough Article: “Formation and persistence of polyglutamine aggregates in mistranslating cells”
2021

Silver Poster Award, Canadian Student Health Research Forum
University of Manitoba, Winnipeg, MB, Canada
2020

Dr. Bishnu D. Sanwal Graduate Performance Award
University of Western Ontario, London, ON, Canada
2019

National Clinical Research Center for Child Health Travel Award.
Zhejiang University, Hangzhou, China
2019

National Sciences and Engineering Research Council Postgraduate Scholarship-
Doctoral
2018

Ontario Graduate Scholarship (offer declined)
2018

Western Graduate Research Scholarship (annual)
2016-2021

Western Scholarship of Distinction
2012

Related Work Experience:

Teaching Assistant
Biochemistry 4415b – Chemical Biology and Synthetic Biology
University of Western Ontario
2017-2020

Guest Lecturer
Biochemistry 9555 – Advanced Laboratory Research and Seminar Series
University of Western Ontario
2021

Biochemistry Graduate Student's Association Co-Chair
University of Western Ontario
2019-2020

Biochemistry Graduate Student's Association Visiting Speaker Coordinator
University of Western Ontario
2018-2019

Conference Volunteer
Canadian Chemistry Conference and Exhibition, Quebec City, QC, Canada
2019

Volunteer: Western Synthetic Biology Research Program
University of Western Ontario
2017-2018

Publications:

Rozik, P., **Lant, J.T.**, Szabla, R., Kiri, R., Wright, D.E., Junop, M., O'Donoghue, P. (2021). A novel fluorescent reporter sensitive to serine mis-incorporation. (accepted in *RNA Biology*)

Lant, J.T., Kiri, R., Duennwald, M.L., O'Donoghue, P. (2021). Formation and persistence of polyglutamine aggregates in mistranslating cells. *Nucleic Acids Research*

Berg, M.D., Giguere, D.J., Dron, J.S., **Lant, J.T.**, Genereaux, J., Liao, C., Wang, J., Robinson, J., Gloor, G.B., Hegele, R.A., O'Donoghue, P., Brandl, C.J. (2019). Targeted sequencing reveals expanded genetic diversity of human transfer RNAs. *RNA biology*, 16(11), 1574-1585.

Lant, J.T., Berg, M.D., Heinemann, I.U., Brandl, C.J., O'Donoghue, P. (2019). Pathways to disease from natural variations in human cytoplasmic tRNAs. *Journal of Biological Chemistry*.

Abdelhameed, M., Aly, S., **Lant, J. T.**, Zhang, X., & Charpentier, P. (2018). Energy/Electron Transfer Switch for Controlling Optical Properties of Silicon Quantum Dots. *Scientific reports*, 8(1), 17068.

Slattery, S. S., Diamond, A., Wang, H., Therrien, J. A., **Lant, J. T.**, Jazey, T., ... & Edgell, D. R. (2018). An expanded plasmid-based genetic toolbox enables Cas9 genome editing and stable maintenance of synthetic pathways in *Phaeodactylum tricornutum*. *ACS synthetic biology*.

Lant, J.T., Berg, M.D. Sze, D.H.W., Hoffman, K.S., Akinpelu, I.C., Turk, M., Heinemann, I.U., Duennwald, M.L., Brandl, C.J., and O'Donoghue, P. (2017) Visualizing tRNA-dependent mistranslation in human cells. *RNA Biology*.

Wolfs, J. M., Hamilton, T. A., **Lant, J. T.**, Laforet, M., Zhang, J., Salemi, L. M., ... & Edgell, D. R. (2016). Biasing genome-editing events toward precise length deletions with an RNA-guided TevCas9 dual nuclease. *Proceedings of the National Academy of Sciences*, 201616343.

Presentations:

Talks

- | | |
|--|------|
| Biochemistry Fall Graduate Symposium, London, ON, Canada. | 2020 |
| Title: <i>Natural human tRNA variants alter the behaviour of mammalian cells and model of disease.</i> | |
| Maud L. Menten Memorial Fall Symposium, London, ON, Canada. | 2020 |
| Title: <i>Developing a dual fluorescent assay for inhibitors of SARS-CoV2 Spike protein binding in human cell culture.</i> | |
| Canadian Student Health Research Forum, Winnipeg, MB, Canada. | 2020 |
| Title: <i>Mistranslating tRNAs alter the formation and persistence of polyglutamine aggregates in cells.</i> | |
| 12 th International Symposium on Aminoacyl-tRNA synthetases, Hangzhou, China. | 2019 |
| Title: <i>Mistranslating tRNAs alter the formation and persistence of polyglutamine aggregates in cells.</i> | |
| mRNA Turnover: Mechanisms, Regulation and their Implication in Infectious and Age-Related Diseases, Montreal, QC, Canada. | 2019 |
| Title: <i>Natural tRNA variants in human cytoplasmic tRNAs as modifiers of neurodegenerative disease.</i> | |
| Canadian Chemistry Conference and Exhibition 2019, Quebec City, QC, Canada. | 2019 |
| Title: <i>Natural tRNA variation and visualizing mistranslation in human cells.</i> | |
| Biochemistry Fall Graduate Symposium, London, ON, Canada. | 2018 |
| Title: <i>Natural tRNA variation and visualizing mistranslation in human cells.</i> | |

Posters

- Harold B. Stewart Lecture and Research Showcase, London, ON, Canada. 2020
 Title: *Mistranslating tRNAs alter the formation and persistence of polyglutamine aggregates in cells.*
- SynBio4, Waterloo, ON, Canada. 2019
 Title: *Natural tRNA variants in human cytoplasmic tRNAs as modifiers of neurodegenerative disease.*
- Neuroscience Research Day, London, ON, Canada. 2019
 Title: *Natural tRNA variants in human cytoplasmic tRNAs as modifiers of neurodegenerative disease.*
- London Health Research Day, London, ON, Canada. 2019
 Title: *Natural tRNA variation and visualizing mistranslation in human cells.*
- Rustbelt RNA Meeting, Columbus, OH, USA. 2018
 Title: *Natural tRNA variation and visualizing mistranslation in human cells.*
- Synthetic Biology Symposium 3.0, London, ON, Canada. 2018
 Title: *Understanding tRNA mutations and the 'hidden language' of protein synthesis.*
- Inventing the Future: Symposium on Synthetic Biology 2.0, London, ON, Canada. 2017
 Title: *The awesome power of tRNA engineering: encoding phosphothreonine in E. coli and tRNA-dependent mistranslation in human cell culture.*
- Harold B. Stewart Lecture and Research Showcase, London, ON, Canada. 2017
 Title: *Hijacking selenocysteine translation for synthetic biology: Recoding phosphorylated serine and threonine and applications of mistranslation in Huntington's disease.*